[redacted]

[redacted]

NASA TECHNICAL MEMORANDUM

NASA TM X-2954

NASA TM X-2954

EFFECT OF WING MOUNTED NACELLES ON A 42° SWEPT SUPERCRITICAL WING CONFIGURATION AT NEAR-SONIC SPEEDS

by Linwood W. McKinney, Joseph F. Herman, and Lawrence A. Bodin

Langley Research Center
Hampton, Va. 23665

NATIONAL AERONAUTICS AND SPACE ADMINISTRATION • WASHINGTON, D. C. • MARCH 1974

[redacted]

CONFIDENTIAL

1. Report No.	2. Government Accession No.	3. Recipient's Catalog No.
NASA TM X-2954		

4. Title and Subtitle	5. Report Date
EFFECT OF WING-MOUNTED NACELLES ON A 42° SWEPT SUPERCRITICAL WING CONFIGURATION AT NEAR-SONIC SPEEDS (U)	March 1974
	6. Performing Organization Code

7. Author(s)	8. Performing Organization Report No.
Linwood W. McKinney, Joseph F. Herman, and Lawrence A. Bodin	L-9267
	10. Work Unit No.
9. Performing Organization Name and Address	760-64-60-01
NASA Langley Research Center Hampton, Va. 23665	11. Contract or Grant No.
	13. Type of Report and Period Covered
12. Sponsoring Agency Name and Address	Technical Memorandum
National Aeronautics and Space Administration Washington, D.C. 20546	14. Sponsoring Agency Code

15. Supplementary Notes

Joseph F. Herman and Lawrence A. Bodin are associated with Hampton Technical Center of Ling-Temco-Vought Aerospace Corporation.

16. Abstract

An investigation has been made to asses the effect of wing-mounted nacelles on a supercritical wing configuration at near-sonic Mach numbers. The investigation was made by utilizing the Cornell Aeronautical Laboratory 8-foot transonic tunnel and covered a Mach number range from 0.90 to 0.99. Force data and pressure measurements at selected locations were obtained.

The investigation with the nacelles on included the effect of spanwise location of the nacelle (semispan locations of 35 and 70 percent) and the effect of area ruling for the nacelles located at the 35-percent semispan station. Tests were also made with the outboard nacelle extended forward so that it was directly adjacent to the inboard nacelle location. These tests provided a direct assessment of the extent of the nacelle interference flow field in a lateral direction.

17. Key Words (Suggested by Author(s))

Wing-mounted nacelles
Transonic speed
Supercritical wing
Transport configuration
Pressure and force data

21. No. of Pages	22. Price
148	

EFFECT OF WING-MOUNTED NACELLES ON A 42° SWEPT SUPERCRITICAL WING CONFIGURATION AT NEAR-SONIC SPEEDS*

By Linwood W. McKinney, Joseph F. Herman,** and Lawrence A. Bodin**
Langley Research Center

SUMMARY

An investigation has been made to assess the effect of wing-mounted nacelles on a supercritical wing configuration at near-sonic Mach numbers. The investigation was made by utilizing the Cornell Aeronautical Laboratory 8-foot transonic tunnel and covered a Mach number range from 0.90 to 0.99. Force data and pressure measurements at selected locations were obtained.

In order to make a realistic assessment of the effects of nacelle installation, it was necessary to optimize the configuration with the nacelles both off and on. Tests with the nacelles off indicated that a strong interaction existed between the wing and fuselage pressure fields. Small changes in the local fuselage contour affected the fuselage shock location and strength which resulted in significant changes in wing performance at near-sonic Mach numbers.

The investigation with the nacelles on included the effect of spanwise location of the nacelle (semispan locations of 35 and 70 percent) and the effect of area ruling for the nacelles located at the 35-percent semispan station. Tests were also made with the outboard nacelle extended forward so that it was directly adjacent to the inboard nacelle location. These tests provided a direct assessment of the extent of the nacelle interference flow field in a lateral direction.

The nacelle installation tests indicated that the nacelle at the outboard location had a more pronounced effect on the wing than at the inboard location. Moving the nacelle laterally from 35-percent semispan to 70-percent semispan had essentially no effect on the pressures induced by the nacelle on the fuselage and indicated that both the outboard and inboard nacelles should be included in the area distribution. The increase in local curvature obtained when the nacelle area was removed from the fuselage circumferentially produced shocks off the fuselage at Mach numbers of 0.95 and greater that offset the drag

---

*Title, Unclassified.

**Associated with Hampton Technical Center of Ling-Temco-Vought Aerospace Corporation.

reduction which should have been obtained because of the improved area distribution. Area ruling for the inboard nacelle by removing area from the underside of the fuselage reduced the drag due to nacelle installation to a level approximately corresponding to that of the isolated nacelle.

INTRODUCTION

The development of the NASA supercritical airfoil section at the Langley Research Center has offered the possibility of efficient cruise at near-sonic speeds. This development provides the potential for a significant payoff in commercial aviation. As a result of this potential, the National Aeronautics and Space Administration is engaged in a continuing research program aimed at the development of a technology base for the design of transport aircraft utilizing supercritical technology.

Past investigations have demonstrated the performance characteristics of the supercritical wing section (refs. 1 to 11) and initial integrated configuration studies have been made utilizing aft fuselage mounted engines to avoid possible adverse nacelle-pylon-wing interference (ref. 12). However, there are several attractive advantages to wing-mounted engines in transport design, such as improved balance capabilities for large aircraft, possible wing-bending relief and greater freedom in horizontal-tail placement for stability and control considerations. Therefore, one of the research areas currently under consideration is the integration of wing-mounted nacelles on a transport configuration designed to operate at near-sonic speeds.

It is generally assumed that successful nacelle integration at speeds near Mach 1.0 will depend primarily on providing an area ruling of the complete configuration corresponding to that for a minimum pressure drag body of revolution while avoiding components with severe local surface contours. Therefore, an investigation was undertaken to determine the effectiveness of local contouring on the fuselage to account for wing-mounted nacelles in the overall area distribution.

The investigation was made by the Langley Research Center utilizing the Cornell Aeronautical Laboratory 8-foot transonic wind tunnel. Technical assistance was provided by the Hampton Technical Center of Ling-Temco-Vought Aerospace Corporation.

COEFFICIENTS AND SYMBOLS

All coefficients are based on the geometry of the reference wing panel which does not include the leading-edge glove or the trailing-edge extension. (See fig. 1.) Moments are referenced to the quarter-chord point of the mean geometric chord which is located

at fuselage station 73.40 cm (28.898 in.). Values are given in both SI and U.S. Customary Units. The measurements and calculations were made in U.S. Customary Units.

b	wing span, 114.3 cm (45 in.)
c	local streamwise wing chord
$\bar{c}$	wing-panel mean geometric chord, 18.087 cm (7.121 in.)
C_A	axial-force coefficient, $\frac{\text{Axial force}}{qS}$
C_D	drag coefficient, $\frac{\text{Drag}}{qS}$
$\Delta C_{D,i}$	nacelle internal drag coefficient
C_L	lift coefficient, $\frac{\text{Lift}}{qS}$
$C_{m_{\bar{c}/4}}$	pitching-moment coefficient, $\frac{\text{Pitching moment}}{qS\bar{c}}$
C_N	normal-force coefficient, $\frac{\text{Normal force}}{qS}$
C_p	pressure coefficient, $\frac{p_{local} - p_{static}}{q}$
M	free-stream Mach number
p	pressure, N/m^2 (lb/ft^2)
q	free-stream dynamic pressure, N/m^2 (lb/ft^2)
r	radius, cm (in.)
S	wing panel reference area, 0.1928 m^2 (2.075 ft^2)
t	thickness, cm (in.)
x	distance measured from leading edge of local wing chord, positive toward wing trailing edge, cm (in.)

y distance measured laterally from plane of symmetry, cm (in.)

z distance measured along a line perpendicular to x and y, cm (in.)

α angle of attack, referred to fuselage reference line, deg

η percent semispan station, $\frac{y}{b/2}$

Subscripts:

l lower

u upper

APPARATUS AND PROCEDURES

Tests

The investigations were conducted by Langley Research Center personnel utilizing the Cornell Aeronautical Laboratory 8-foot variable-density wind tunnel. The facility has an 8-foot-square perforated test section with a porosity of 22 percent. The configurations were generally tested over a Mach number range from 0.90 to 0.99 at a constant Reynolds number of 9.84×10^6 per meter (3.0×10^6 per foot).

Wind-Tunnel Models

A two-view drawing of the general configuration is presented in figure 1. A typical longitudinal development of fuselage cross sections is presented in figure 2. For this investigation the horizontal tail was not included on the model.

The model wing has an aspect ratio of 6.77, a panel taper ratio of 0.36, and 42.24^o of sweepback at the quarter-chord line. The wing area of the basic panel, including the fuselage intercept, is 0.1928 m^2 (2.075 ft^2), and the reference mean geometric chord is 18.087 cm (7.121 in.) in length. Table I presents the wing coordinates. Figure 3 presents the measured twist distribution of the wing including the original incidence. (See table I.) The wing was tested with the incidence increased 0.5^o by rotating the wing about fuselage station (FS) 39.90 cm (15.71 in.) and water line (WL) -1.55 cm (-0.61 in.). The wing was constructed of aluminum and was instrumented with flush surface static-pressure orifices in streamwise rows on the upper and lower surfaces at semispan stations of 22, 32.3, and 37.7 percent. The same wing was used for all tests.

The fuselage was constructed in a manner such that material could be added or removed to investigate the effects of longitudinal development of cross-sectional area on aerodynamic characteristics. Initial investigations were conducted with a wing—body—vertical-tail configuration, designated configuration B. This body was modified by extending the nose 5.08 cm (2 in.) and redefining the cross-sectional area progression based upon an area distribution presented in reference 12. The body was instrumented with flush surface static-pressure orifices located between fuselage stations 35.56 cm (14 in.) and 91.44 cm (36 in.) on the top center line, on the right side above the wing (WL = 0) and on the bottom center line for selected configurations.

Wing-mounted flowthrough nacelles were used to investigate the effect of spanwise location on aerodynamic characteristics. Nacelles were located at 35-percent and then at 70-percent wing semispan. Figure 4(a) presents the pertinent geometry of the basic pylon-nacelle installations at 35- and 70-percent semispan. Ordinates for the pylon, measured normal to the leading edge, are presented in table II. Figure 4(b) presents a schematic sketch of the extended pylon which was also mounted at the 70-percent semispan station and located the nacelles so that they were at the same longitudinal station as the inboard nacelle location. (See fig. 5(j).) This extended pylon is not considered to be a practical arrangement, but was used to isolate spanwise and chordwise effects.

The model vertical tail had an aspect ratio of 1.34, a taper ratio of 0.306, 45° sweepback at the quarter-chord line, and a symmetrical airfoil section.

Several model photographs are shown in figure 5.

Boundary-Layer Transition

Boundary-layer trips were applied to the wing and tail surfaces by using the technique described in references 13 to 15 to simulate full-scale Reynolds number boundary-layer shock-induced separation characteristics. This technique requires that laminar flow be maintained ahead of the trip, and, therefore, caution was exercised to maintain a very smooth surface ahead of the trip. The wing transition strips were located as shown in figure 6.

The transition strips on the vertical tail were located at 31 percent of the local streamwise chord. Number 120 carborundum grains were used. The fuselage transition strip was applied 3.81 cm (1.5 in.) aft of the fuselage nose with number 100 carborundum grains. Transition strips for the flowthrough nacelles were located 0.9525 cm (0.375 in.) behind the inlet leading edge. Strips of number 120 carborundum grains were applied inside and outside. Transition strips on the nacelle pylons were located 0.254 cm (0.10 in.) measured normal to the leading edge. Number 120 carborundum grains were used. All model transition strips were 0.127 cm (0.05 in.) wide.

Measurements

Aerodynamic forces and moments were measured with an internally mounted six-component strain-gage balance. Measurements of the local static pressure along streamwise chord lines were obtained for selected wing semispan stations. In addition, local static pressures were measured along the top center line, along the right side (WL = 0), and along the bottom center line of selected fuselage configurations. Pressures were measured with internally mounted scanivalves.

Force measurements were taken over a Mach range varying from 0.90 to 0.99 for angles of attack that generally varied from -0.5° to 5.5°. Pressure data were obtained in the angle-of-attack range of 1° to 4°. Pressure data presented in this report are for a lift coefficient of approximately 0.40.

Corrections

Measured axial force and drag data presented herein have been corrected to a condition of free-stream static pressure acting on an area of 19.32 cm^2 (3.0 in^2). To be consistent with reference 12, this area represented the cross-sectional area of the sting. Where applicable, the axial force and drag have been reduced by the estimated skin friction on the interior surfaces of the flowthrough nacelles as presented in figure 7. Corrections have been made to the measured angle of attack for model support system deflections. Further corrections to the measured angle of attack have been made for tunnel airflow angularity.

Accuracy

The accuracy of the force and moment measurements, as determined by calibration of the balance, is given in coefficient form as follows:

Normal force	±0.0009
Pitching moment	±0.00025
Axial force	±0.00017

Pressure measurements were measured with an accuracy of ±11.97 N/m^2 (±0.25 lb/ft^2). Mach number measurements were accurate to ±0.002. Angles of attack are estimated to be within $\pm 0.05^{\circ}$.

RESULTS AND DISCUSSION

In order to make a realistic assessment of the effects of wing-mounted nacelle installations at near-sonic speeds, it is necessary to optimize both the nacelles-on and

nacelles-off configurations. Therefore, an investigation was made to optimize the wing-body configuration prior to nacelle installation. The importance of applying the area-rule concept in this speed range and at the same time providing a fuselage shape that conforms to the wing streamlines for control of the isobars on the wing, has been recognized for some time. However, practical experience in applying these principles and assessing their sensitivity has been limited because of wing performance prior to the development of the NASA supercritical section. Because of this general lack of experience, a rather detailed discussion of the wing-body optimization is presented.

Optimization of Wing-Body

The initial model (model B) was designed to a preliminary sonic area distribution. (See fig. 8.) Initial tests of this model configuration indicated excessive drag rise at Mach numbers above $M = 0.95$. Subsequent to model construction, an improved sonic area distribution presented in reference 12 was developed. Therefore, the initial model B was modified to conform to this area distribution. (See fig. 9, model B_1.) In the development of these total area distributions, consideration has been given to the second-order effect caused by the expansion of the supersonic stream tube above the wing at lifting conditions. The area associated with this effect is designated in the figure as equivalent area due to lift. The effect of lift compensation in the area distribution has been verified by previous experimental work and is discussed in some detail in references 12, 16, and 17. A comparison of the drag rise characteristics at $C_L = 0.4$ for these two models is presented in figure 10. This C_L is considered to be near the cruise lift condition for a typical near-sonic transport. The basic data are contained in figure 11. The drag rise for the B_1 configuration was delayed at low lift coefficients $(C_L = 0.2)$ but at $C_L = 0.4$ essentially no effect was obtained. A further examination of the forces on the body axes (fig. 11) indicates that the axial component of force was reduced by the modification represented by configuration B_1 over the complete Mach number range, the largest reduction occurring at the high normal-force coefficients. However, a reduction in normal force with angle of attack is also indicated. The reductions in axial force were expected with the improved area distribution. The anticipated reductions in drag were not realized, however, because of the reduced normal-force curve slope, since at an angle of attack normal force is the predominant contributor to drag.

Since the same wing was used on both configurations (models B and B_1), the reduction in lift-curve slope was attributed to an interference associated with an oblique shock of the fuselage. The wing used in this investigation was not identical to the wing used in reference 12 in that significant differences existed in section shape in the region of the wing glove near the fuselage, as well as differences in span and twist. Since the pressures on the side of the fuselage are influenced greatly by the wing pressure field, it was

assumed that the fuselage contours were not optimum, and at the critical speed ($M > 0.95$) for this model, shocks were emanating from the side of the fuselage.

A comparison of the area distribution for the B and B_1 configurations (fig. 12) indicates rather significant differences. In modifying the model to the area distribution shown for the B_1 configuration and maintaining the maximum fineness ratio (9.05), the nose of the model was extended 5.08 cm (2 in.) which, in effect, moved the wing rearward. These changes caused the fuselage area distribution to close to a minimum more rapidly with higher rates of change in the slope of the surface; this condition might result in an adverse interference on the wing.

A third model configuration (model B_2) was therefore investigated, which had the maximum area further aft while maintaining a smooth area progression and the curvature of the fuselage in the region of the wing root was reduced. (See figs. 13 and 14.) The drag rise characteristics for the B_1 and B_2 configurations are compared in figure 15. The B_2 configuration shows a more severe drag divergence. An examination of the data indicates that this condition resulted from a further reduction in wing performance and to some extent, a less desirable overall area distribution.

A comparison of wing pressure distributions measured at $\eta = 0.220$, 0.323, and 0.377 for the B, B_1, and B_2 configurations is presented in figure 16 for Mach numbers of 0.90, 0.95, and 0.98 and a lift coefficient of approximately 0.40. The pressure data at Mach numbers of 0.95 and 0.98 indicate a reduction in the suction pressures over the first 30 percent of the chord and a significant loss of pressure recovery over the trailing-edge section of the wing This condition resulted in both increased drag and reduced lift for a given angle of attack. Fluorescent oil-flow visualization studies made during the tests correlated well with these data and the effects can be attributed to a strong shock emanating from the side of the fuselage and extending across the wing as indicated by the sketch in figure 17. The fuselage shock occurred aft of the transition strips on the wing glove and the shock—boundary-layer interaction on the wing glove near the fuselage was minimized by the high-energy turbulent boundary layer. As the shock extended spanwise across the transition strip, the shock—boundary-layer interaction in the laminar boundary layer ahead of the transition induced separation that significantly altered the flow over the remainder of the wing span. For the B_1 configuration, it appeared that the shock interaction with the wing was probably very similar to the B_2 configuration, but somewhat less severe.

Although the area progression for the fuselage of the B_2 configuration looked more favorable from total area considerations, these pressure results indicate a highly unfavorable local interaction of the curvature at the wing root with the wing upper surface contour. Therefore, the model was restored to the B_1 lines and an attempt was made to solve the local problems associated with that area distribution. To aid in this task, a

series of pressure orifices were installed in the fuselage on the top center line, bottom center line, and along the side 2.54 cm (1 in.) above the wing surface as indicated in figure 1.

The changes in area distribution resulting from the local fuselage modifications on the B_1 configuration, designated B_{1a} and B_{1b}, are shown in figure 18. The modifications reduced the curvature on the side of the fuselage in the area of the wing root. The effect of the reduced curvature on the wing and fuselage pressures are shown in figures 19 and 20 for Mach numbers of 0.90, 0.95, and 0.98. A sketch showing the relationship of the pressures to the wing location is also shown on the fuselage pressures. In general, for the B_1 configuration, a high negative peak pressure existed on the side of the fuselage. Reducing the curvature on the B_{1a} configuration reduced the pressure peak and smoothed the distribution. A further small reduction of the fuselage curvature (model B_{1b}) had only a small effect on the fuselage pressures. The effect of these changes on the drag is summarized in figure 21 where a significant reduction is shown for the B_{1b} configuration at Mach numbers above 0.95. The basic data are presented in figure 22. Since the overall smoothness of the area distribution has deteriorated with the modifications, the improvement in drag is the result of reducing the interference on the wing associated with the shock off the fuselage.

A further attempt to smooth the overall area distribution was investigated by reducing the maximum cross-sectional area of configuration B_{1b} to configuration B_{1c} as shown in figure 23. This reduction was accomplished by removing material from the fuselage above the wing. The effect of this modification on the drag rise characteristics is presented in figure 24 and the basic data are presented in figures 25 to 27. The large increase in drag shown for Mach numbers above 0.95 (fig. 24) was caused by a strong shock again occurring on the fuselage. The presence of this shock is highly visible in the pressure distribution of both the wing and fuselage. (See figs. 25 and 26.)

The strong interaction of the wing and fuselage pressure field at near-sonic speeds is generally known; however, these results illustrate the extreme sensitivity to relatively small changes in local fuselage contour. It should not be concluded from the results presented in this report, however, that the total area-rule requirement and conditions for elimination of adverse local effects cannot be satisfied simultaneously. The present investigation considered modifications only to the fuselage contour and it is believed that more severe fuselage contours which would result in a more favorable area distribution could be tolerated if accompanied by small changes in the shape of the wing glove section near the fuselage. This change in the wing glove section would be expected to produce a further improvement in drag at the near-sonic Mach numbers. However, the reason for attempting to optimize the wing-body configuration in this investigation, as stated earlier, was to provide a base for assessing nacelle installation effects. It was not practical at this point to modify the wing glove in order to effect further optimization of the wing-body

and since the B_{1b} configuration exhibited reasonable drag rise characteristics at the design point $(C_L = 0.40)$ with a relatively smooth area distribution, it was used as a base for the nacelle-installation tests.

Nacelle Installation Effects

The investigation conducted on the wing—body—vertical-tail configuration without nacelles verified, as expected, the strong interaction between the pressure fields on the fuselage and wing glove and indicated the extreme sensitivity of these pressure fields to small changes in local fuselage contour at near-sonic speeds. In view of these effects and the anticipated negative pressure increment on the fuselage resulting from the presence of the nacelle-pylon in the flow field, tests were made with the nacelles installed without changing the configuration area ruling. These tests provided a qualitative assessment of the direct effect of the nacelle on the wing and fuselage and also served as a base from which to evaluate the effectiveness of applying the area rule to the configuration to account for the nacelles.

Effect of not applying the area rule for nacelles.- The effect of nacelles located at the 35-percent and then at the 70-percent semispan station was investigated. The data obtained from these tests are presented in figures 28 to 33. The drag data are summarized in figure 28 for $C_L = 0.40$ in terms of both total drag and the incremental drag resulting from nacelle installation. The measured drag for the isolated nacelle-pylon combination obtained in a previous investigation is also included for reference. At $C_L = 0.40$, both configurations (nacelles inboard and nacelles outboard) exhibited a significant drag rise above a Mach number of $M = 0.95$ with no appreciable difference between the two locations. At a Mach number of 0.98, the ΔC_D due to the nacelles was 2.3 times the drag of the isolated nacelle. The negligible difference in drag shown for the two locations at $C_L = 0.40$ may have been somewhat fortuitous, however, since the shape of the drag polars are markedly different for the two locations as Mach number is increased. (See fig. 29.) At Mach numbers of 0.95 and greater, the nacelles when at the inboard location have a more severe drag penalty than when at the outboard location for the low lift coefficients, but at the higher lift coefficients $(C_L$ greater than approximately $0.40)$ the reverse is generally true. The nacelles at the inboard location produced an improvement in drag due to lift compared with the nacelles off baseline at the high lift coefficients that resulted in drag levels equal to or less than the nacelles off baseline at the highest lift coefficients for some Mach numbers. However, in comparing the drag polars, it should be kept in mind that the nacelles-off configuration was optimized for $C_L = 0.40$ and at the higher lift coefficients flow separation was present on the wing. With the nacelles installed at the 35-percent semispan station, a vortex off the pylon (visible with fluorescent oil techniques) energized the boundary layer in the region of the

juncture between the wing panel and highly swept glove and delayed separation on the wing. Therefore, the apparent improvement in drag due to lift at the high lift coefficient with the nacelles installed at the 35-percent semispan station would not be expected if the wing was designed for a higher lift coefficient. It is believed that the results obtained around the design condition $(C_L = 0.40)$ are most realistic.

The effect of the nacelle-pylon on the wing pressure distribution is presented in figure 30 for $C_L \approx 0.40$ at Mach numbers of 0.90, 0.95, and 0.98. These limited pressure distributions show a slight improvement in pressure recovery at the trailing edge with the nacelle inboard even for the case for a lift coefficient of 0.40. The effect of moving the nacelle to the outboard location produces a rise in pressure over the wing leading edge and a loss in pressure recovery at the trailing edge for Mach numbers of both 0.95 and 0.98.

The effect of nacelle installation on the surface pressures on the top center line, side, and bottom center line of the fuselage are presented in figure 31 for Mach numbers of 0.90, 0.95, and 0.98. A comparison of the pressures obtained with the nacelles at the inboard location with the nacelles-off case indicates a direct effect of the nacelle on the fuselage. More negative pressures were obtained in the vicinity of the nacelle with a stronger shock occurring on both the top and bottom of the fuselage. A comparison of the pressure distribution with the nacelles moved outboard with the nacelles-off case also indicates some increase in the negative pressure on the fuselage adjacent to the nacelle, but less pronounced than that with the nacelle inboard, and the fuselage pressures generally reflect the trend seen on the wing.

Theory indicates that near Mach 1.0 disturbances propagate infinitely far from the source in a direction normal to the flow. Therefore, it would be expected that varying the nacelle location spanwise would have a minimal effect on the influence of the nacelle at the fuselage. In this test, however, the nacelle at the outboard station had a pronounced effect on the wing (fig. 30); it is not clear whether the increments seen in fuselage pressure are a direct result of the nacelle or are a result of changes in the wing pressure distribution reflected on the fuselage. Since part of the objective of the investigation was to assess the applicability of the area-rule concept to nacelles mounted outboard on the wing, additional tests were made with the outboard nacelle extended forward so that it was directly adjacent to the inboard nacelle location as indicated in figure 5. These tests, although not a practical configuration, provided a direct assessment of the extent of the nacelle interference flow field in a lateral direction at near-sonic Mach numbers. The tests were made at a later time in the investigation and slight differences in the fuselage lines resulted in a slightly different fuselage pressure distribution on the nacelles off-base configuration. Therefore, the data are presented in terms of increments in pressure coefficient on the fuselage due to the nacelle and are compared with data from the earlier

installations in figure 32 for Mach numbers of 0.95 and 0.98. At a Mach number of 0.95 (fig. 32(a)) the negative pressure peak on the fuselage is diminished as the nacelle is moved laterally (position 1 to position 3). Also, the nacelle in the outboard location has essentially no effect on the pressure at the bottom center line of the fuselage. At a Mach number of 0.98 (fig. 32(b)), where the flow field around the airplane would be expected to be supercritical, moving the nacelle laterally had essentially no effect on the peak negative pressures induced on the fuselage. The effect of the nacelle is essentially independent of lateral location. Based on these data, it is concluded that for efficient nacelle integration at near-sonic speeds, both the inboard and outboard nacelle should be included in the total area distribution.

The limited wing pressure distributions presented earlier in this paper (fig. 30) with the nacelles installed without changing the configuration area ruling indicated that the interference field from the outboard nacelle resulted in a loss in pressure recovery on the wing. The elimination of this interference would appear to require careful redesign of the nacelle-pylon-wing combination which was beyond the scope of this investigation. In general, the effect obtained from applying the area rule to the aircraft components is dependent on the local flow field that the components are immersed in. Therefore, it was felt that application of the area rule to the fuselage for the outboard nacelle on this configuration prior to elimination of the nacelle-wing interference effects could lead to erroneous conclusions with regard to the benefits of applying the area rule. Tests were made, however, to assess the effectiveness of the area rule for the nacelles at the inboard location.

Effect of application of area rule for inboard nacelles.- The effect of area ruling for the inboard nacelles was investigated by removing an amount of cross-sectional area from the fuselage equivalent to that associated with the nacelles and pylons. In one case, the area was removed from the fuselage circumferentially, and, in a second case, all area was removed below the wing. Area distributions for these two configurations are presented in figures 33 and 34. A summary of the drag characteristics taken at $C_L = 0.40$ is presented in figure 35 and the basic data are presented in figures 36 to 38. It will be observed that removing the area circumferentially resulted in an improvement in drag compared with that for the case in which the area rule was not applied; however, taking the area for the nacelles from the fuselage below the wing reduced the drag due to the nacelles to a level approximately corresponding to the isolated nacelles up to a Mach number of 0.94 with a slight difference at the higher Mach numbers.

The differences in drag shown for the two configurations area ruled for the nacelles which had comparable area distributions are the result of local effects on the fuselage. Earlier tests indicated that the drag of the configuration was very sensitive to the contours of the upper fuselage in the region above the wing at Mach numbers of 0.95 and above.

The addition of the nacelles produced higher velocities and associated negative pressure peaks in this region. For the case where fuselage area was removed circumferentially, the curvature of the fuselage was increased in the region adjacent to the nacelle. The high local velocities associated with the increased curvature combined with the velocity induced by the nacelle resulted in strong shocks off the fuselage at $M = 0.95$ and above. The interaction of this shock with the wing tended to offset drag improvements that should have been obtained because of the improved area distribution. The presence of the shock is visible in the fuselage pressure distributions presented in figure 38. One approach to eliminating this problem, which might provide a practical solution, would be to modify the wing glove locally to compensate for the influence of the nacelle pressure field.

Removing equivalent nacelle cross-sectional area below the wing resulted in a concaved region in the bottom of the fuselage with relatively high local curvature. The pressure tubes on the lower surface of the fuselage were destroyed in order to remove the required amount of material, and a direct assessment of the effects of the changes in curvature on the fuselage pressure is not available. However, schlieren observations during the tests indicated that the shocks were not changed significantly and this observation appears to be substantiated by the force data. It should be pointed out that a shock is always present on the bottom of the fuselage at near-sonic Mach numbers because of the cusp in the lower surface of the wing. The addition of the nacelles increases the shock strength somewhat, but the pressure aft of the shock recovers to near the same level with nacelles both on and off. (See fig. 38.) Therefore, small changes in shock strength would not be expected to make significant changes in the drag.

CONCLUDING REMARKS

These exploratory tests indicated that with the nacelles off, a strong interaction existed between the wing and fuselage pressure field. Small changes in the local fuselage contour affected the fuselage shock location and strength which resulted in significant changes in wing performance at near-sonic Mach numbers.

The investigation with the nacelles on included the effect of spanwise location of the nacelle (semispan locations of 35 and 70 percent) and the effect of area ruling for the nacelles located at the 35-percent semispan station. Tests were also made with the outboard nacelle extended forward so that it was directly adjacent to the inboard nacelle location. These tests provided a direct assessment of the extent of the nacelle interference flow field in a lateral direction.

The nacelle installation tests indicated that the nacelle at the outboard location had a more pronounced effect on the wing than at the inboard location. Moving the nacelle laterally from 35-percent semispan to 70-percent semispan had essentially no effect on

the pressures induced by the nacelle on the fuselage and indicated that both the outboard and inboard nacelles should be included in the area distribution. The increase in local curvature obtained when the nacelle area was removed from the fuselage circumferentially produced shocks off the fuselage at Mach numbers of 0.95 and greater that offset the drag reduction which should have been obtained because of the improved area distribution. Area ruling for the inboard nacelle by removing area from the underside of the fuselage reduced the drag due to nacelle installation to a level approximately corresponding to that of the isolated nacelle.

Langley Research Center,
National Aeronautics and Space Administration,
Hampton, Va., November 26, 1973.

REFERENCES

1. Anon.: Supercritical Wing Technology – A Progress Report on Flight Evaluations. NASA SP-301, 1972.

2. Palmer, W. E.; Elliot, D. W.; and White, J. E.: Flight and Wind-Tunnel Evaluation of a 17% Thick Supercritical Airfoil on a T-2C Airplane. NR71H-150 (Contract N00019-70-C-0474), North American Rockwell Corp., July 31, 1971.
   Vol. I – Basic Report. (Available from DDC as AD 517 436L.)
   Vol. II – Flight Measured Wing Wake Profiles and Surface Pressures. (Available from DDC as AD 517 437L.)

3. Ferris, James C.: Aerodynamic Characteristics of a Model With a 17-Percent-Thick Supercritical Wing. NASA TM X-2551, 1972.

4. Harris, Charles D.: Wind-Tunnel Investigation of Effects of Trailing-Edge Geometry on a NASA Supercritical Airfoil Section. NASA TM X-2336, 1971.

5. Harris, Charles D.; and Blackwell, James A., Jr.: Wind-Tunnel Investigation of Effects of Rear Upper Surface Modification on an NASA Supercritical Airfoil. NASA TM X-2454, 1972.

6. Harris, Charles D.: Aerodynamic Characteristics of Two NASA Supercritical Airfoils With Different Maximum Thicknesses. NASA TM X-2532, 1972.

7. Harris, Charles D.: Wind-Tunnel Measurements of Aerodynamic Load Distribution on an NASA Supercritical-Wing Research Airplane Configuration. NASA TM X-2469, 1972.

8. Bartlett, Dennis W.; and Re, Richard J.: Wind-Tunnel Investigation of Basic Aerodynamic Characteristics of a Supercritical Wing Research Airplane Configuration. NASA TM X-2470, 1972.

9. Harris, Charles D.; and Bartlett, Dennis W.: Tabulated Pressure Measurements on an NASA Supercritical-Wing Research Airplane Model With and Without Fuselage Area-Rule Additions at Mach 0.25 to 1.00. NASA TM X-2634, 1972.

10. Harris, Charles D.; and Bartlett, Dennis W.: Wind-Tunnel Investigation of Effects of Underwing Leading-Edge Vortex Generators on a Supercritical-Wing Research Airplane Configuration. NASA TM X-2471, 1972.

11. Jordan, Frank L., Jr.: Investigation at Near-Sonic Speed of Some Effects of Humidity on the Longitudinal Aerodynamic Characteristics of a NASA Supercritical Wing Research Airplane Model. NASA TM X-2618, 1972.

12. Langhans, Richard A.; and Flechner, Stuart G.: Wind-Tunnel Investigation at Mach Numbers From 0.25 to 1.01 of a Transport Configuration Designed To Cruise at Near-Sonic Speeds. NASA TM X-2622, 1972.

13. Loving, Donald L.: Wind-Tunnel—Flight Correlation of Shock-Induced Separated Flow. NASA TN D-3580, 1966.

14. Blackwell, James A., Jr.: Preliminary Study of Effects of Reynolds Number and Boundary-Layer Transition Location on Shock-Induced Separation. NASA TN D-5003, 1969.

15. Braslow, Albert L.; and Knox, Eugene C.: Simplified Method for Determination of Critical Height of Distributed Roughness Particles for Boundary-Layer Transition at Mach Numbers From 0 to 5. NACA TN 4363, 1958.

16. Loving, Donald L.: A Transonic Wind-Tunnel Investigation of the Effect of Modifications to an Indented Body in Combination With a 45° Sweptback Wing. NACA RM L53F02, 1953.

17. Bartlett, Dennis W.; and Harris, Charles D.: Aerodynamic Characteristics of an NASA Supercritical-Wing Research Airplane Model With and Without Fuselage Area-Rule Additions at Mach 0.25 to 1.00. NASA TM X-2633, 1972.

TABLE I.- WING AIRFOIL COORDINATES

x/c	z_u/c for –	z_l/c for –	z_u/c for –	z_l/c for –
	η = 0.1042; c = 45.895 cm (18.069 in.); x = 0 at fuselage station 32.512 cm (12.80 in.)		η = 0.1932; c = 31.359 cm (12.346 in.); x = 0 at fuselage station 48.209 cm (18.98 in.)	
0	-0.0225	-0.0225	-0.0497	-0.0497
.0025	-.0153	-.0296	-.0418	-.0562
.0050	-.0119	-.0331	-.0390	-.0592
.0100	-.0075	-.0376	-.0346	-.0641
.0150	-.0043	-.0410	-.0315	-.0676
.0250	.0003	-.0465	-.0265	-.0729
.0500	.0078	-.0555	-.0178	-.0824
.0750	.0140	-.0618	-.0124	-.0885
.1000	.0182	-.0664	-.0086	-.0926
.1500	.0242	-.0728	-.0043	-.0985
.2000	.0283	-.0776	-.0023	-.1019
.2500	.0305	-.0808	-.0017	-.1039
.3000	.0307	-.0828	-.0021	-.1046
.4000	.0263	-.0834	-.0042	-.1026
.5000	.0173	-.0797	-.0084	-.0975
.5500	.0124	-.0751	-.0113	-.0939
.6000	.0074	-.0700	-.0148	-.0894
.6500	.0024	-.0642	-.0187	-.0843
.7000	-.0031	-.0584	-.0230	-.0789
.7500	-.0086	-.0525	-.0278	-.0728
.8000	-.0146	-.0468	-.0329	-.0668
.8500	-.0212	-.0434	-.0384	-.0620
.9000	-.0279	-.0424	-.0441	-.0599
.9500	-.0343	-.0435	-.0502	-.0603
1.0000	-.0424	-.0448	-.0582	-.0622

TABLE I.- WING AIRFOIL COORDINATES – Continued

x/c	z_u/c for –	z_l/c for –	z_u/c for –	z_l/c for –
	η = 0.2578; c = 23.995 cm (9.447 in.); x = 0 at fuselage station 57.506 cm (22.64 in.)		η = 0.3111; c = 20.759 cm (8.173 in.); x = 0 at fuselage station 62.205 cm (24.49 in.)	
0	-0.0796	-0.0796	-0.1014	-0.1014
.0025	-.0711	-.0868	-.0941	-.1080
.0050	-.0679	-.0901	-.0909	-.1113
.0100	-.0636	-.0948	-.0870	-.1156
.0150	-.0604	-.0981	-.9841	-.1188
.0250	-.0564	-.1030	-.0793	-.1233
.0500	-.0494	-.1108	-.0719	-.1300
.0750	-.0446	-.1161	-.0668	-.1344
.1000	-.0410	-.1197	-.0629	-.1378
.1500	-.0359	-.1240	-.0572	-.1422
.2000	-.0325	-.1265	-.0535	-.1444
.2500	-.0304	-.1277	-.0512	-.1453
.3000	-.0291	-.1280	-.0496	-.1452
.4000	-.0293	-.1256	-.0493	-.1431
.5000	-.0321	-.1205	-.0511	-.1376
.5500	-.0345	-.1169	-.0525	-.1327
.6000	-.0371	-.1121	-.0540	-.1281
.6500	-.0400	-.1065	-.0561	-.1216
.7000	-.0431	-.0998	-.0581	-.1137
.7500	-.0464	-.0922	-.0607	-.1050
.8000	-.0503	-.0849	-.0639	-.0967
.8500	-.0545	-.0793	-.0675	-.0906
.9000	-.0595	-.0766	-.0721	-.0879
.9500	-.0659	-.0774	-.0782	-.0896
1.0000	-.0751	-.0798	-.0879	-.0925

TABLE I.- WING AIRFOIL COORDINATES – Continued

x/c	z_u/c for –	z_l/c for –	z_u/c for –	z_l/c for –
	η = 0.3516; c = 19.342 cm (7.615 in.); x = 0 at fuselage station 64.948 cm (25.57 in.)		η = 0.3864; c = 18.514 cm (7.289 in.); x = 0 at fuselage station 66.929 cm (26.35 in.)	
0	-0.1144	-0.1144	-0.1237	-0.1237
.0025	-.1075	-.1216	-.1155	-.1320
.0050	-.1042	-.1248	-.1125	-.1353
.0100	-.0999	-.1289	-.1085	-.1392
.0150	-.0970	-.1318	-.1057	-.1418
.0250	-.0926	-.1356	-.1017	-.1455
.0500	-.0856	-.1418	-.0950	-.1511
.0750	-.0804	-.1462	-.0904	-.1552
.1000	-.0766	-.1495	-.0870	-.1580
.1500	-.0712	-.1534	-.0815	-.1616
.2000	-.0675	-.1552	-.0777	-.1632
.2500	-.0649	-.1559	-.0751	-.1639
.3000	-.0635	-.1558	-.0733	-.1635
.4000	-.0624	-.1532	-.0715	-.1607
.5000	-.0629	-.1475	-.0713	-.1551
.5500	-.0637	-.1425	-.0716	-.1509
.6000	-.0646	-.1379	-.0721	-.1455
.6500	-.0658	-.1307	-.0729	-.1387
.7000	-.0677	-.1225	-.0741	-.1301
.7500	-.0696	-.1131	-.0761	-.1206
.8000	-.0725	-.1043	-.0785	-.1111
.8500	-.0759	-.0977	-.0817	-.1046
.9000	-.0805	-.0949	-.0858	-.1010
.9500	-.0867	-.0971	-.0917	-.1025
1.0000	-.0967	-.1018	-.1007	-.1105

TABLE I.- WING AIRFOIL COORDINATES – Continued

x/c	z_u/c for –	z_l/c for –	z_u/c for –	z_l/c for –
	η = 0.4251; c = 17.910 cm (7.051 in.); x = 0 at fuselage station 69.113 cm (27.21 in.)		η = 0.4638; c = 17.308 cm (6.814 in.); x = 0 at fuselage station 71.272 cm (28.06 in.)	
0	-0.1319	-0.1319	-0.1404	-0.1404
.0025	-.1239	-.1402	-.1325	-.1487
.0050	-.1208	-.1433	-.1295	-.1517
.0100	-.1167	-.1471	-.1255	-.1554
.0150	-.1140	-.1498	-.1228	-.1581
.0250	-.1100	-.1536	-.1188	-.1618
.0500	-.1036	-.1591	-.1124	-.1673
.0750	-.0990	-.1628	-.1079	-.1709
.1000	-.0957	-.1655	-.1048	-.1734
.1500	-.0910	-.1685	-.1004	-.1764
.2000	-.0874	-.1702	-.0971	-.1776
.2500	-.0849	-.1703	-.0939	-.1779
.3000	-.0825	-.1700	-.0912	-.1771
.4000	-.0799	-.1669	-.0884	-.1736
.5000	-.0788	-.1612	-.0864	-.1678
.5500	-.0788	-.1572	-.0862	-.1636
.6000	-.0791	-.1515	-.0860	-.1579
.6500	-.0794	-.1444	-.0863	-.1506
.7000	-.0806	-.1356	-.0873	-.1417
.7500	-.0823	-.1259	-.0886	-.1318
.8000	-.0843	-.1165	-.0902	-.1223
.8500	-.0872	-.1097	-.0930	-.1153
.9000	-.0913	-.1064	-.0972	-.1121
.9500	-.0971	-.1079	-.1030	-.1139
1.0000	-.1063	-.1161	-.1122	-.1221

TABLE I.- WING AIRFOIL COORDINATES – Continued

x/c	z_u/c for –	z_l/c for –	z_u/c for –	z_l/c for –
	η = 0.5024; c = 16.703 cm (6.576 in.); x = 0 at fuselage station 73.431 cm (28.91 in.)		η = 0.5411; c = 16.096 cm (6.337 in.); x = 0 at fuselage station 75.565 cm (29.75 in.)	
0	-0.1495	-0.1495	-0.1597	-0.1597
.0025	-.1417	-.1576	-.1518	-.1676
.0050	-.1388	-.1608	-.1488	-.1705
.0100	-.1350	-.1645	-.1451	-.1743
.0150	-.1324	-.1671	-.1426	-.1768
.0250	-.1285	-.1708	-.1385	-.1803
.0500	-.1221	-.1760	-.1321	-.1854
.0750	-.1177	-.1797	-.1278	-.1888
.1000	-.1145	-.1820	-.1244	-.1909
.1500	-.1100	-.1850	-.1194	-.1937
.2000	-.1066	-.1856	-.1155	-.1941
.2500	-.1031	-.1855	-.1121	-.1937
.3000	-.1000	-.1846	-.1096	-.1927
.4000	-.0967	-.1810	-.1056	-.1889
.5000	-.0943	-.1748	-.1027	-.1823
.5500	-.0939	-.1707	-.1021	-.1785
.6000	-.0936	-.1652	-.1017	-.1738
.6500	-.0934	-.1572	-.1010	-.1644
.7000	-.0940	-.1478	-.1012	-.1545
.7500	-.0951	-.1382	-.1023	-.1455
.8000	-.0969	-.1291	-.1037	-.1359
.8500	-.0995	-.1216	-.1064	-.1288
.9000	-.1034	-.1186	-.1100	-.1252
.9500	-.1093	-.1203	-.1160	-.1271
1.0000	-.1186	-.1287	-.1255	-.1355

TABLE I.- WING AIRFOIL COORDINATES – Continued

x/c	z_u/c for –	z_l/c for –	z_u/c for –	z_l/c for –
	η = 0.5797; c = 15.623 cm (6.151 in.); x = 0 at fuselage station 77.724 cm (30.60 in.)		η = 0.6184; c = 15.091 cm (5.913 in.); x = 0 at fuselage station 79.883 cm (31.45 in.)	
0	-0.1689	-0.1689	-0.1801	-0.1801
.0025	-.1613	-.1768	-.1725	-.1878
.0050	-.1584	-.1797	-.1696	-.1906
.0100	-.1548	-.1834	-.1661	-.1942
.0150	-.1521	-.1857	-.1634	-.1965
.0250	-.1482	-.1890	-.1595	-.1997
.0500	-.1418	-.1941	-.1530	-.2049
.0750	-.1373	-.1970	-.1484	-.2074
.1000	-.1339	-.1991	-.1449	-.2092
.1500	-.1284	-.2010	-.1392	-.2108
.2000	-.1244	-.2014	-.1352	-.2112
.2500	-.1211	-.2008	-.1317	-.2103
.3000	-.1184	-.1996	-.1288	-.2088
.4000	-.1139	-.1954	-.1238	-.2043
.5000	-.1106	-.1885	-.1203	-.1973
.5500	-.1097	-.1839	-.1190	-.1925
.6000	-.1089	-.1776	-.1180	-.1861
.6500	-.1084	-.1699	-.1173	-.1783
.7000	-.1084	-.1605	-.1170	-.1688
.7500	-.1089	-.1502	-.1174	-.1583
.8000	-.1106	-.1411	-.1187	-.1491
.8500	-.1132	-.1342	-.1213	-.1422
.9000	-.1174	-.1317	-.1252	-.1396
.9500	-.1238	-.1344	-.1315	-.1421
1.0000	-.1342	-.1442	-.1418	-.1521

TABLE I.- WING AIRFOIL COORDINATES – Continued

x/c	z_u/c for –	z_l/c for –	z_u/c for –	z_l/c for –
	η = 0.6570; c = 14.343 cm (5.674 in.); x = 0 at fuselage station 82.042 cm (32.30 in.)		η = 0.6916; c = 13.807 cm (5.436 in.); x = 0 at fuselage station 83.972 cm (33.06 in.)	
0	-0.1919	-0.1919	-0.2046	-0.2046
.0025	-.1843	-.1995	-.1972	-.2112
.0500	-.1815	-.2023	-.1945	-.2150
.0100	-.1782	-.2060	-.1910	-.2185
.0150	-.1755	-.2084	-.1883	-.2208
.0250	-.1715	-.2113	-.1842	-.2238
.0500	-.1649	-.2162	-.1776	-.2282
.0750	-.1603	-.2186	-.1730	-.2306
.1000	-.1567	-.2201	-.1695	-.2319
.1500	-.1511	-.2215	-.1636	-.2330
.2000	-.1466	-.2213	-.1590	-.2328
.2500	-.1431	-.2204	-.1553	-.2314
.3000	-.1401	-.2188	-.1520	-.2295
.4000	-.1349	-.2141	-.1466	-.2246
.5000	-.1307	-.2066	-.1419	-.2168
.5500	-.1290	-.2016	-.1400	-.2117
.6000	-.1279	-.1953	-.1385	-.2052
.6500	-.1270	-.1875	-.1376	-.1972
.7000	-.1263	-.1775	-.1367	-.1874
.7500	-.1267	-.1673	-.1365	-.1769
.8000	-.1278	-.1581	-.1375	-.1678
.8500	-.1299	-.1510	-.1396	-.1610
.9000	-.1339	-.1484	-.1434	-.1580
.9500	-.1402	-.1510	-.1496	-.1605
1.0000	-.1501	-.1608	-.1607	-.1704

TABLE I.-WING AIRFOIL COORDINATED – Continued

x/c	z_u/c for –	z_l/c for –	z_u/c for –	z_l/c for –
	η = 0.7343; c = 13.200 cm (5.197 in.); x = 0 at fuselage station 86.36 cm (34.00 in.)		η = 0.7729; c = 12.593 cm (4.958 in.); x = 0 at fuselage station 88.519 cm (34.85 in.)	
0	-0.2182	-0.2182	-0.2328	-0.2328
.0025	-.2109	-.2255	-.2256	-.2400
.0050	-.2083	-.2285	-.2228	-.2427
.0100	-.2047	-.2317	-.2191	-.2460
.0150	-.2021	-.2340	-.2167	-.2484
.0250	-.1980	-.2372	-.2126	-.2513
.0500	-.1911	-.2410	-.2062	-.2552
.0750	-.1867	-.2432	-.2015	-.2571
.1000	-.1831	-.2445	-.1977	-.2512
.1500	-.1770	-.2455	-.1913	-.2589
.2000	-.1722	-.2450	-.1869	-.2585
.2500	-.1683	-.2434	-.1813	-.2559
.3000	-.1649	-.2414	-.1780	-.2540
.4000	-.1591	-.2361	-.1726	-.2485
.5000	-.1540	-.2281	-.1674	-.2405
.5500	-.1520	-.2228	-.1652	-.2350
.6000	-.1503	-.2161	-.1632	-.2281
.6500	-.1491	-.2080	-.1616	-.2200
.7000	-.1481	-.1983	-.1605	-.2102
.7500	-.1477	-.1879	-.1600	-.1998
.8000	-.1483	-.1785	-.1602	-.1903
.8500	-.1501	-.1717	-.1621	-.1836
.9000	-.1538	-.1687	-.1655	-.1806
.9500	-.1602	-.1712	-.1718	-.1828
1.0000	-.1714	-.1807	-.1825	-.1922

TABLE I.- WING AIRFOIL COORDINATES – Continued

x/c	z_u/c for –	z_l/c for –	z_u/c for –	z_l/c for –
	η = 0.8116; c = 11.989 cm (4.720 in.); x = 0 at fuselage station 90.678 cm (35.70 in.)		η = 0.8502; c = 11.382 cm (4.481 in.); x = 0 at fuselage station 92.812 cm (36.54 in.)	
0	-0.2483	-0.2483	-0.2653	-0.2653
.0025	-.2411	-.2555	-.2583	-.2724
.0050	-.2385	-.2581	-.2557	-.2750
.0100	-.2349	-.2613	-.2524	-.2782
.0150	-.2324	-.2637	-.2499	-.2804
.0250	-.2285	-.2664	-.2458	-.2831
.0500	-.2221	-.2703	-.2392	-.2866
.0750	-.2173	-.2721	-.2345	-.2886
.1000	-.2134	-.2731	-.2307	-.2897
.1500	-.2070	-.2735	-.2245	-.2901
.2000	-.2022	-.2728	-.2194	-.2890
.2500	-.1978	-.2709	-.2148	-.2868
.3000	-.1941	-.2686	-.2110	-.2844
.4000	-.1876	-.2624	-.2041	-.2779
.5000	-.1820	-.2544	-.1990	-.2687
.5500	-.1797	-.2482	-.1957	-.2631
.6000	-.1773	-.2413	-.1932	-.2562
.6500	-.1757	-.2332	-.1913	-.2478
.7000	-.1744	-.2234	-.1899	-.2381
.7500	-.1737	-.2132	-.1888	-.2281
.8000	-.1738	-.2037	-.1886	-.2185
.8500	-.1753	-.1968	-.1899	-.2114
.9000	-.1785	-.1936	-.1928	-.2081
.9500	-.1845	-.1956	-.1986	-.2098
1.0000	-.1961	-.2047	-.2088	-.2187

TABLE I.- WING AIRFOIL COORDINATES – Concluded

x/c	z_u/c for –	z_l/c for –	z_u/c for –	z_l/c for –
	η = 0.9352; c = 10.051 cm (3.957 in.); x = 0 at fuselage station 97.561 cm (38.41 in.)		η = 0.9676; c = 9.492 cm (3.737 in.); x = 0 at fuselage station 99.416 cm (39.14 in.)	
0	-0.3088	-0.3088	-0.3302	-0.3302
.0025	-.3028	-.3153	-.3238	-.3367
.0050	-.3002	-.3180	-.3209	-.3390
.0100	-.2963	-.3213	-.3174	-.3420
.0150	-.2935	-.3231	-.3148	-.3440
.0250	-.2900	-.3256	-.3110	-.3467
.0500	-.2834	-.3297	-.3040	-.3505
.0750	-.2786	-.3320	-.2992	-.3521
.1000	-.2747	-.3328	-.2952	-.3535
.1500	-.2684	-.3326	-.2884	-.3533
.2000	-.2629	-.3310	-.2834	-.3513
.2500	-.2586	-.3287	-.2794	-.3489
.3000	-.2546	-.3257	-.2754	-.3459
.4000	-.2469	-.3181	-.2672	-.3376
.5000	-.2403	-.3081	-.2605	-.3271
.5500	-.2371	-.3022	-.2571	-.3209
.6000	-.2343	-.2954	-.2539	-.3139
.6500	-.2319	-.2867	-.2511	-.3050
.7000	-.2297	-.2767	-.2492	-.2957
.7500	-.2278	-.2670	-.2478	-.2858
.8000	-.2270	-.2577	-.2468	-.2766
.8500	-.2282	-.2500	-.2466	-.2688
.9000	-.2304	-.2457	-.2484	-.2643
.9500	-.2347	-.2469	-.2537	-.2655
1.0000	-.2451	-.2548	-.2636	-.2732

TABLE II.- INBOARD PYLON ORDINATES (NORMAL TO LEADING EDGE)

x, cm	x, in.	y, cm	y, in.	t/c, percent
0	0	0	0	0
.0376	.0148	.0854	.0336	4.48
.0762	.0300	.1168	.0460	6.13
.1138	.0448	.1394	.0549	7.32
.1525	.0600	.1557	.0613	8.18
.1900	.0748	.1708	.0672	8.97
.2276	.0896	.1821	.0717	9.56
.2657	.1046	.1922	.0757	10.09
.3038	.1196	.2022	.0796	10.62
.3425	.1348	.2097	.0826	10.68
.3800	.1496	.2173	.0855	11.41
.5701	.2244	.2437	.0959	12.79
.7567	.2979	.2610	.1028	13.65
.9500	.3740	.2700	.1063	14.18
1.1400	.4488	.2751	.1083	14.44
1.3301	.5236	.2763	.1088	14.51
1.5210	.5985	.2751	.1083	14.44
1.7101	.6733	.2738	.1078	14.37
1.9002	.7481	.2612	.1029	13.72
2.0902	.8229	.2512	.0989	13.19
2.2802	.8977	.2386	.0940	12.53
2.4696	.9723	.2211	.0870	11.60
2.6603	1.0474	.2022	.0796	10.62
2.8502	1.1221	.1809	.0712	9.49
3.0402	1.1969	.1557	.0613	8.18
3.2302	1.2717	.1269	.0499	6.66
3.4203	1.3466	.0980	.0386	5.14
3.6103	1.4214	.0641	.0252	3.36
3.8100	1.5000	.0264	.0104	1.39

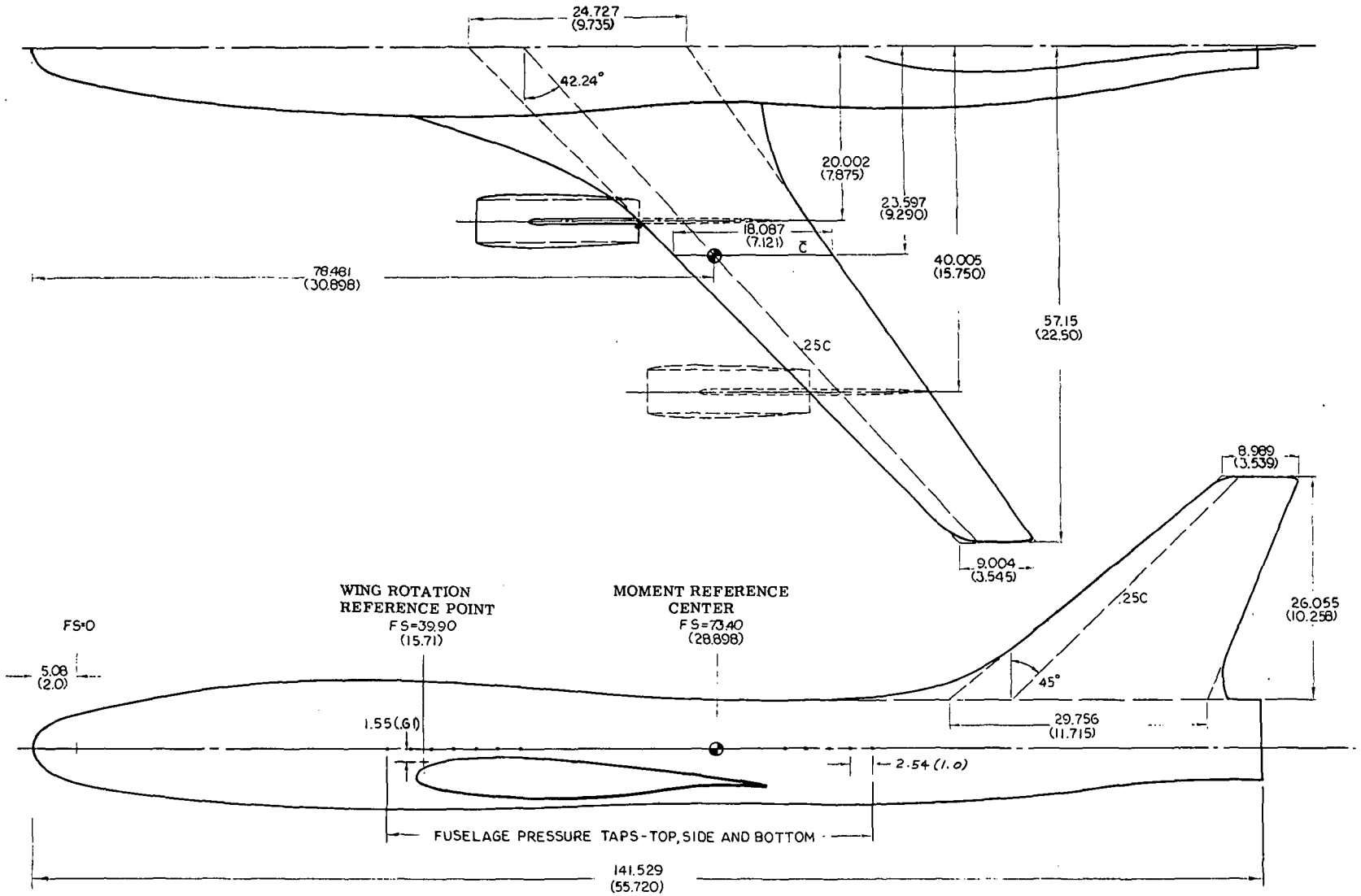

Figure 1.- Pertinent geometric characteristics. Dimensions are in cm (in.).

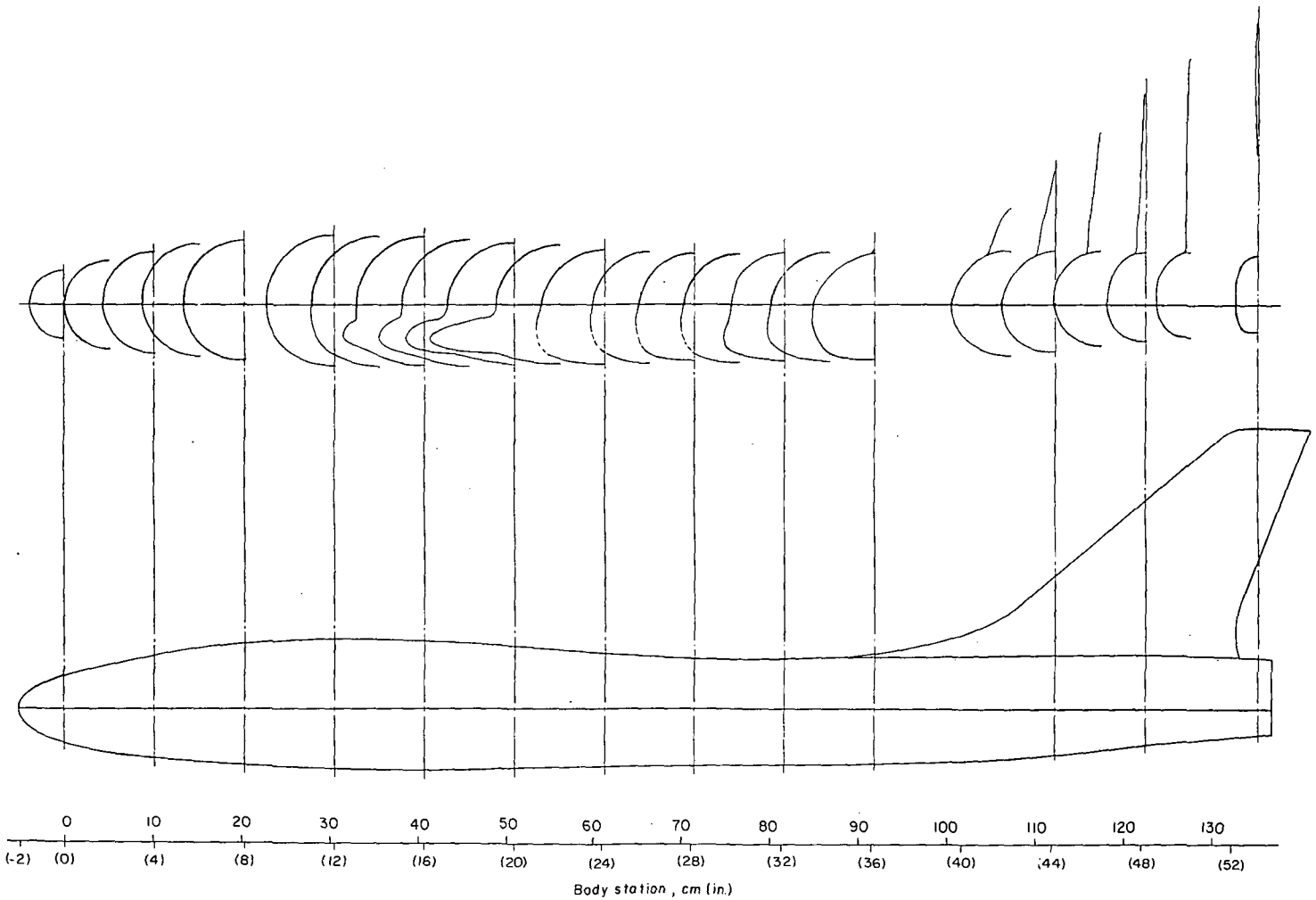

Figure 2.- Typical longitudinal development of fuselage cross sections.

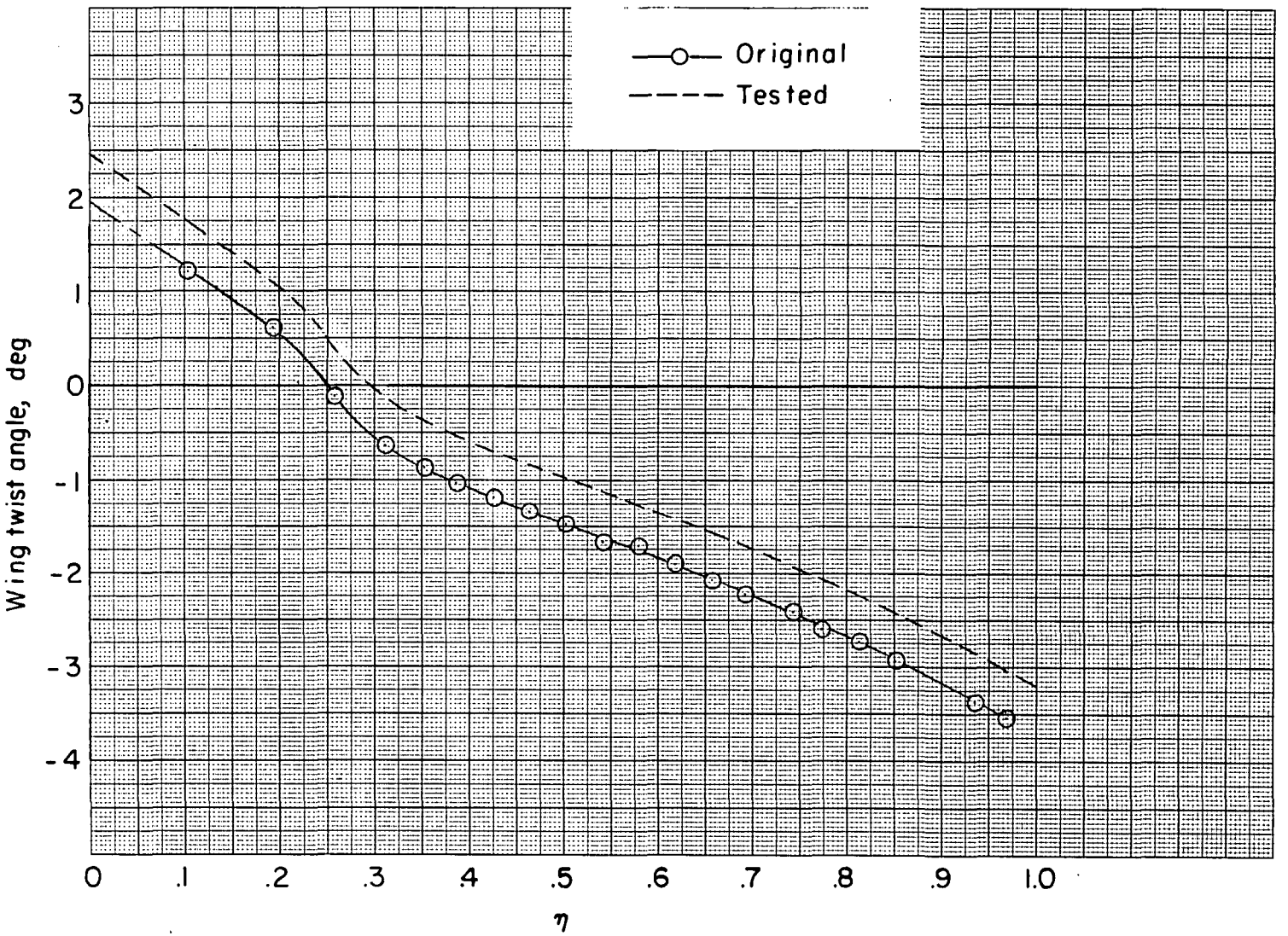

Figure 3.- Measured wing twist distribution.

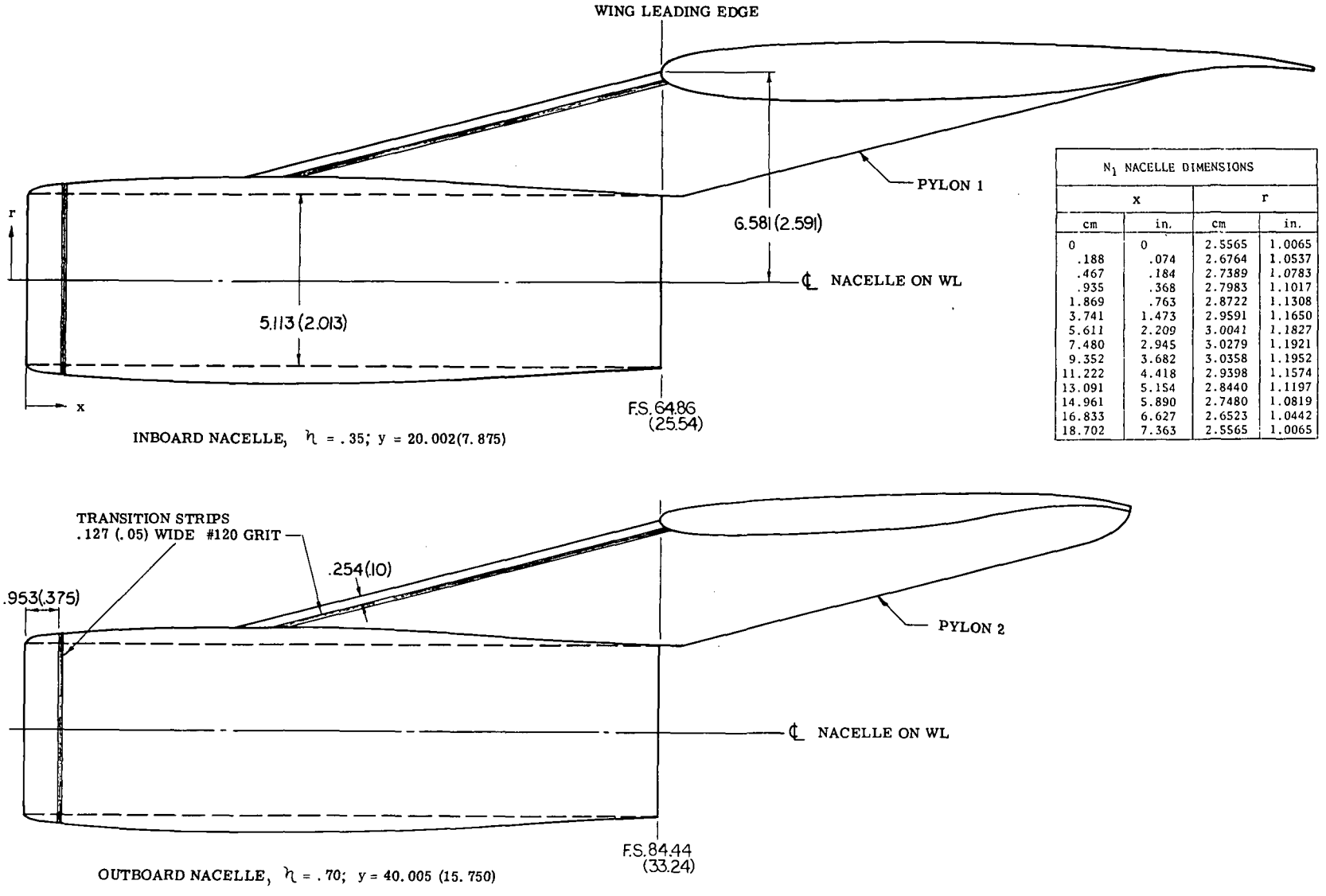

N_1 NACELLE DIMENSIONS			
x		r	
cm	in.	cm	in.
0	0	2.5565	1.0065
.188	.074	2.6764	1.0537
.467	.184	2.7389	1.0783
.935	.368	2.7983	1.1017
1.869	.763	2.8722	1.1308
3.741	1.473	2.9591	1.1650
5.611	2.209	3.0041	1.1827
7.480	2.945	3.0279	1.1921
9.352	3.682	3.0358	1.1952
11.222	4.418	2.9398	1.1574
13.091	5.154	2.8440	1.1197
14.961	5.890	2.7480	1.0819
16.833	6.627	2.6523	1.0442
18.702	7.363	2.5565	1.0065

(a) Basic nacelles and pylons.

Figure 4.- Geometric characteristics. Dimensions are in cm (in.)

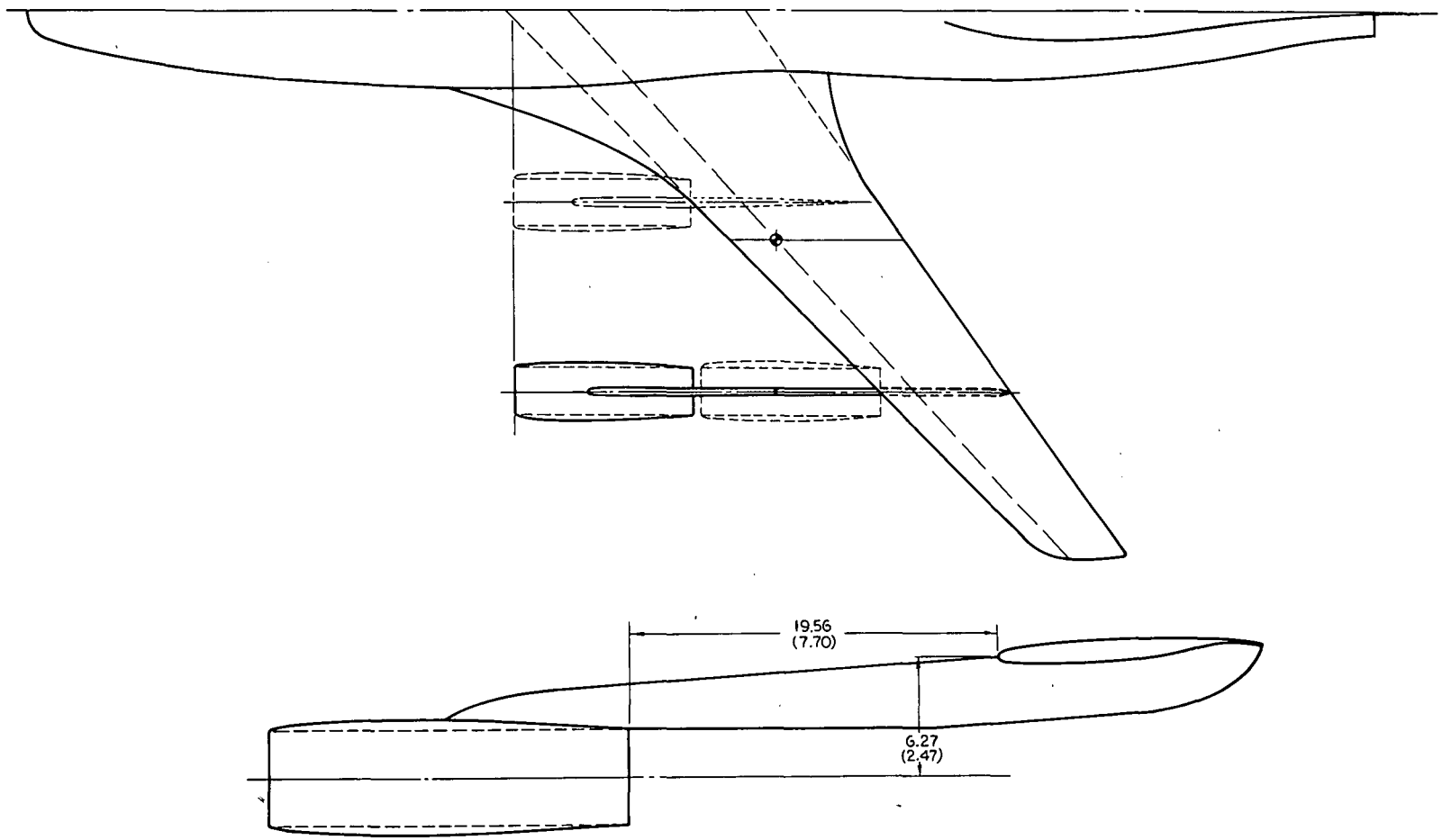

(b) Extended pylon and nacelle configuration.

Figure 4.- Concluded.

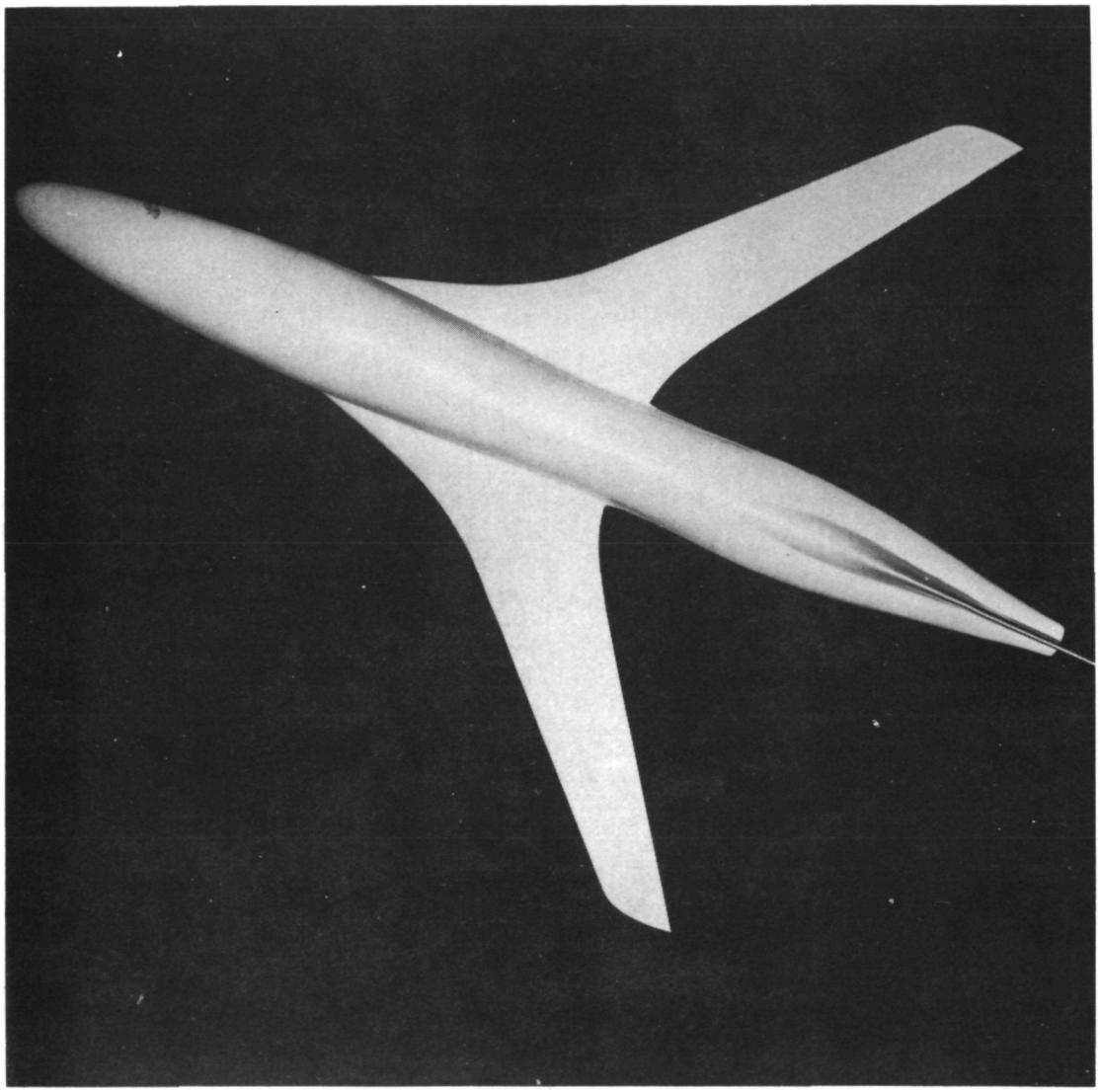

L-73-8022

(a) Planview, configuration B_1.

Figure 5.- Model photographs.

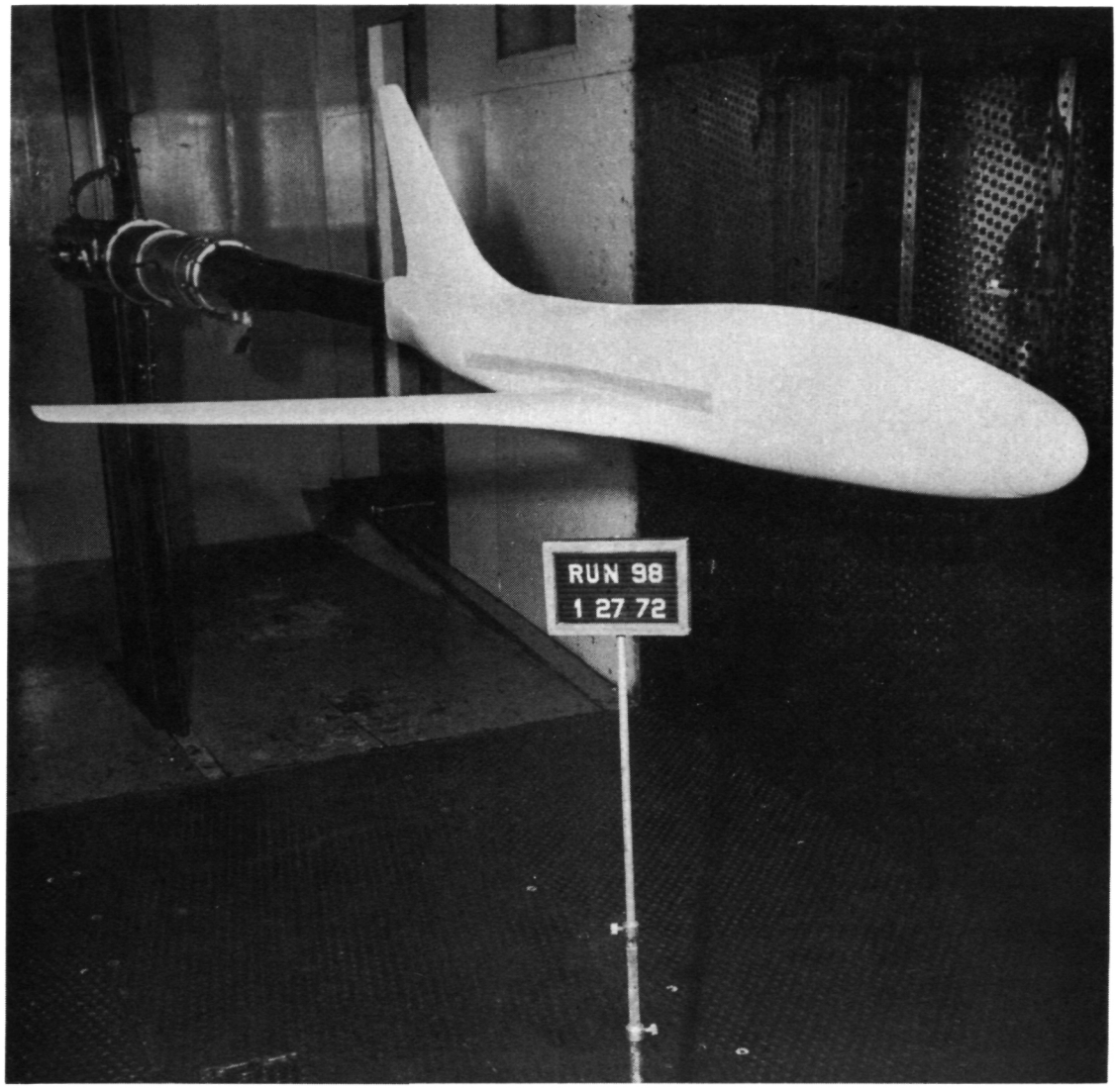

L-73-8023

(b) Front quarter view, configuration B_1.

Figure 5.- Continued.

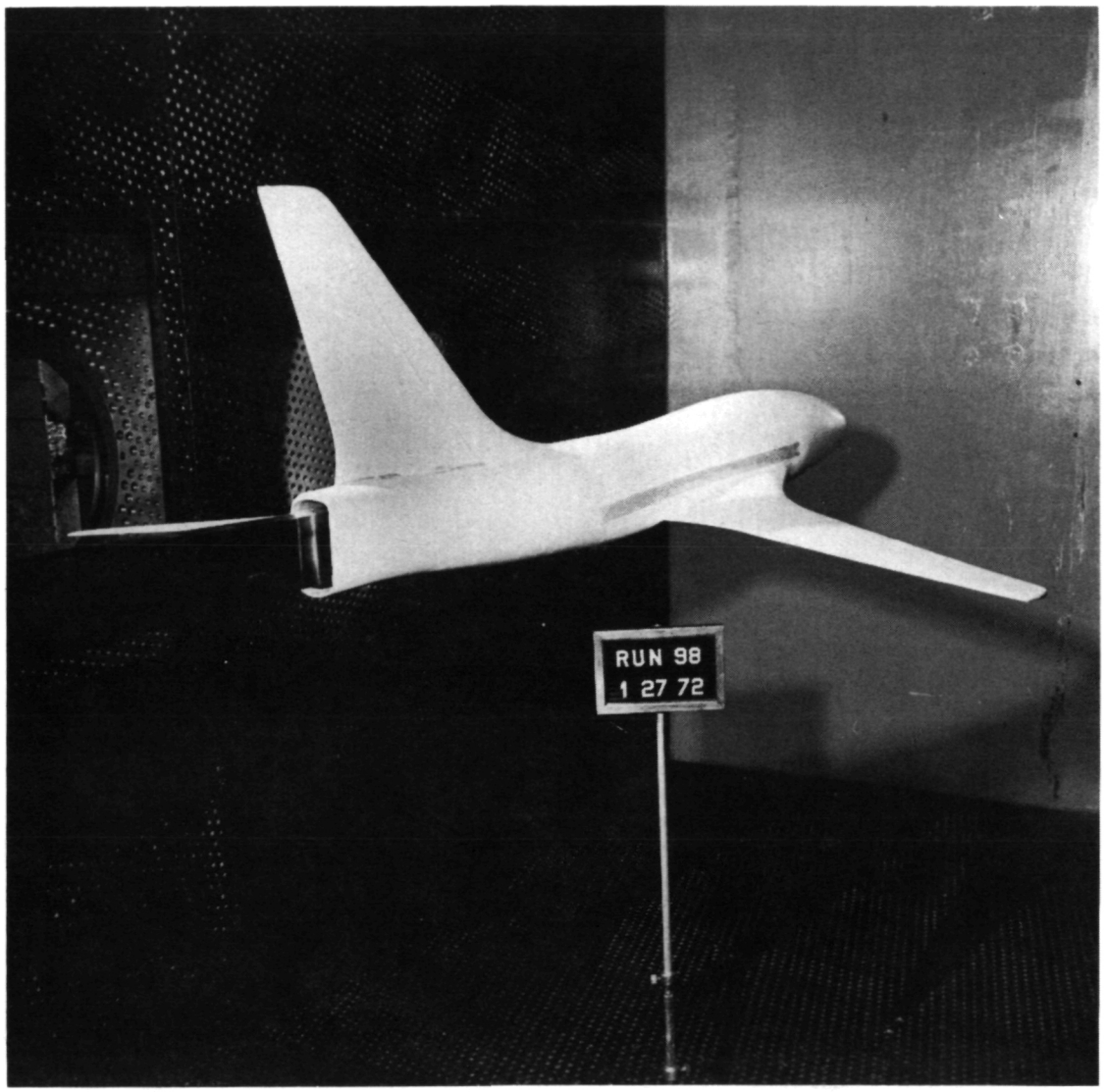

L-73-8024

(c) Rear quarter view, configuration B_1.

Figure 5.- Continued.

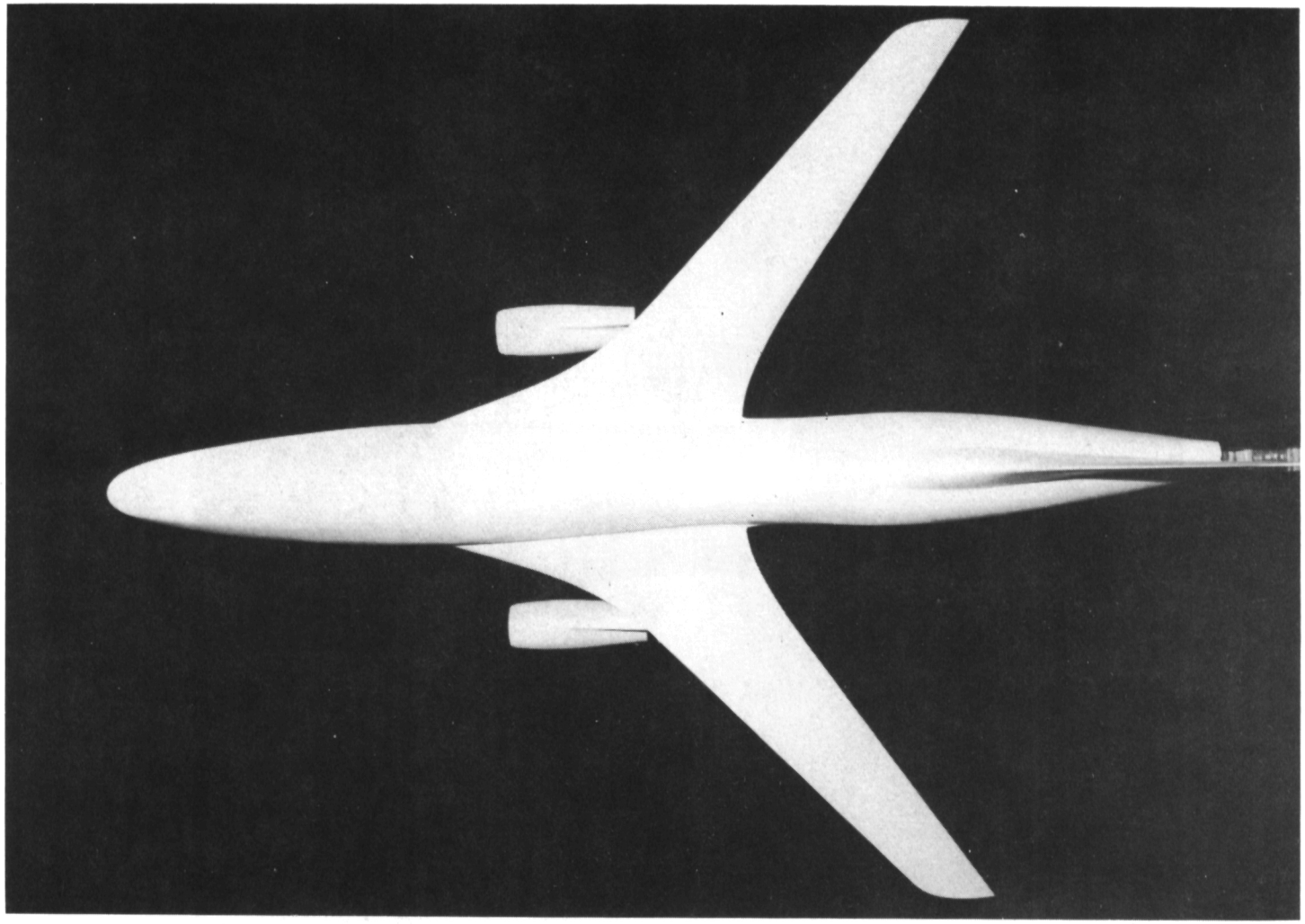

L-73-8025

(d) Planview, nacelles located at 0.35b/2.

Figure 5.- Continued.

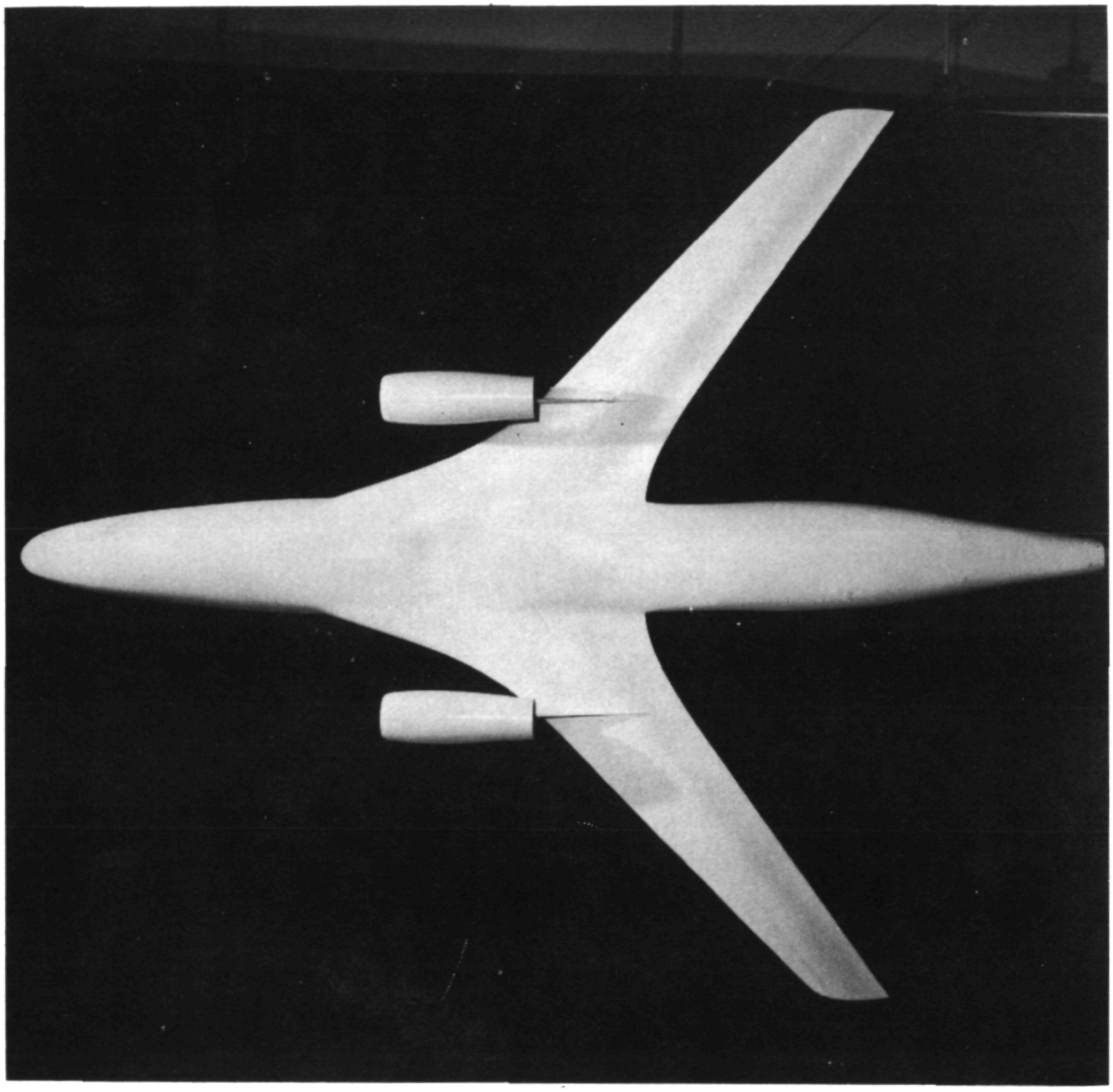

L-73-8026

(e) Bottom view, nacelles located at 0.35b/2.

Figure 5.- Continued.

L-73-8027

(f) B_1 configuration with inboard nacelles, tunnel installation.

Figure 5.- Continued.

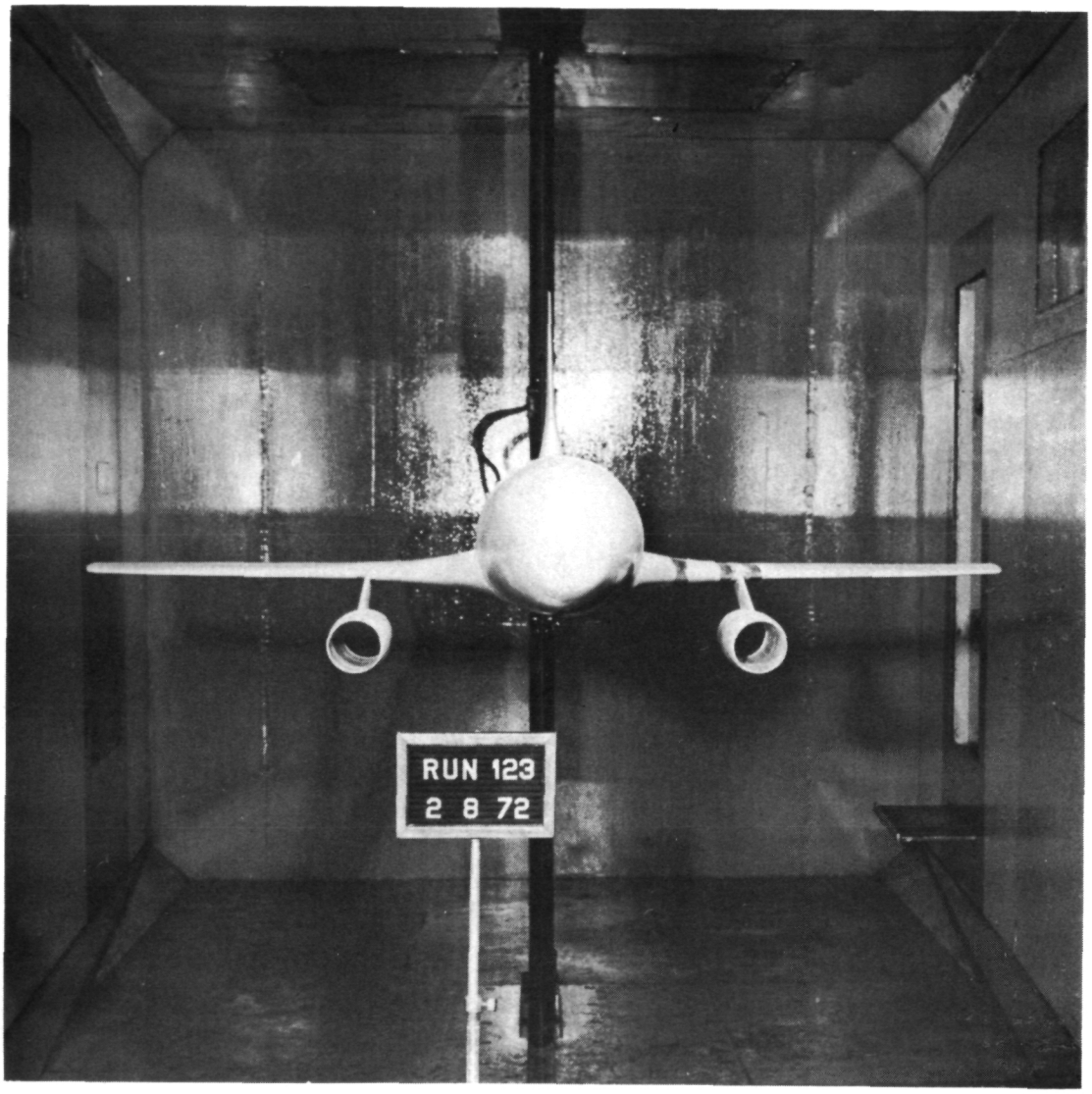

L-73-8028

(g) B_1 configuration with inboard nacelles, tunnel installation.

Figure 5.- Continued.

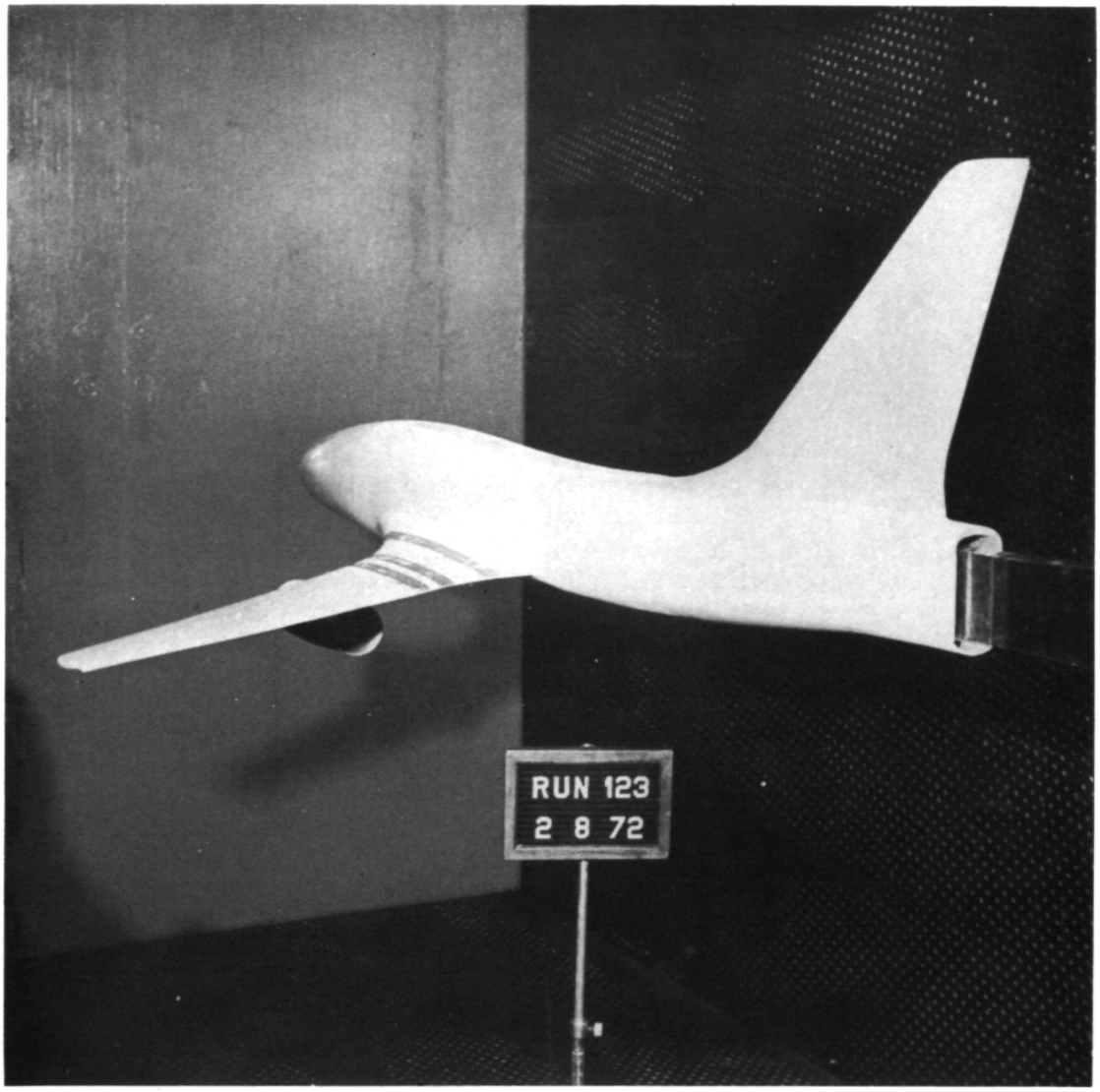

L-73-8029

(h) B_1 configuration with inboard nacelles, tunnel installation.

Figure 5.- Continued.

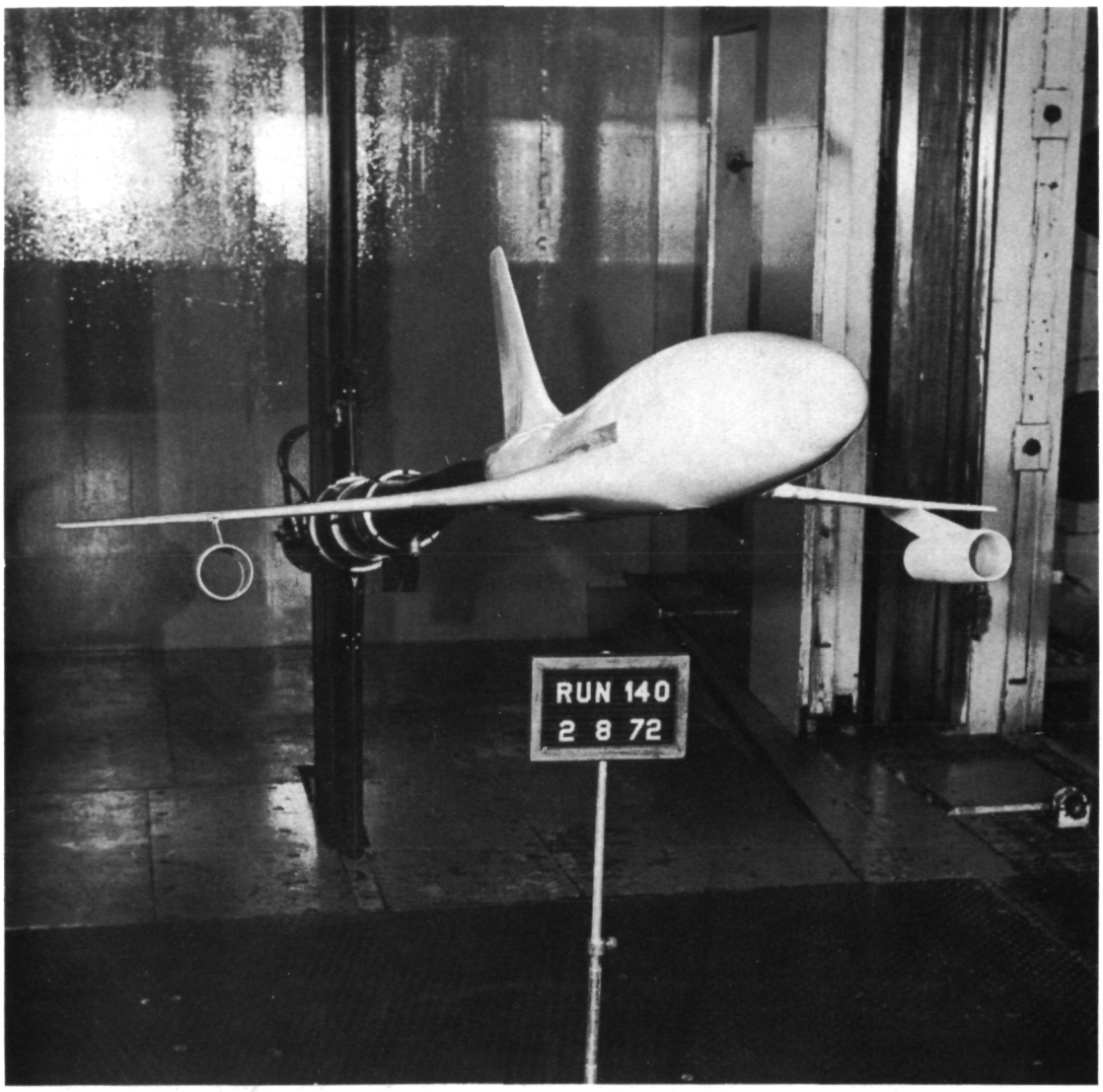

L-73-8030

(i) B_1 configuration with outboard nacelles, tunnel installation.

Figure 5.- Continued.

L-73-8031

(j) Modified B_1 configuration with extended pylons, tunnel installation.

Figure 5.- Continued.

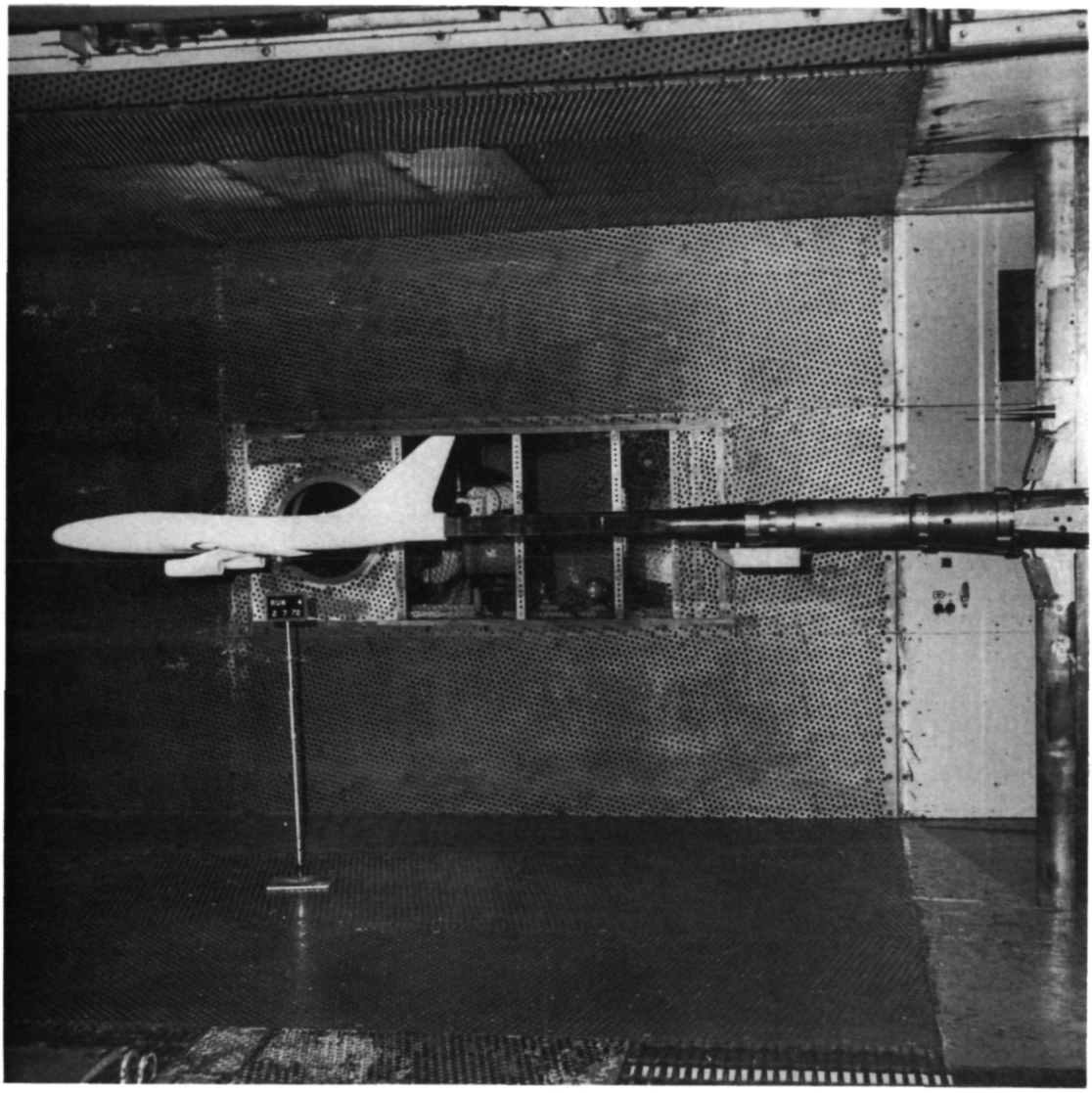

L-73-8032

(k) General tunnel installation.

Figure 5.- Concluded.

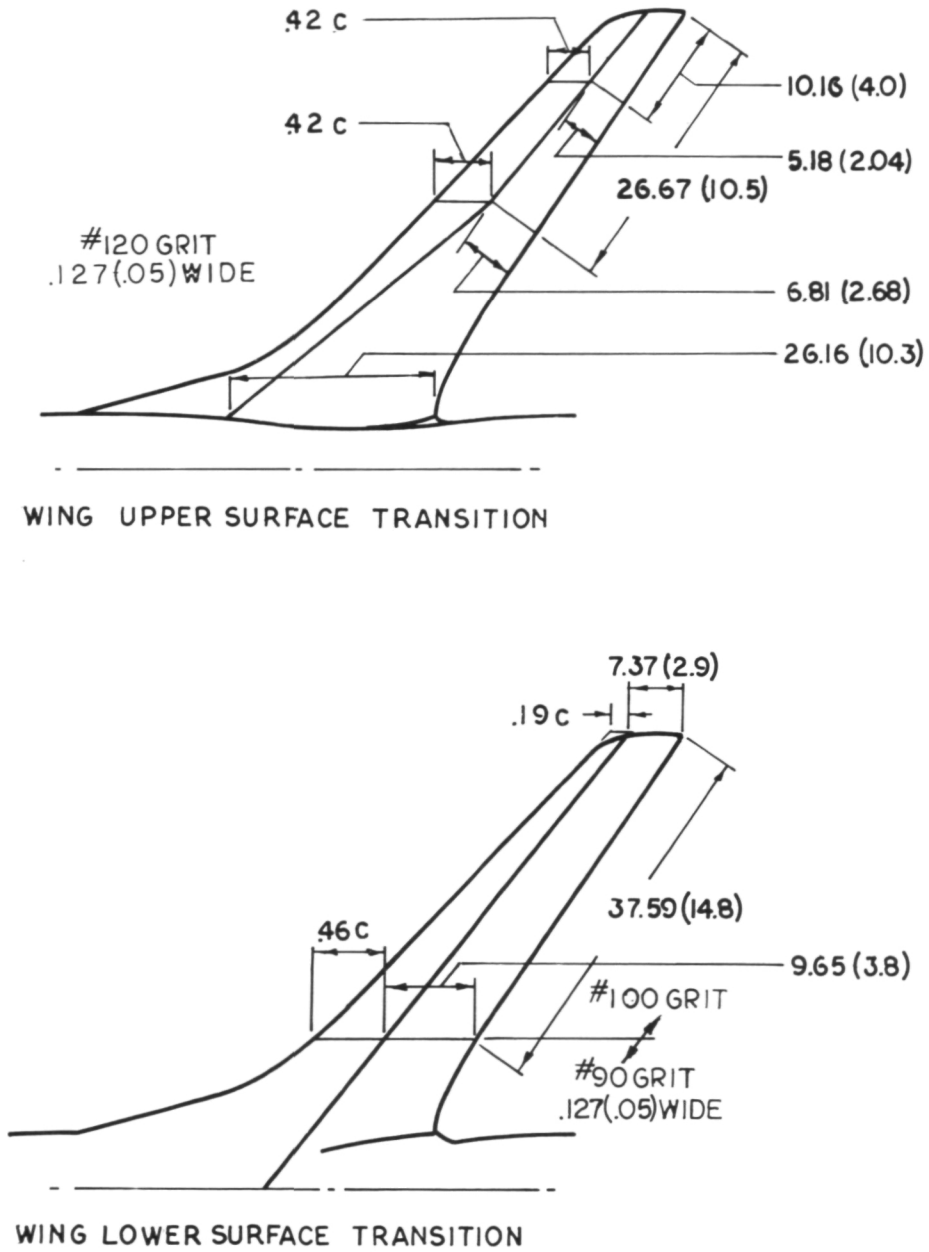

Figure 6.- Boundary-layer transition strip pattern. Dimensions are in cm (in.).

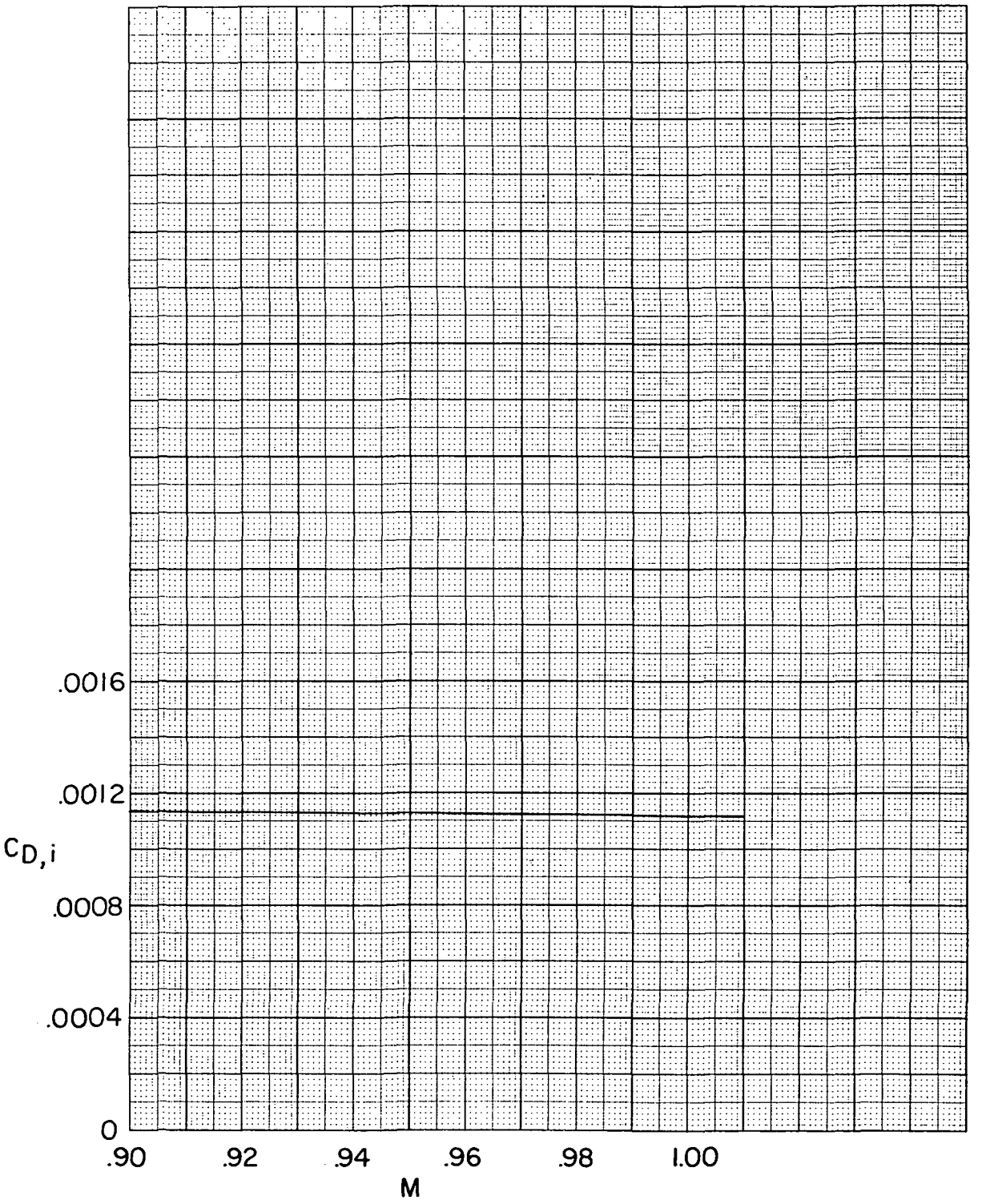

Figure 7.- Internal drag correction based on estimated skin friction. Two nacelles.

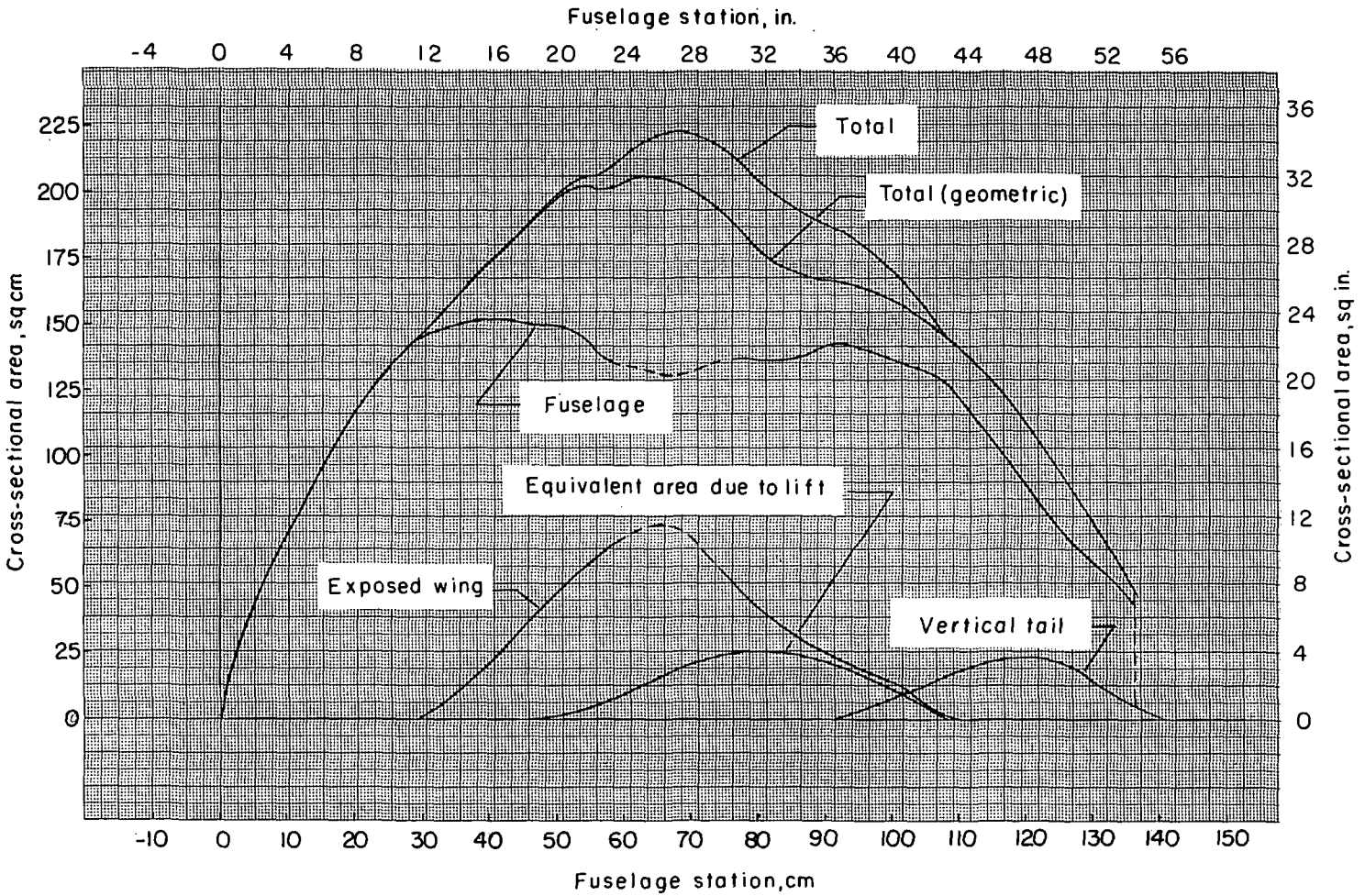

Figure 8.- Cross-sectional area distribution of configuration B.

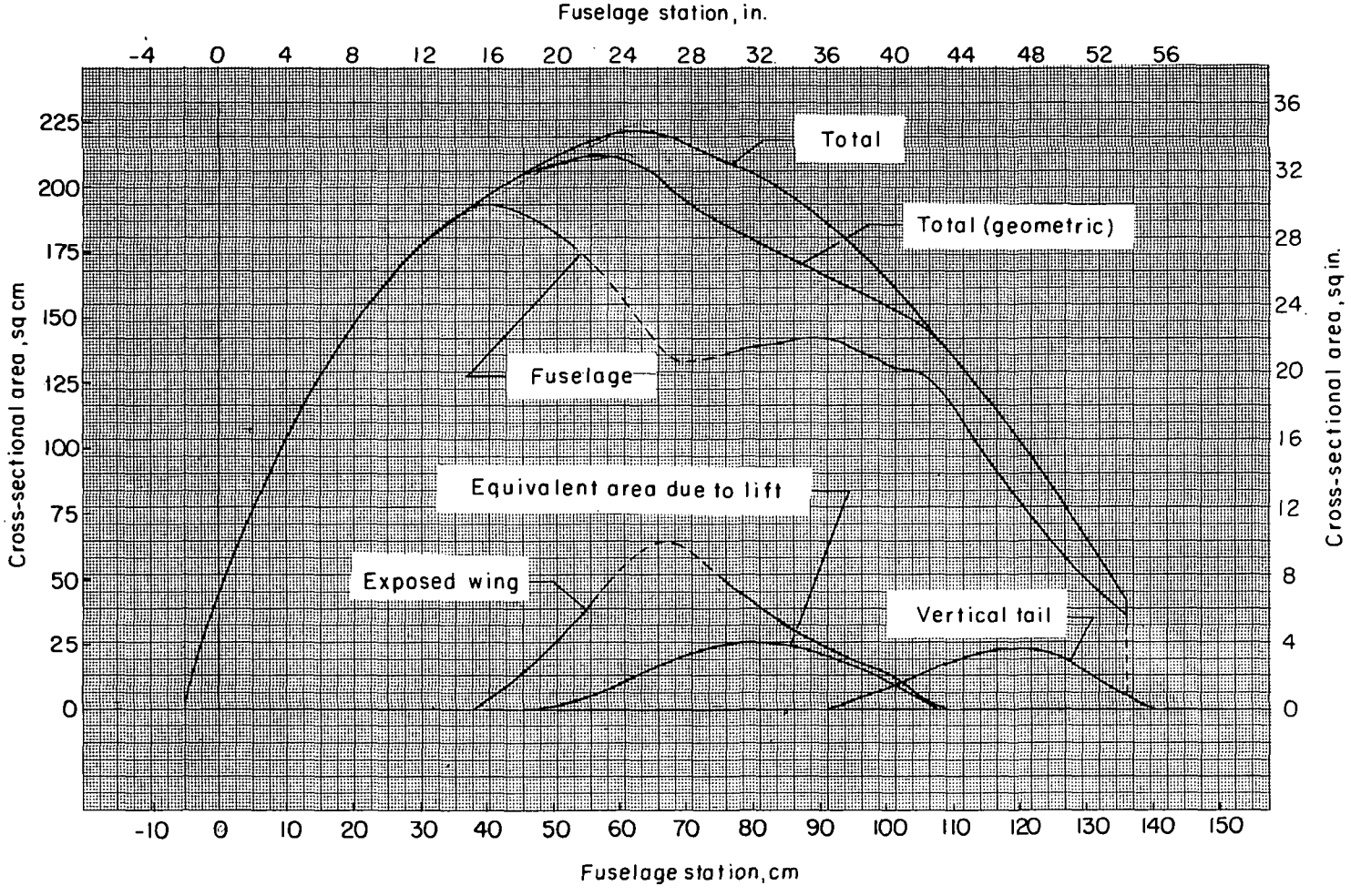

Figure 9.- Cross-sectional area distribution of configuration B_1.

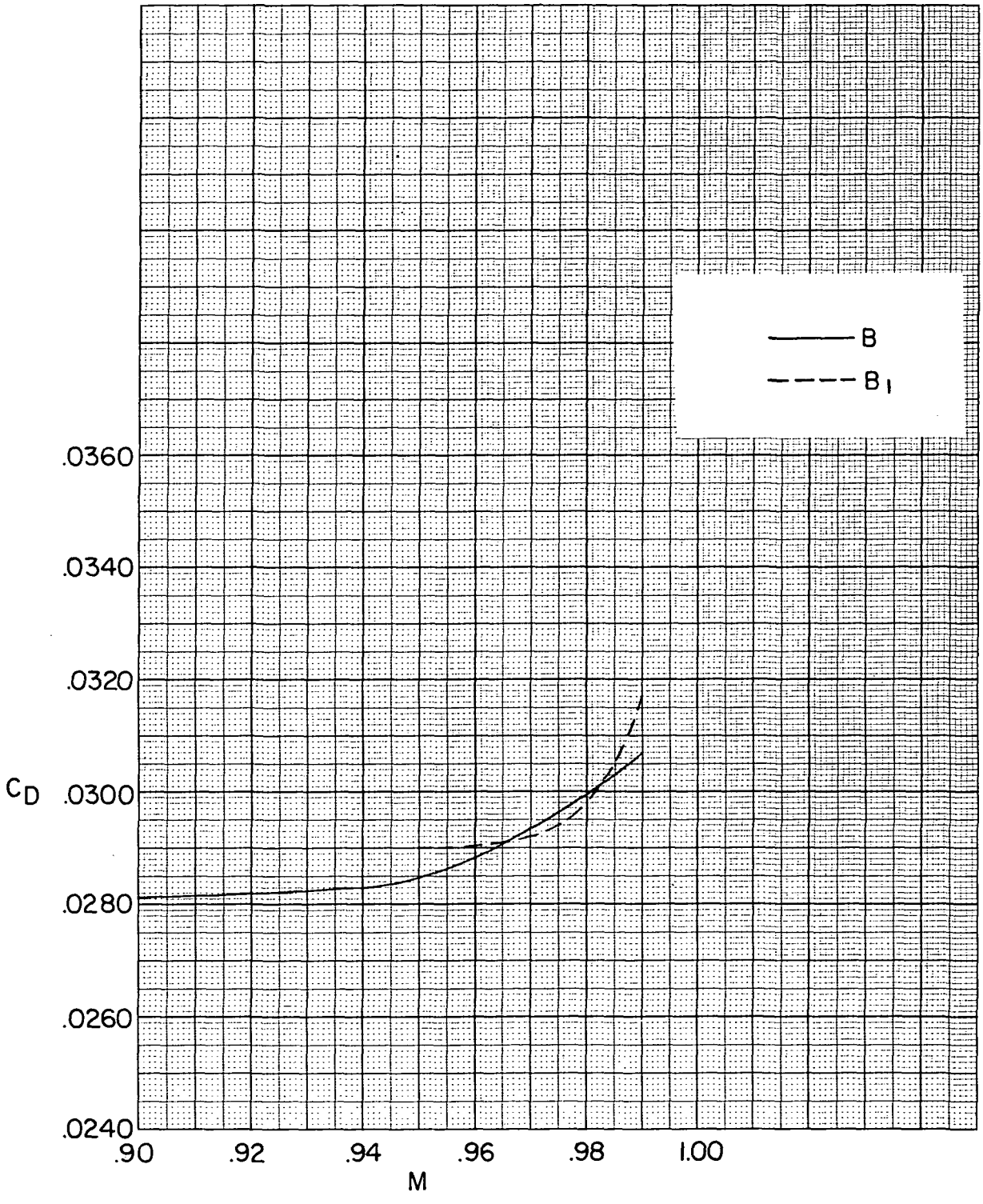

Figure 10.- Comparison of drag rise characteristics for configurations B and B_1, $C_L = 0.40$.

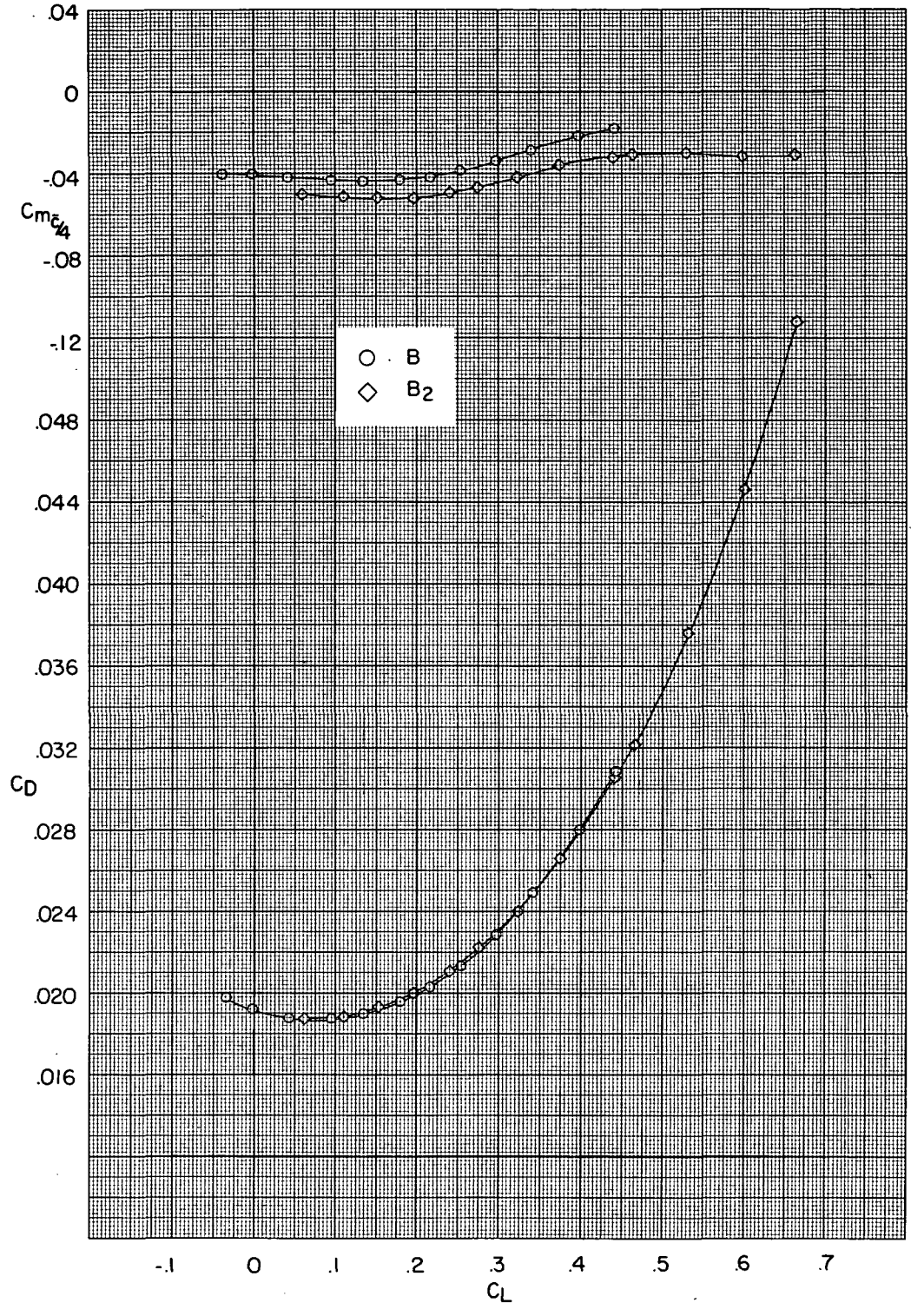

(a) M = 0.90.

Figure 11.- Longitudinal aerodynamic data for configurations B, B_1, and B_2.

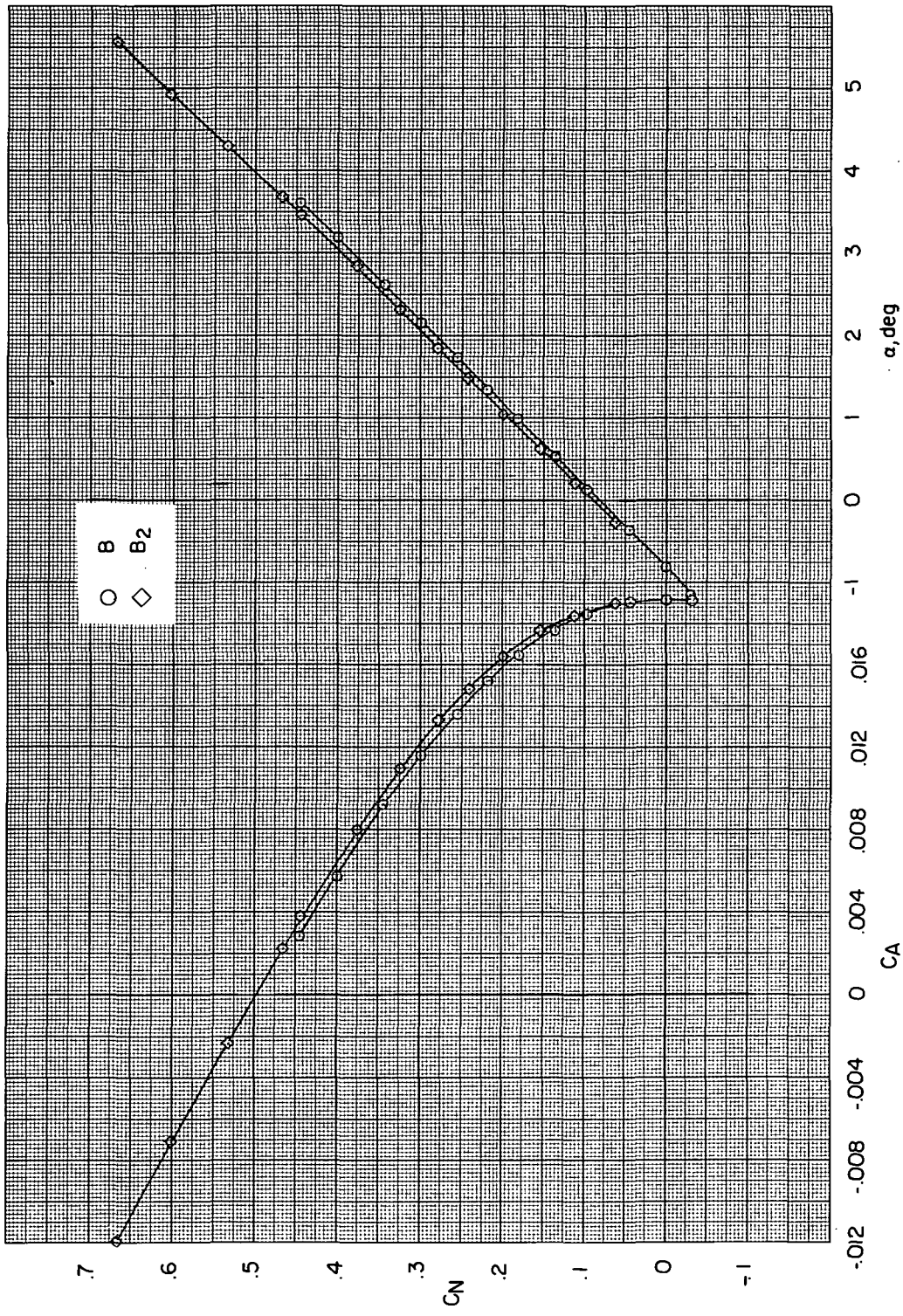

(a) Concluded.

Figure 11.- Continued.

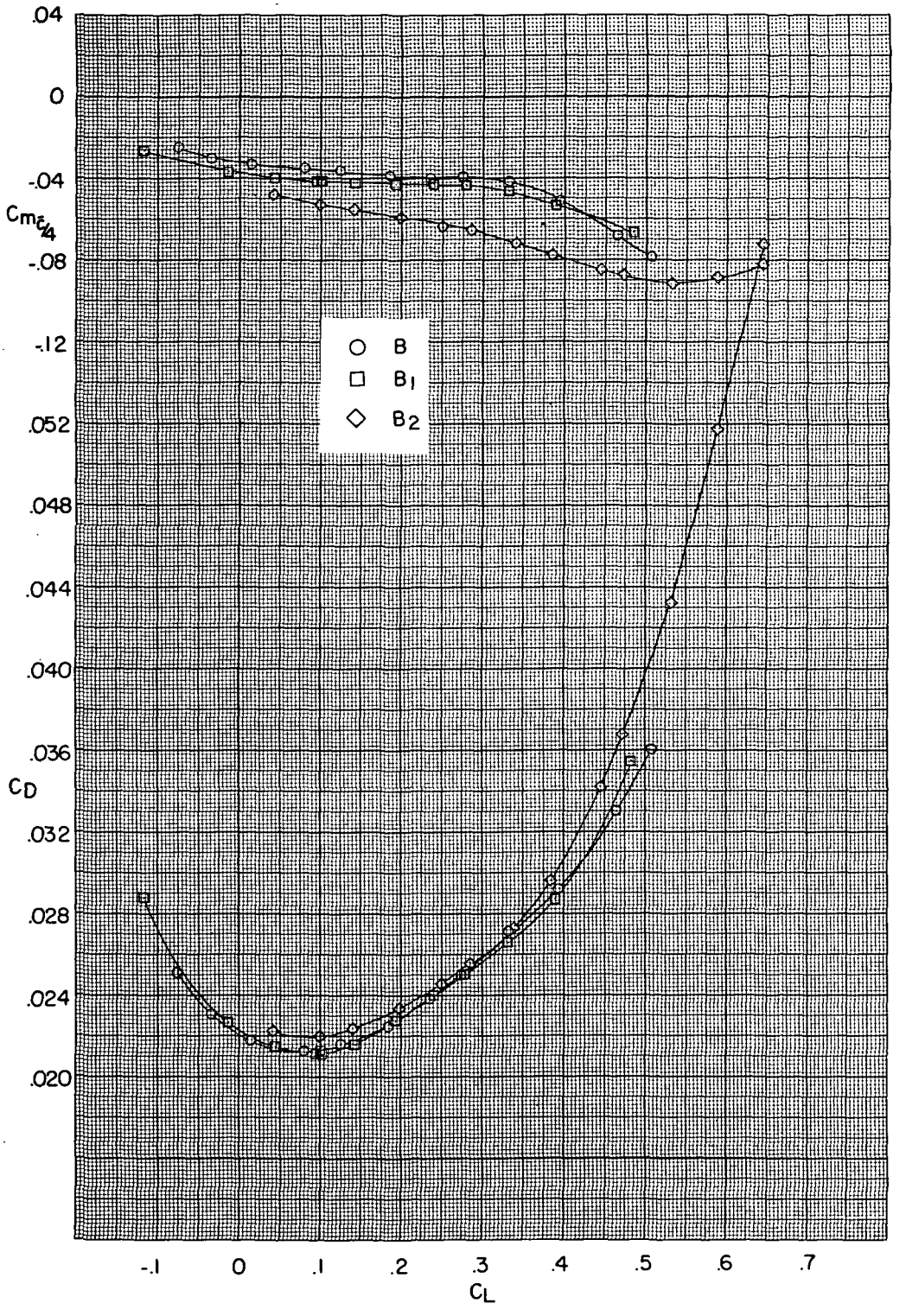

(b) M = 0.95.

Figure 11.- Continued.

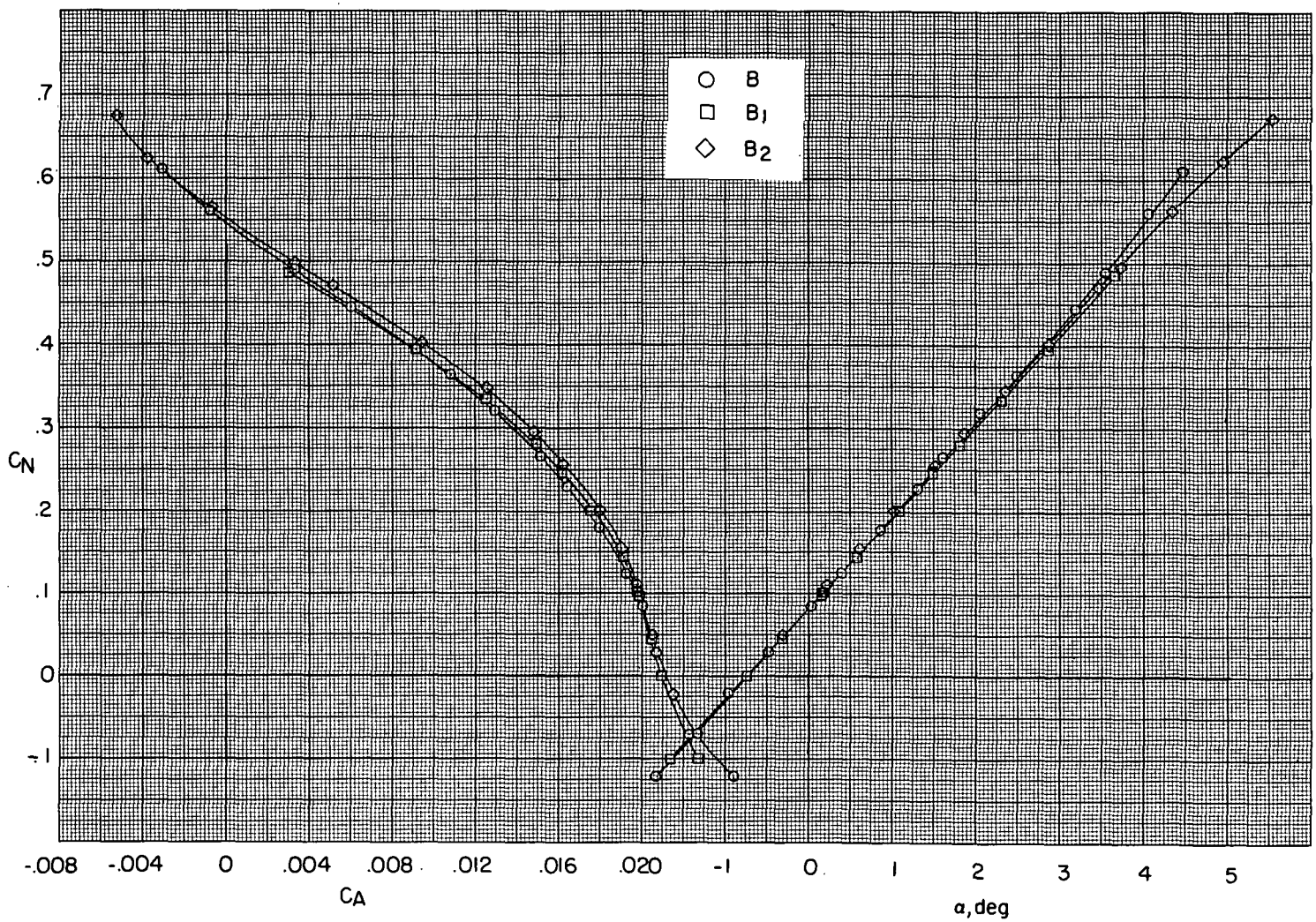

(b) Concluded.

Figure 11.- Continued.

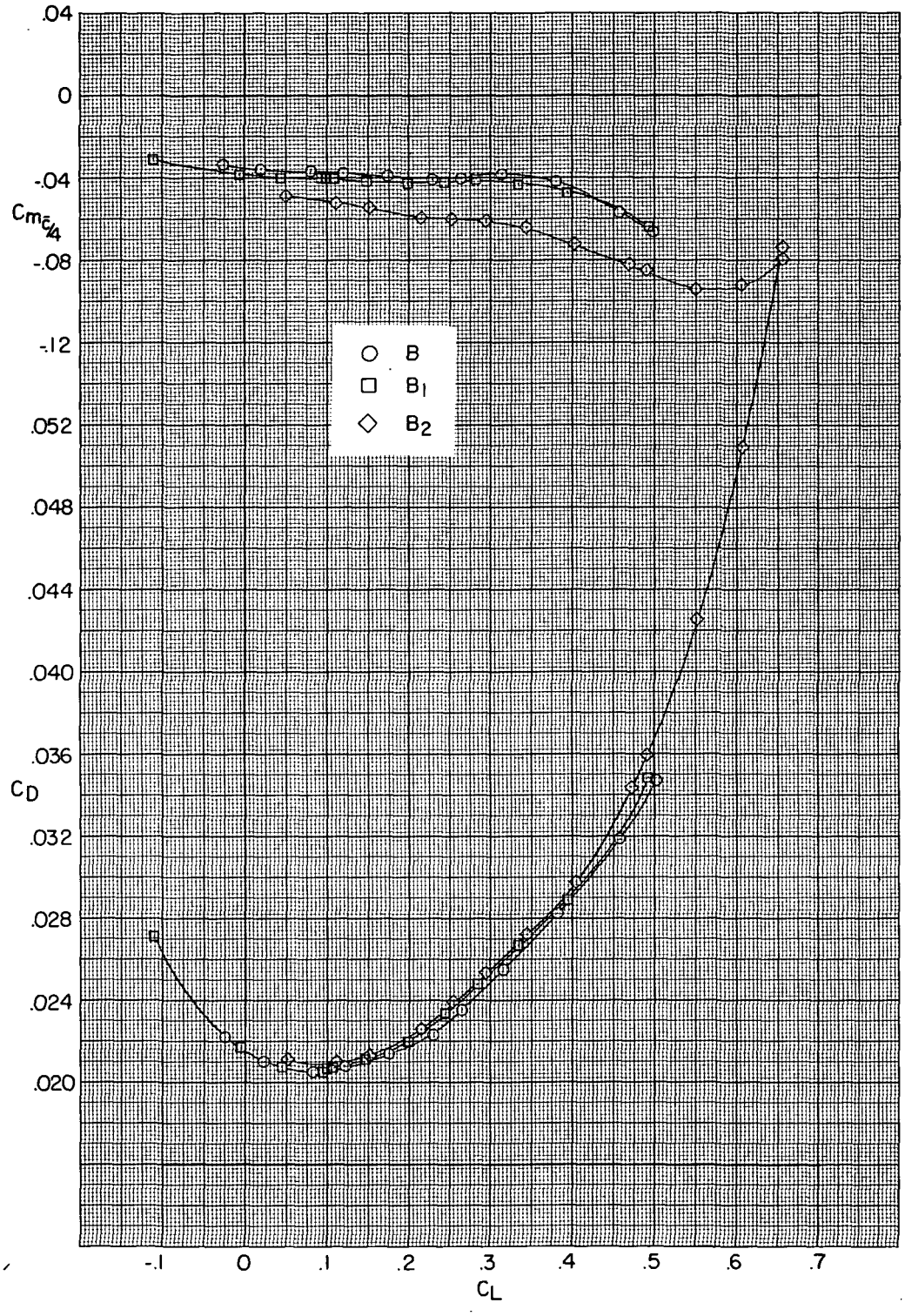

(c) M = 0.96

Figure 11.- Continued.

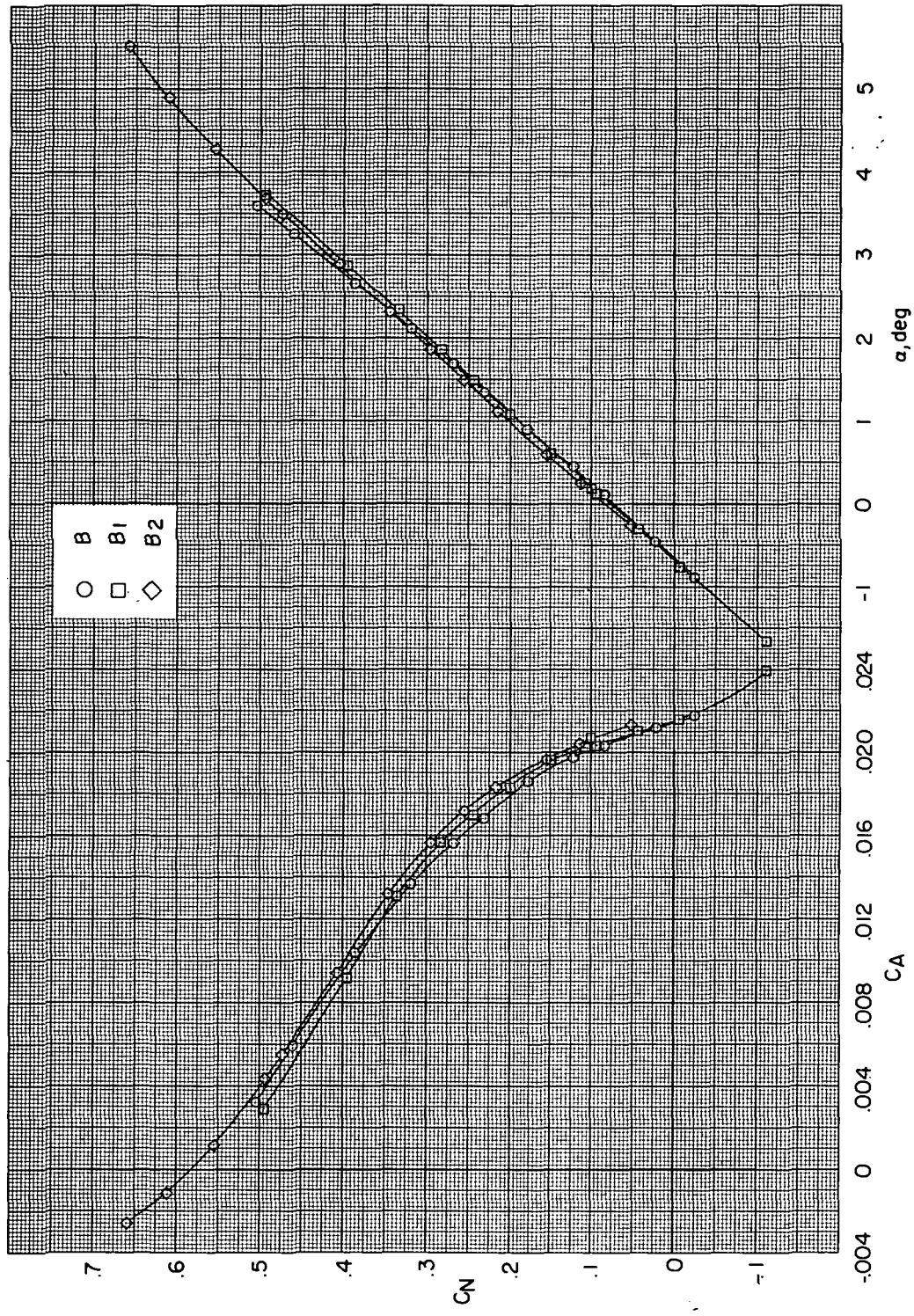

(c) Concluded.

Figure 11.- Continued.

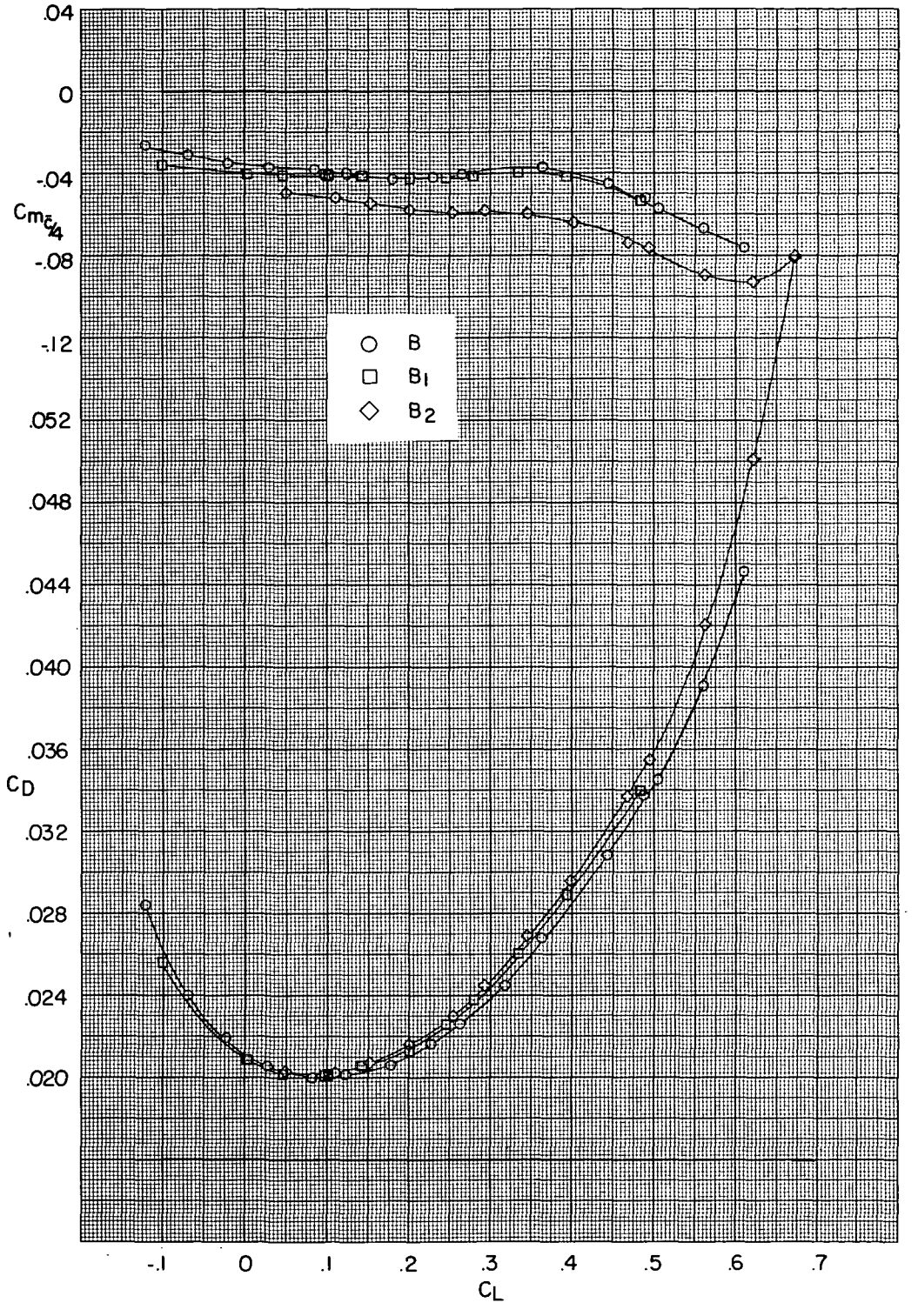

(d) M = 0.97.

Figure 11.- Continued.

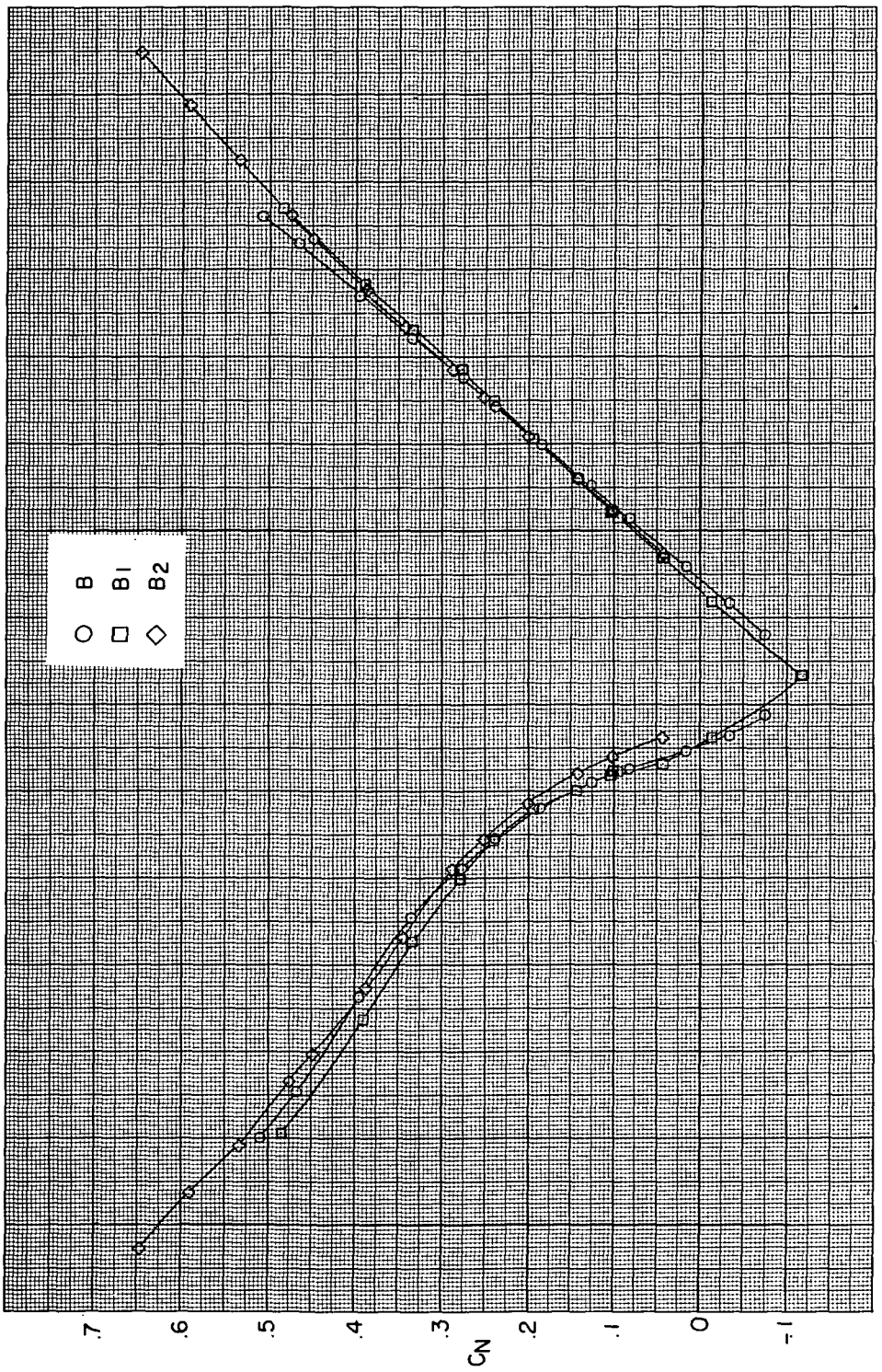

(d) Concluded.

Figure 11.- Continued.

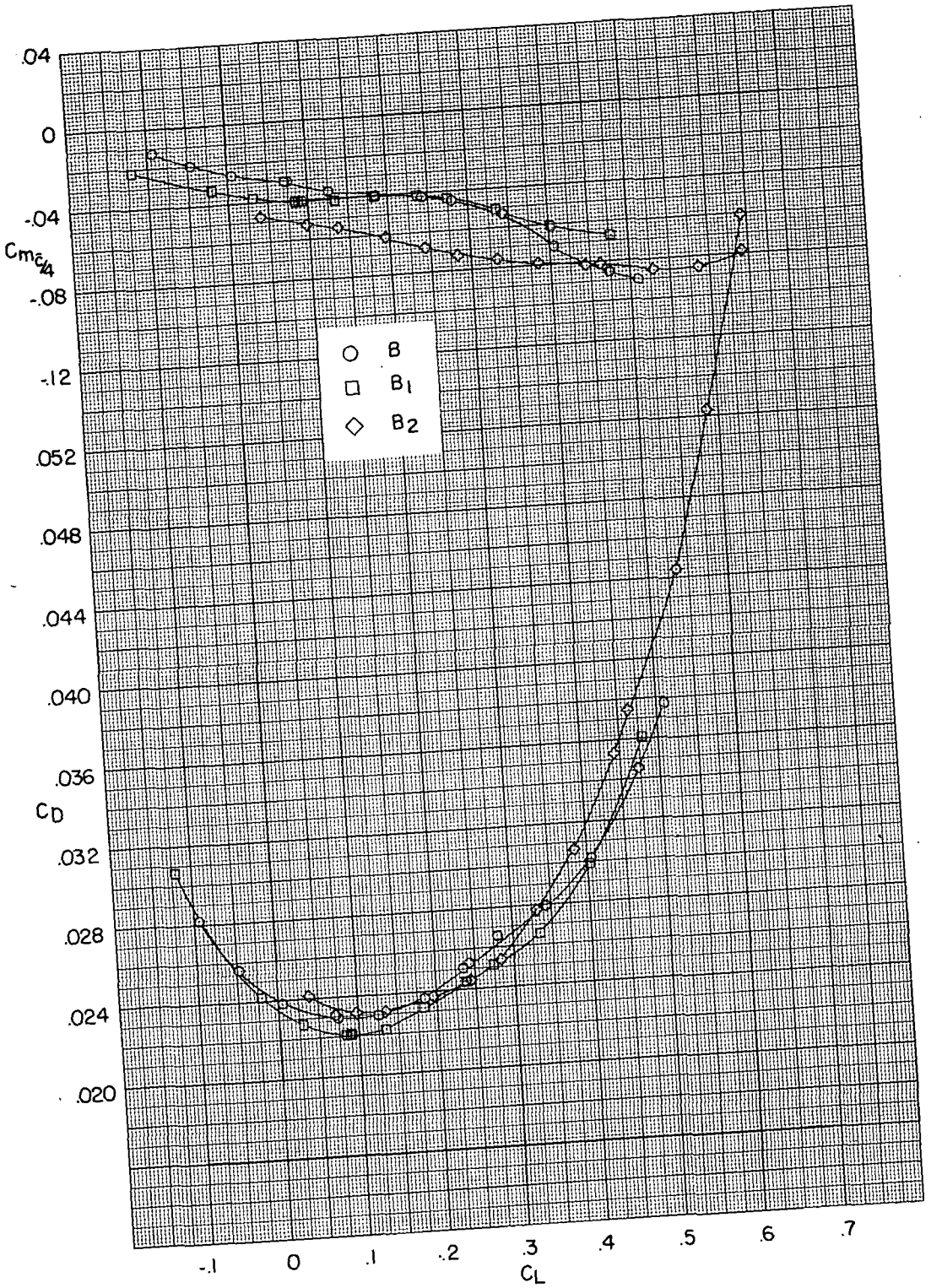

(e) M = 0.98.

Figure 11.- Continued.

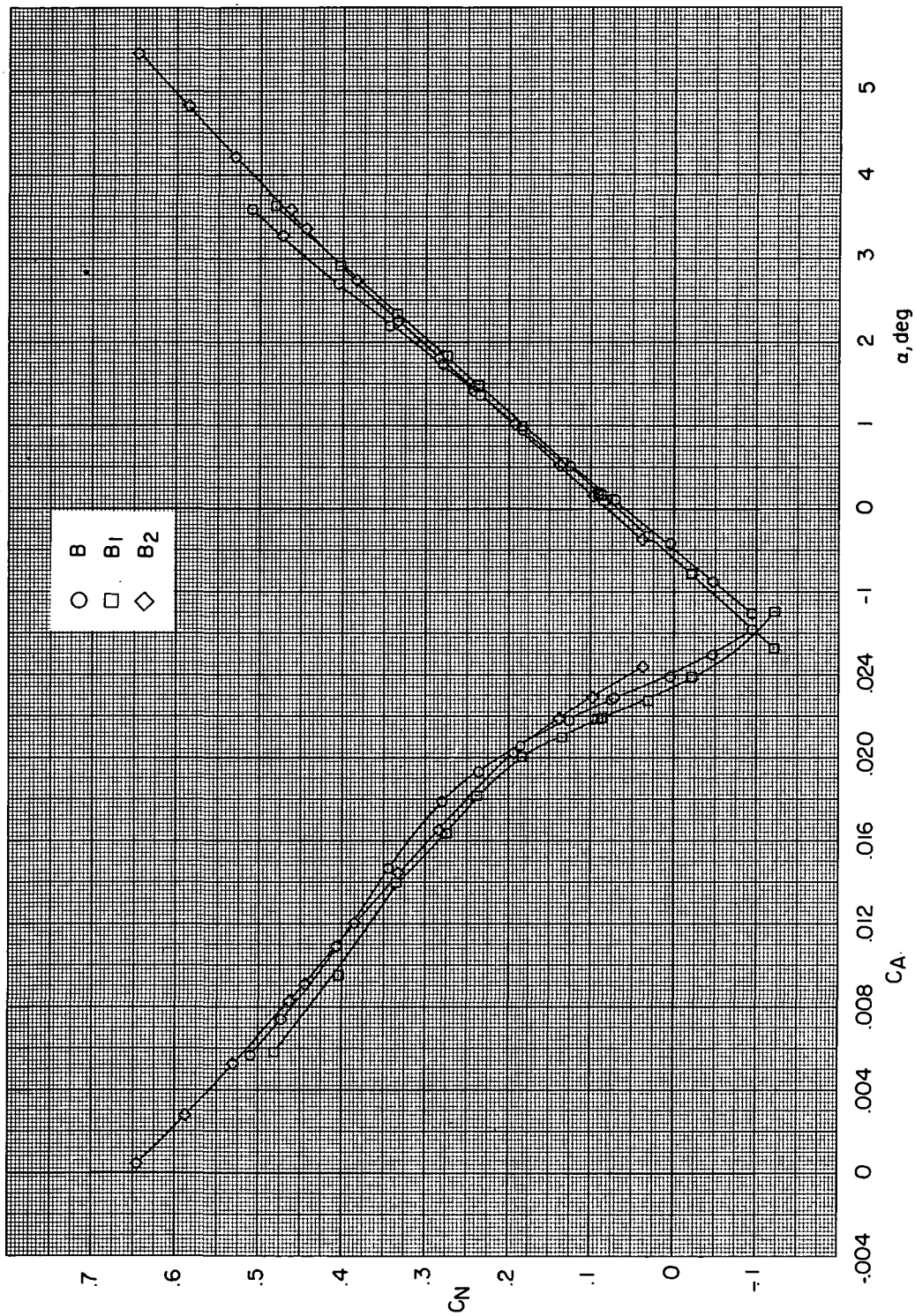

(e) Concluded.

Figure 11.- Continued.

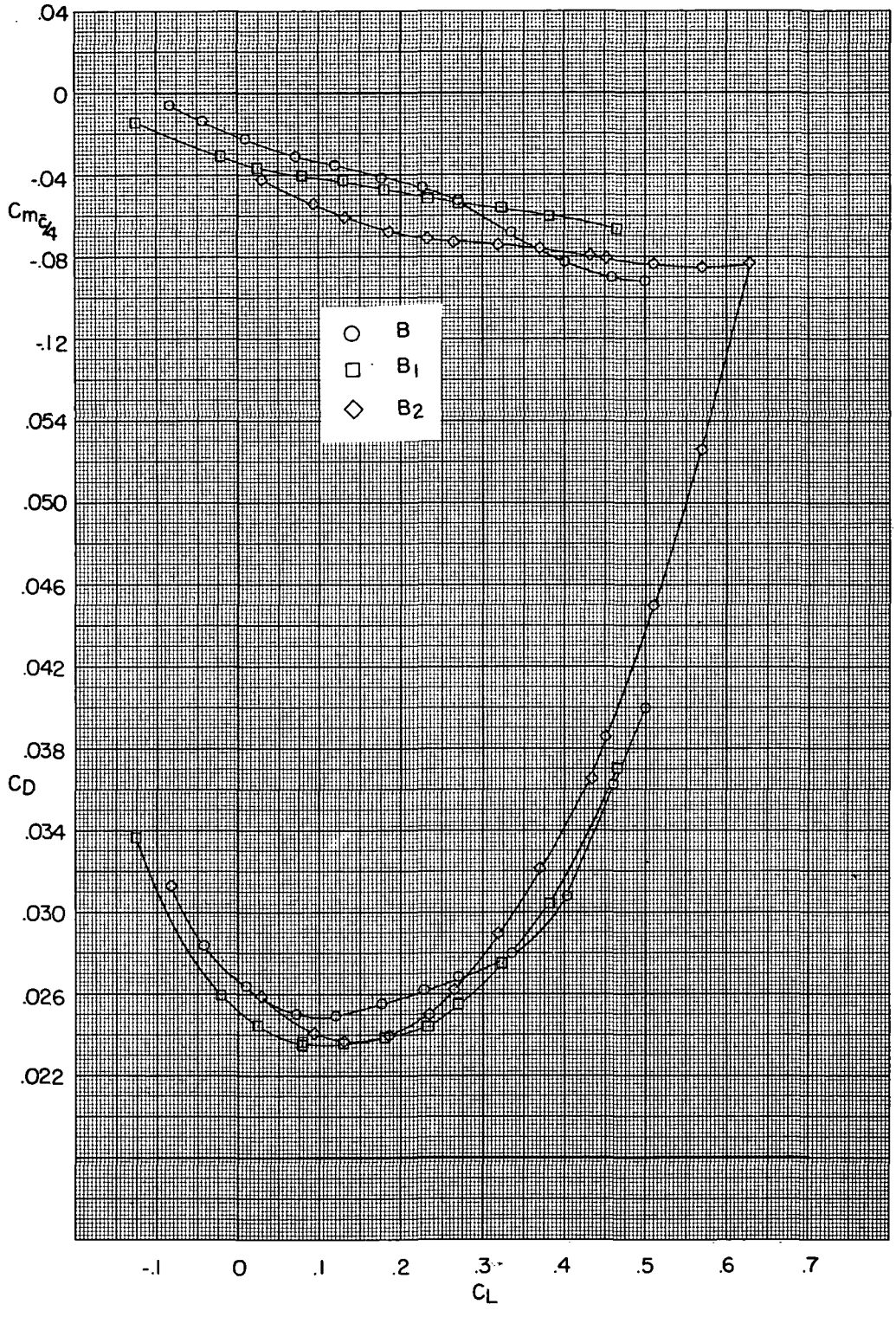

(f) M = 0.99.

Figure 11.- Continued.

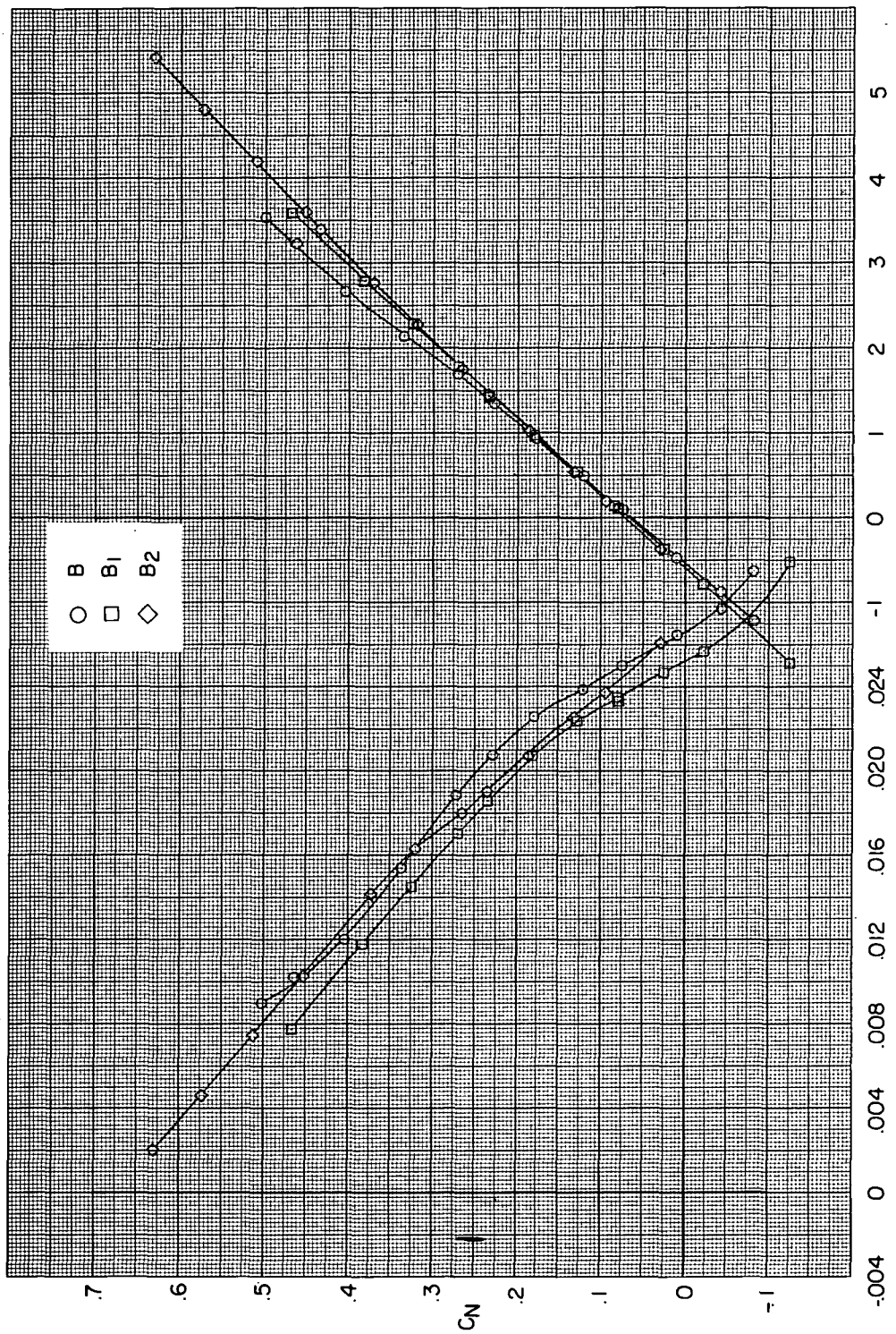

(f) Concluded.

Figure 11.- Concluded.

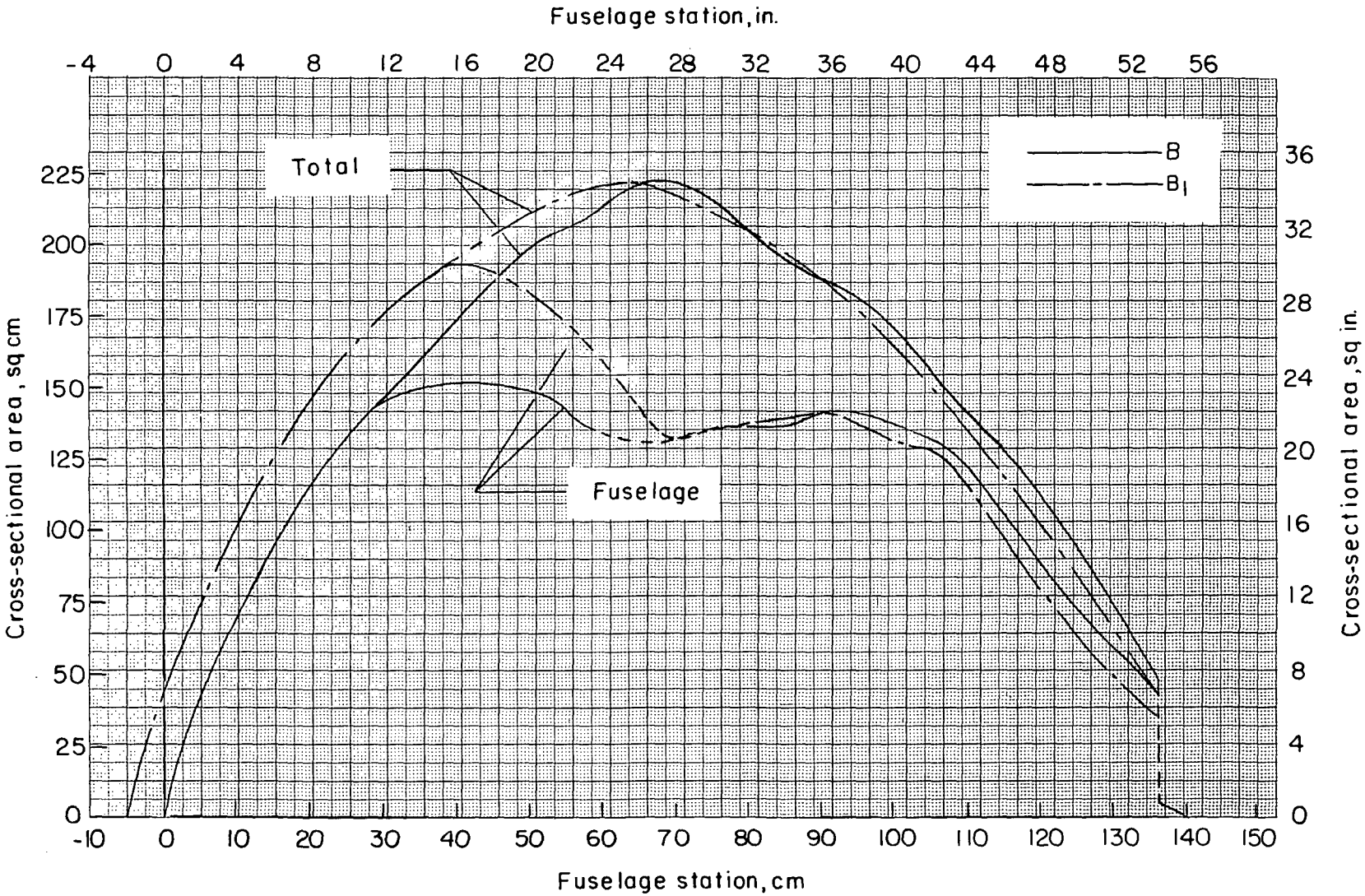

Figure 12.- Comparison of cross-sectional area distributions of configurations B and B_1.

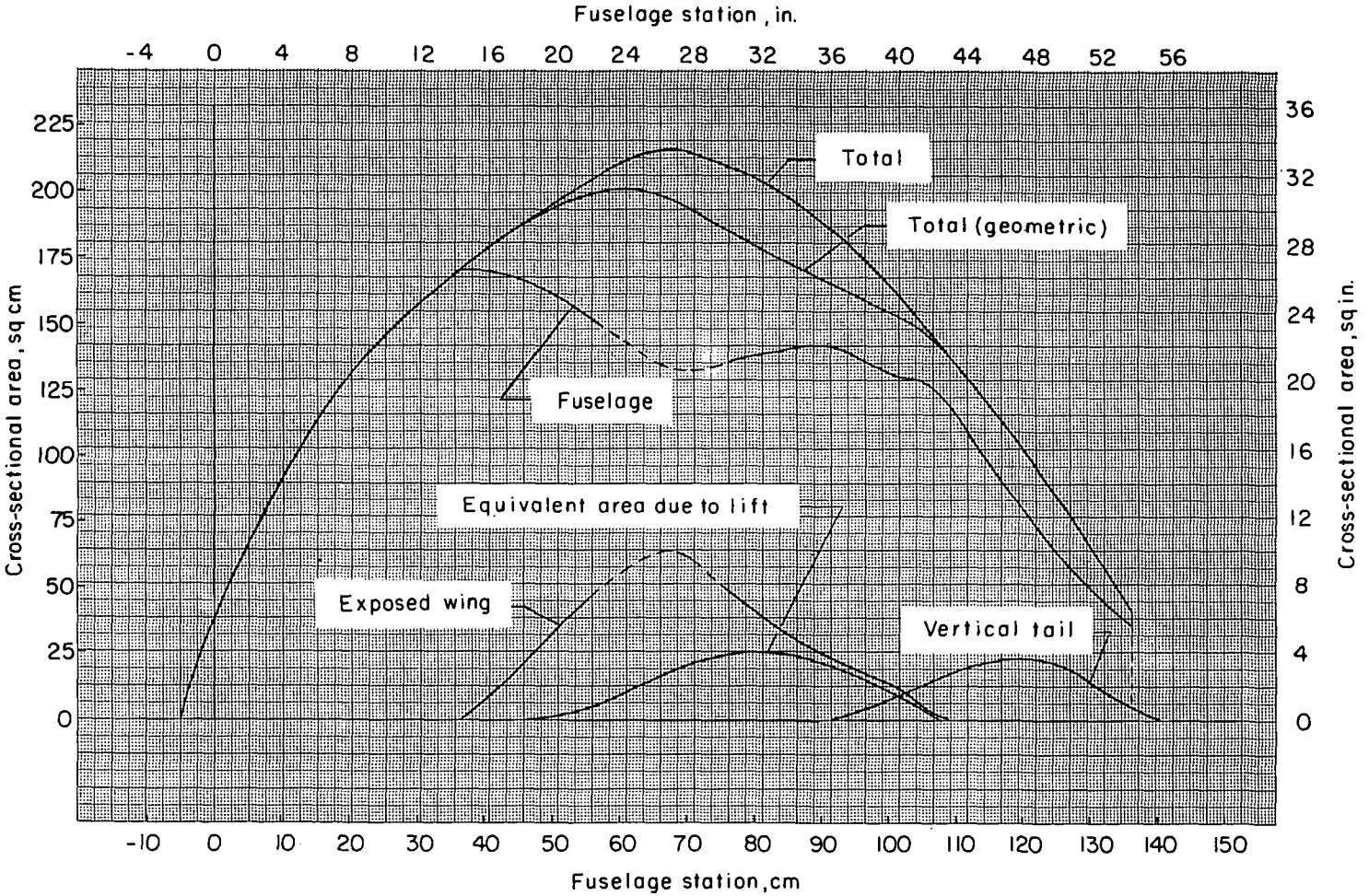

Figure 13.- Cross-sectional area distribution of configuration B_2.

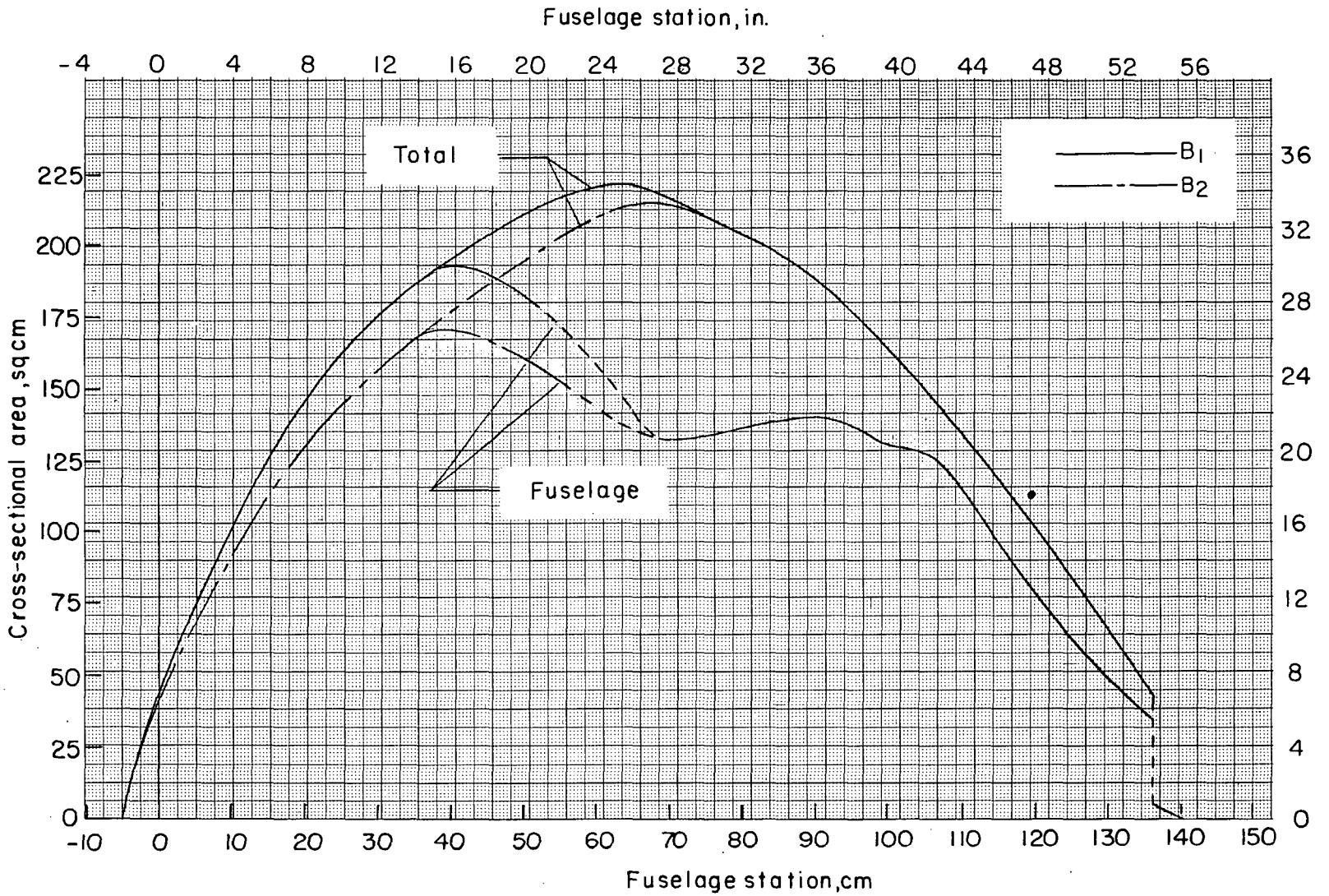

Figure 14.- Comparison of cross-sectional area distributions of configurations B_1 and B_2.

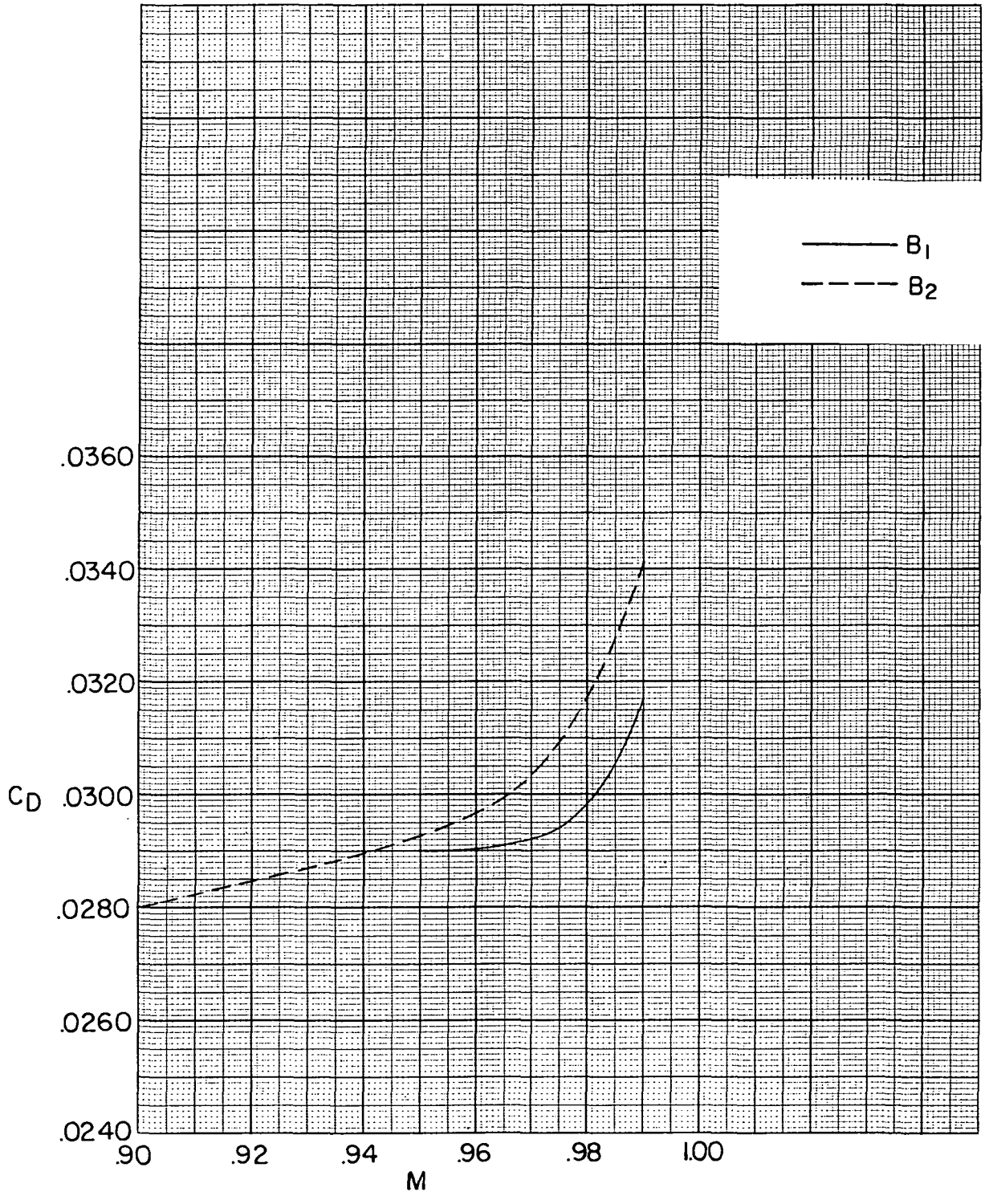

Figure 15.- Comparison of drag-rise characteristics for configurations B_1 and B_2. $C_L = 0.40$.

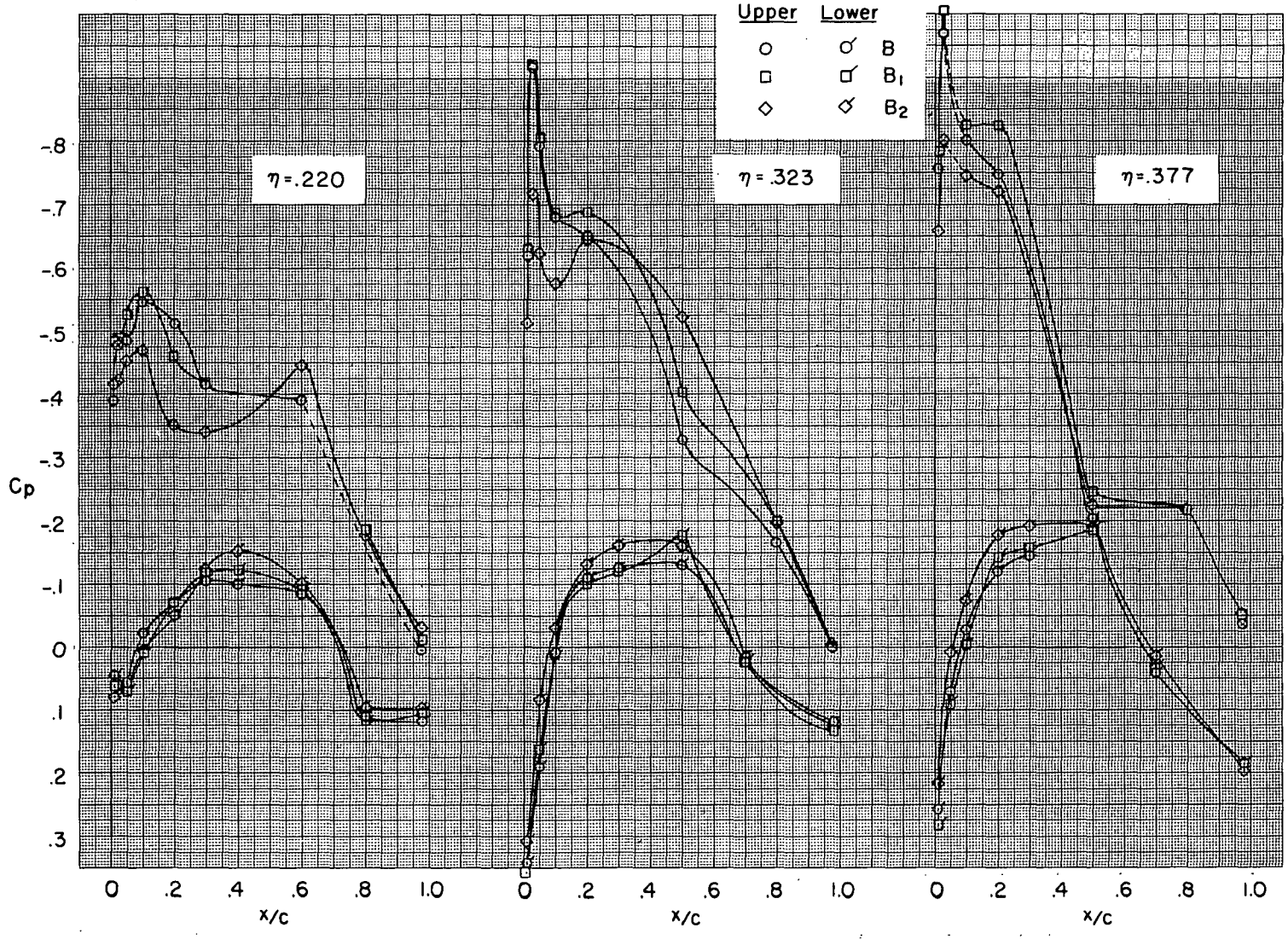

(a) M = 0.90.

Figure 16.- Wing pressure distributions for configurations B, B_1, and B_2. $C_L \approx 0.40$.

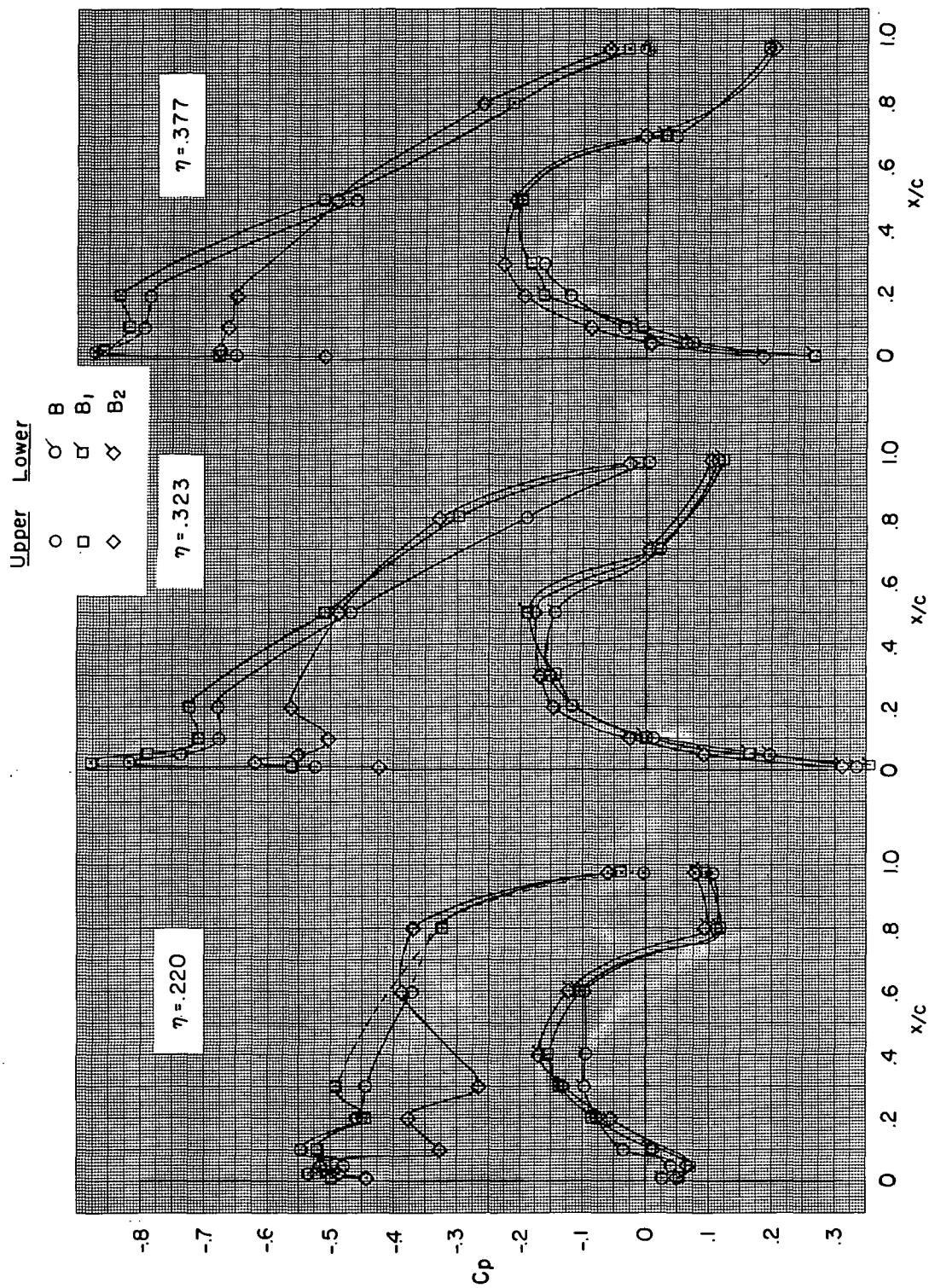

(b) M = 0.95.

Figure 16.- Continued.

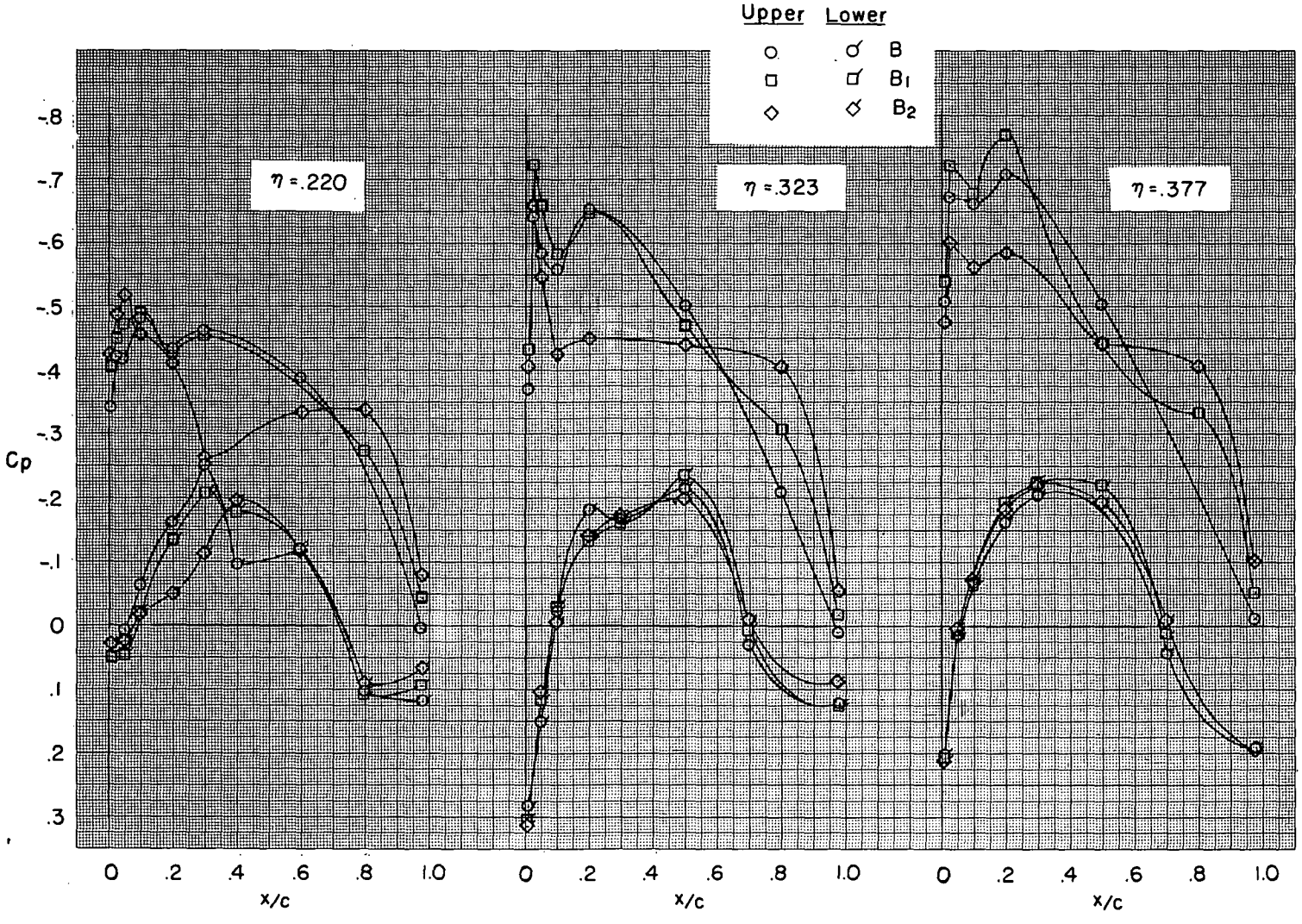

(c) M = 0.98.

Figure 16.- Concluded.

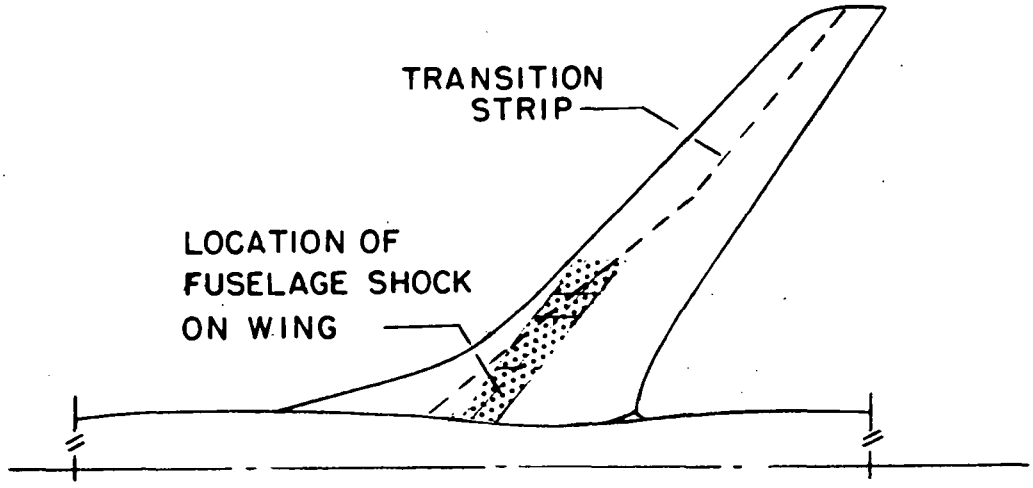

Figure 17.- Sketch illustrating location of fuselage shock on wing.

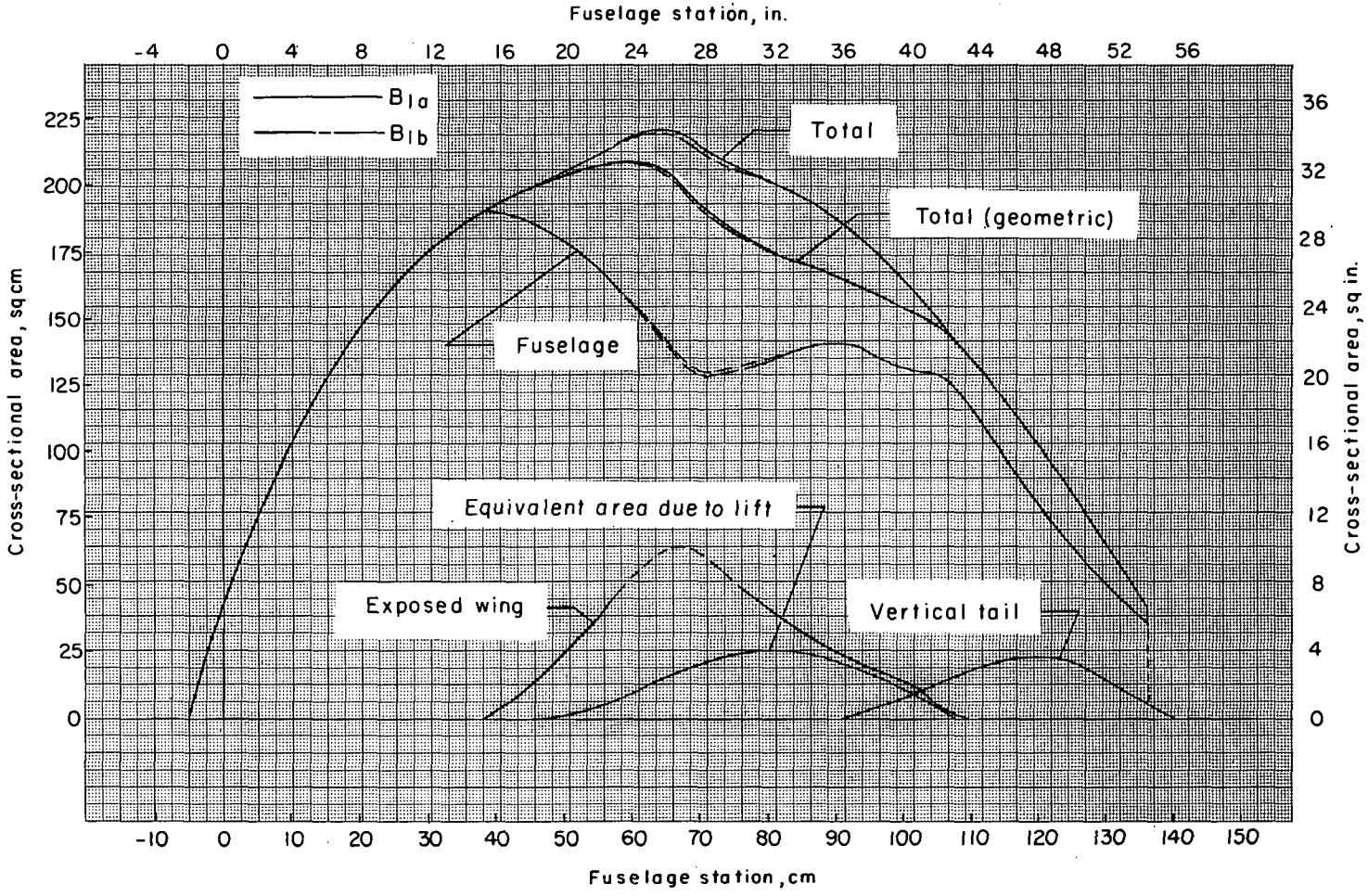

Figure 18.- Comparison of cross-sectional area distributions of configurations B_{1a} and B_{1b}.

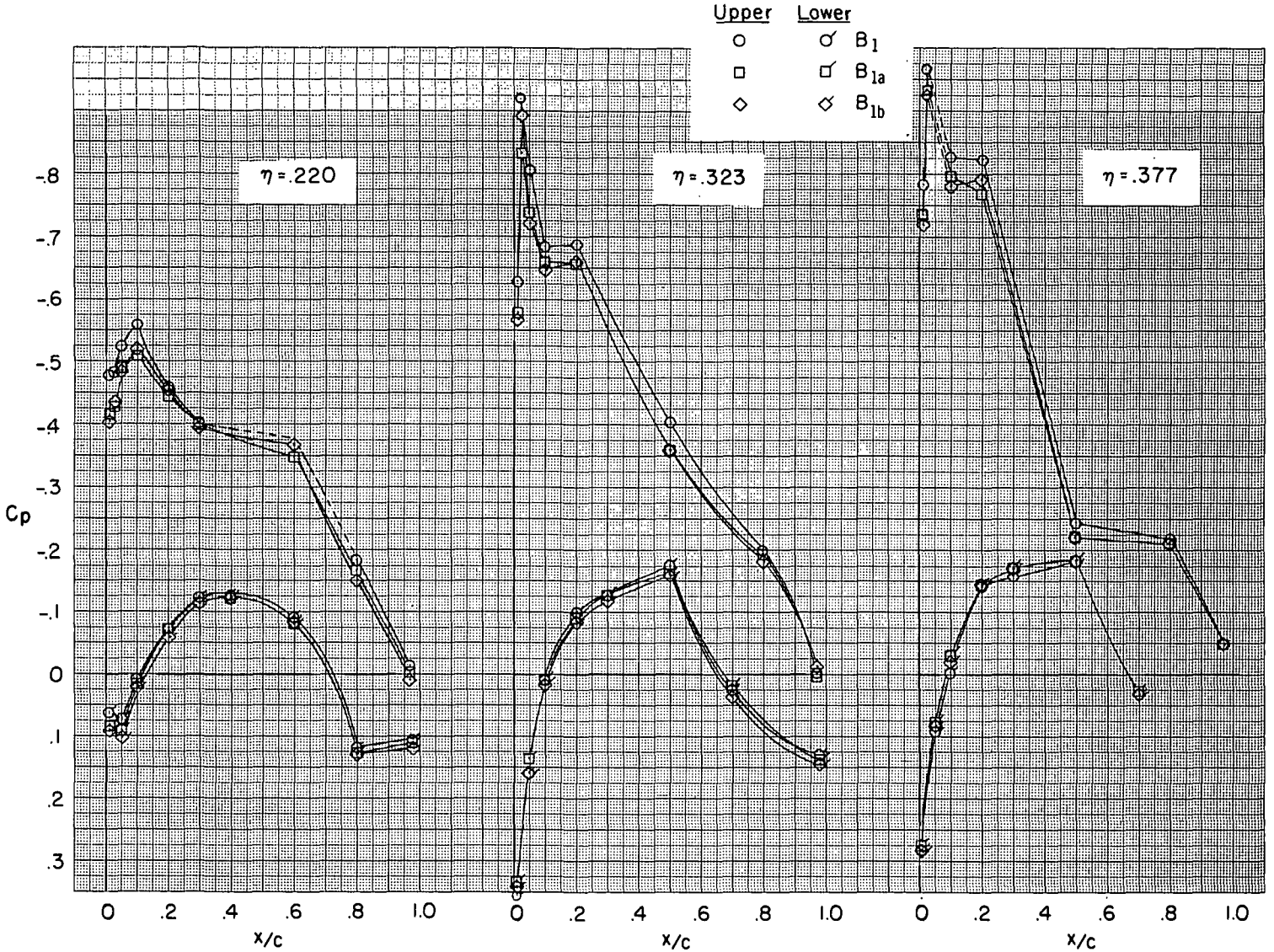

(a) M = 0.90.

Figure 19.- Wing pressure distributions for configurations B_1, B_{1a}, and B_{1b}. $C_L \approx 0.40$.

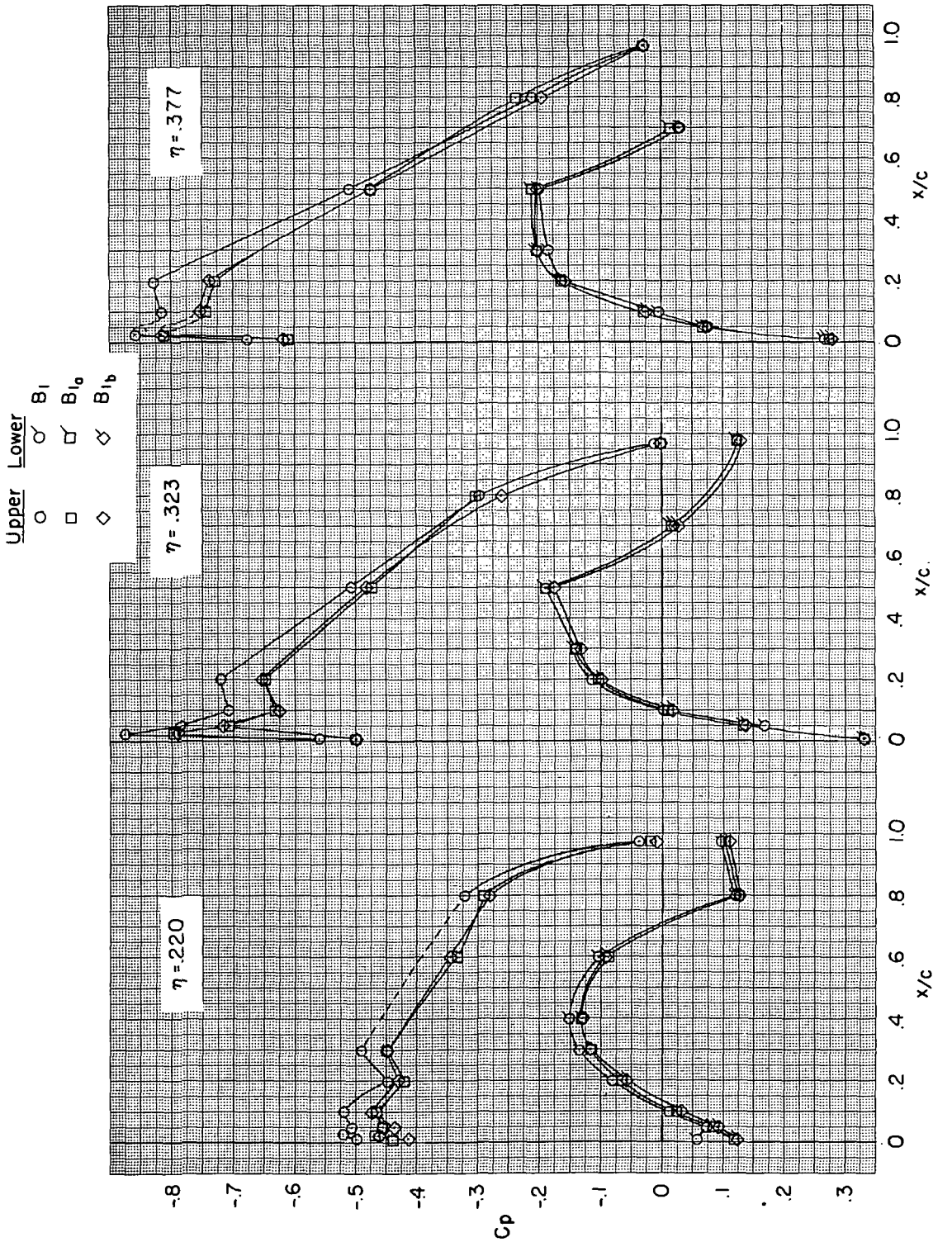

(b) M = 0.95.

Figure 19.- Continued.

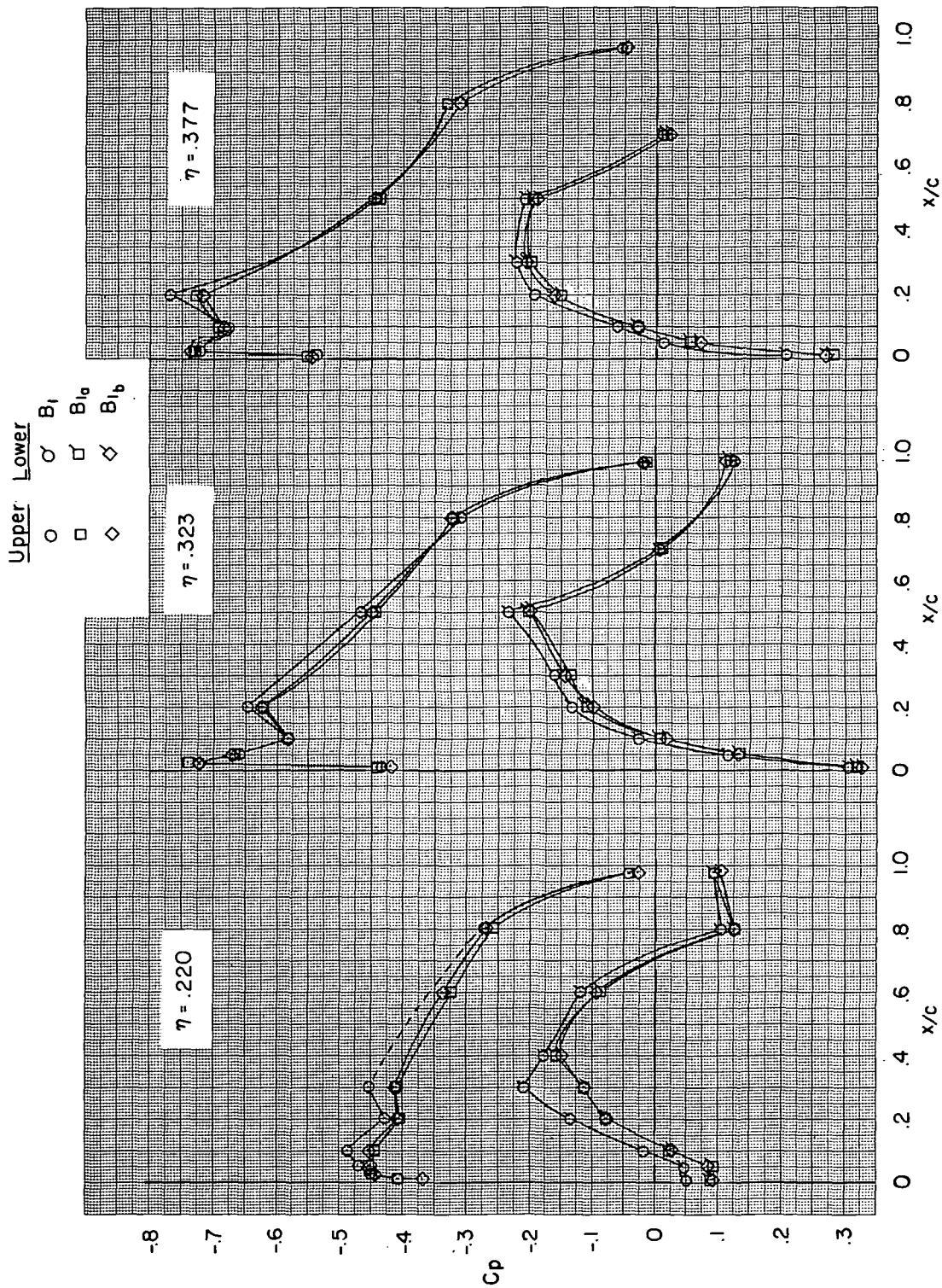

(c) M = 0.98.

Figure 19.- Concluded.

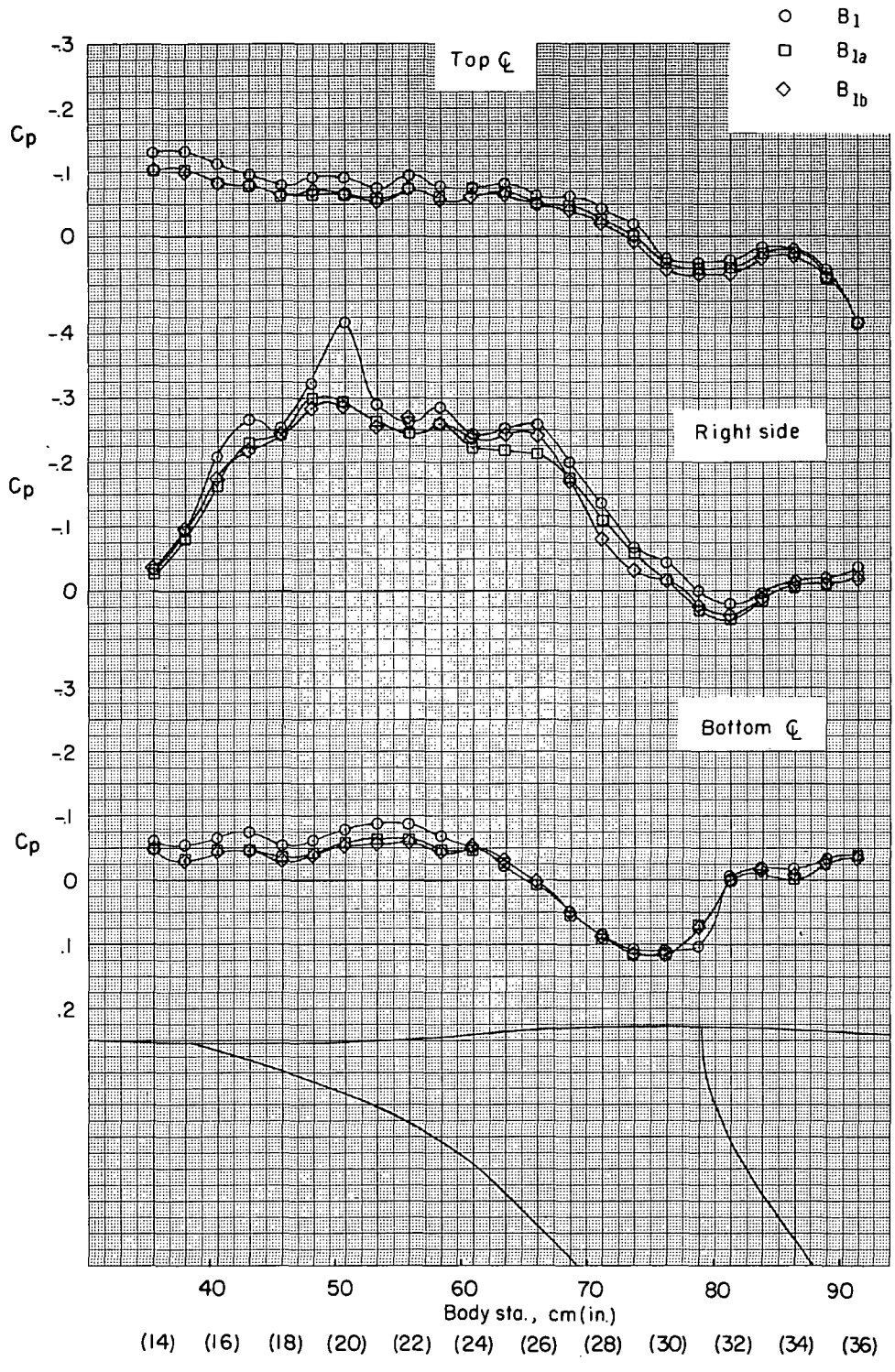

(a) M = 0.90.

Figure 20.- Fuselage pressure distributions for configurations B_1, B_{1a}, and B_{1b}. $C_L \approx 0.40$.

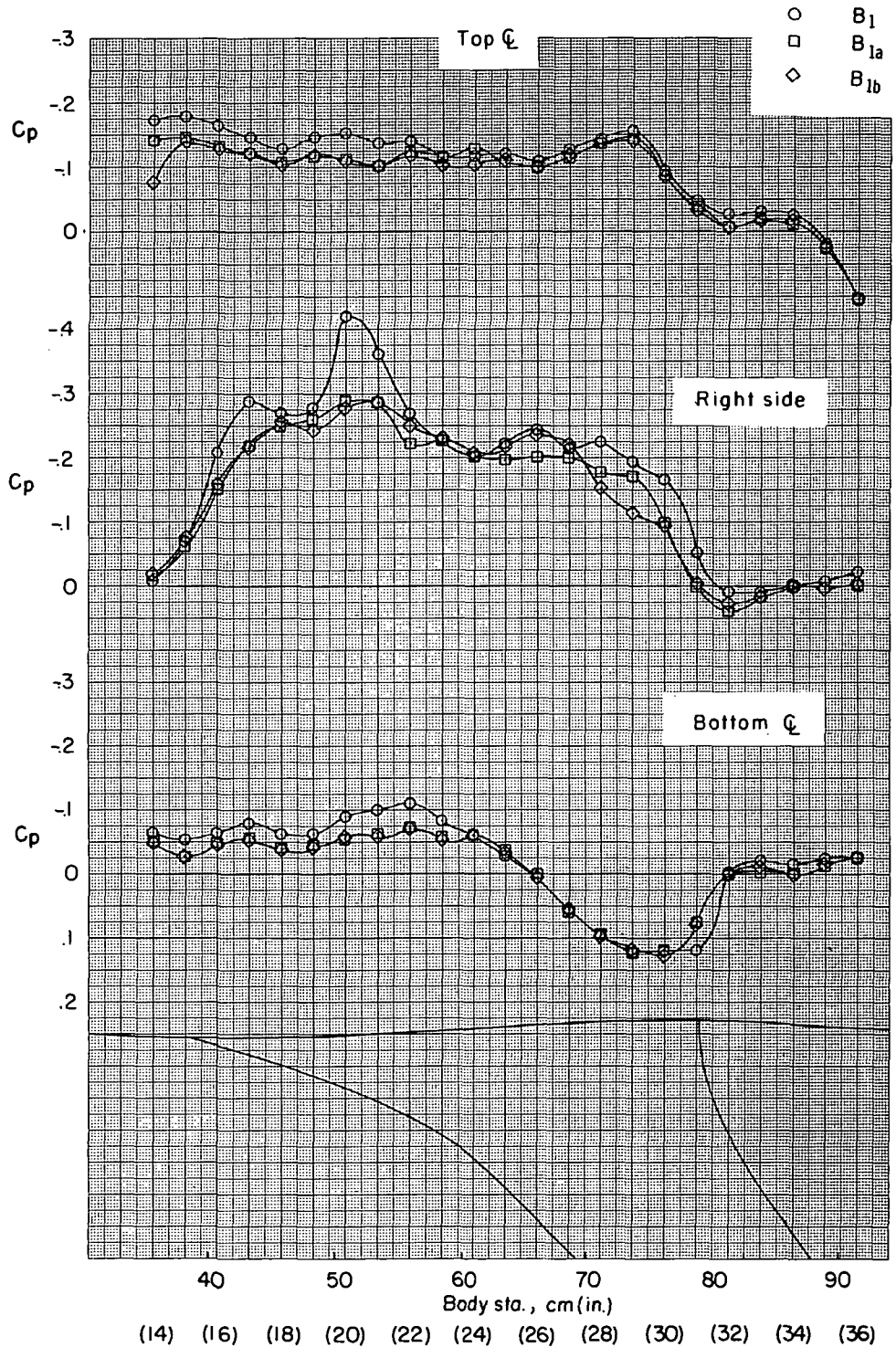

(b) M = 0.95.

Figure 20.- Continued.

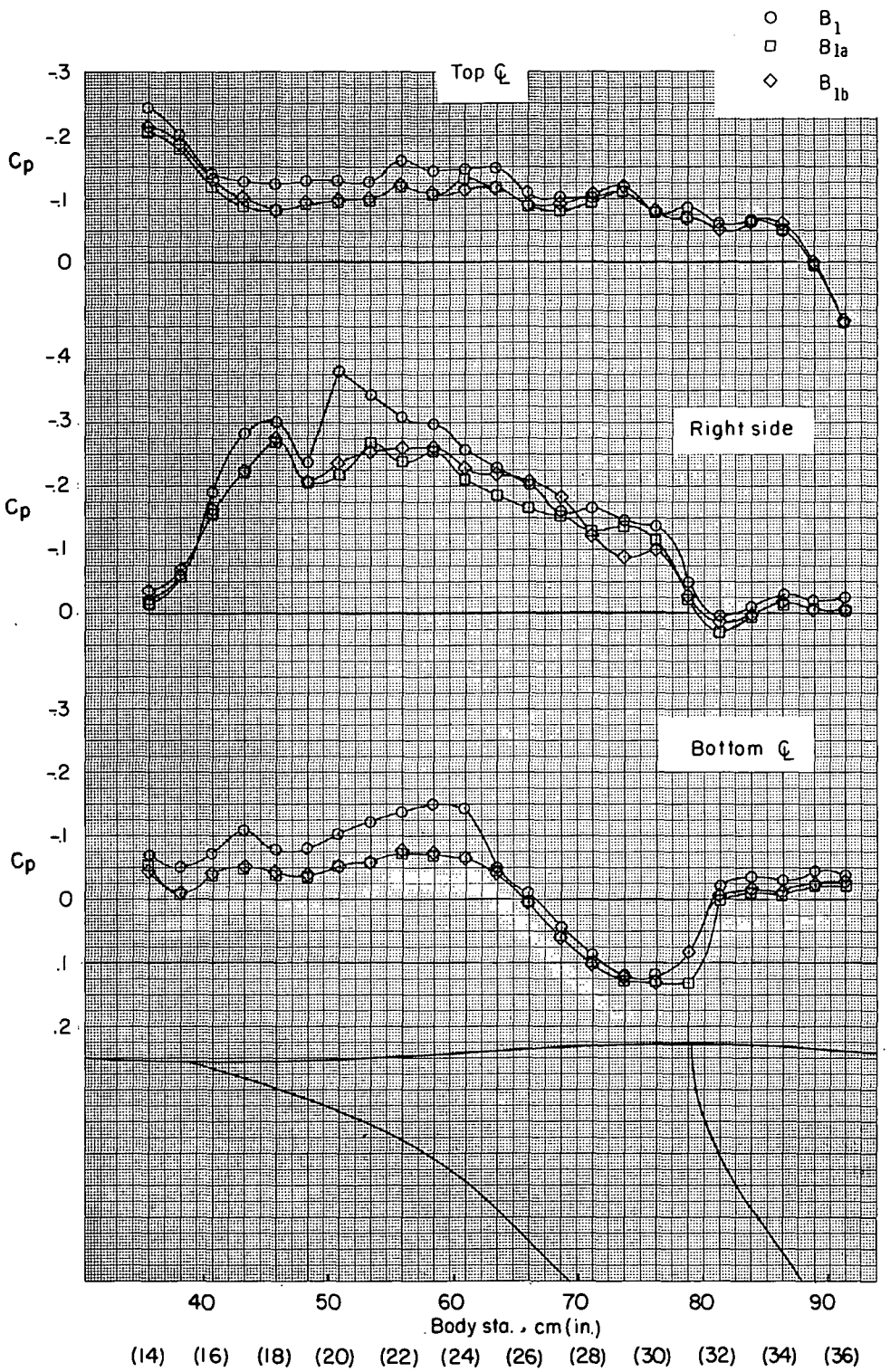

(c) M = 0.98.

Figure 20.- Concluded.

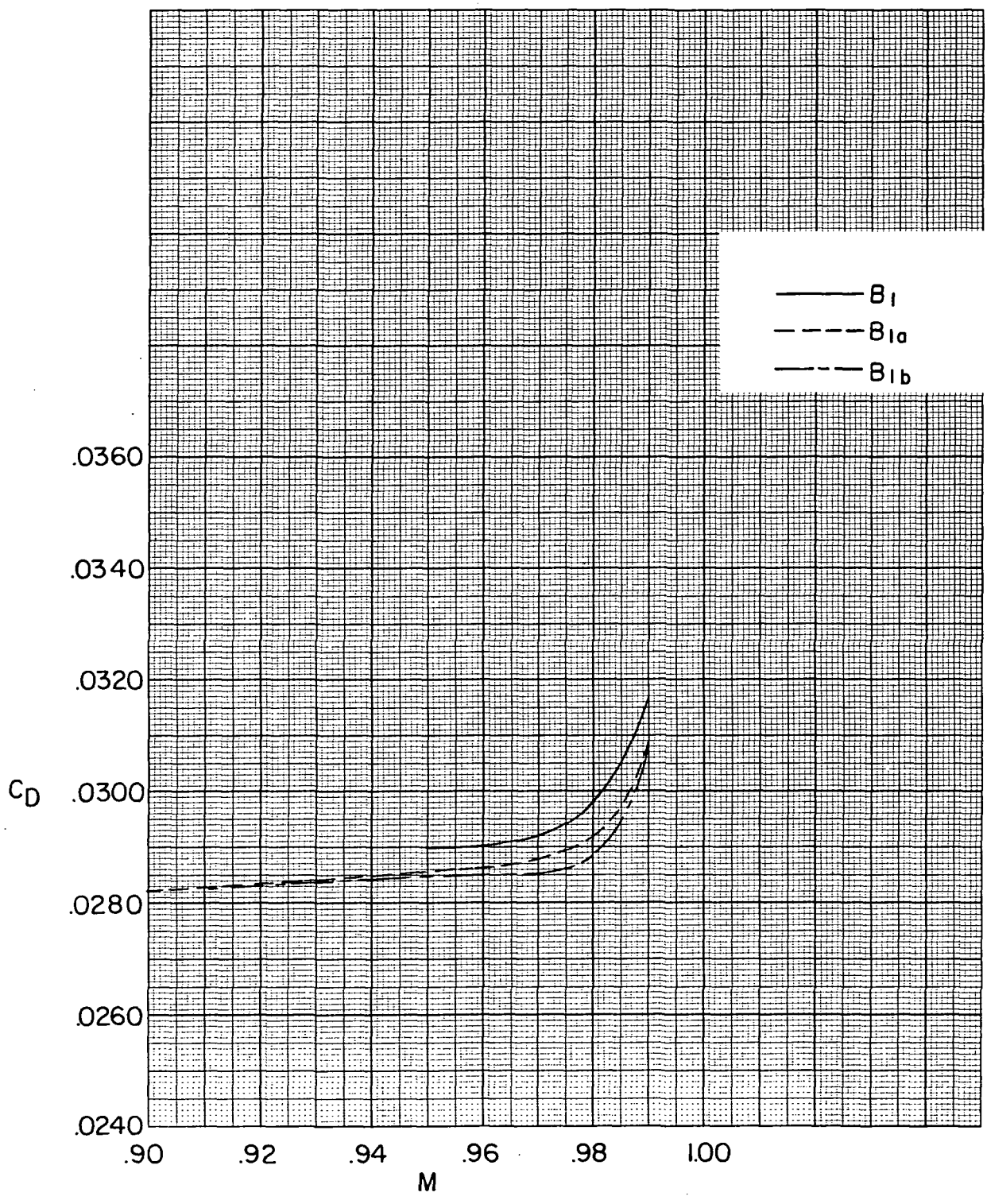

Figure 21.- Comparison of drag-rise characteristics for configurations B_1, B_{1a}, and B_{1b}. $C_L = 0.40$.

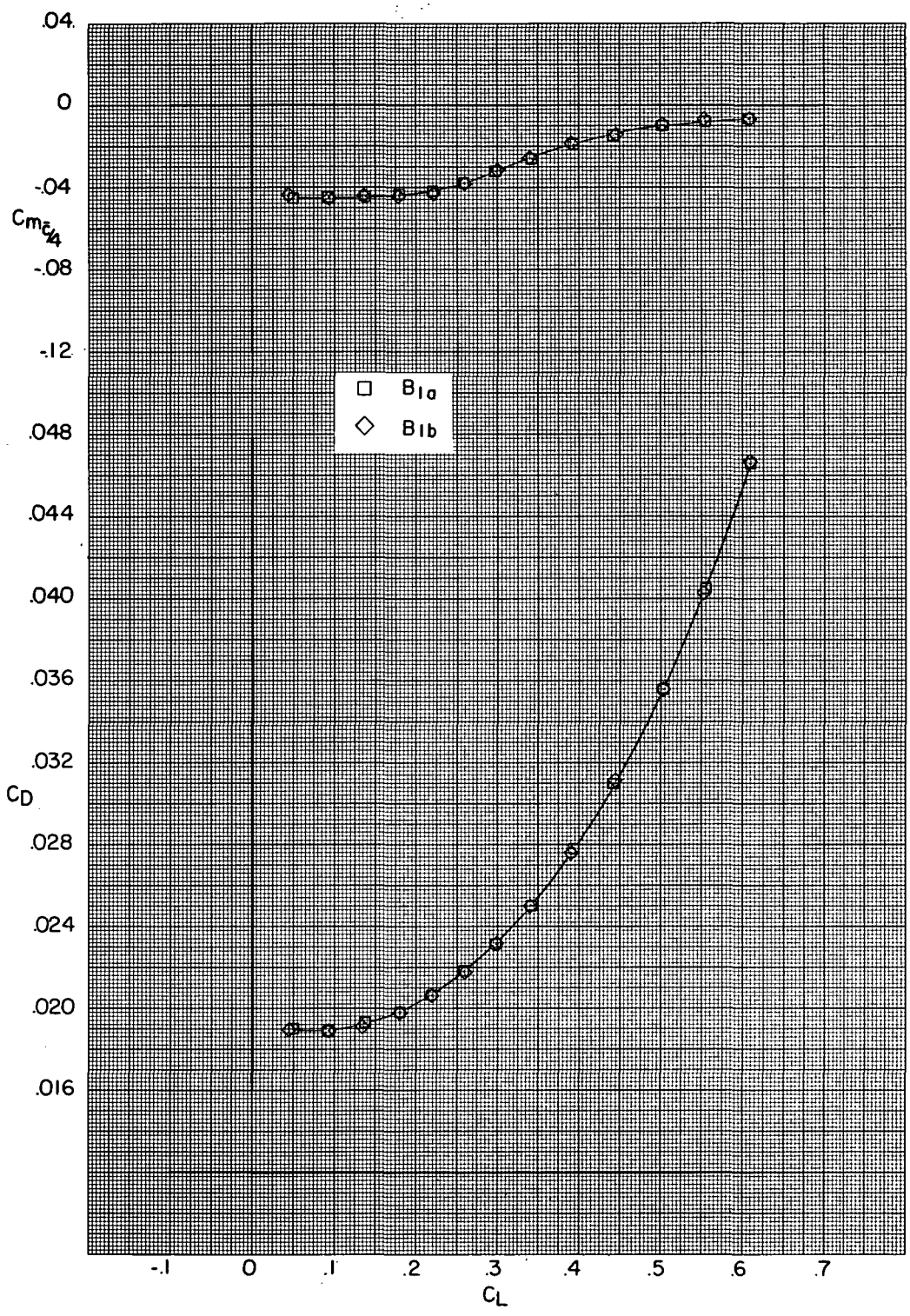

(a) M = 0.90.

Figure 22.- Longitudinal aerodynamic data for configurations B_1, B_{1a}, and B_{1b}.

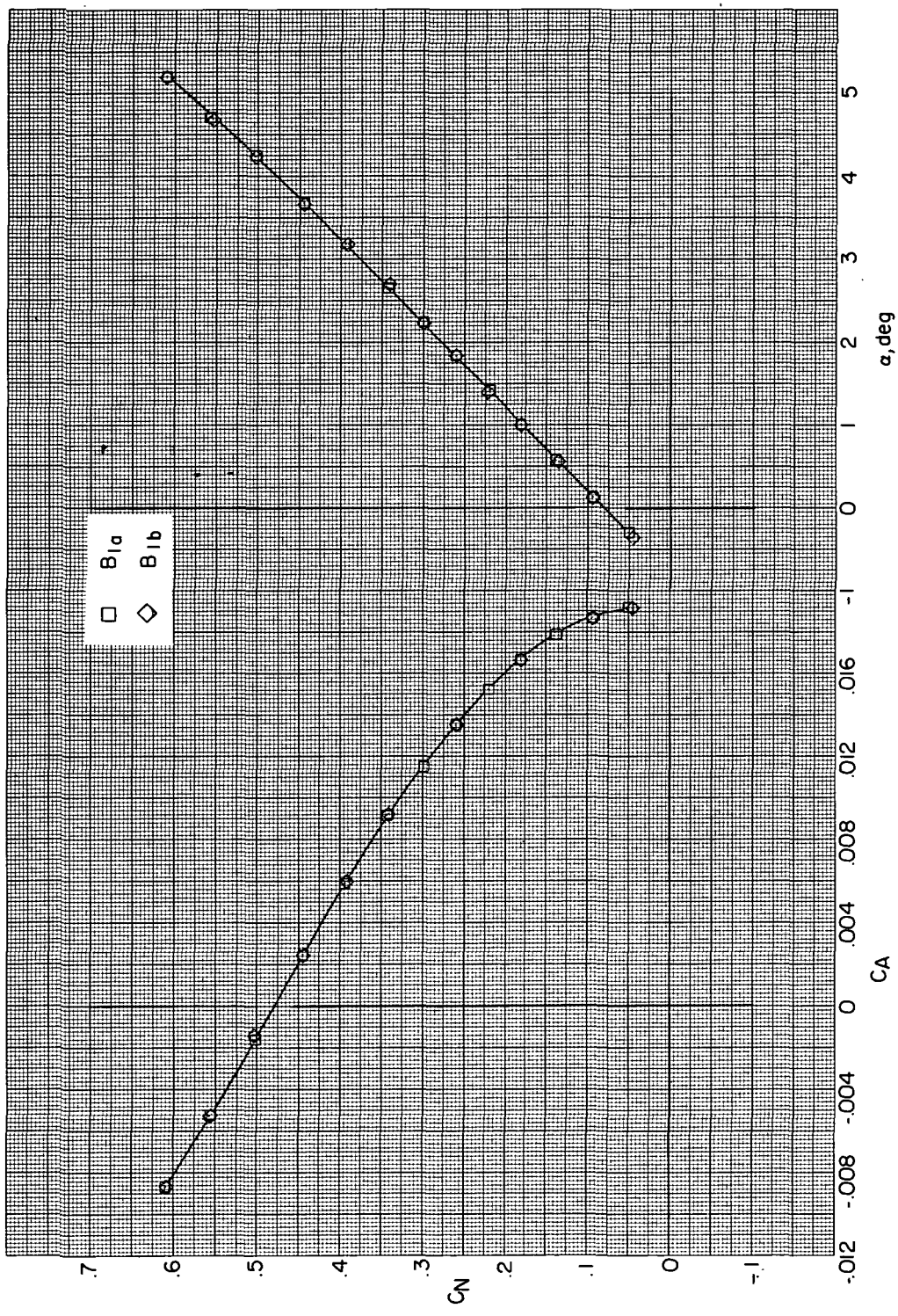

(a) Concluded.

Figure 22.- Continued.

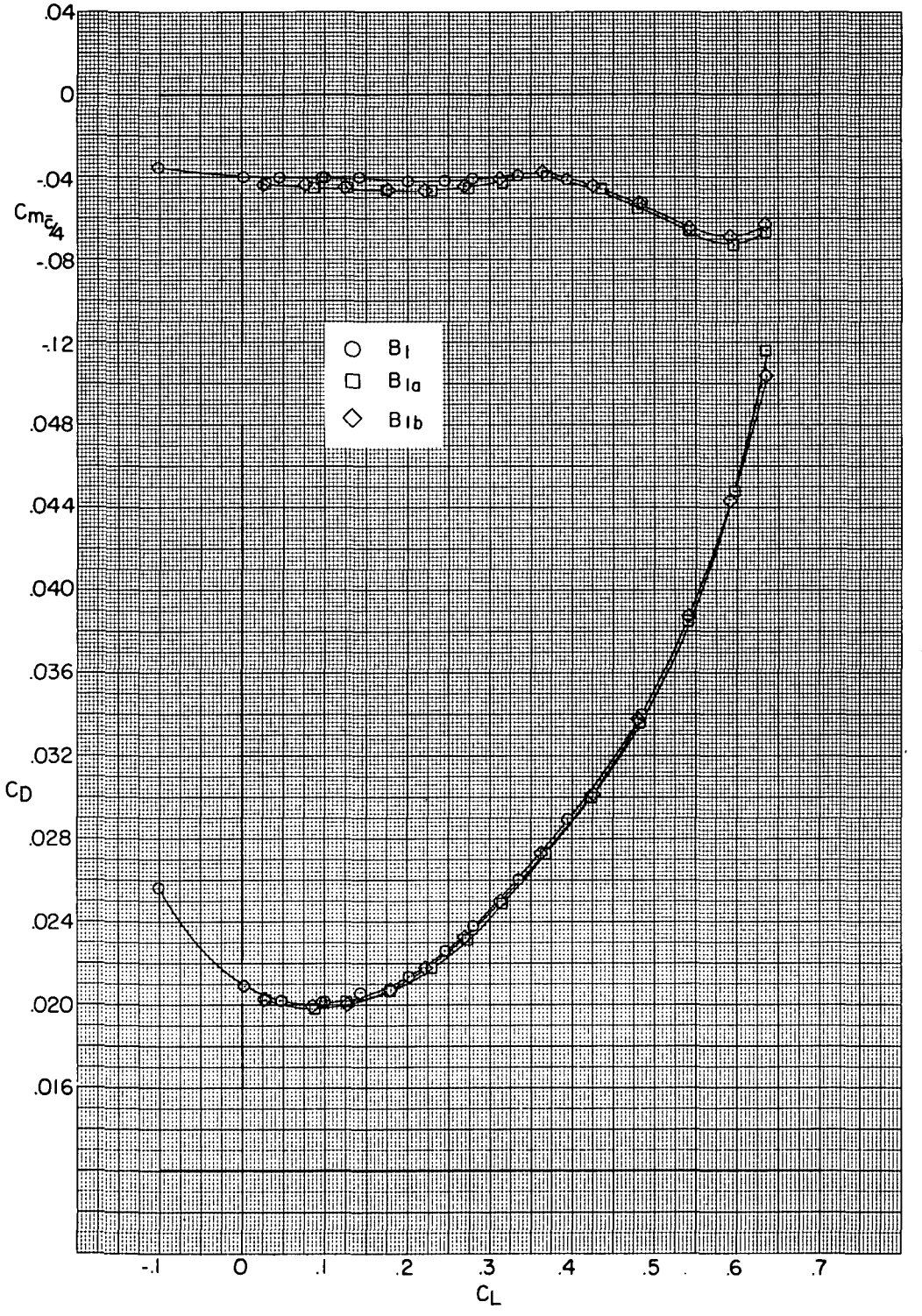

(b) M = 0.95.

Figure 22.- Continued.

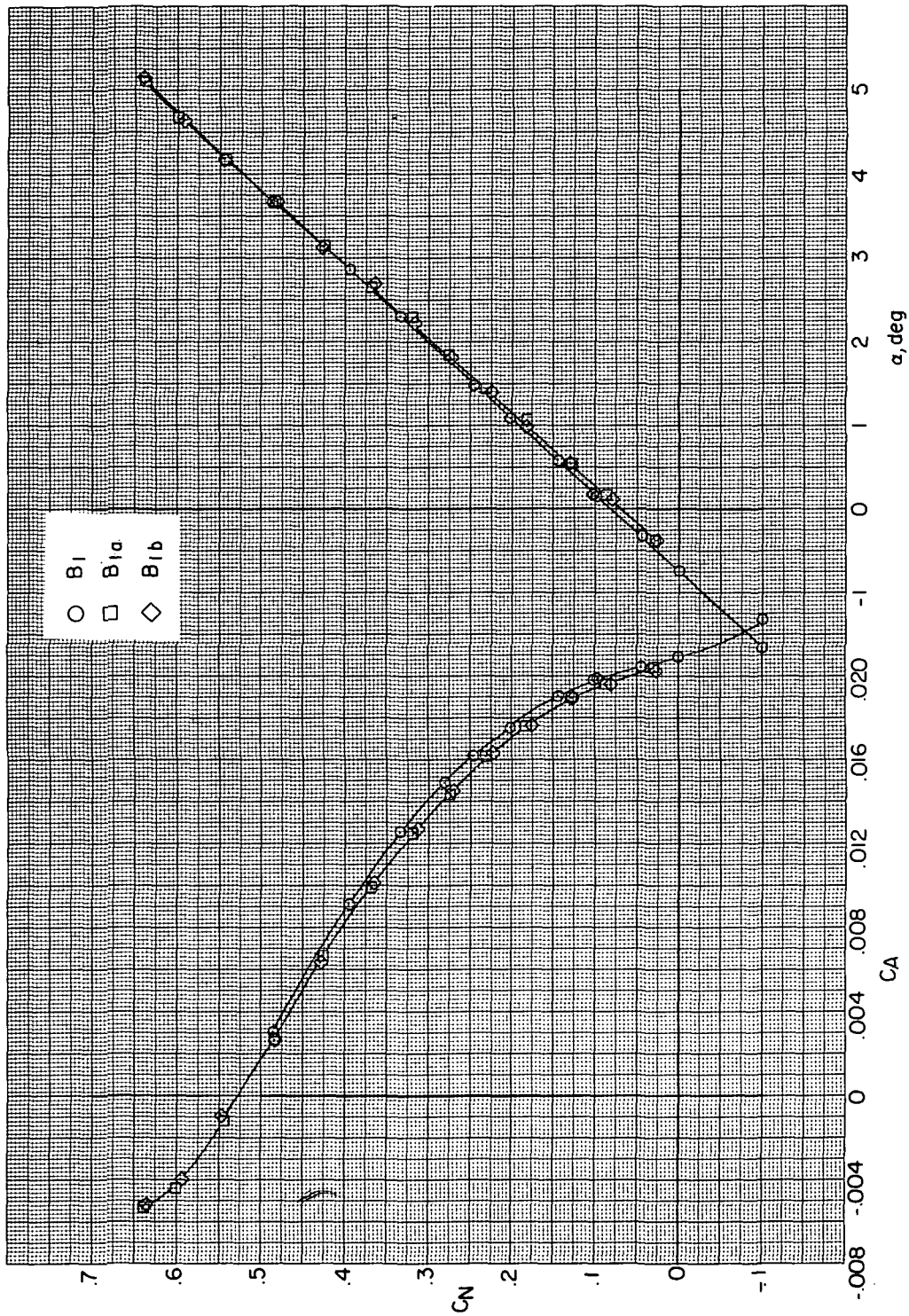

(b) Concluded.

Figure 22.- Continued.

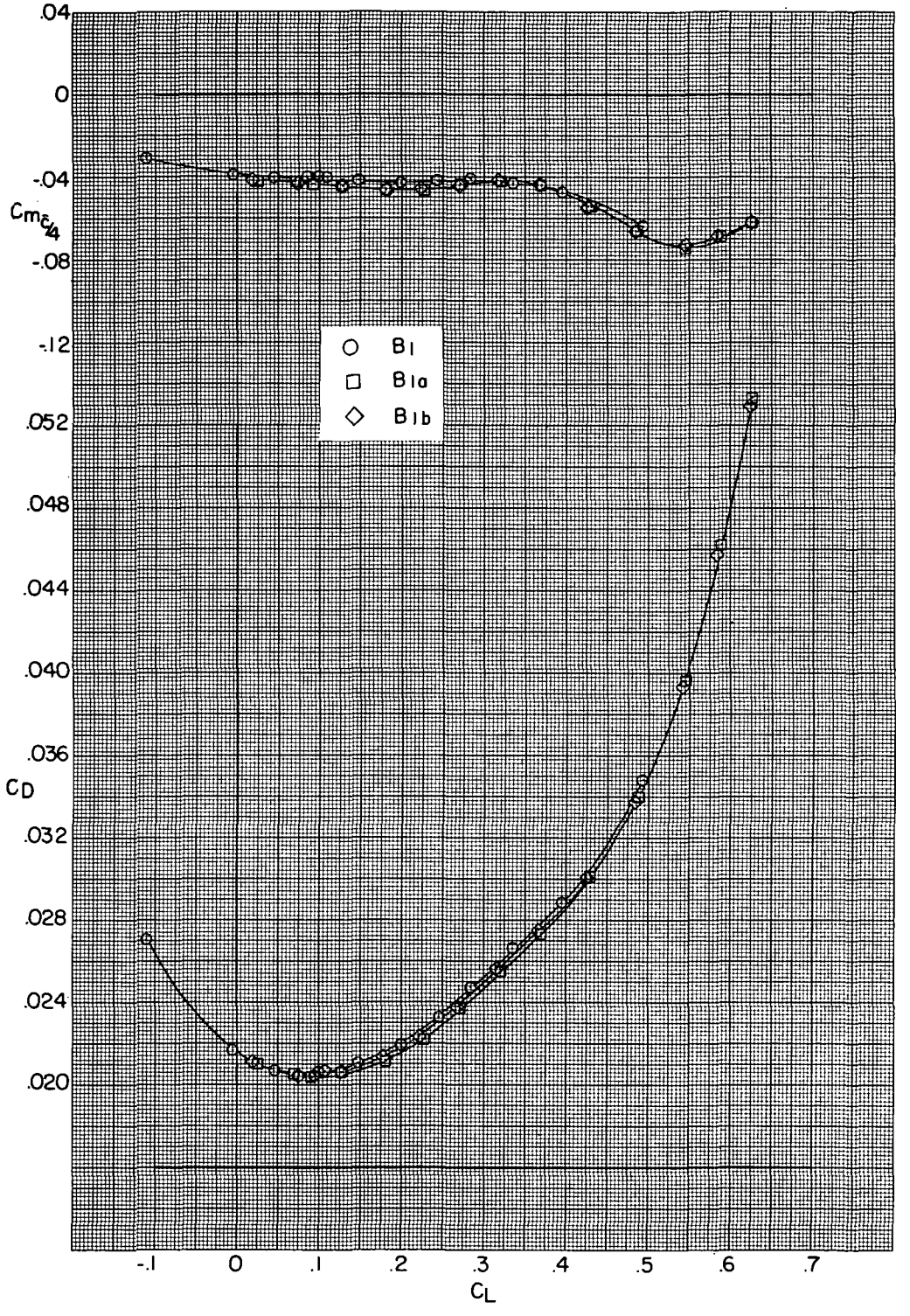

(c) M = 0.96.

Figure 22.- Continued.

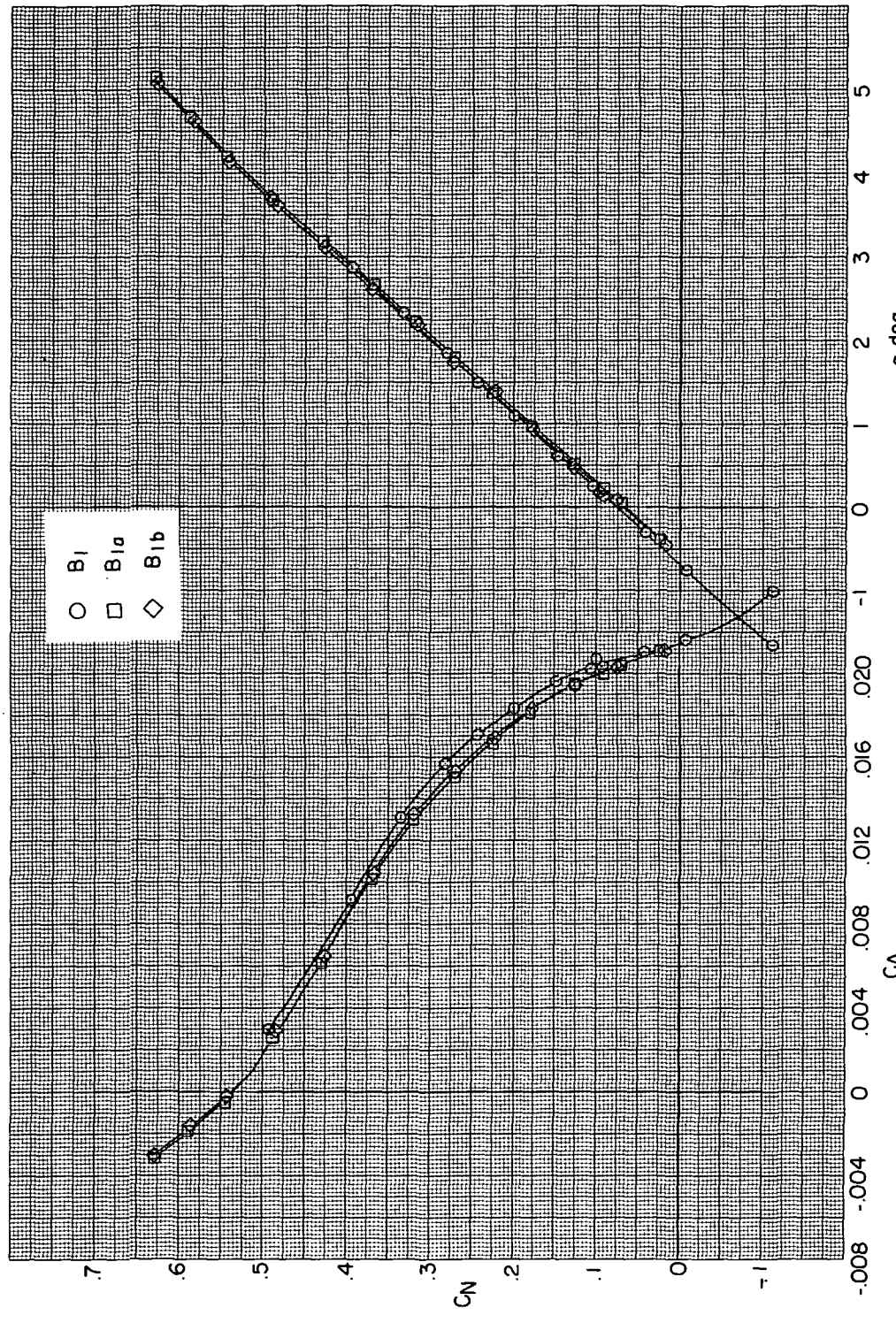

(c) Concluded.

Figure 22.- Continued.

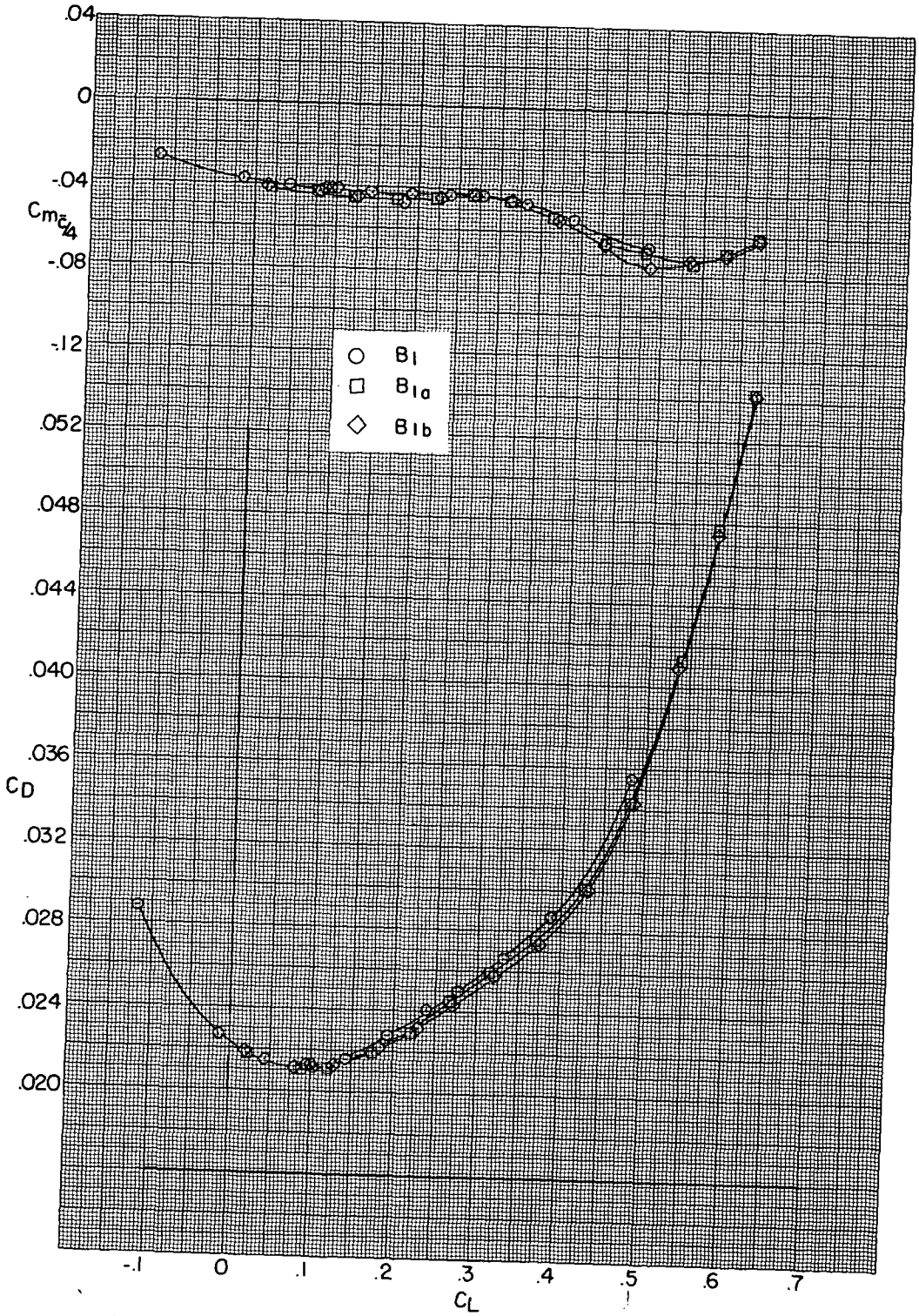

(d) M = 0.97.

Figure 22.- Continued.

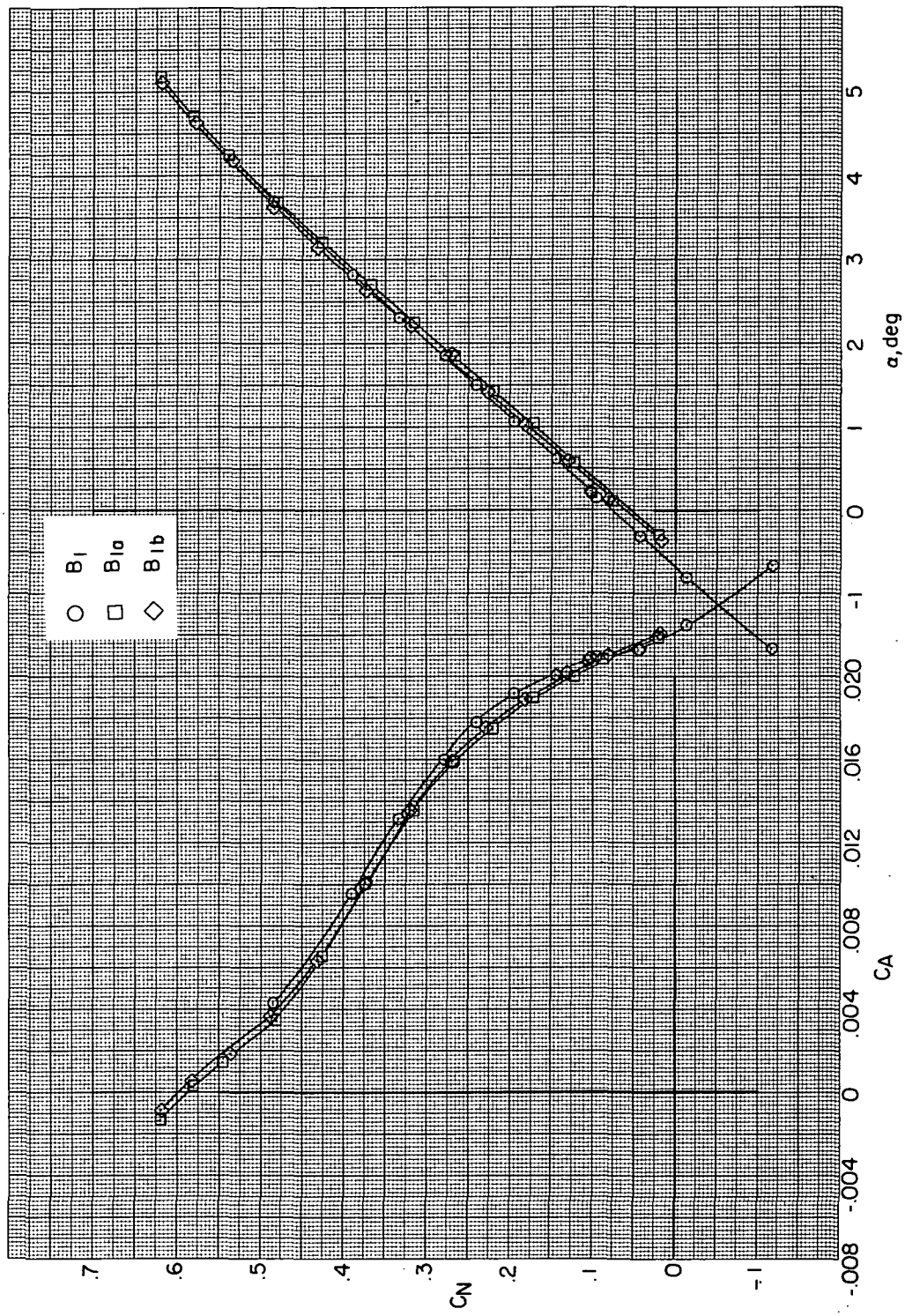

(d) Concluded.

Figure 22.- Continued.

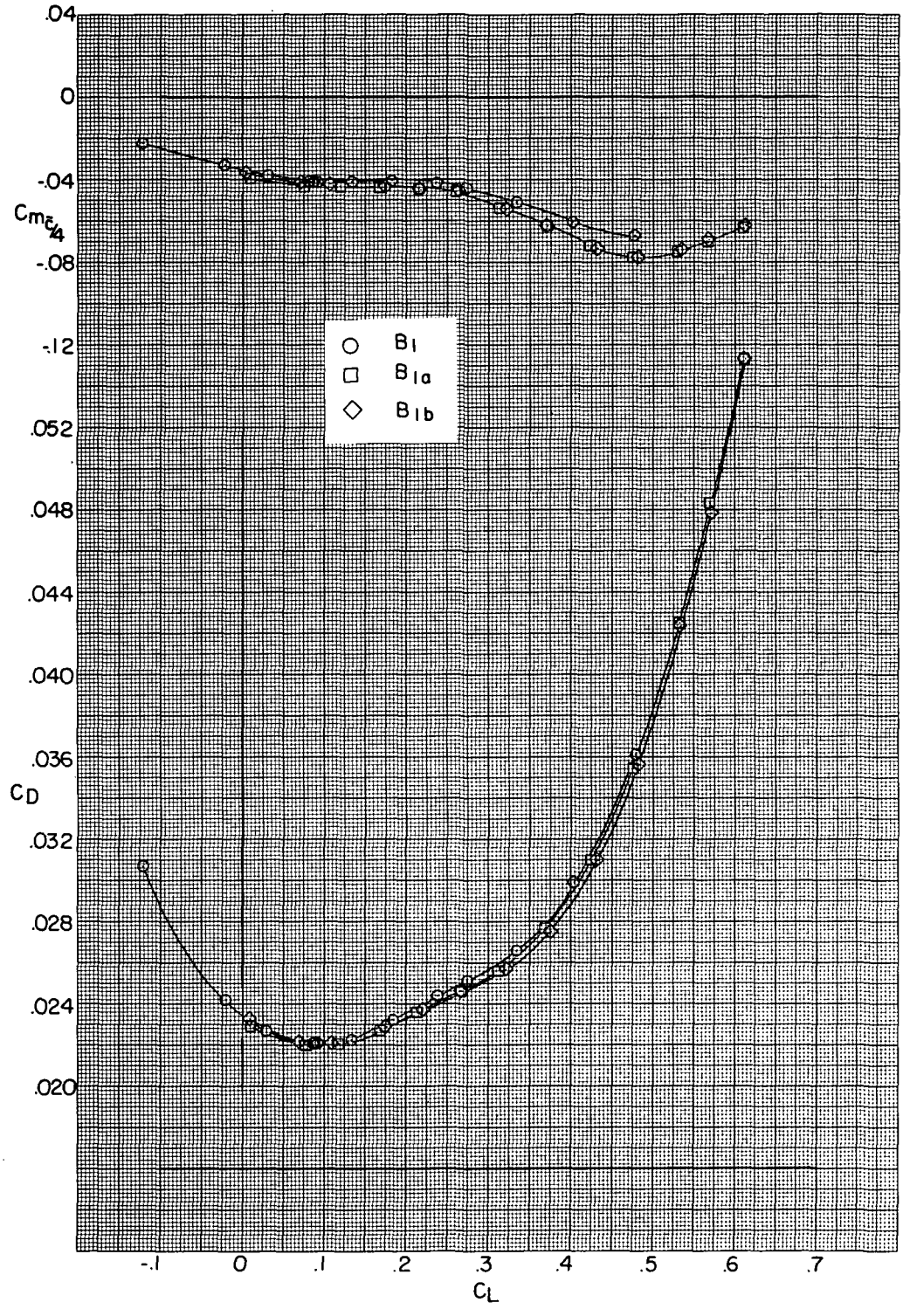

(e) M = 0.98.

Figure 22.- Continued.

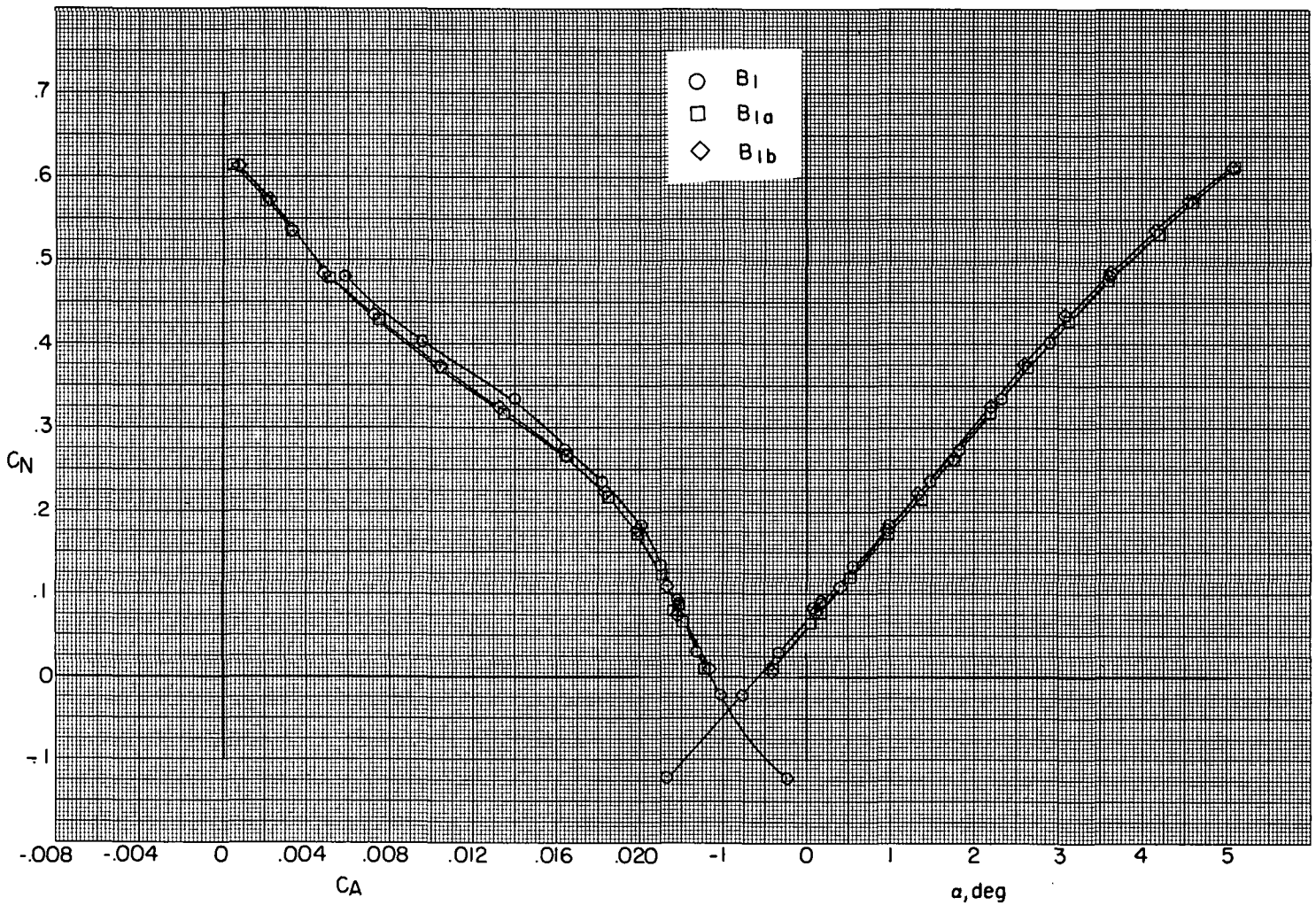

(e) Concluded.

Figure 22.- Continued.

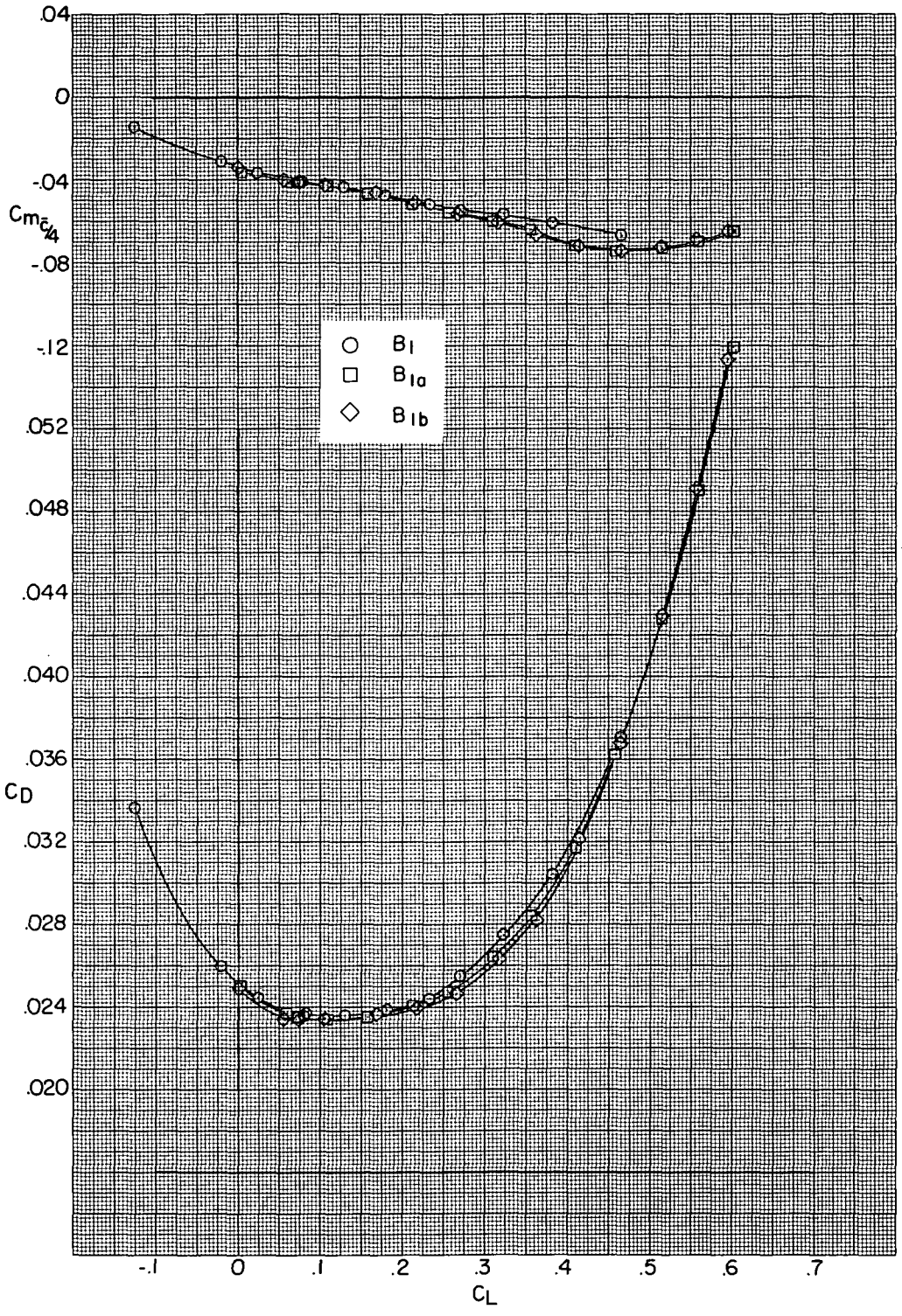

(f) M = 0.99.

Figure 22.- Continued.

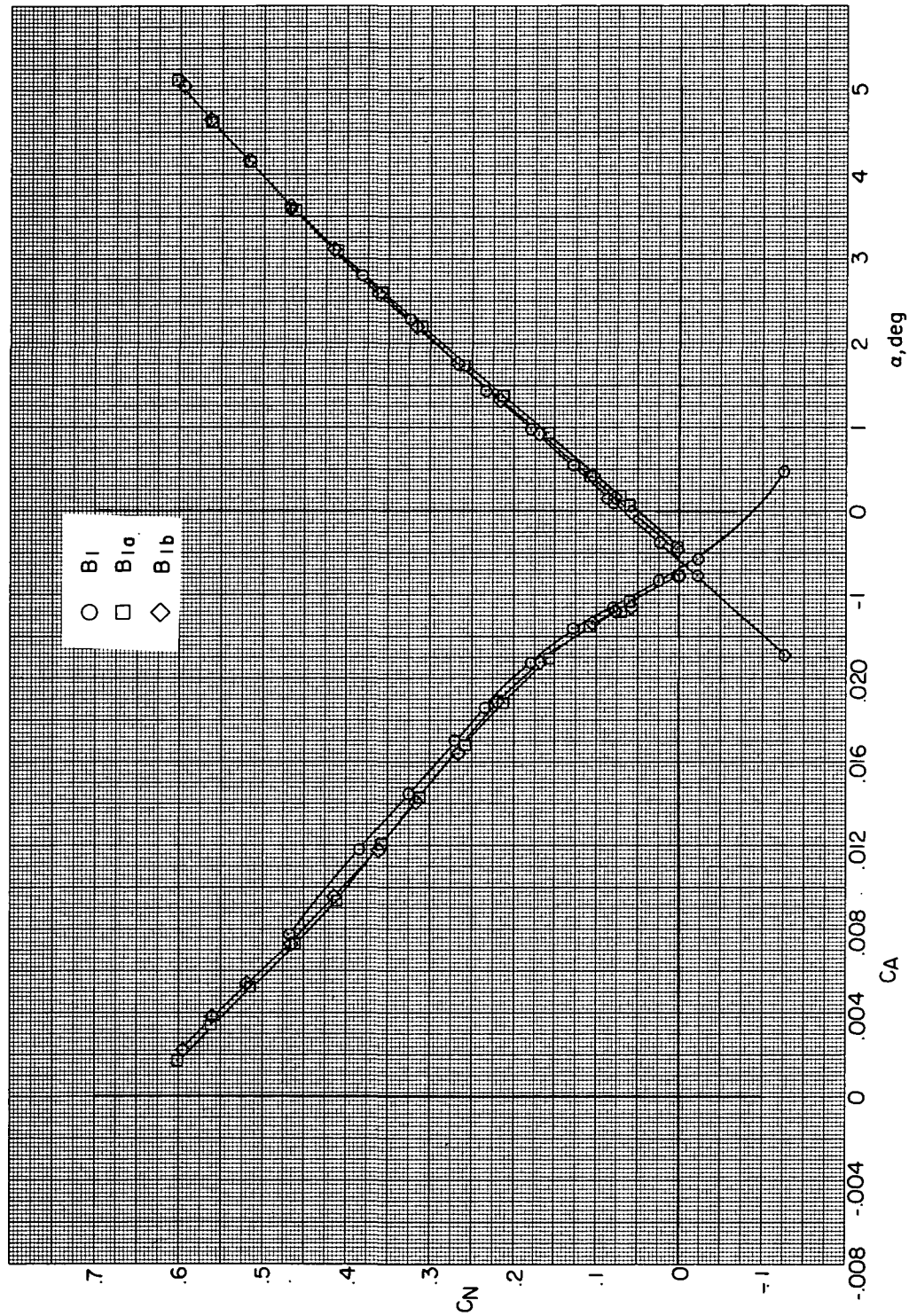

(f) Concluded.

Figure 22.- Concluded.

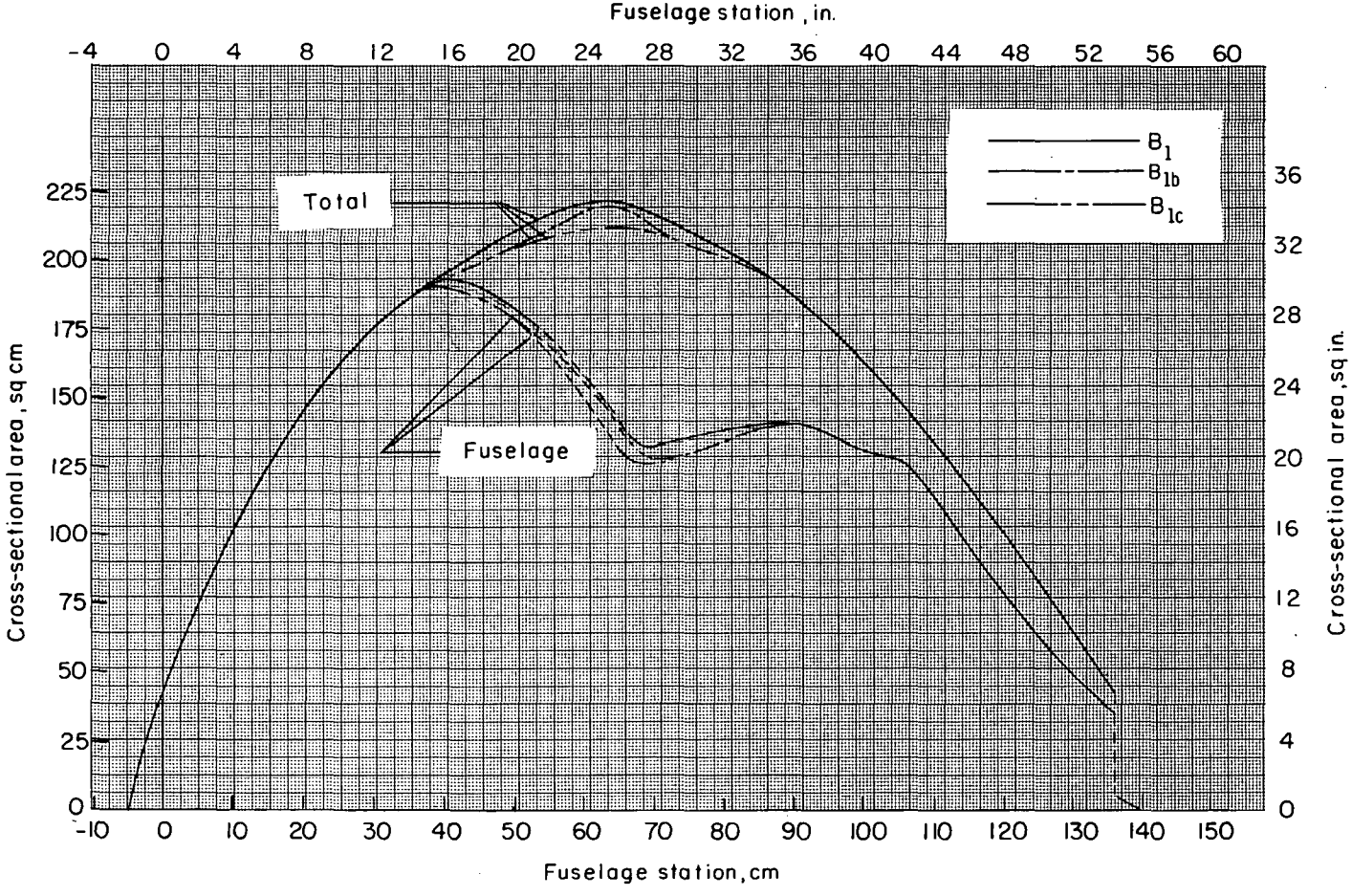

Figure 23.- Comparison of cross-sectional area distributions of configurations B_1, B_{1b}, and B_{1c}.

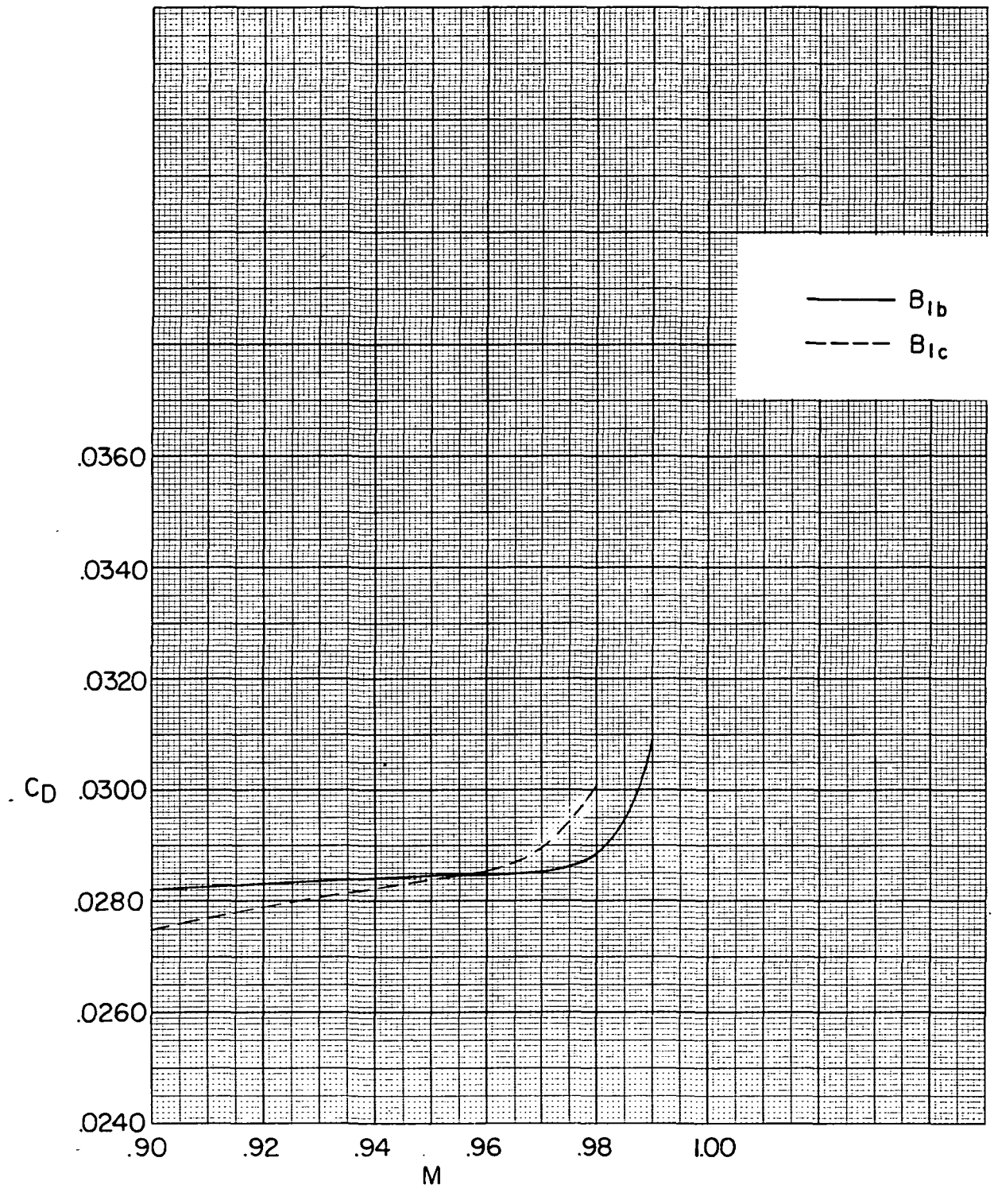

Figure 24.- Comparison of drag-rise characteristics for configurations B_{1b} and B_{1c}. $C_L = 0.40$.

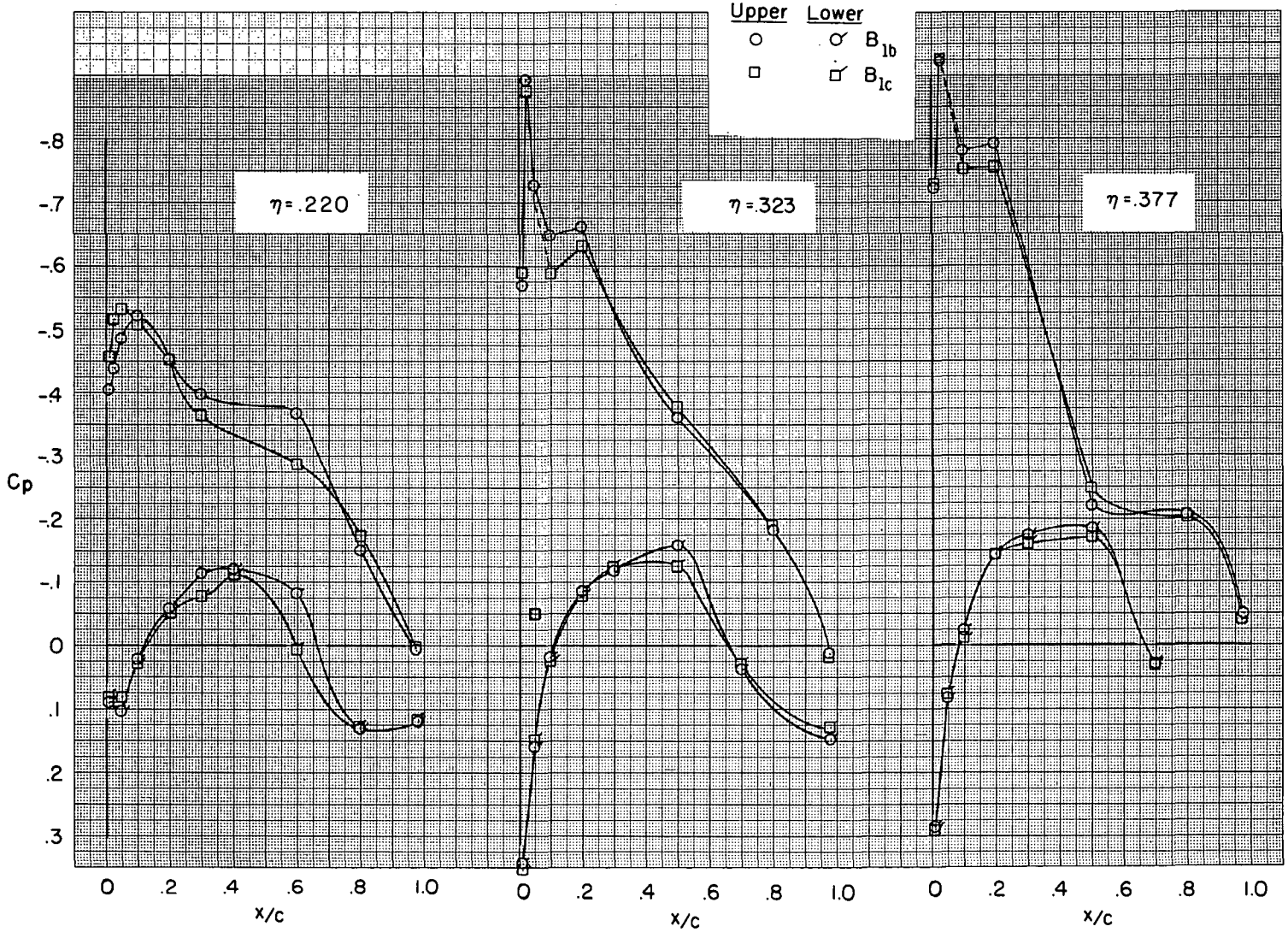

(a) M = 0.90.

Figure 25.- Wing pressure distributions for configurations B_{1b} and B_{1c}. $C_L \approx 0.40$.

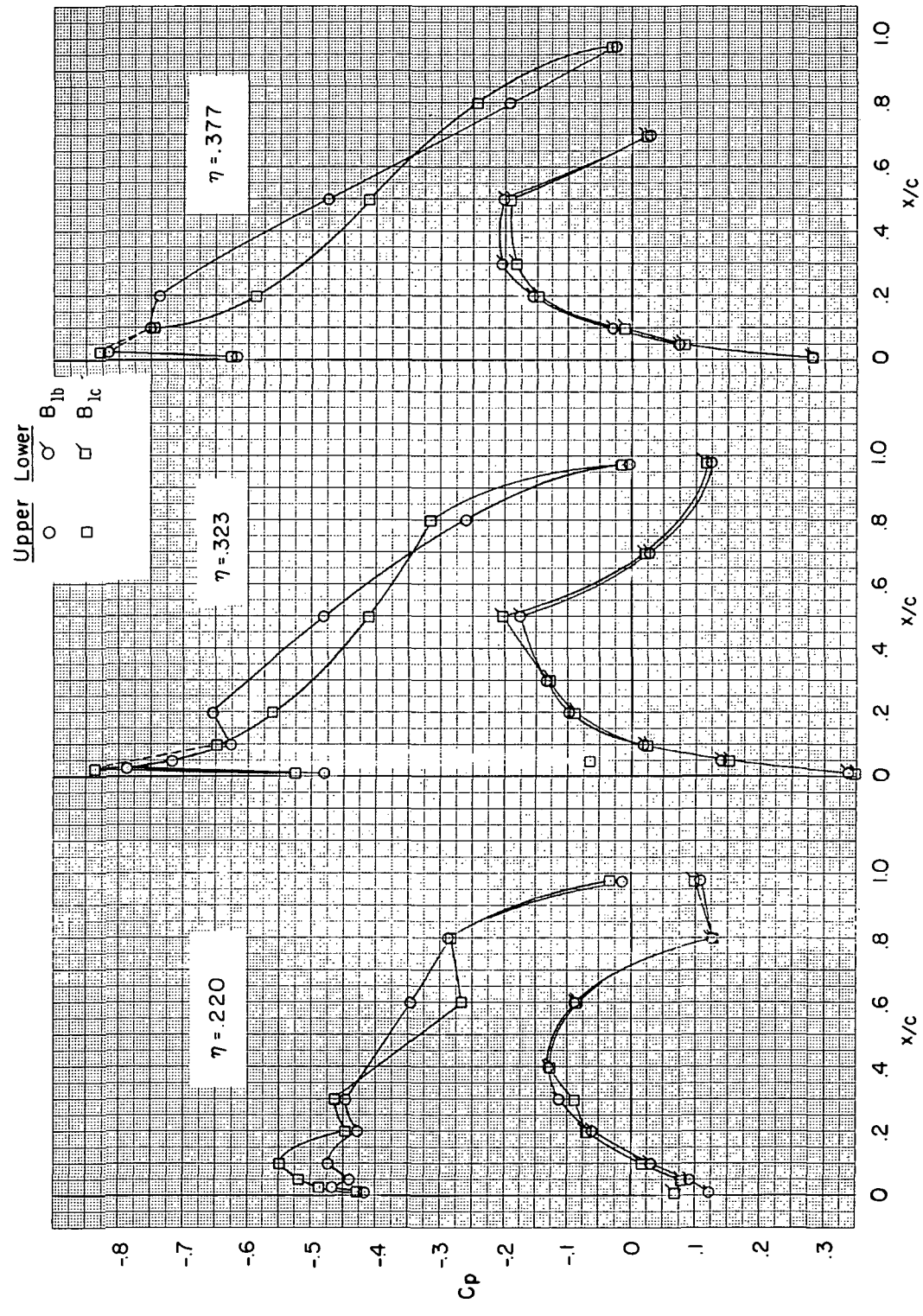

(b) M = 0.95.

Figure 25.- Continued.

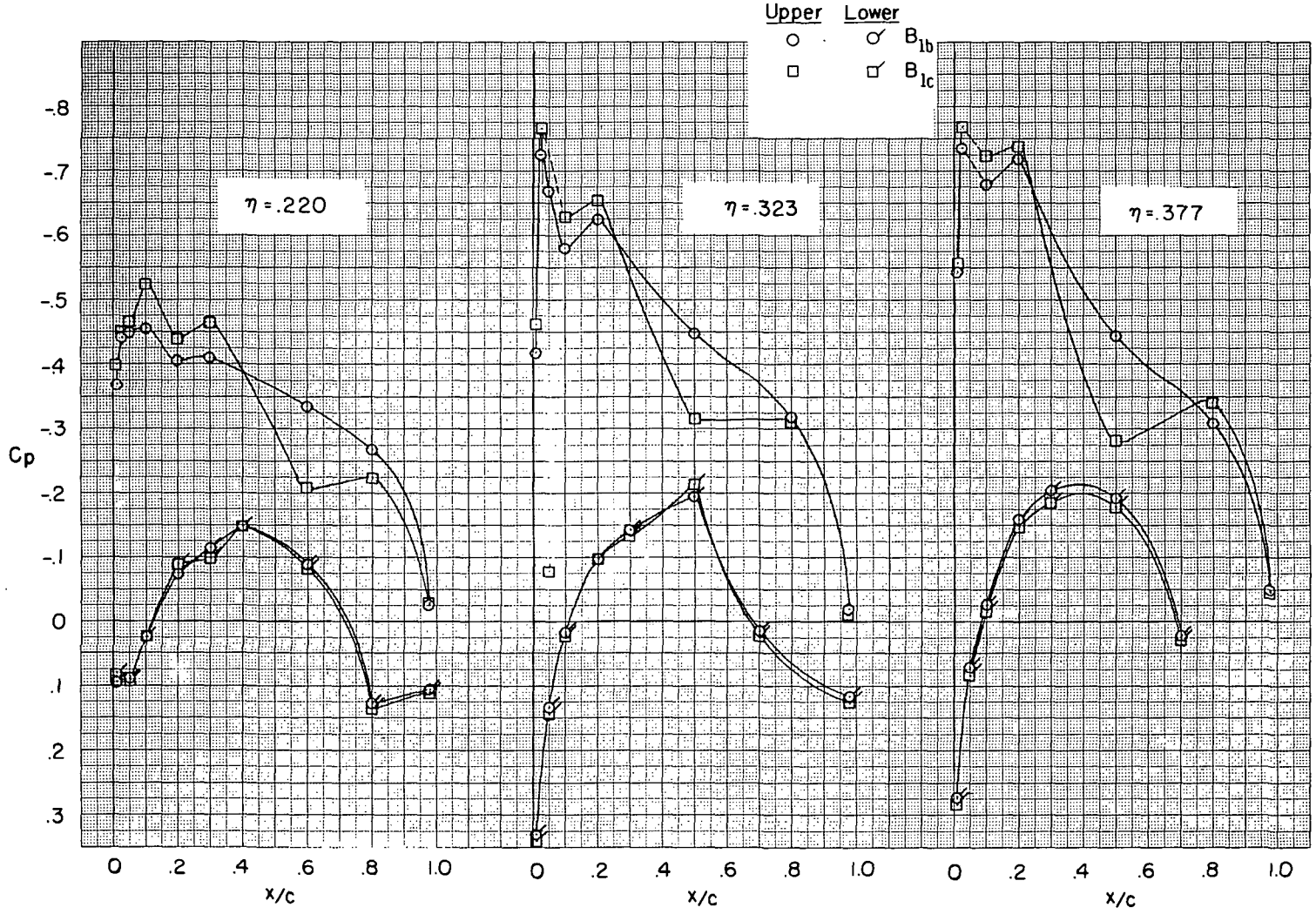

(c) M = 0.98.

Figure 25.- Concluded.

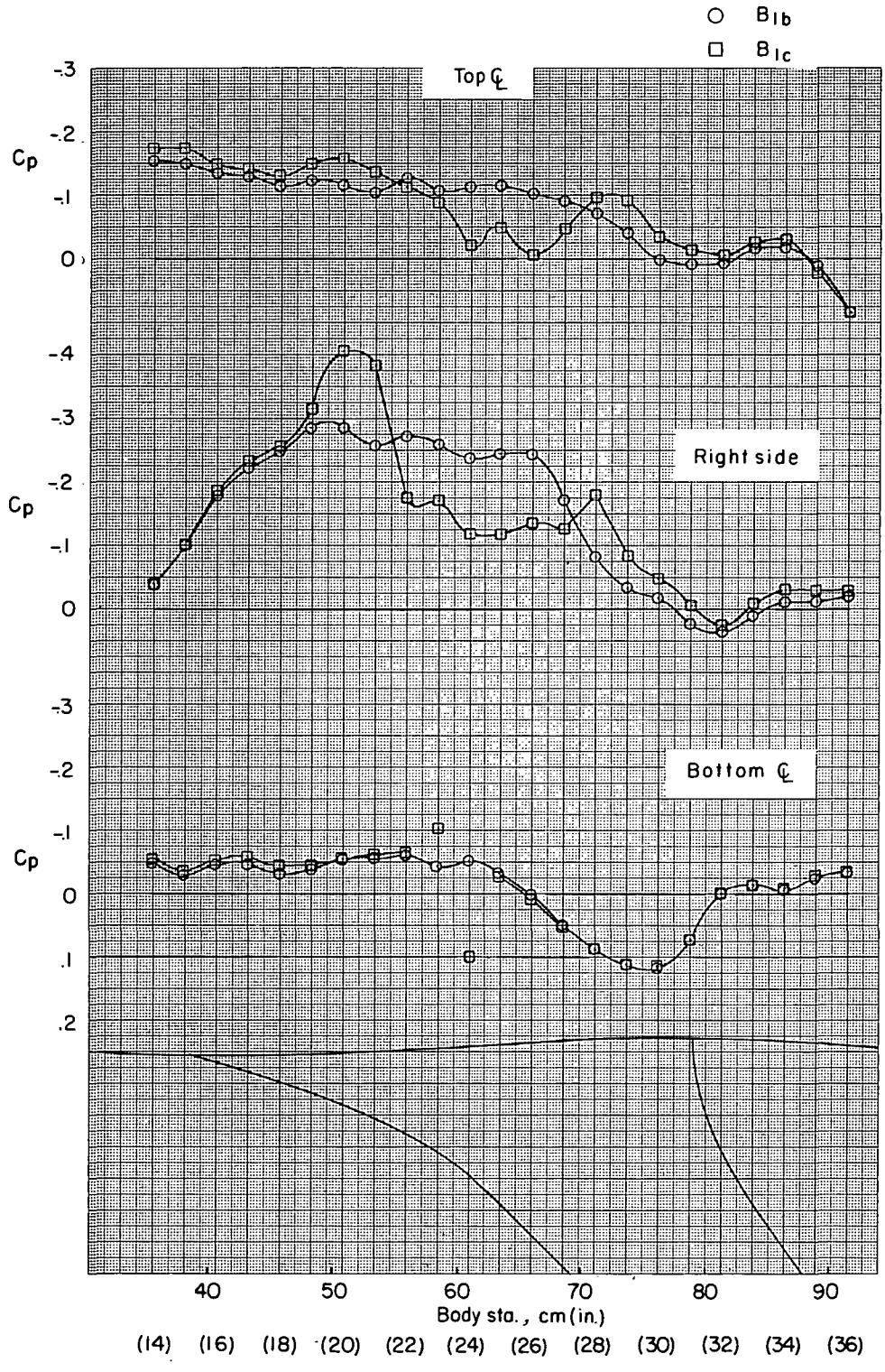

(a) M = 0.90.

Figure 26.- Fuselage pressure distributions for configurations B_{1b} and B_{1c}. $C_L \approx 0.40$.

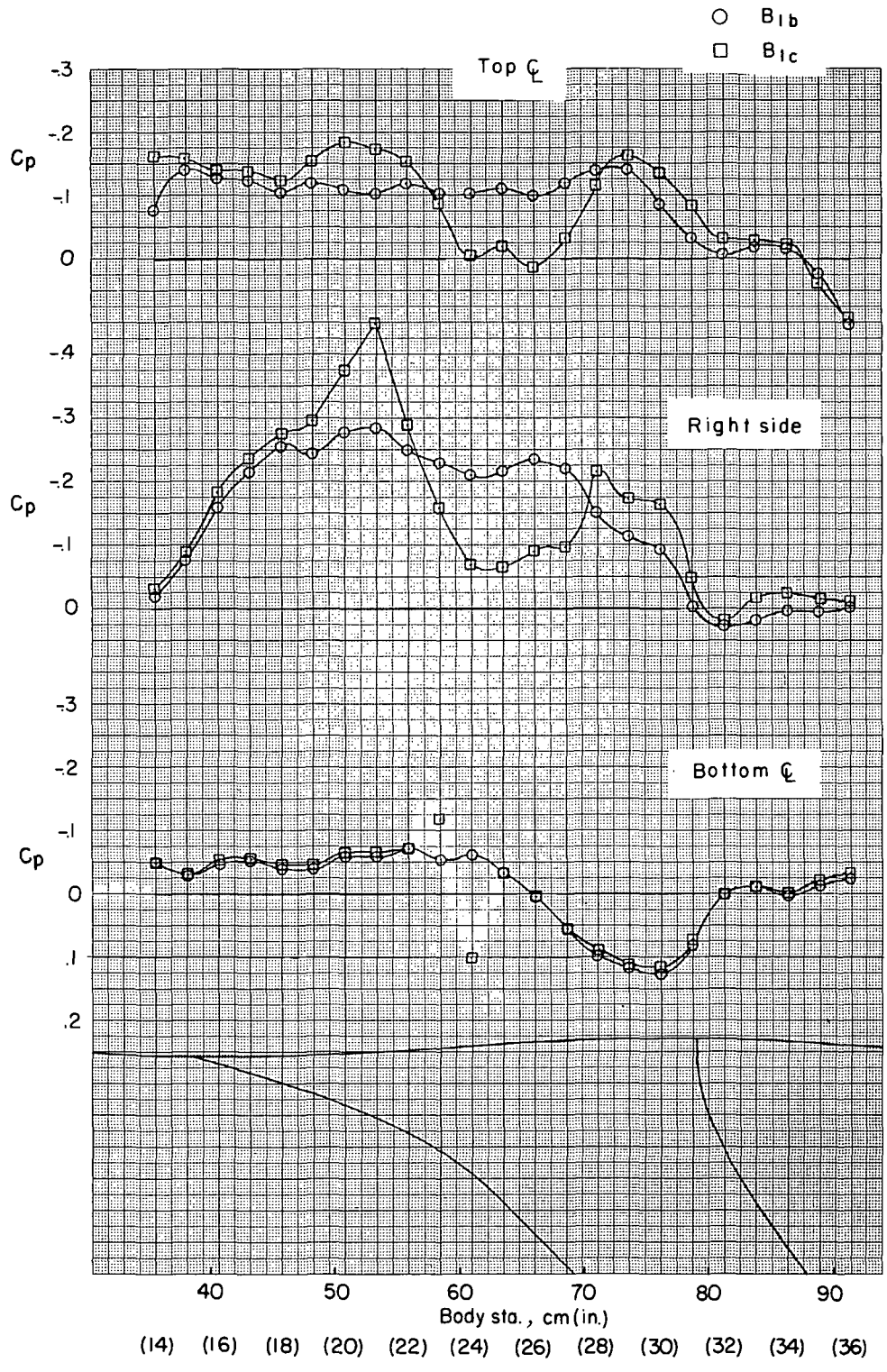

(b) M = 0.95.

Figure 26.- Continued.

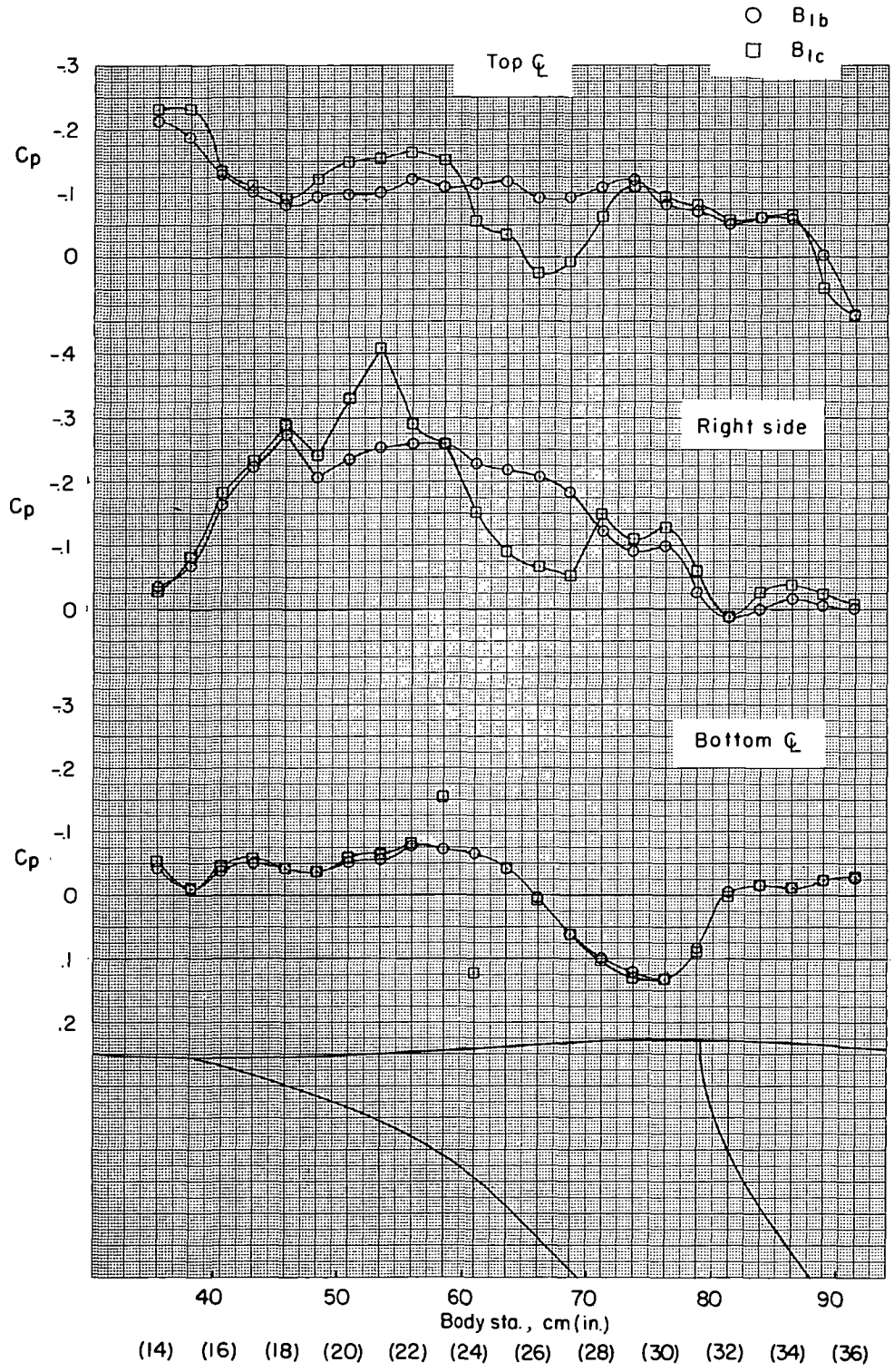

(c) M = 0.98.

Figure 26.- Concluded.

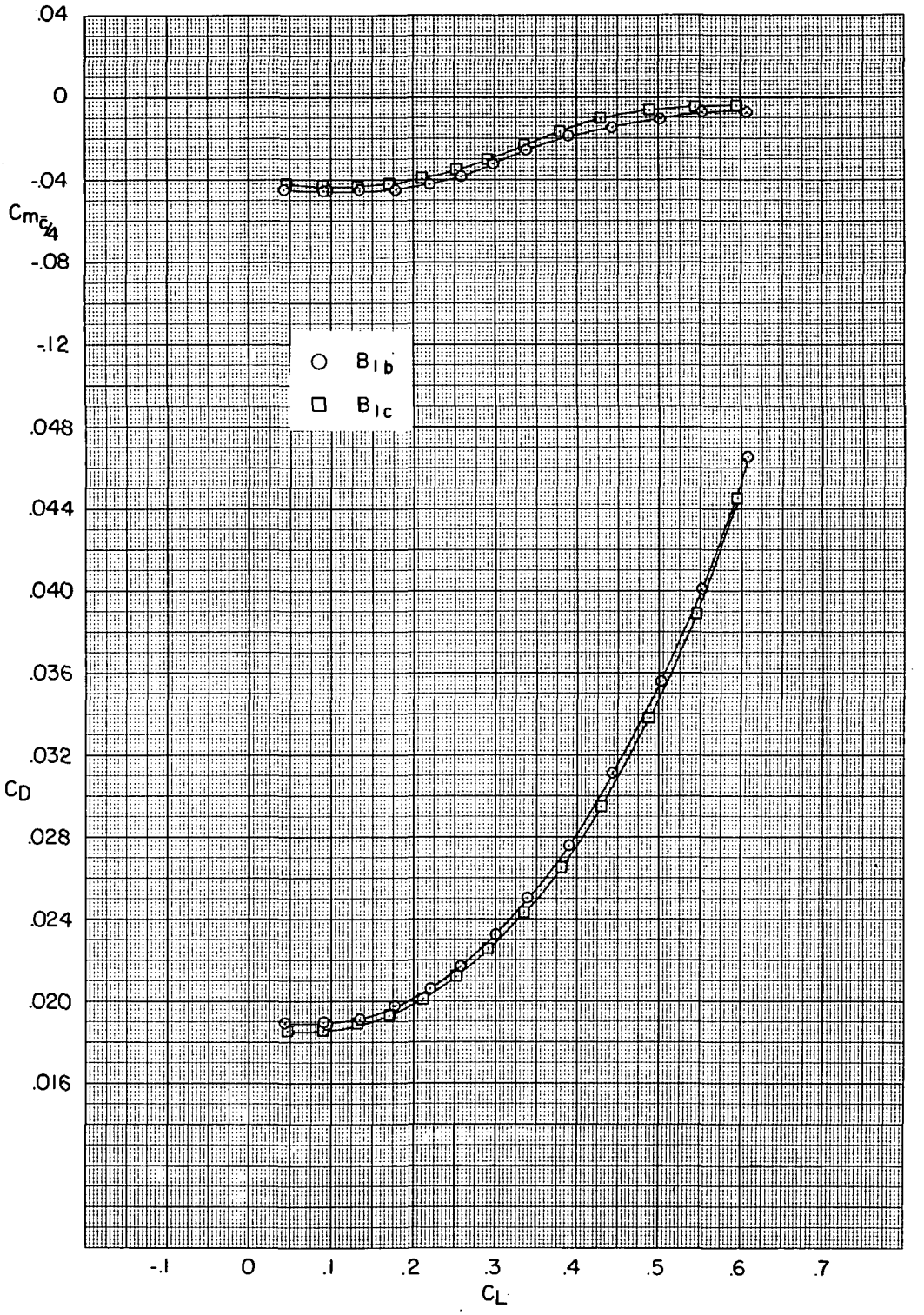

(a) M = 0.90.

Figure 27.- Longitudinal aerodynamic data for configurations B_{1b} and B_{1c}.

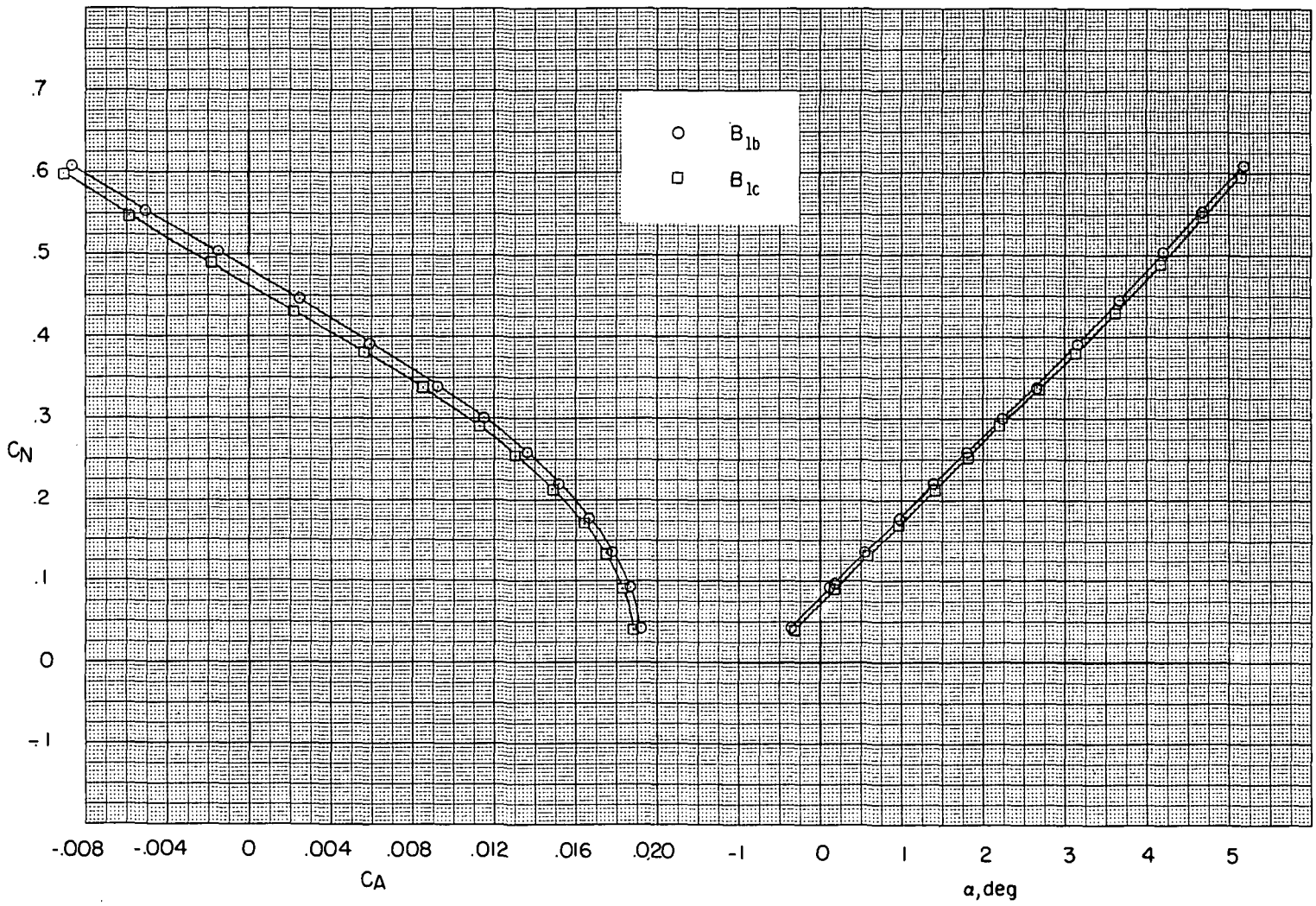

(a) Concluded.

Figure 27.- Continued.

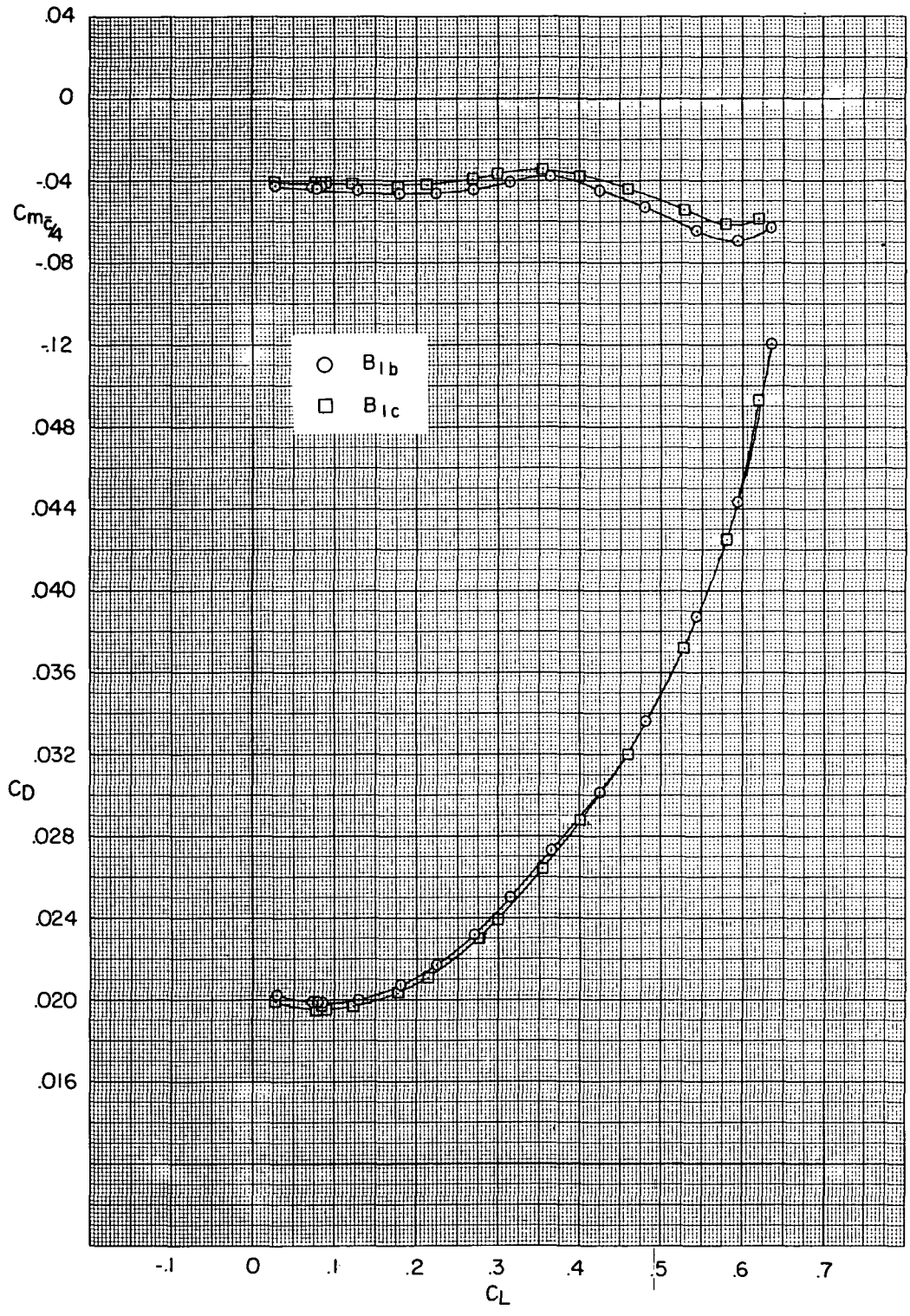

(b) M = 0.95.

Figure 27.- Continued.

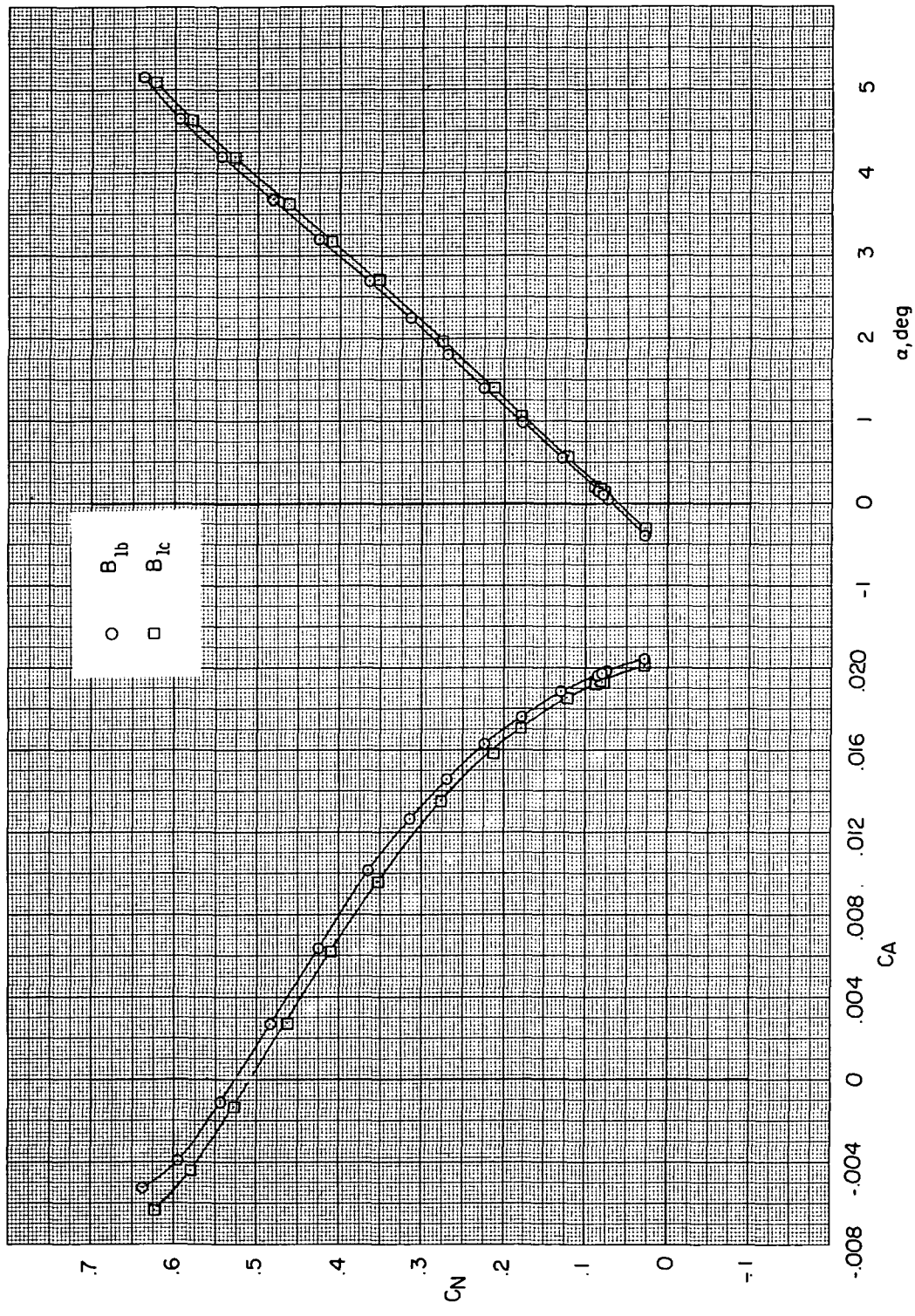

(b) Concluded.

Figure 27.- Continued.

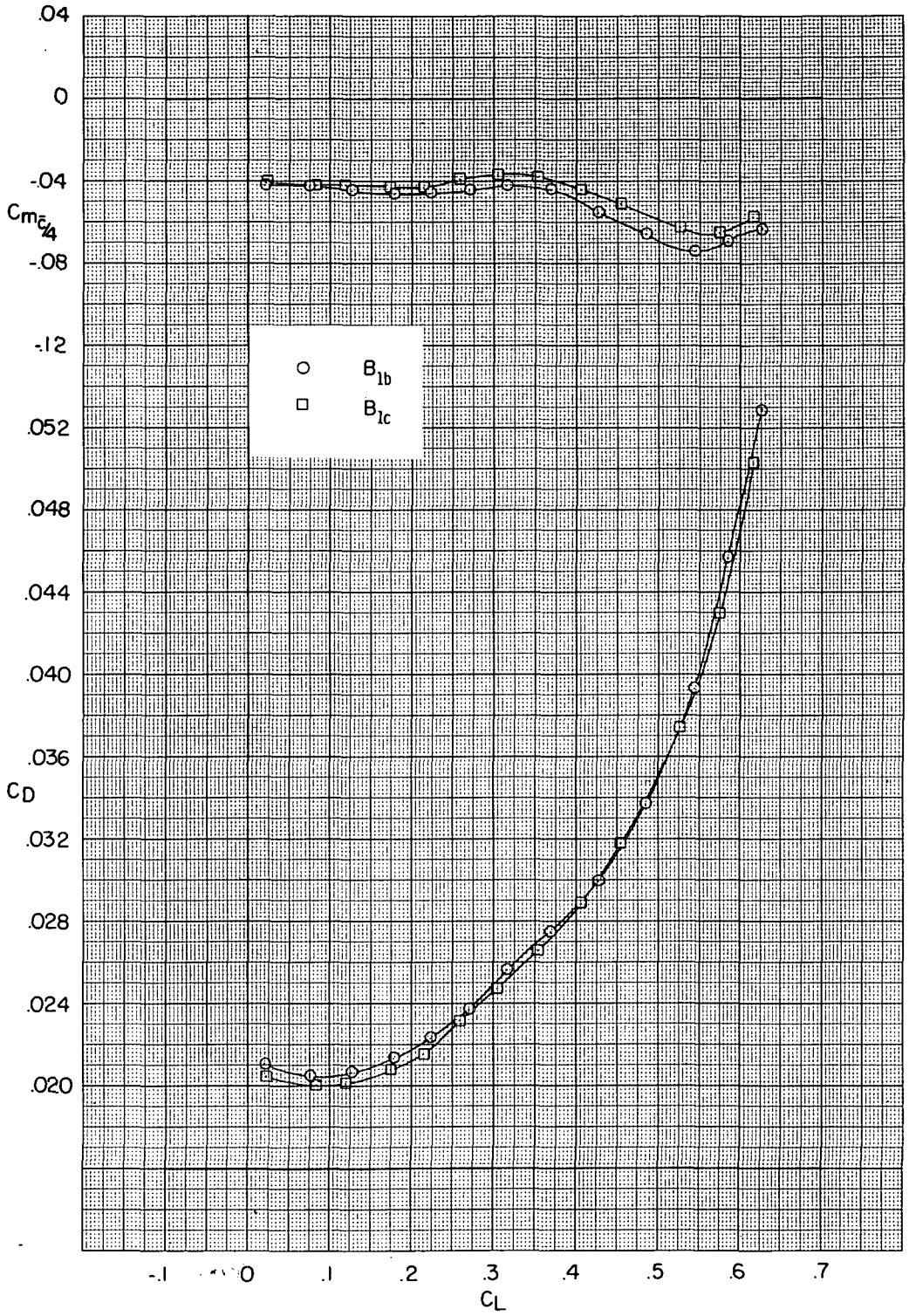

(c) M = 0.96.

Figure 27.- Continued.

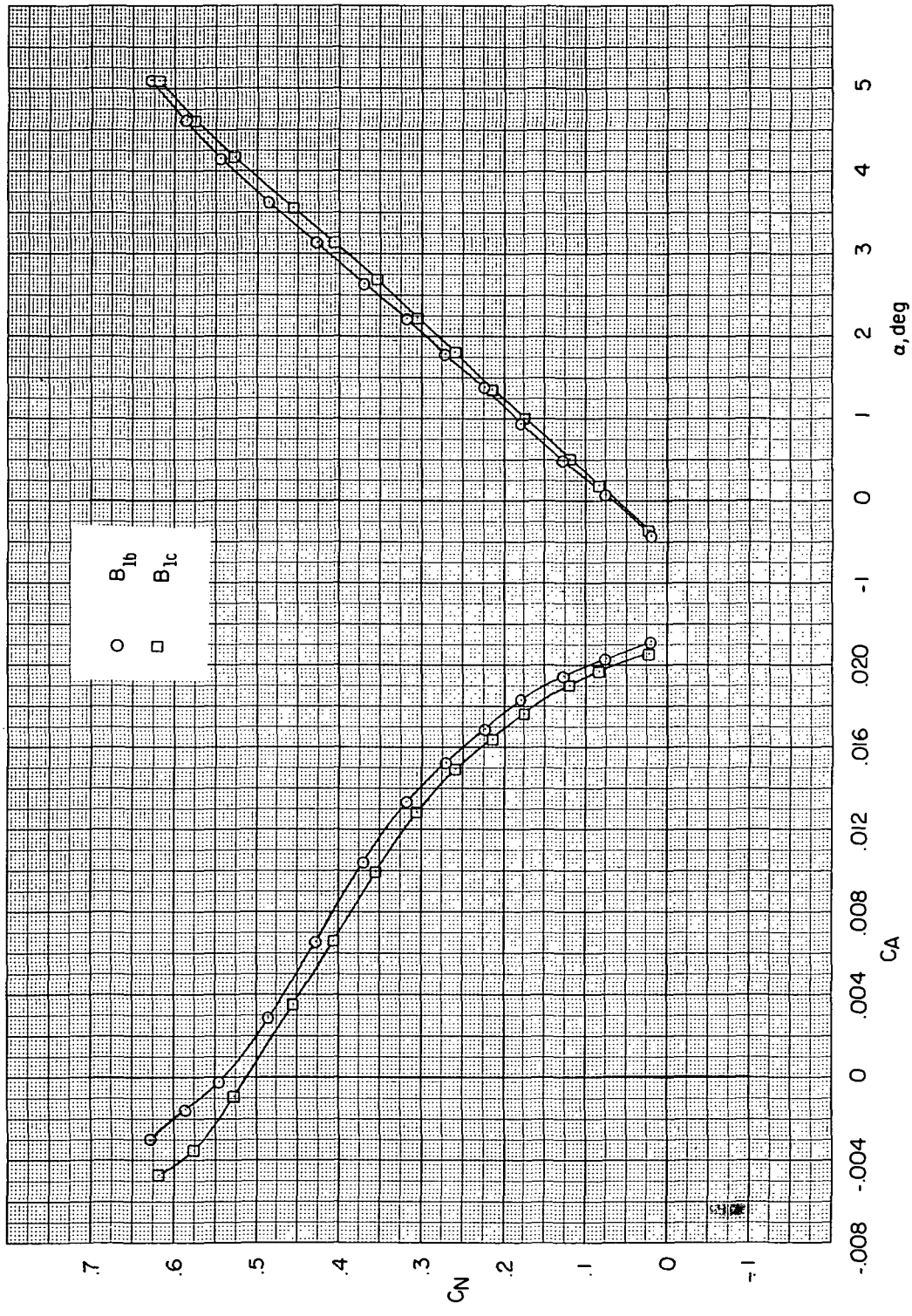

(c) Concluded.

Figure 27.- Continued.

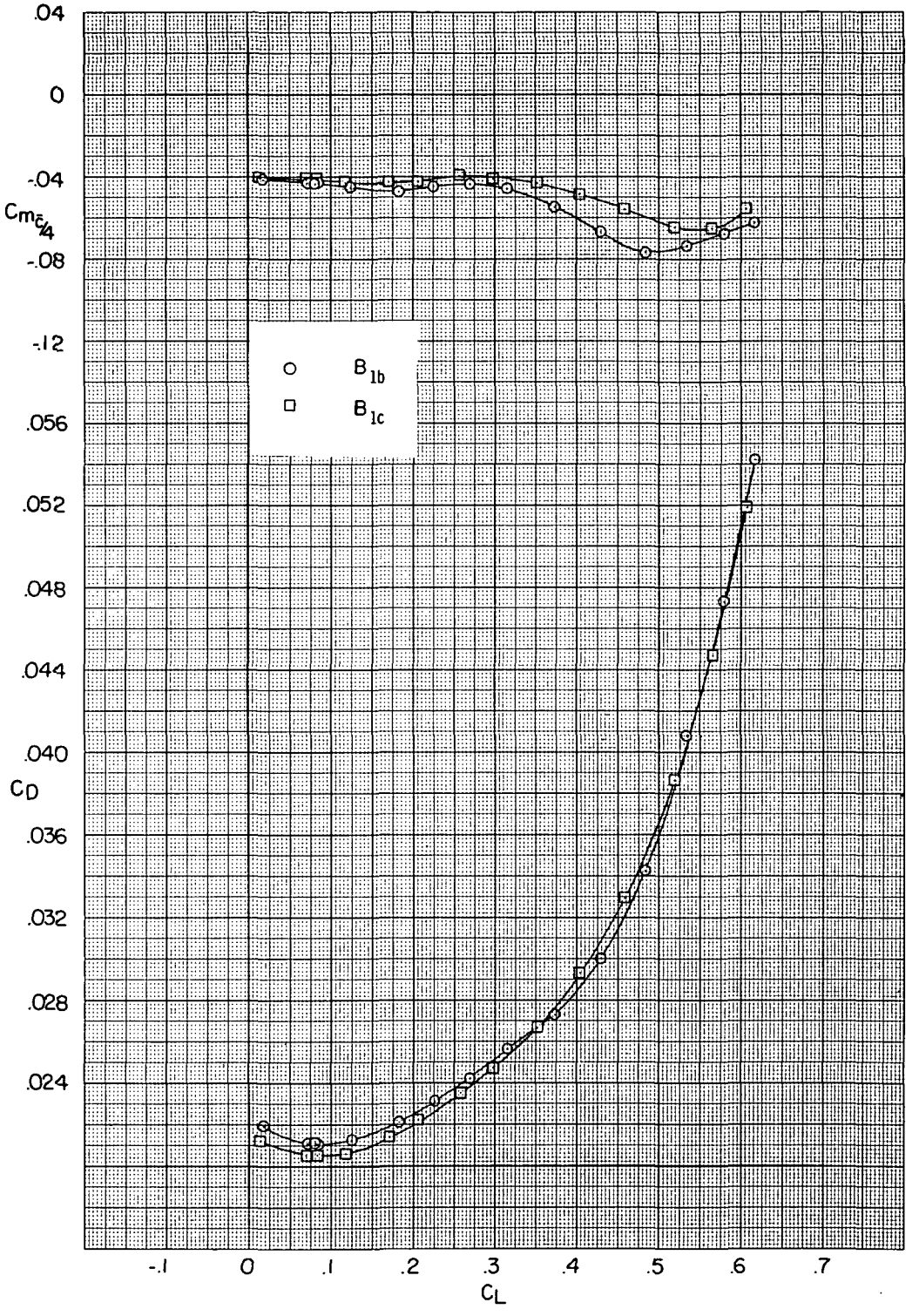

(d) M = 0.97.

Figure 27.- Continued.

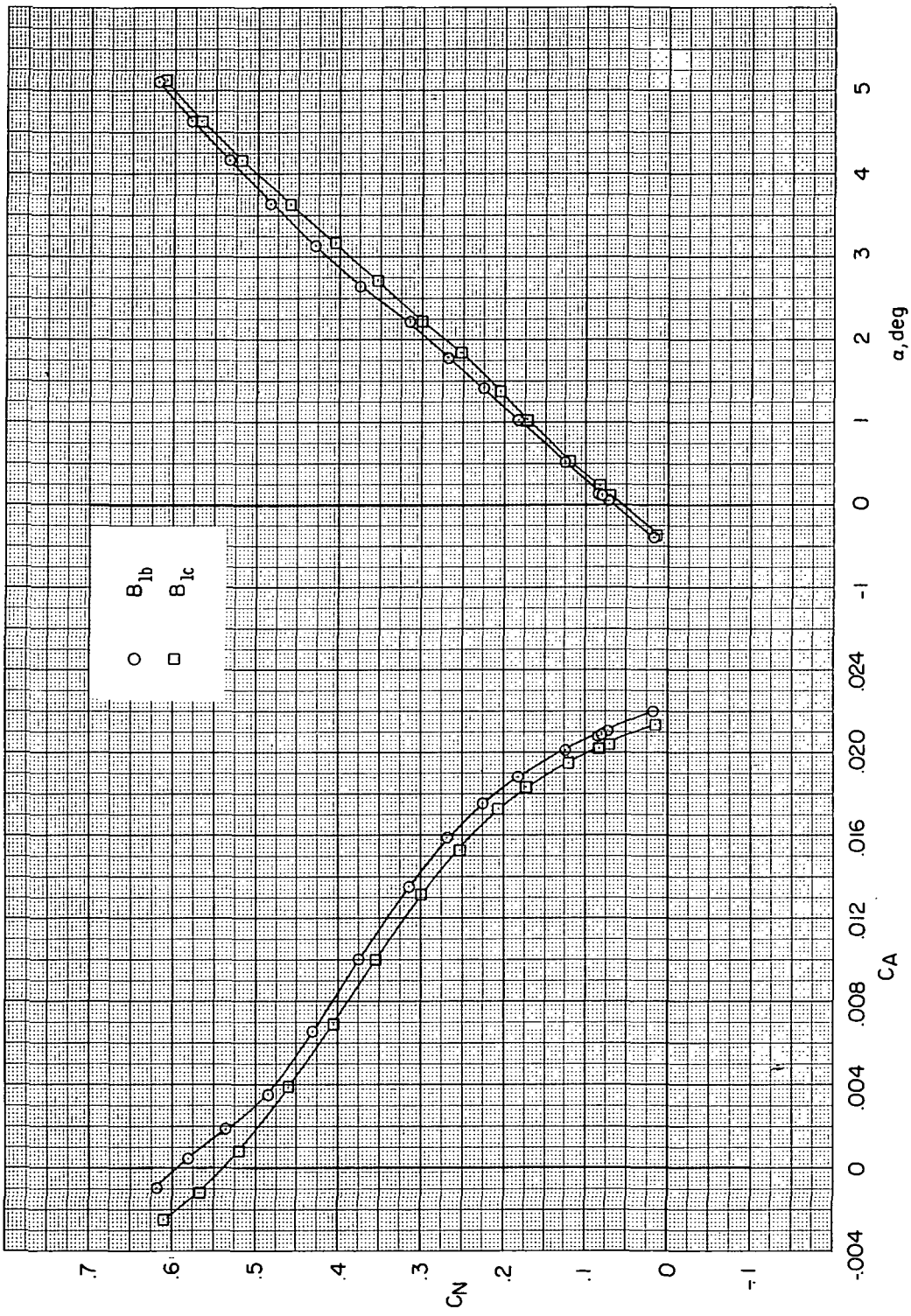

(d) Concluded.

Figure 27.- Continued.

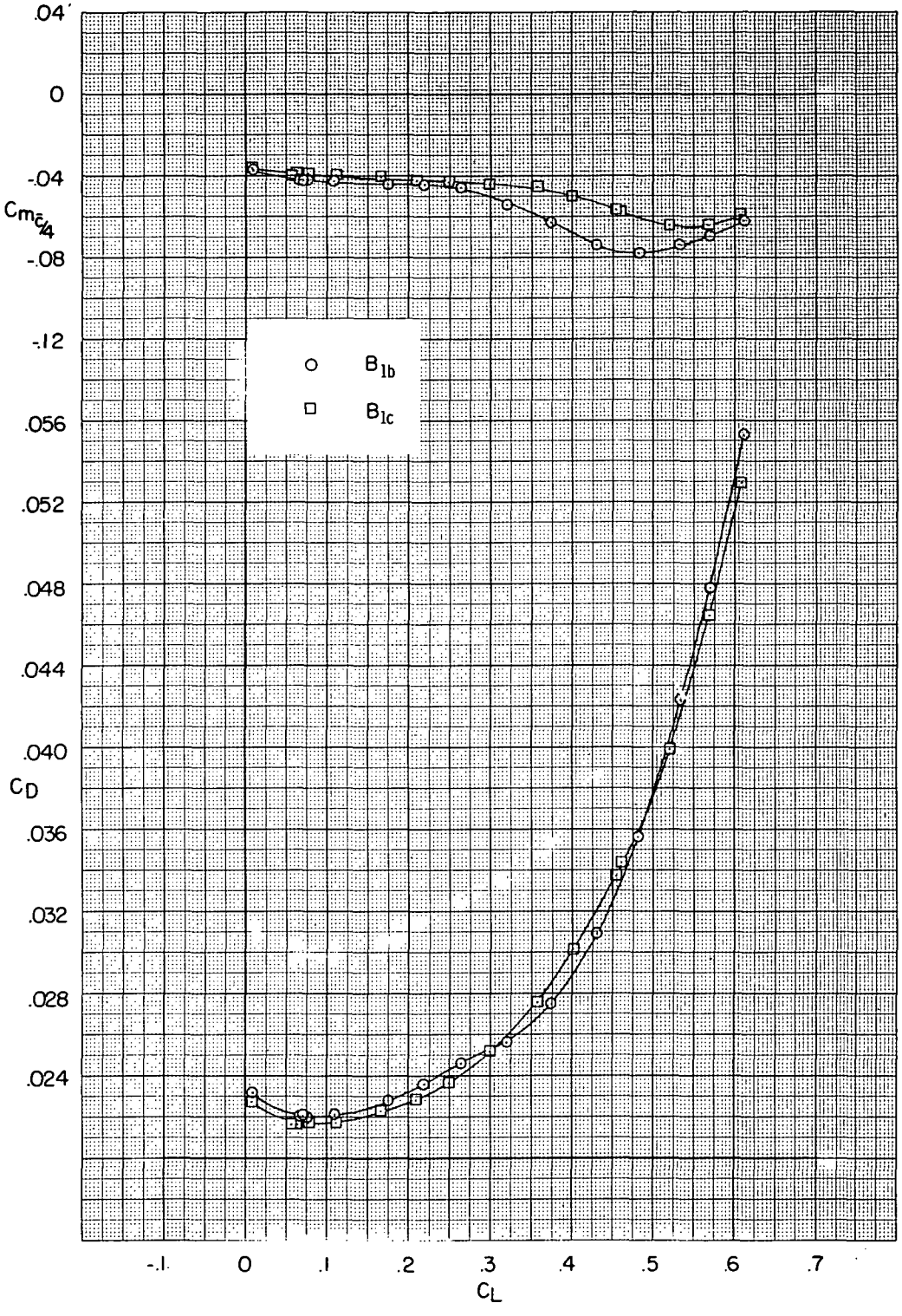

(e) M = 0.98.

Figure 27.- Continued.

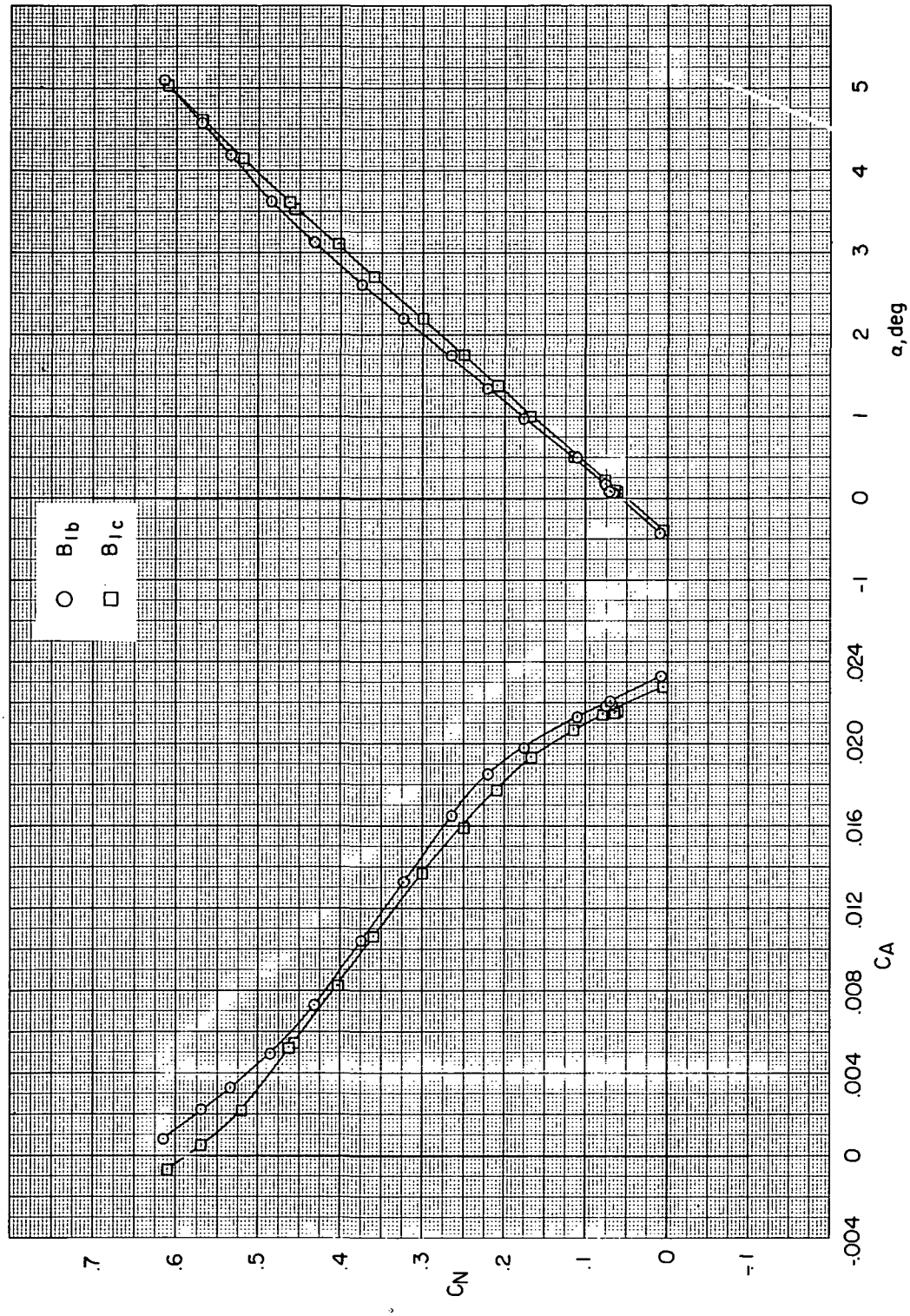

(e) Concluded.

Figure 27.- Concluded.

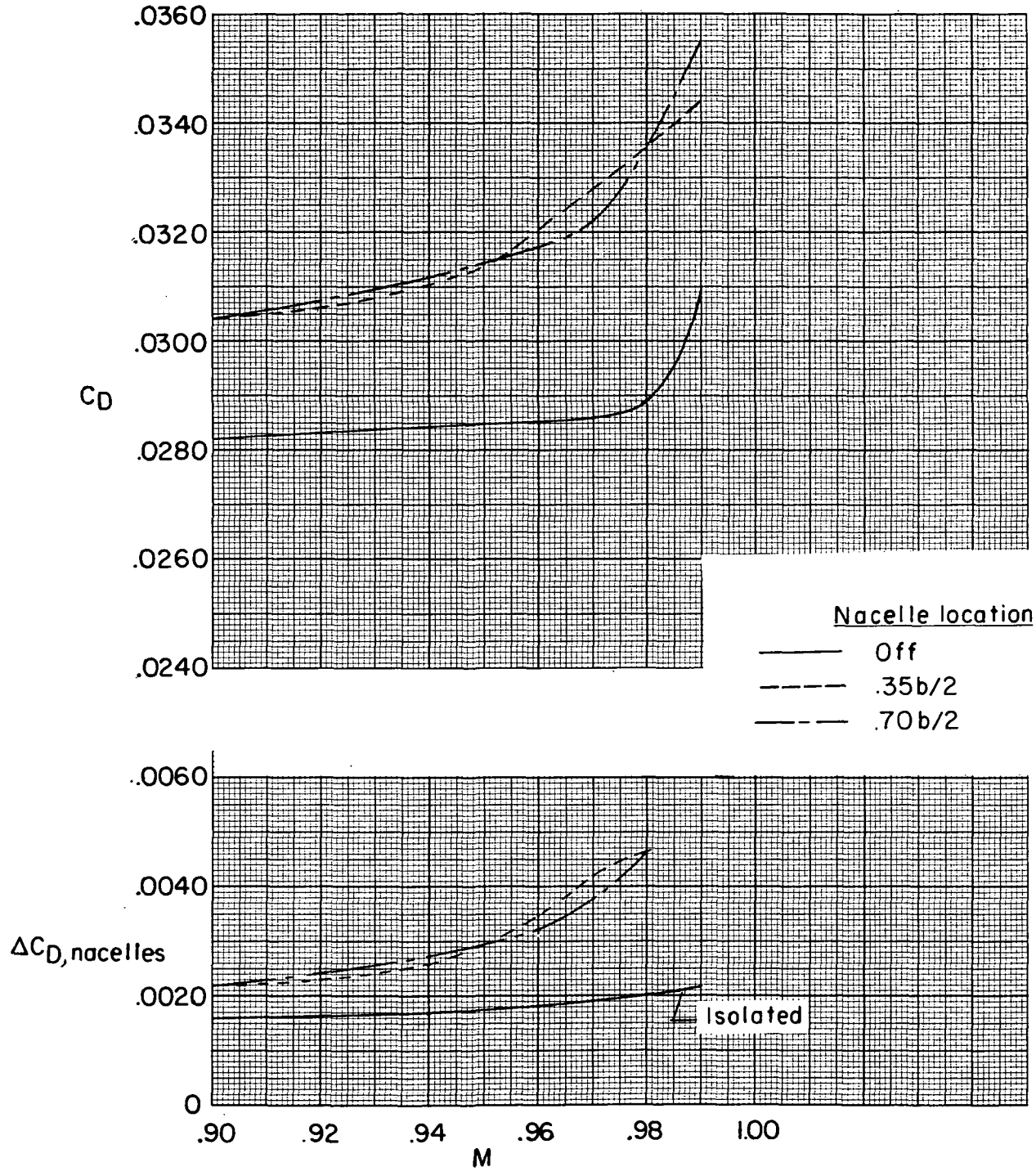

Figure 28.- Summary of nacelle installation on drag. No area ruling for nacelles. $C_L = 0.40$.

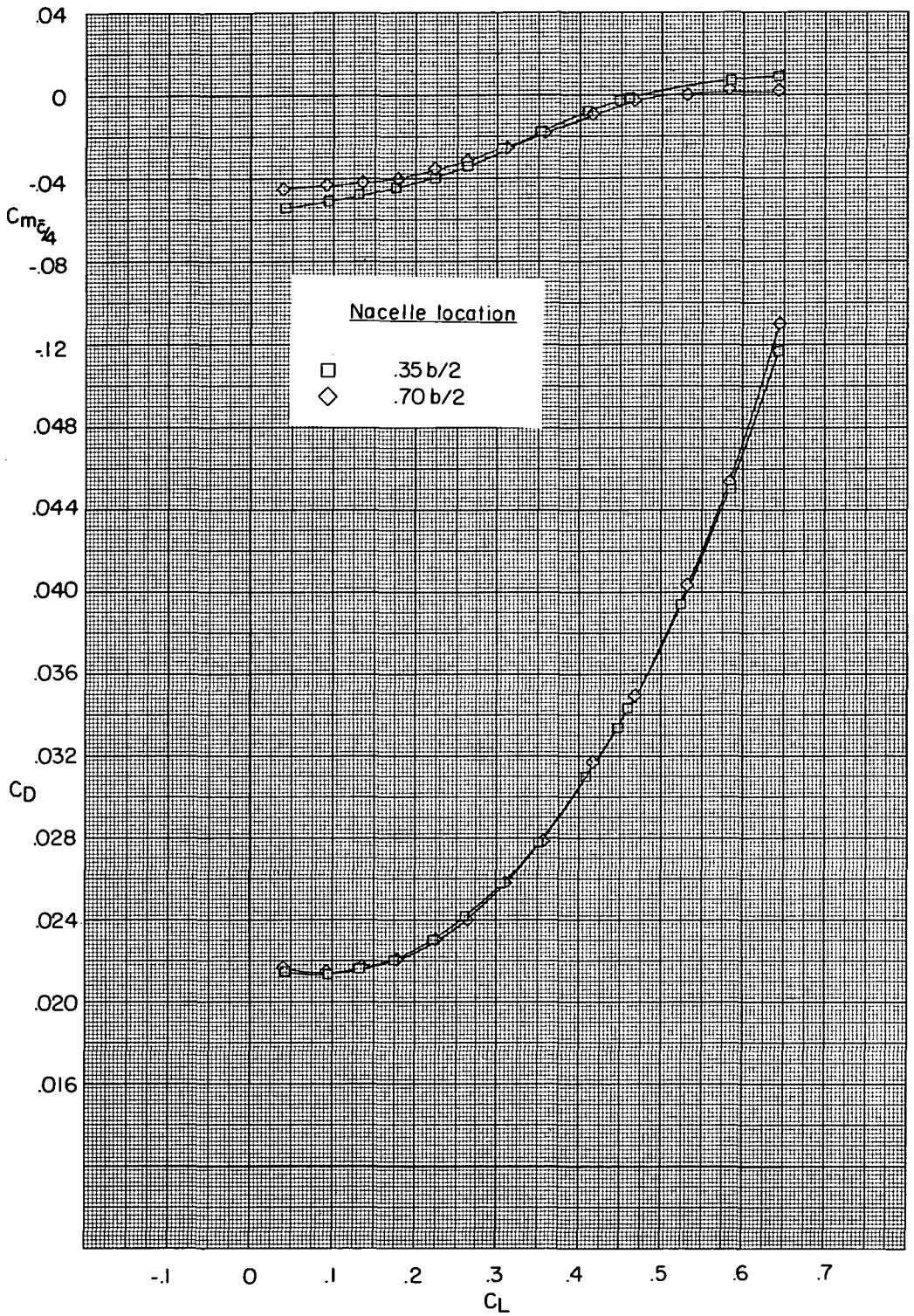

(a) M = 0.90.

Figure 29.- Effect of nacelle location on longitudinal aerodynamic data for the B_1 configuration with no area ruling for nacelles.

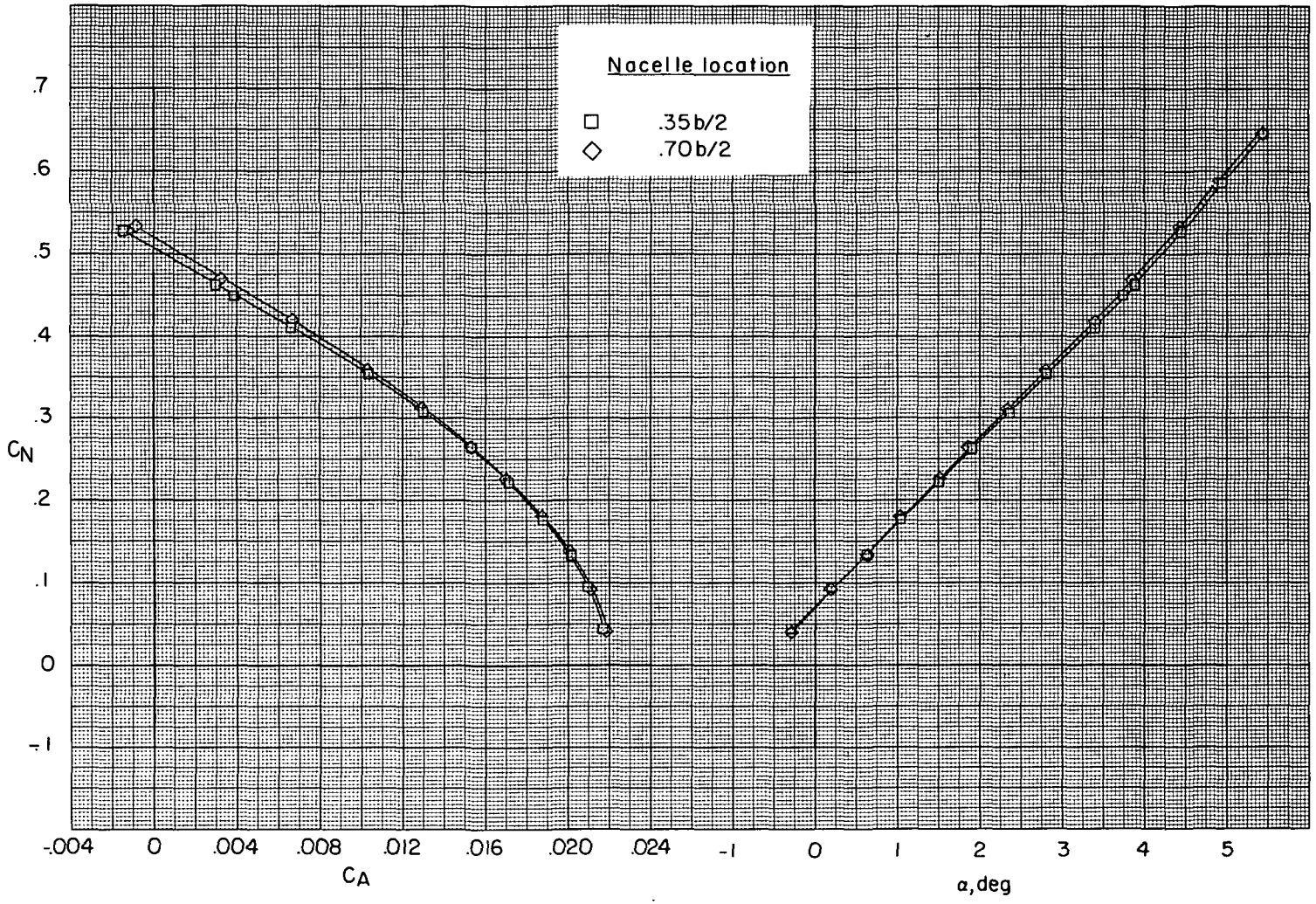

(a) Concluded.

Figure 29.- Continued.

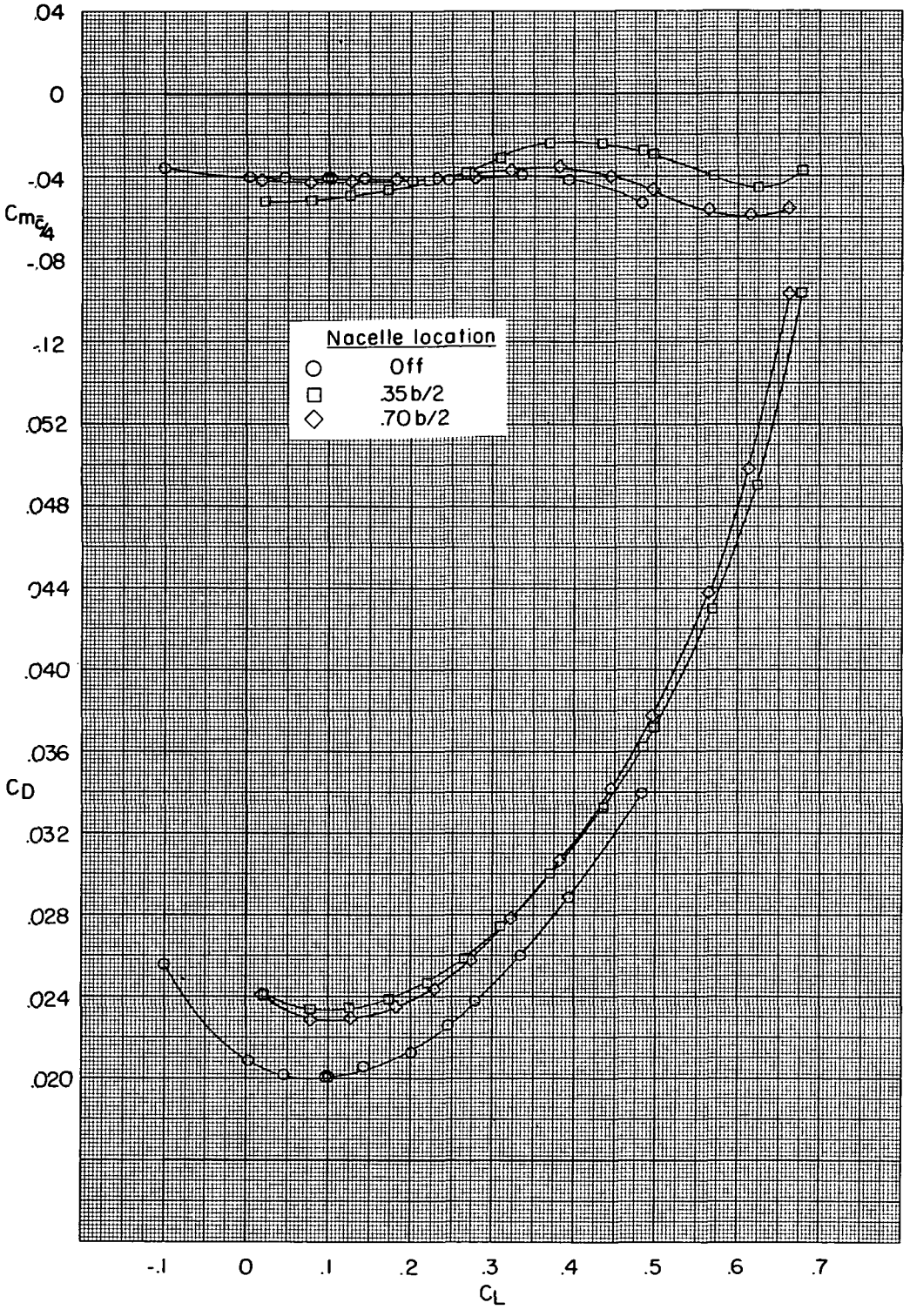

(b) M = 0.95.

Figure 29.- Continued.

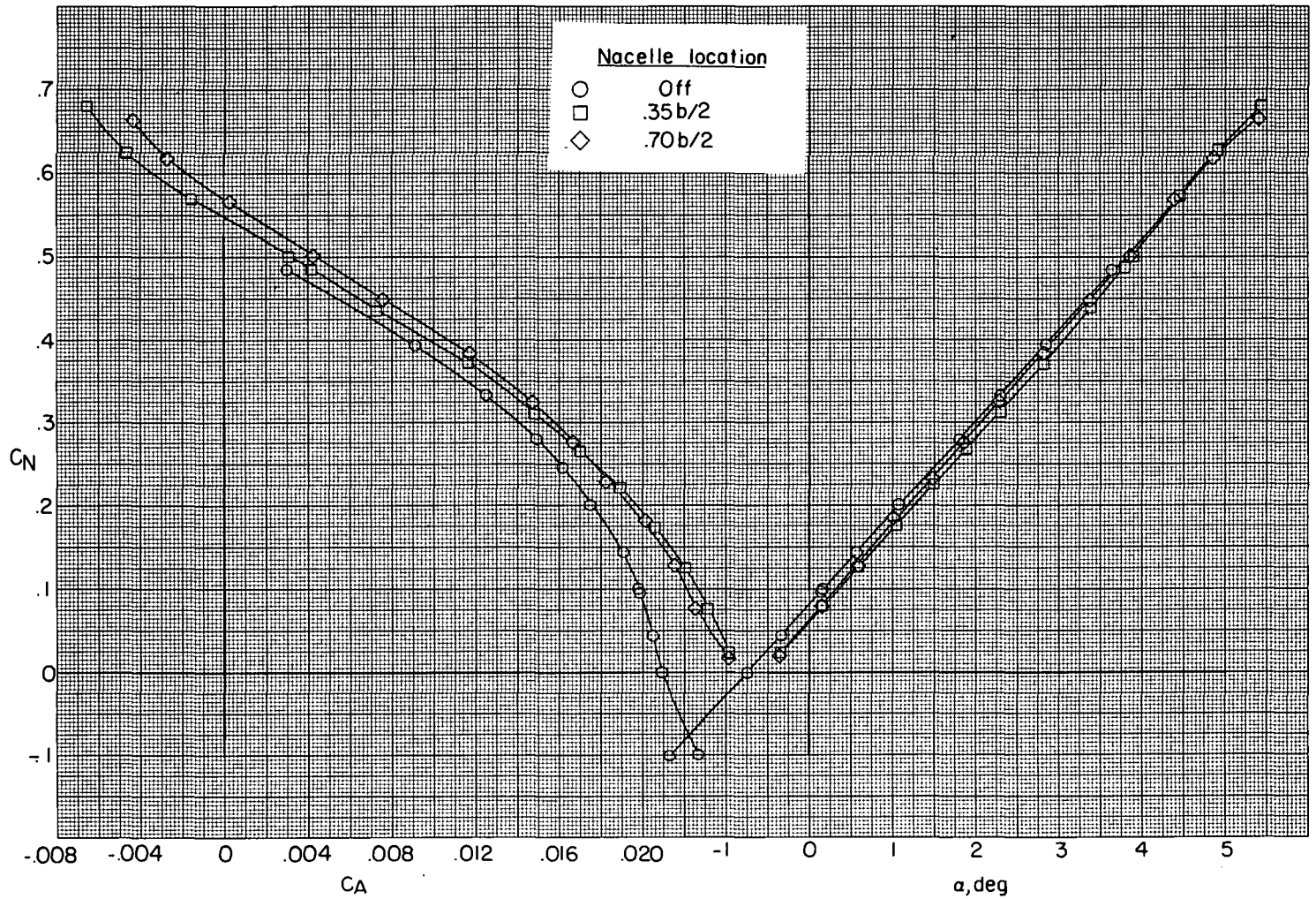

(b) Concluded.

Figure 29.- Continued.

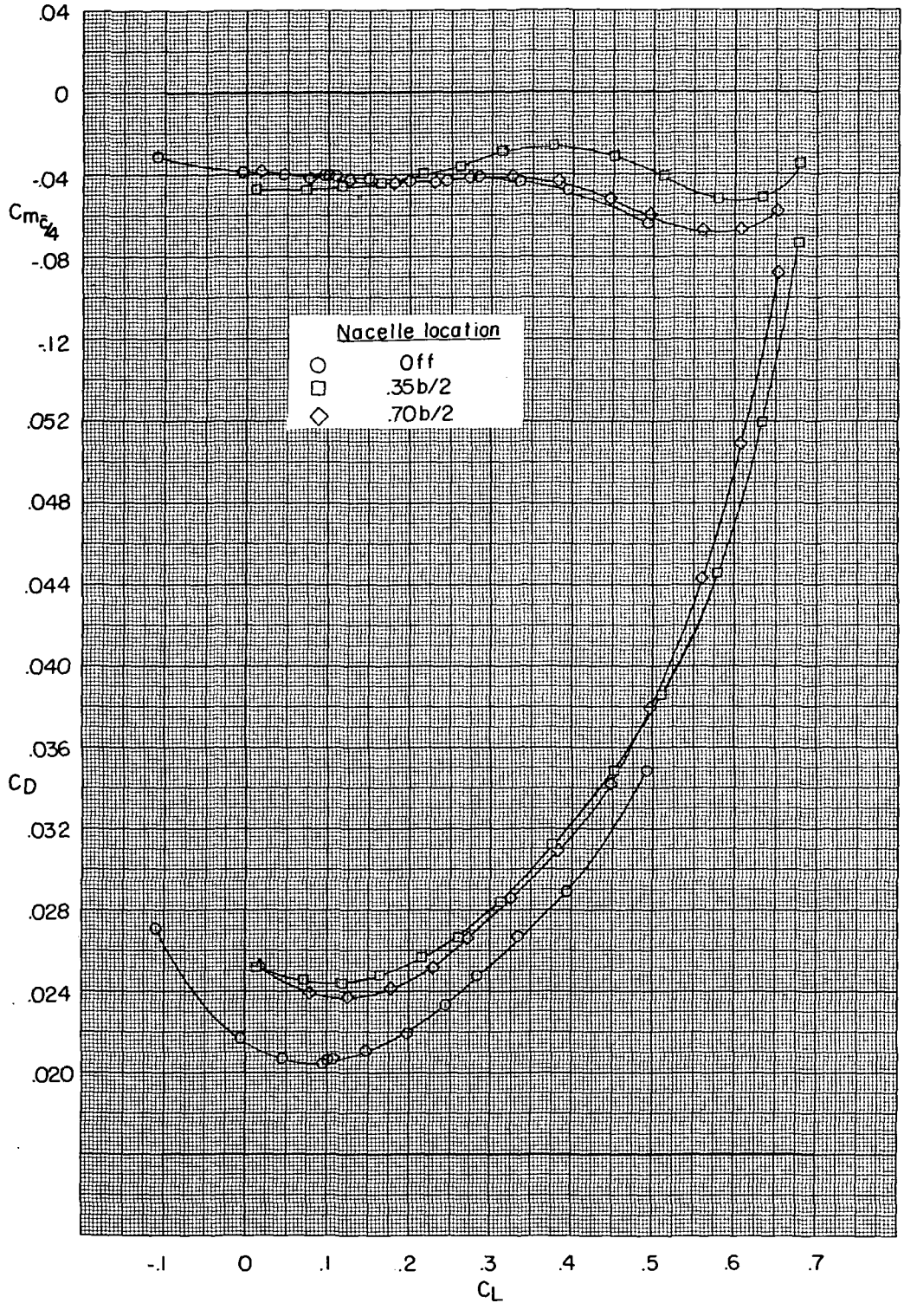

(c) M = 0.96.

Figure 29.- Continued.

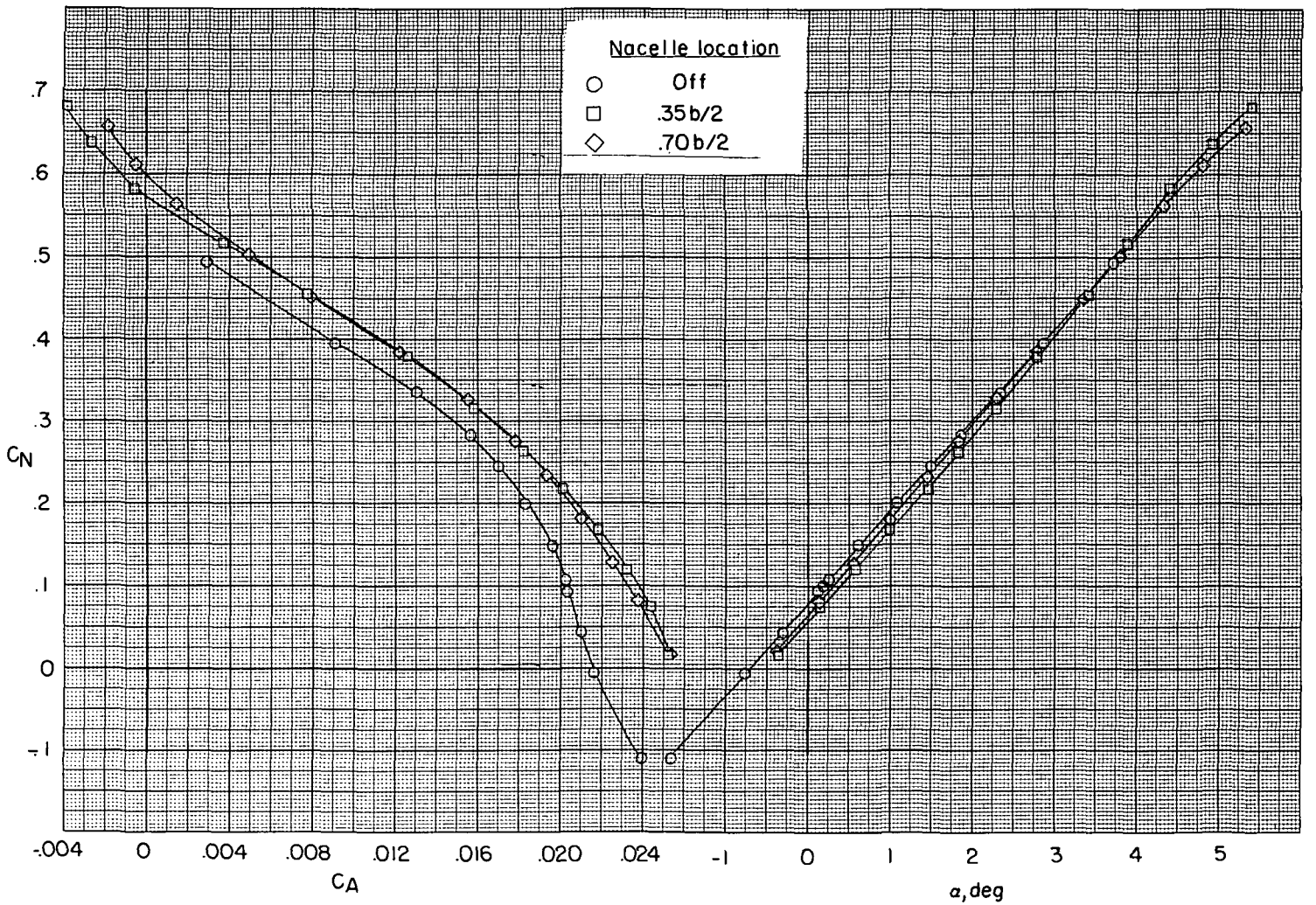

(c) Concluded.

Figure 29.- Continued.

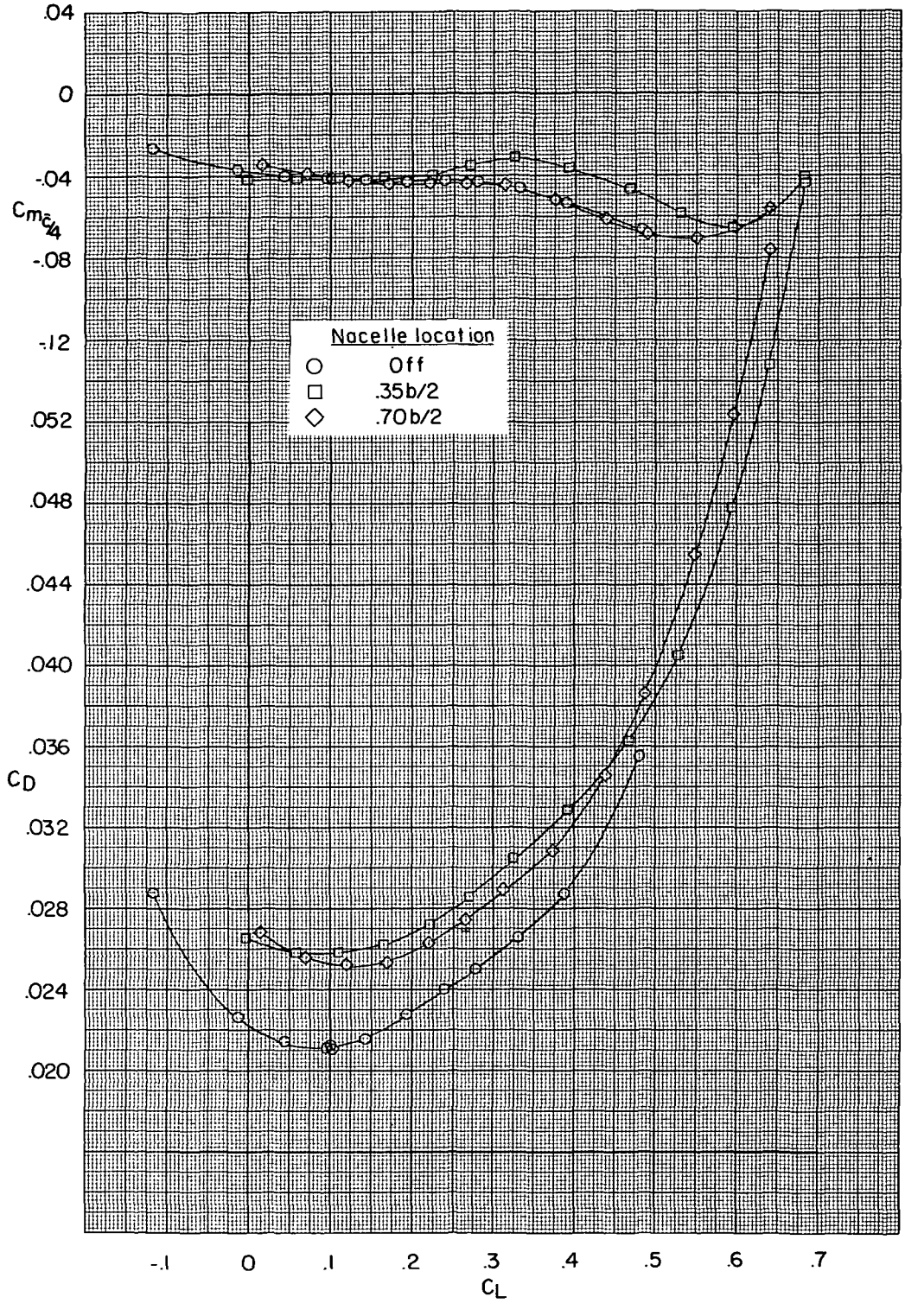

(*d*) $M = 0.97$.

Figure 29.- Continued.

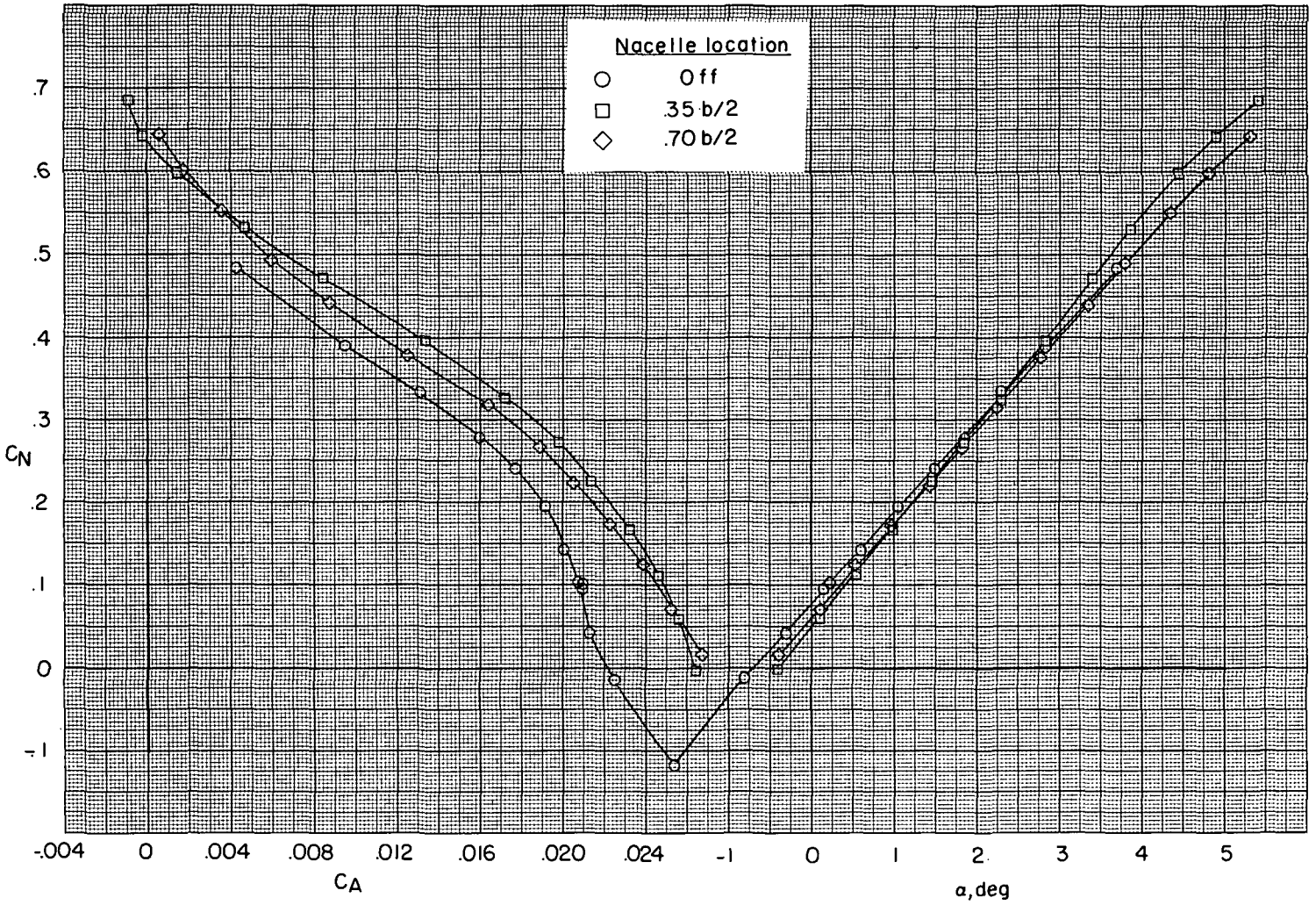

(d) Concluded.

Figure 29.- Continued.

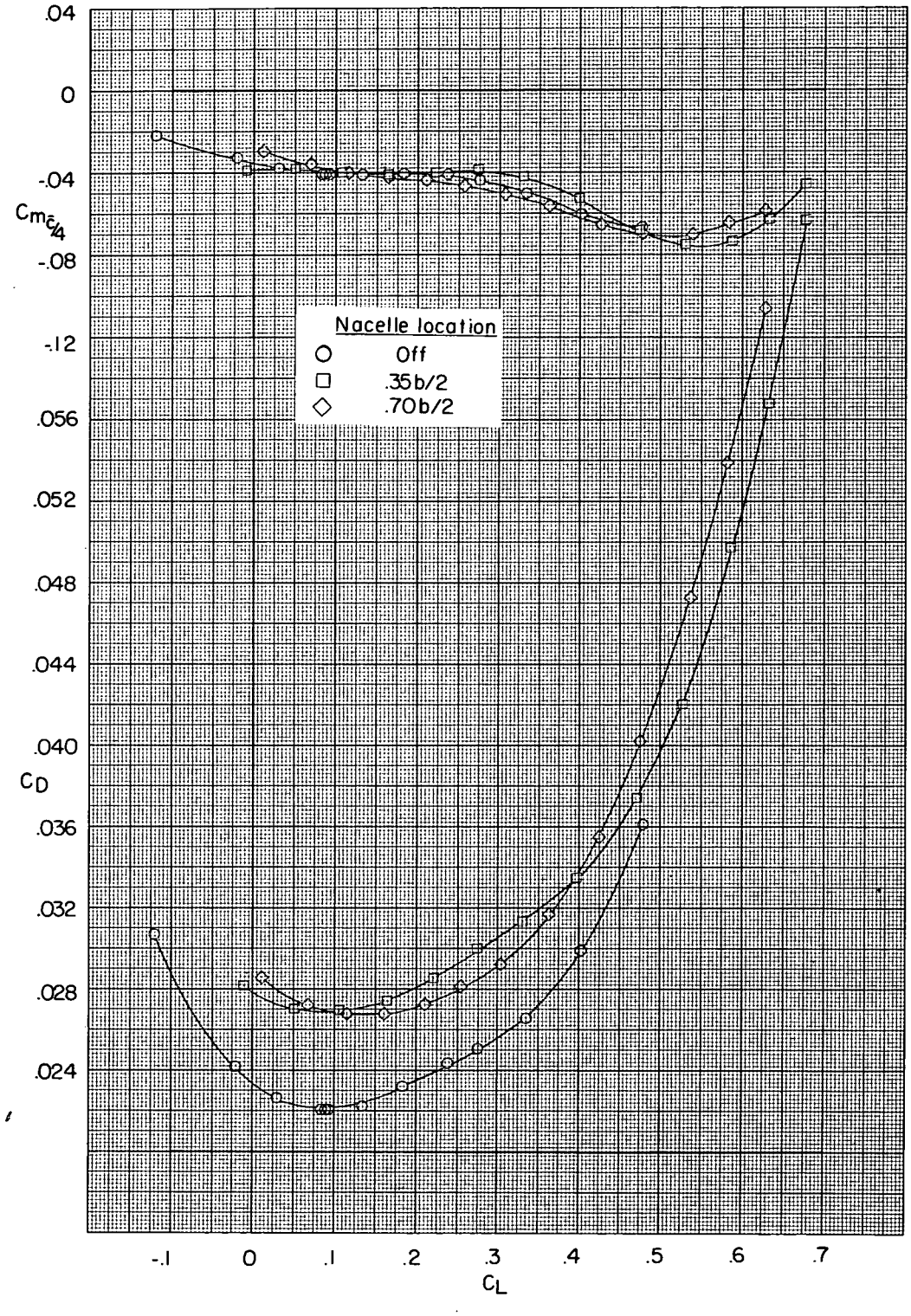

(e) M = 0.98.

Figure 29.- Continued.

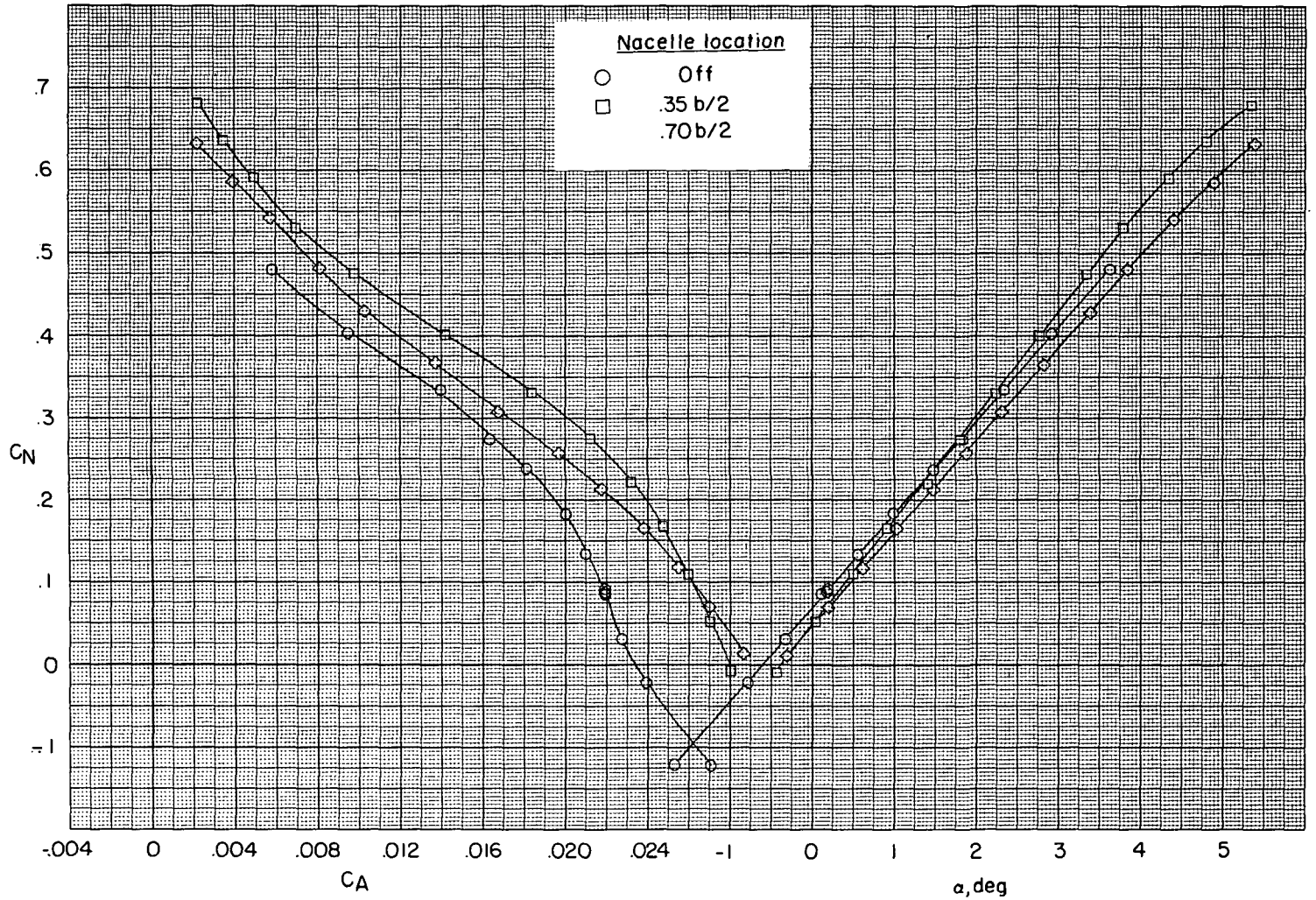

(e) Concluded.

Figure 29.- Continued.

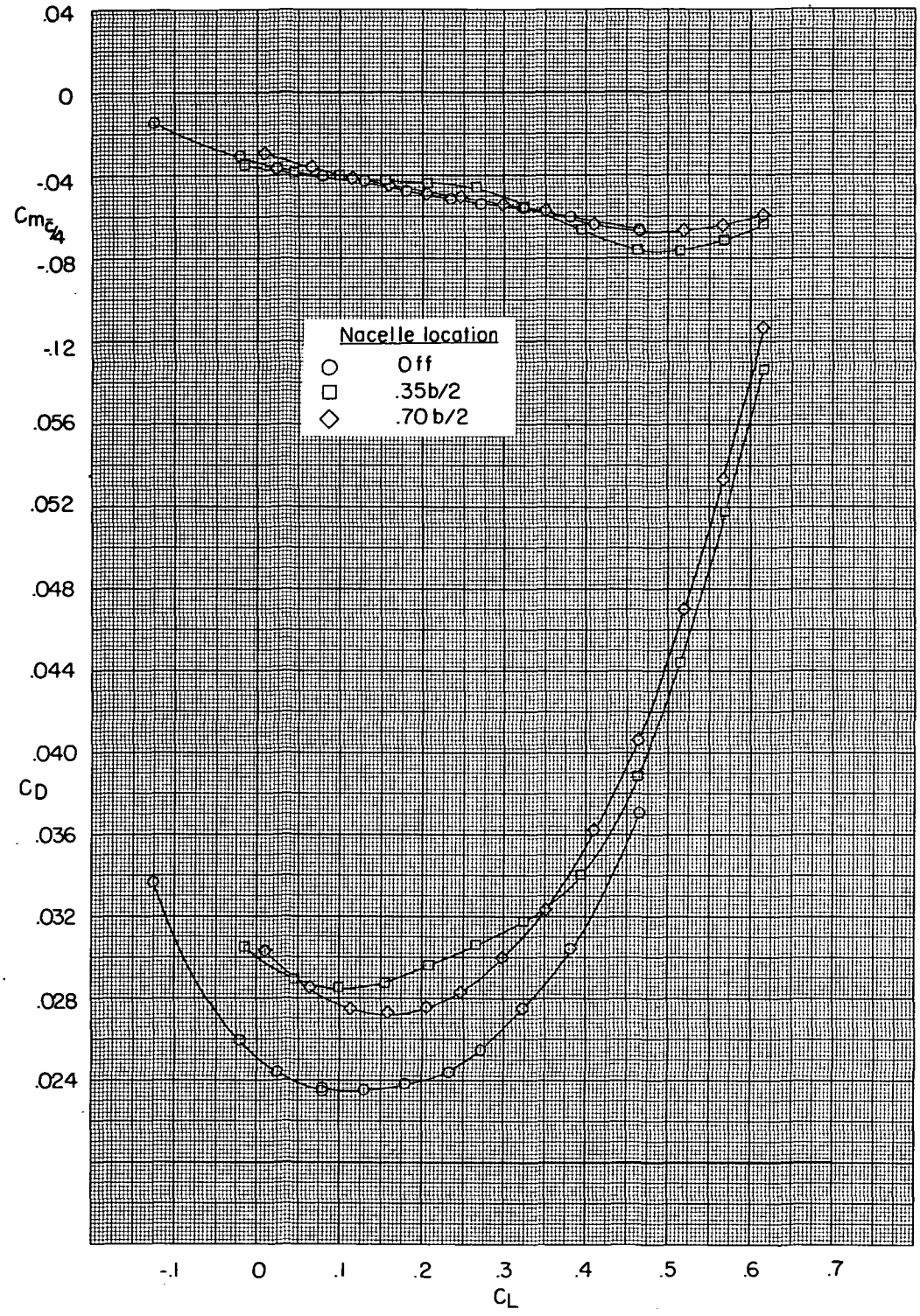

(f) M = 0.99.

Figure 29.- Continued.

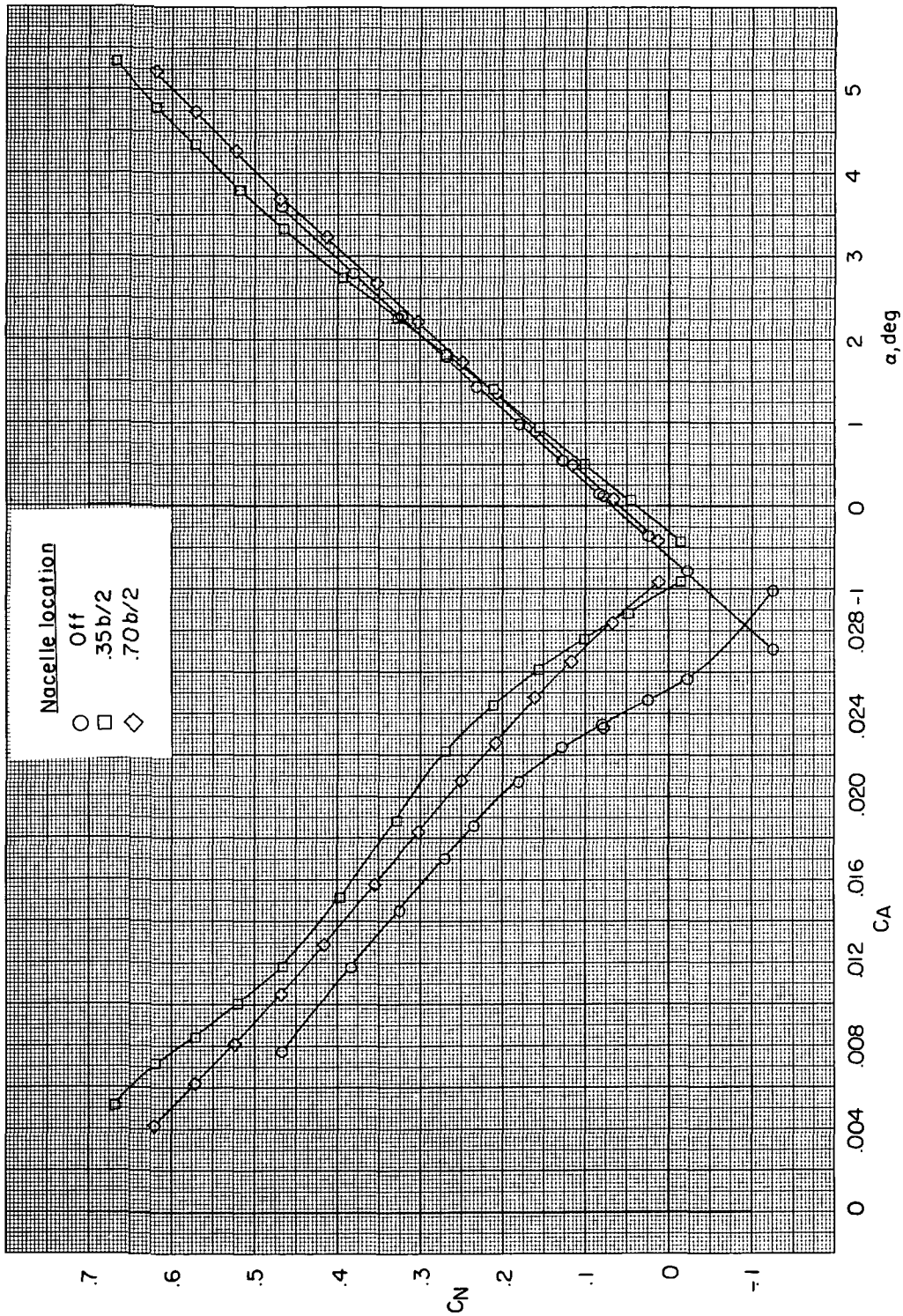

(f) Concluded.

Figure 29.- Concluded.

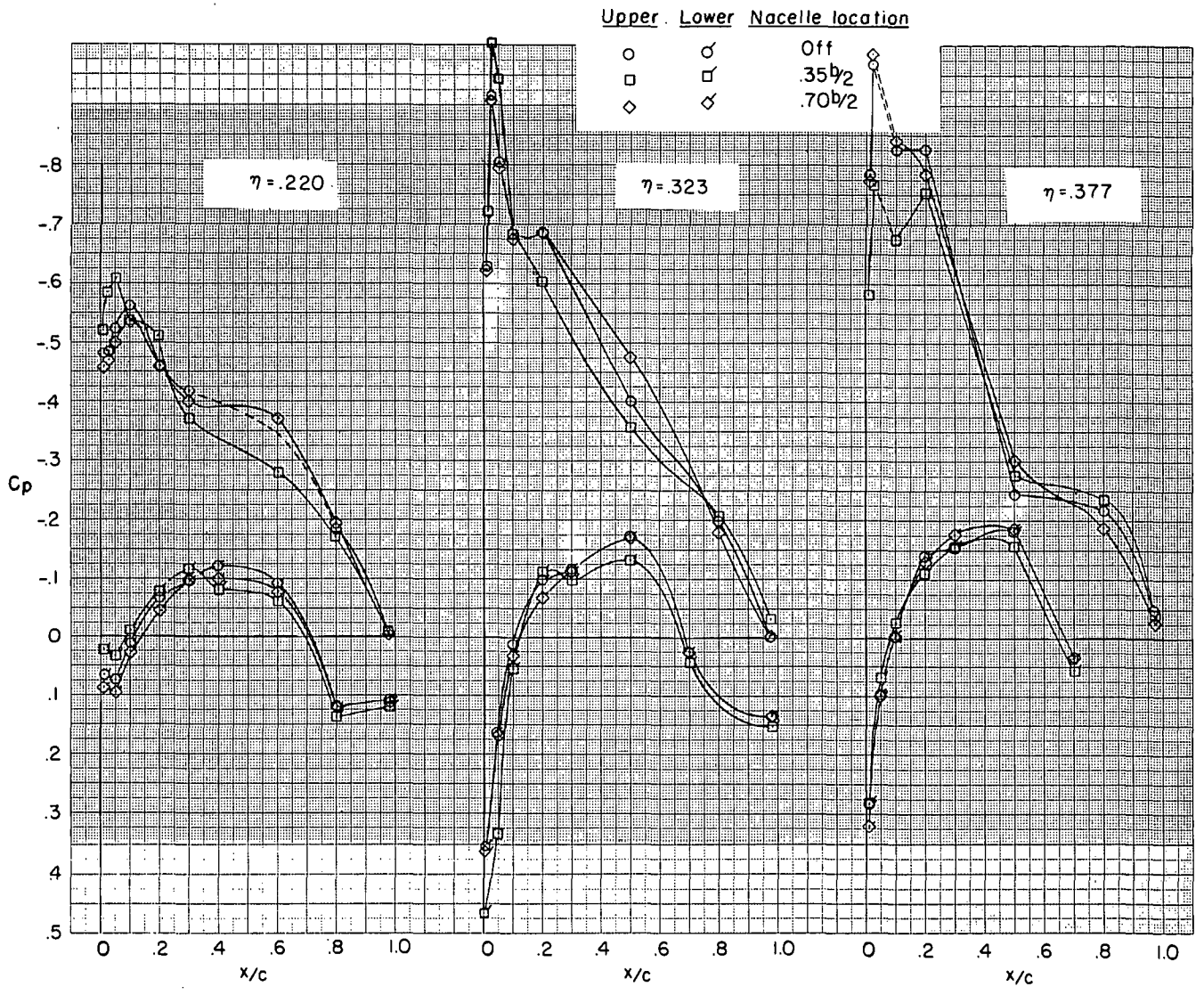

(a) M = 0.90.

Figure 30.- Effect of nacelle location on wing pressure distribution for the B_1 configuration with no area ruling for nacelles. $C_L \approx 0.40$.

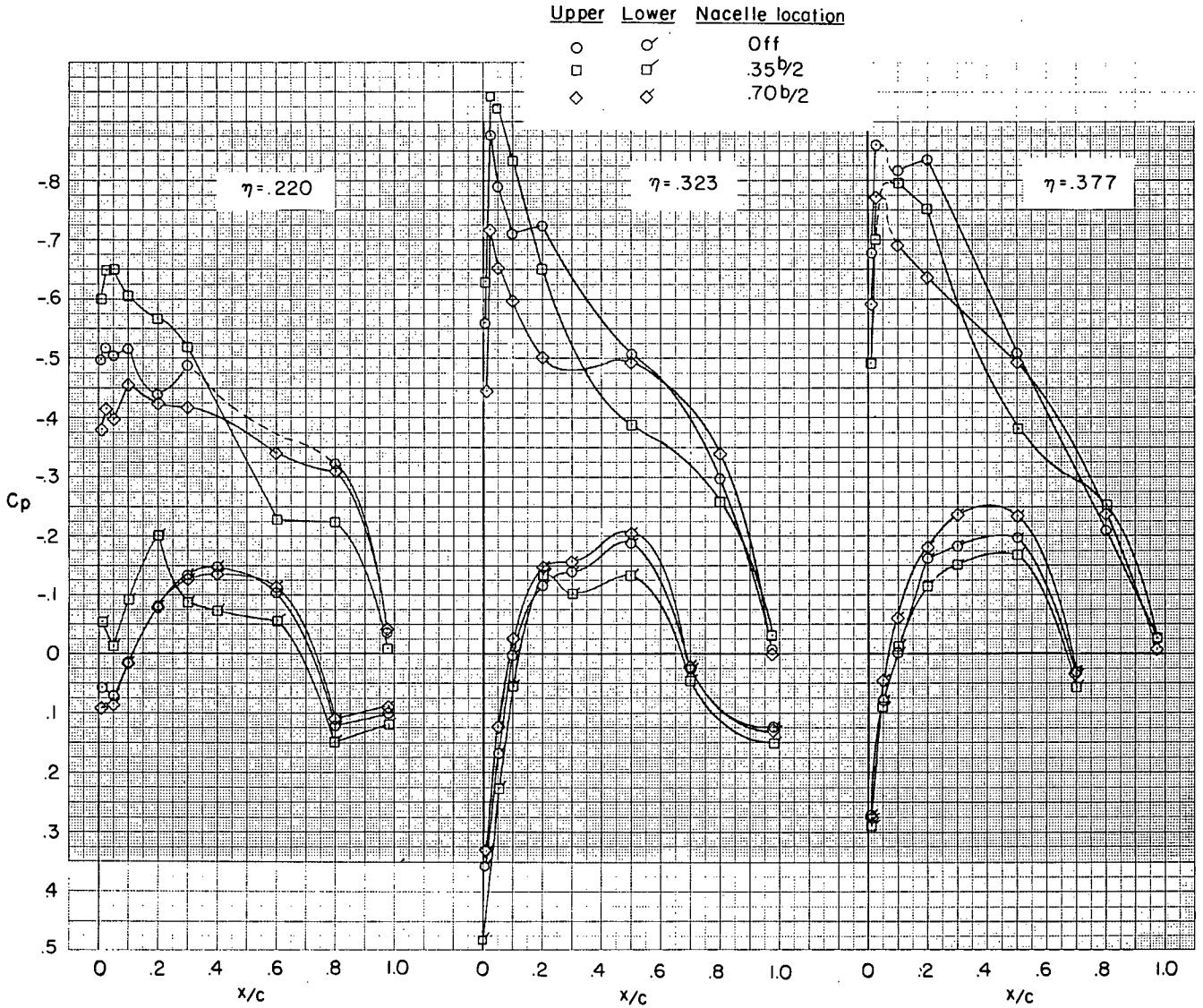

(b) M = 0.95.

Figure 30.- Continued.

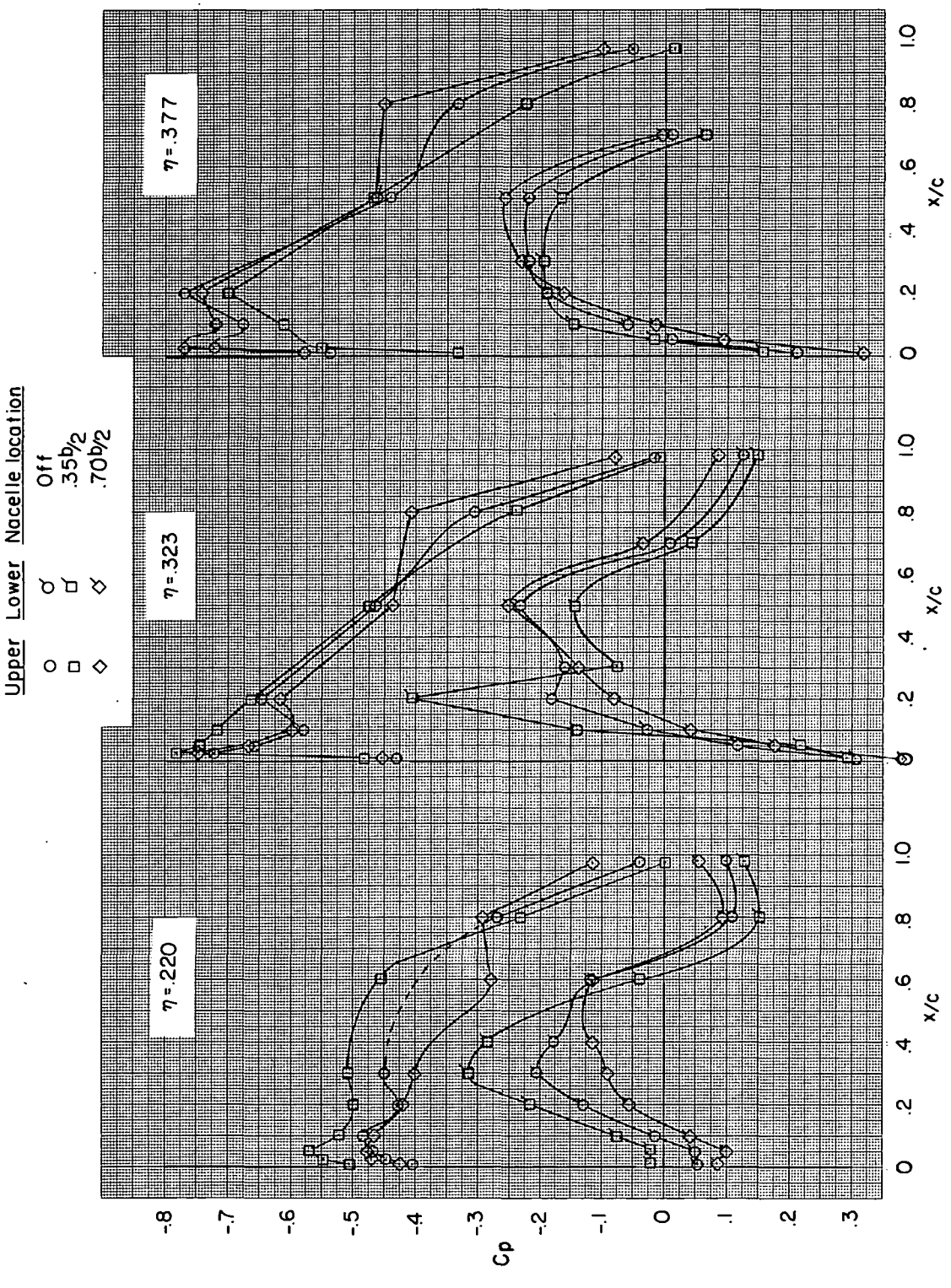

(c) M = 0.98.

Figure 30.- Concluded.

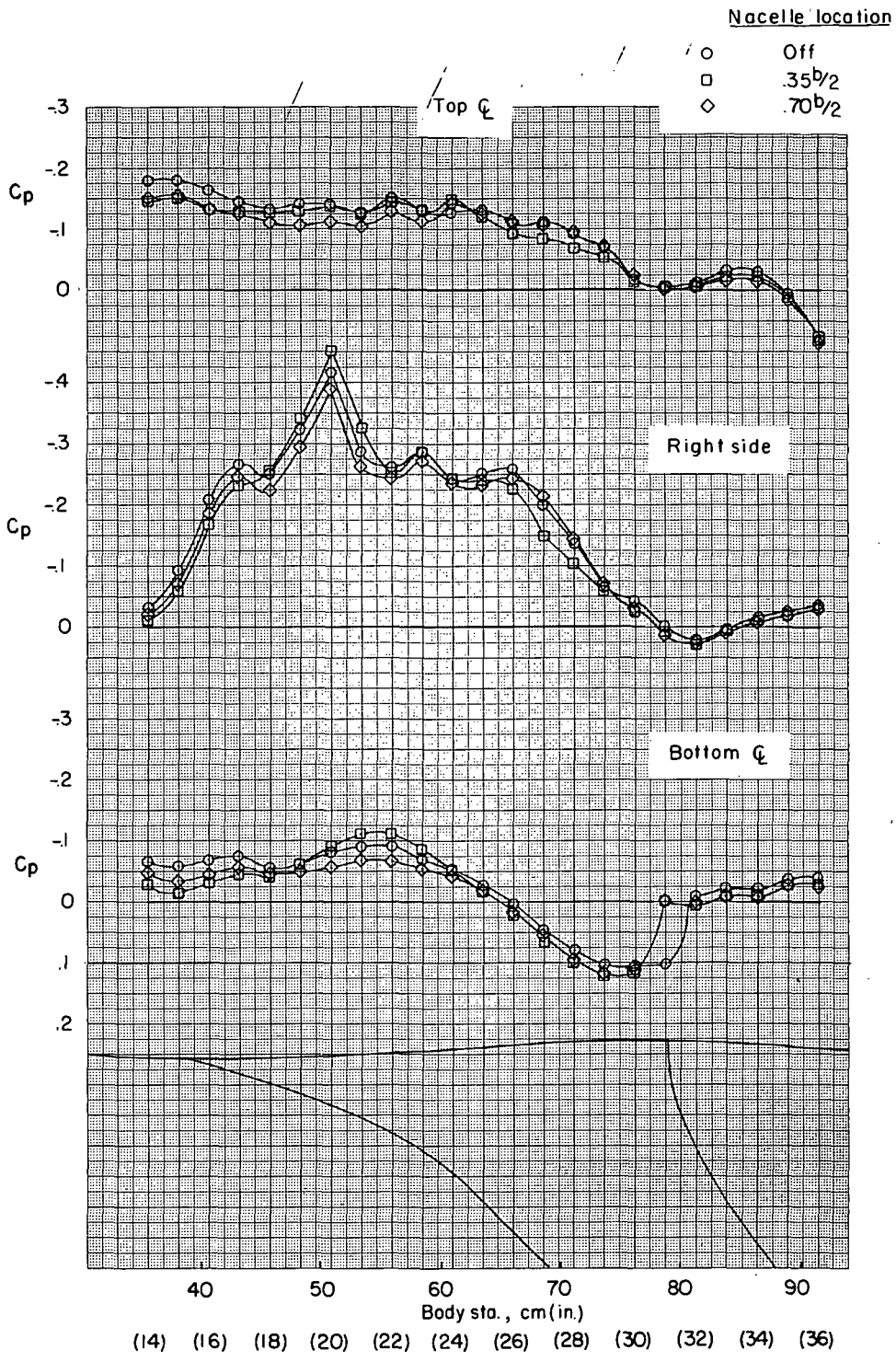

(a) M = 0.90.

Figure 31.- Effect of nacelle location on fuselage pressure distribution for the B_1 configuration with no area ruling for nacelles. $C_L \approx 0.40$.

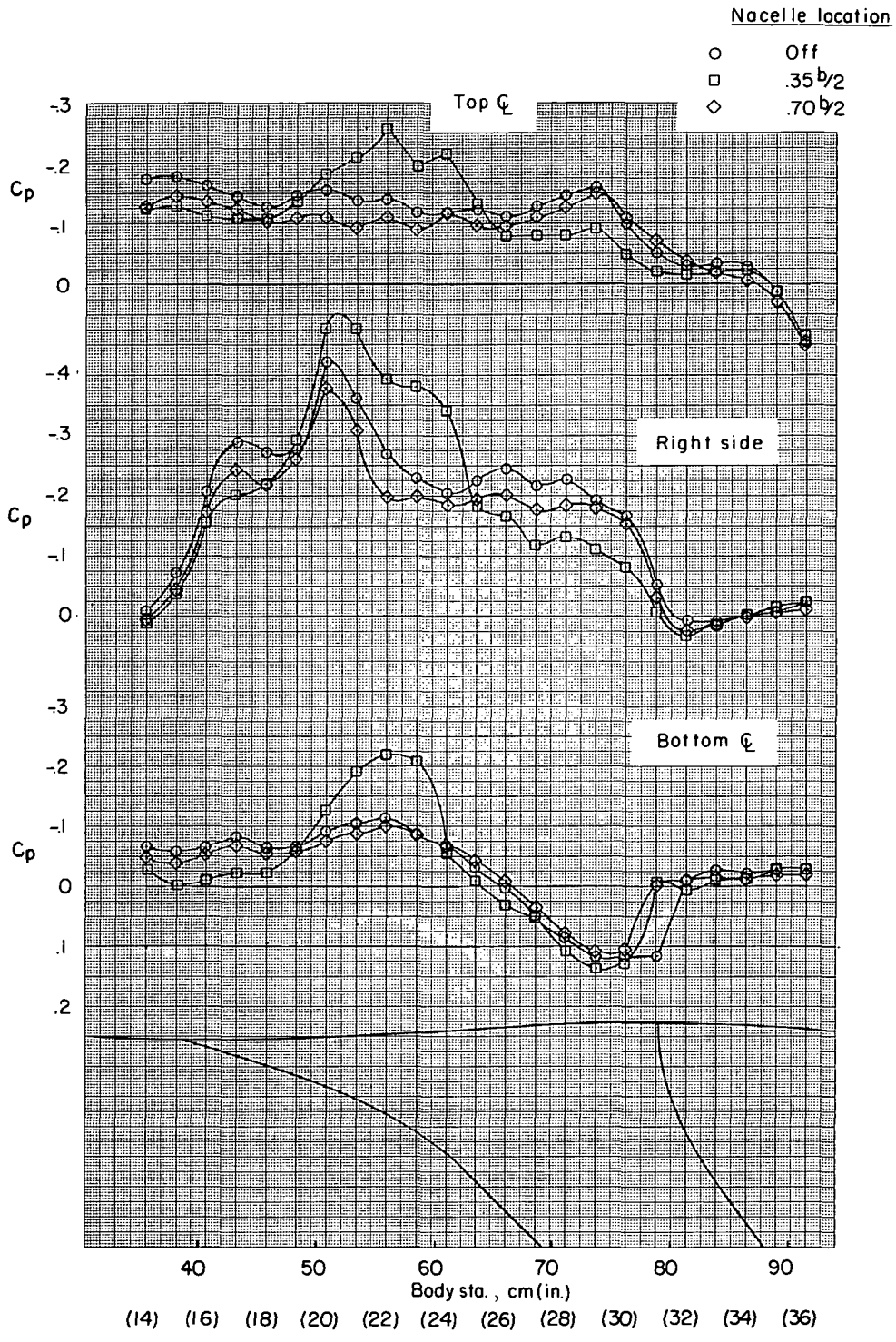

(b) M = 0.95.

Figure 31.- Continued.

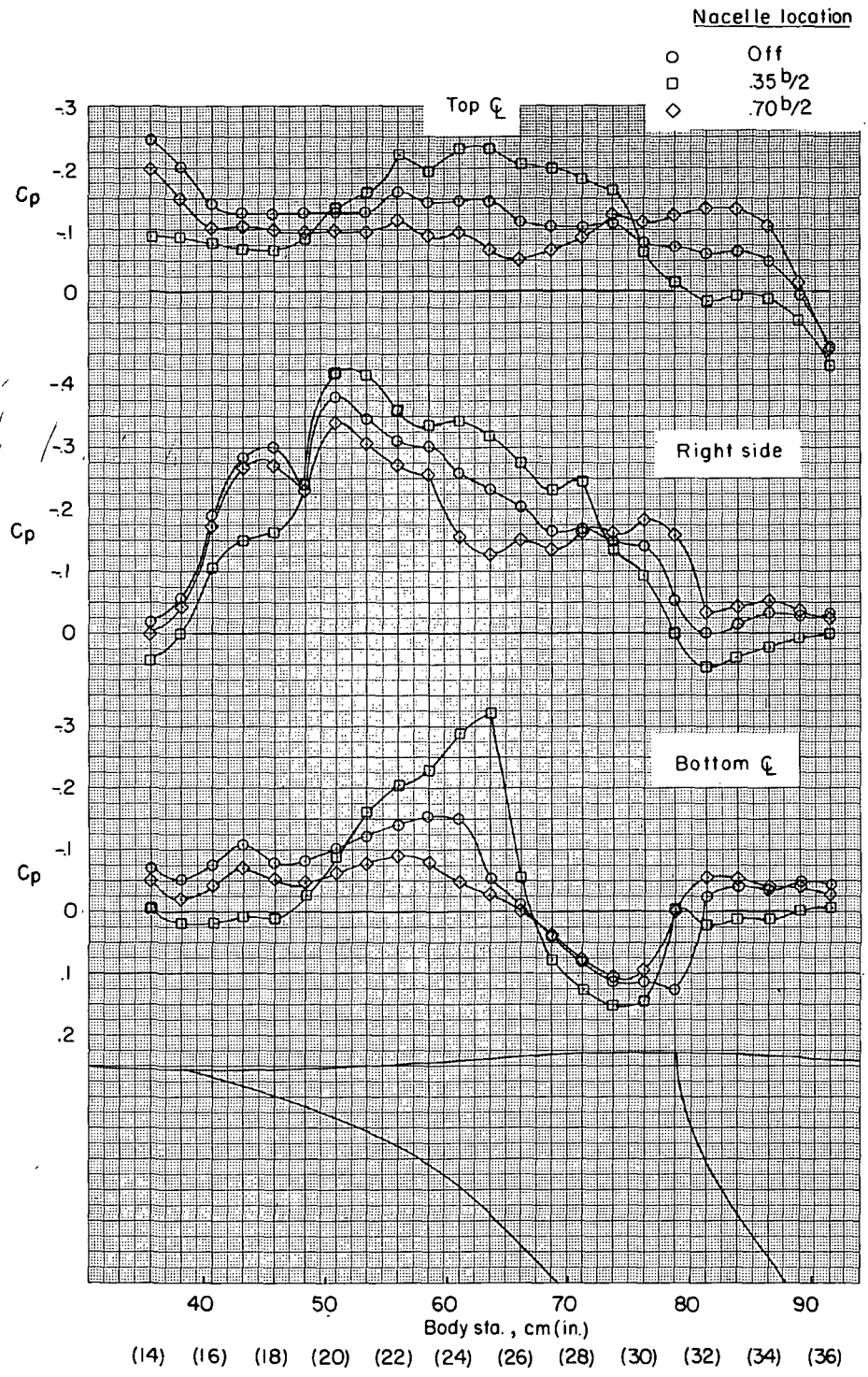

(c) M = 0.98.

Figure 31.- Concluded.

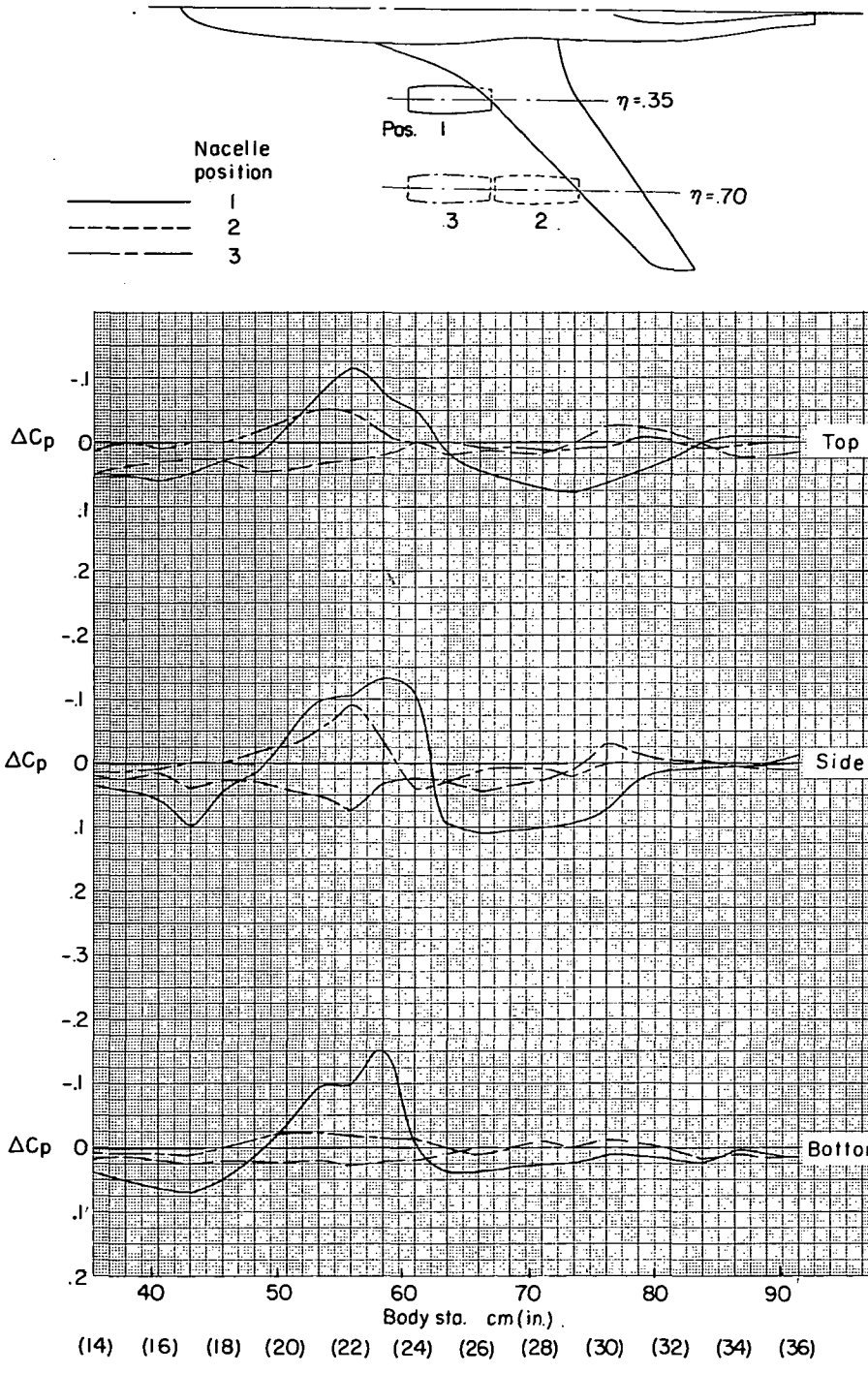

(a) M = 0.95.

Figure 32.- Effect of nacelle position on incremental pressure coefficient on fuselage. $C_L \approx 0.40$.

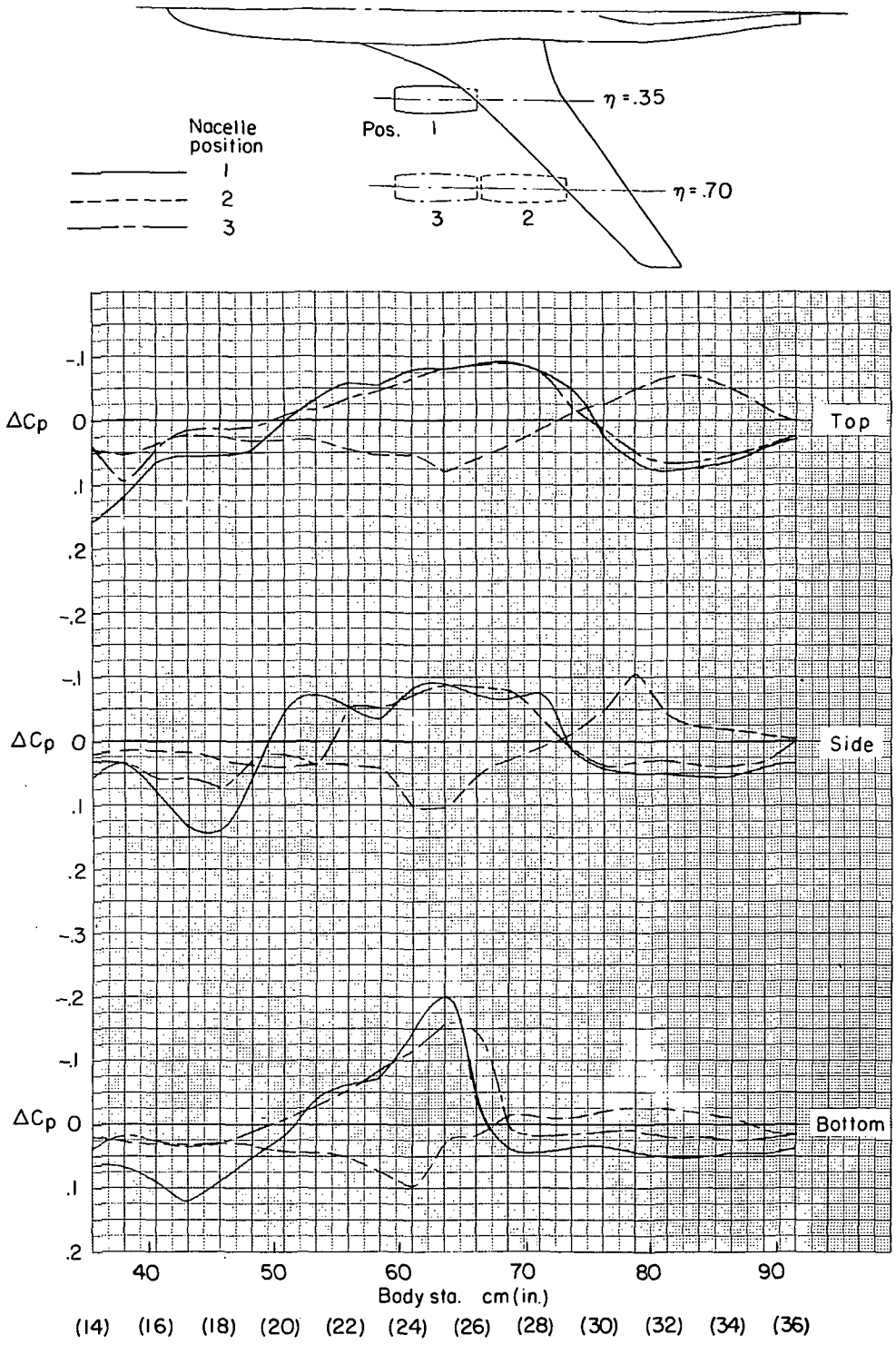

(b) M = 0.98.

Figure 32.- Concluded.

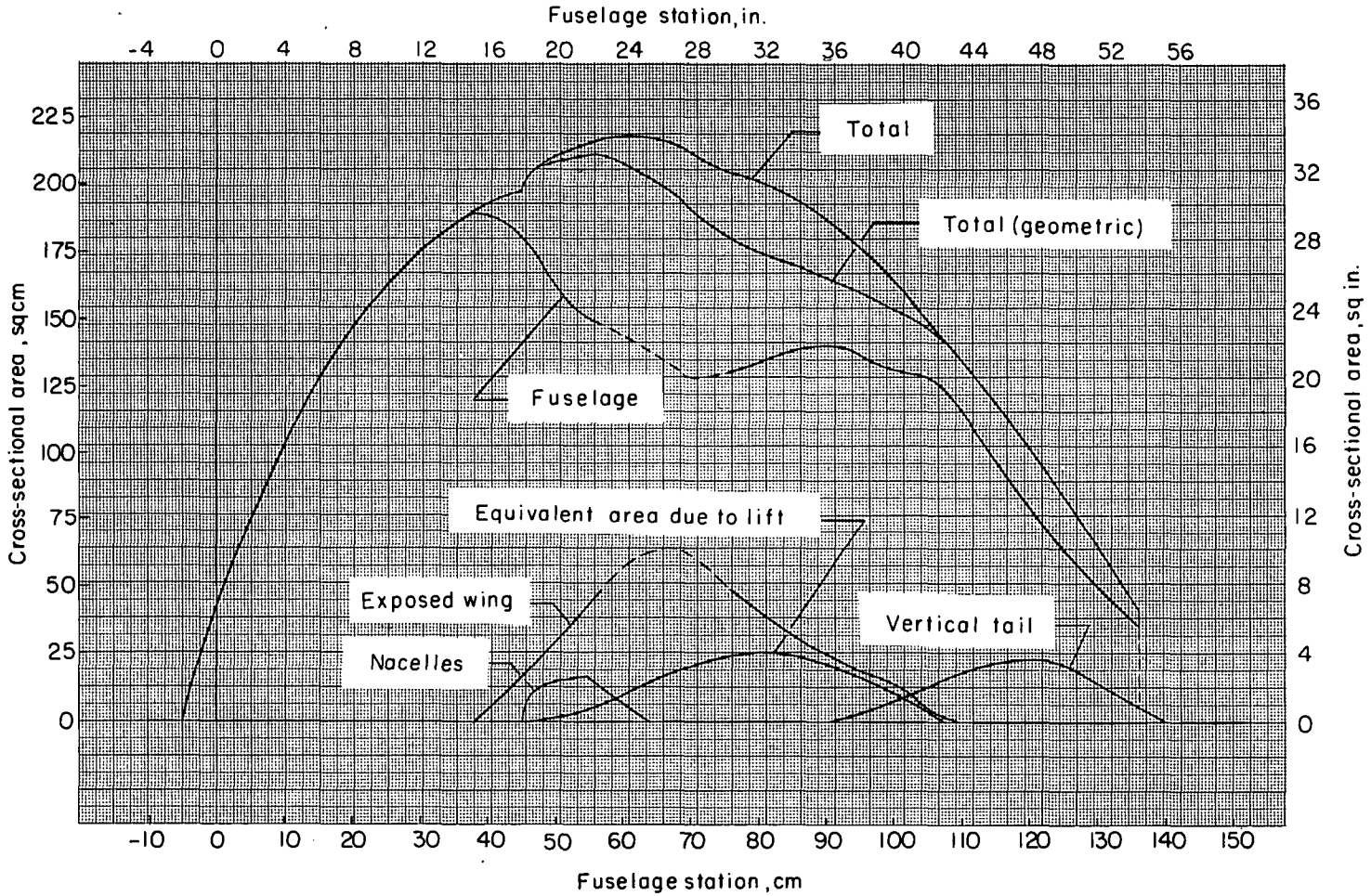

Figure 33.- Cross-sectional area distribution for the nacelles-on configuration with the nacelles at 0.35b/2 and area ruling for the nacelles taken circumferentially.

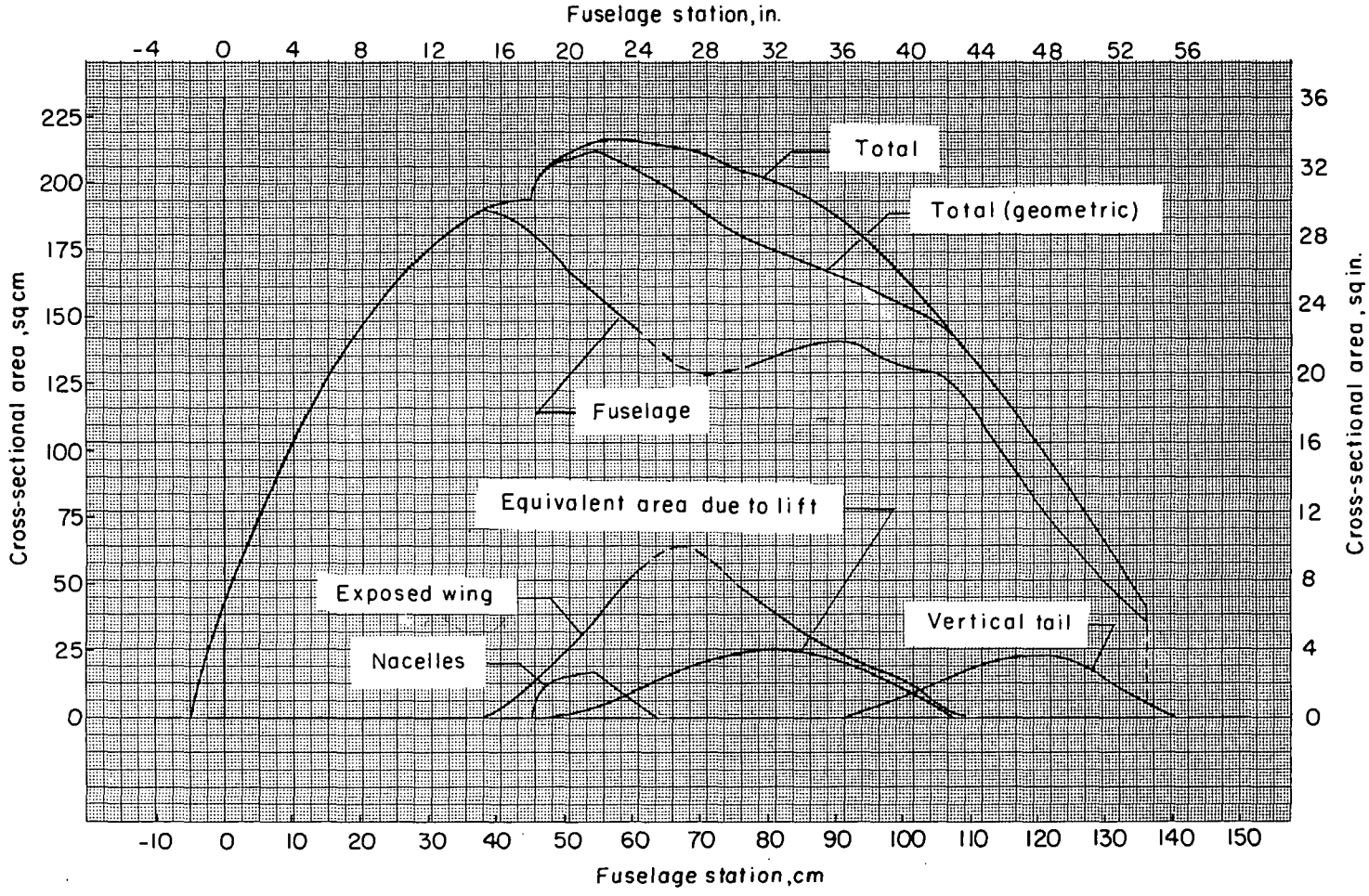

Figure 34.- Cross-sectional area distribution for the nacelles on configuration with the nacelles located at 0.35b/2 and area ruling for the nacelles taken below the wing.

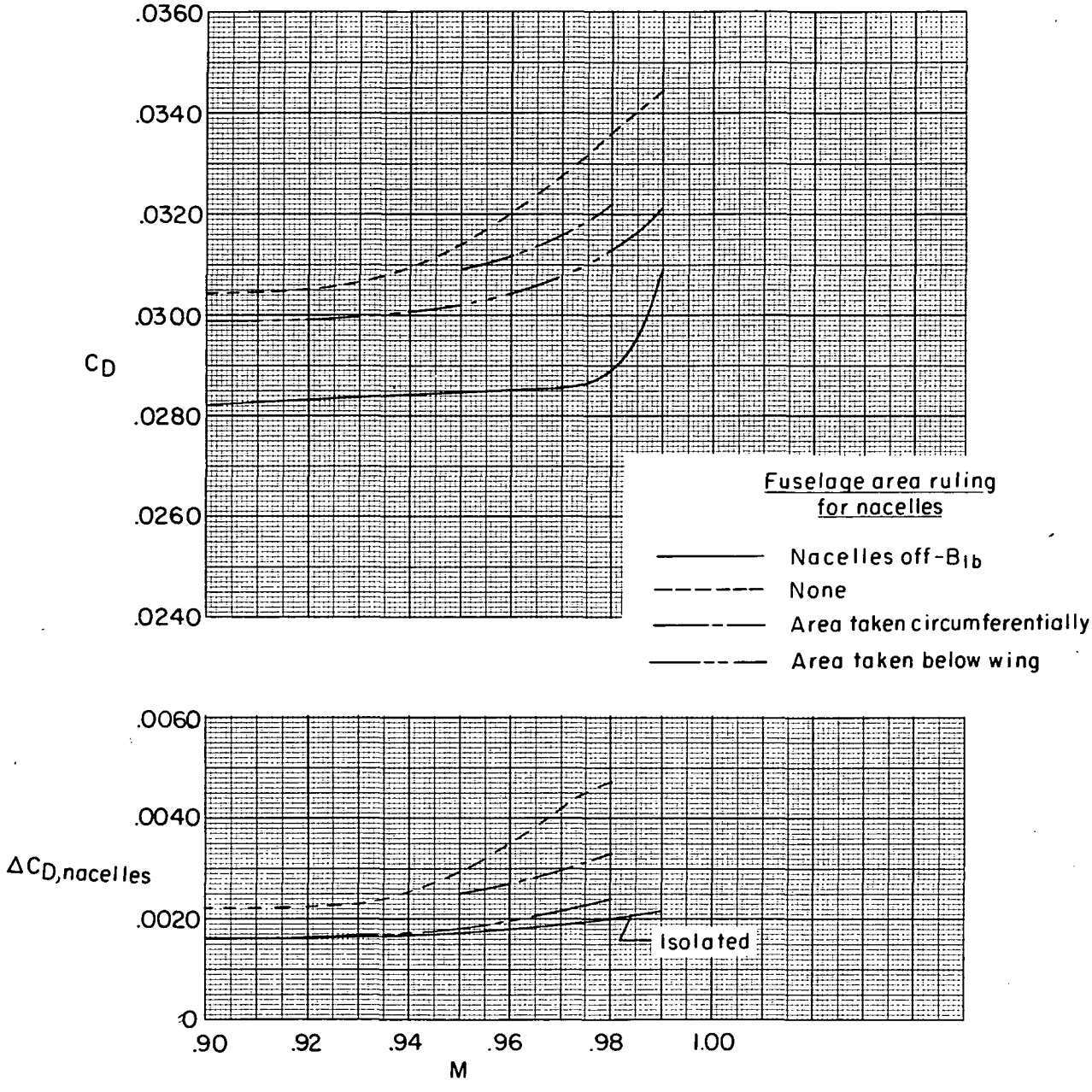

Figure 35.- Summary of nacelle installation drag characteristics. Fuselage area ruled for nacelles. $C_L = 0.40$.

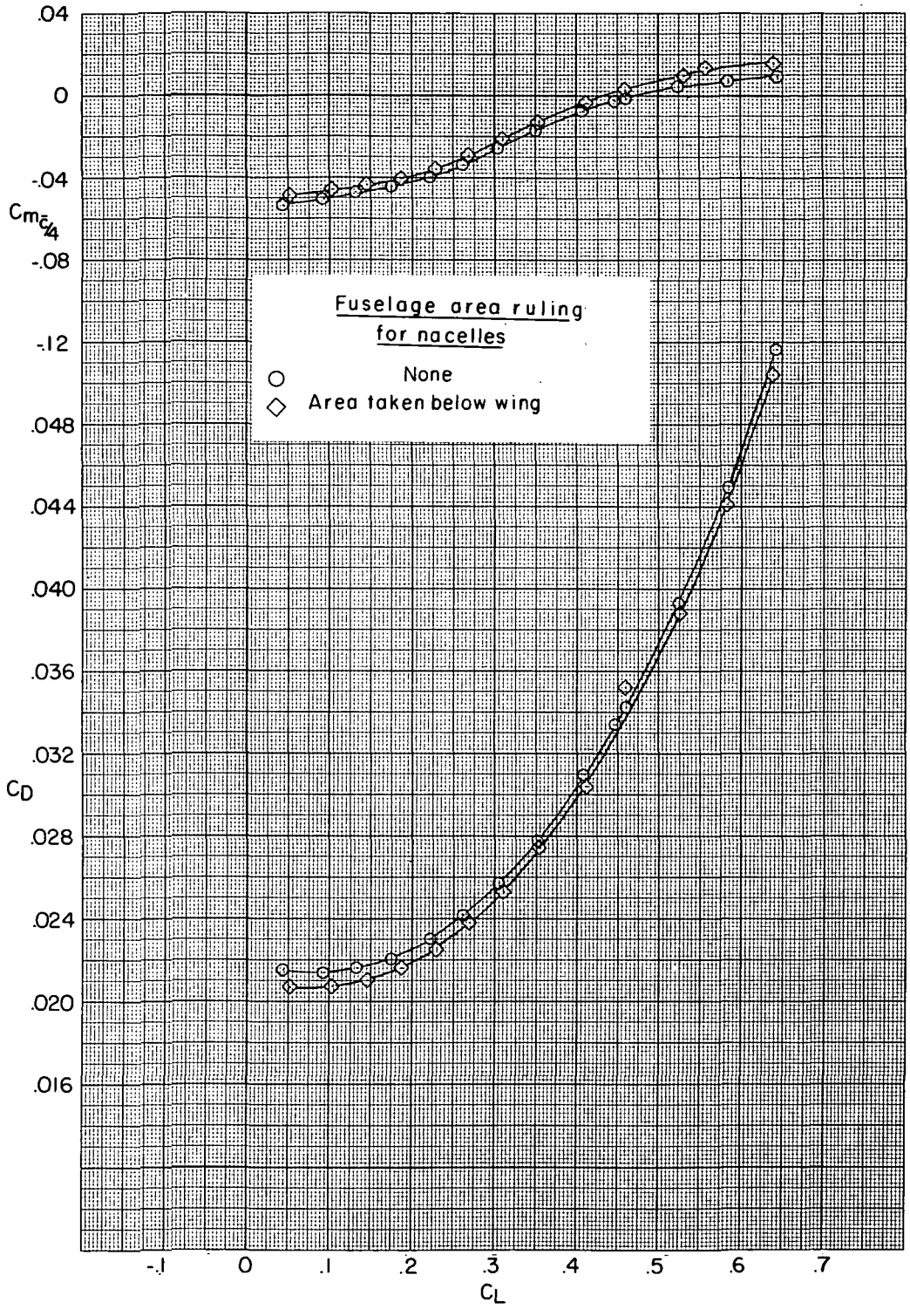

(a) M = 0.90.

Figure 36.- Effect of area ruling for nacelles located at 0.35b/2 on longitudinal aerodynamic characteristics.

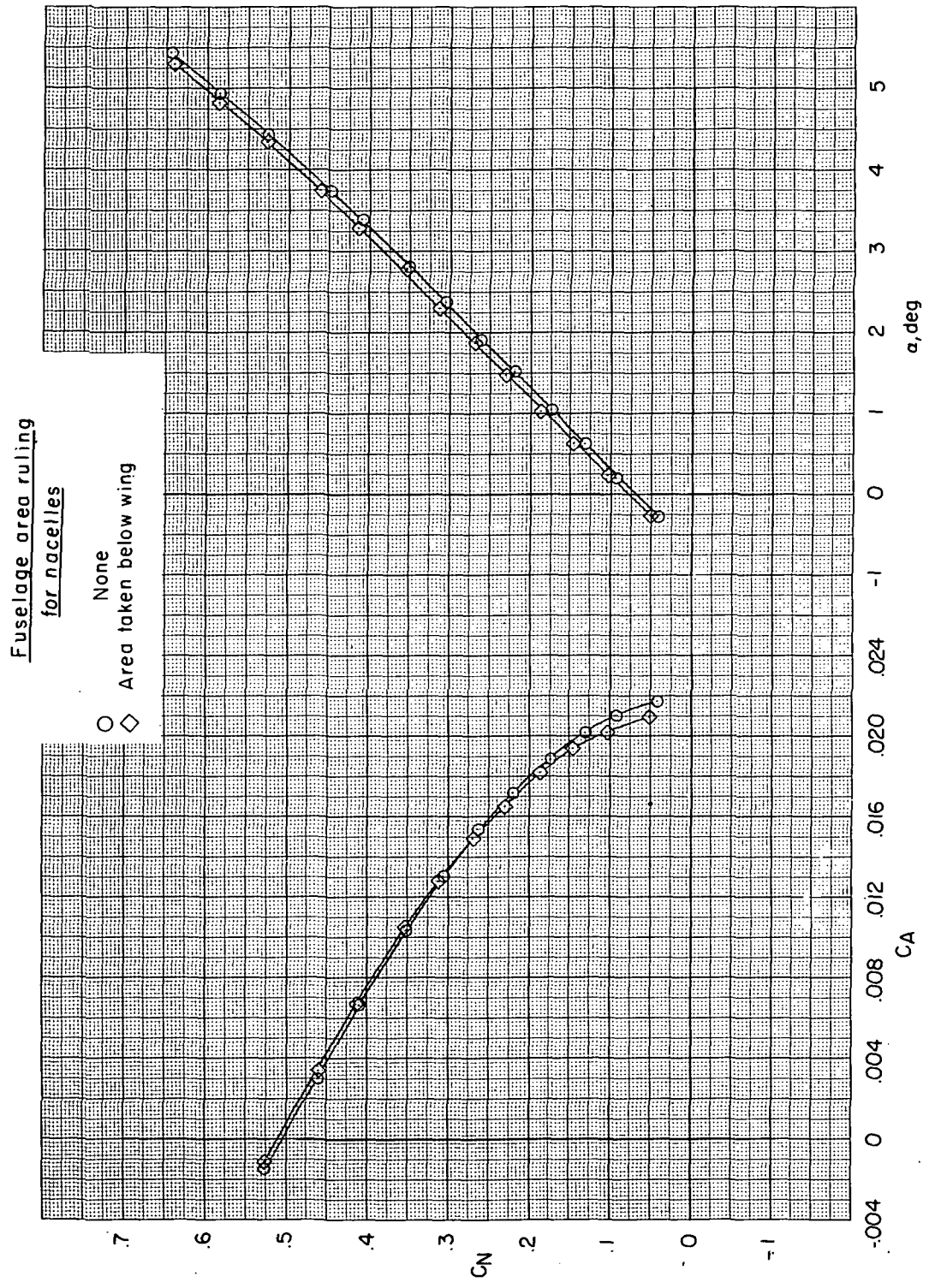

(a) Concluded.

Figure 36.- Continued.

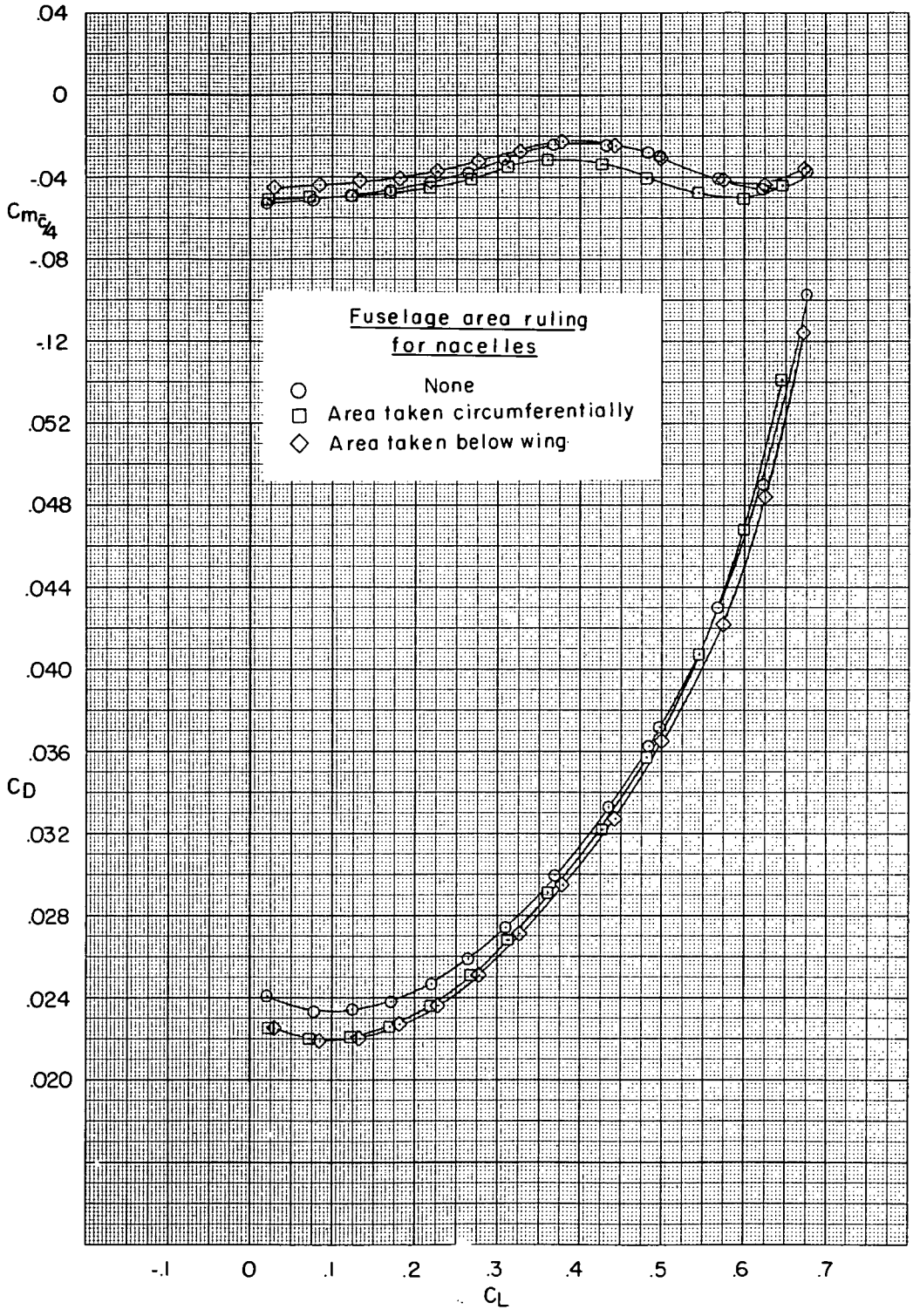

(b) M = 0.95.

Figure 36.- Continued.

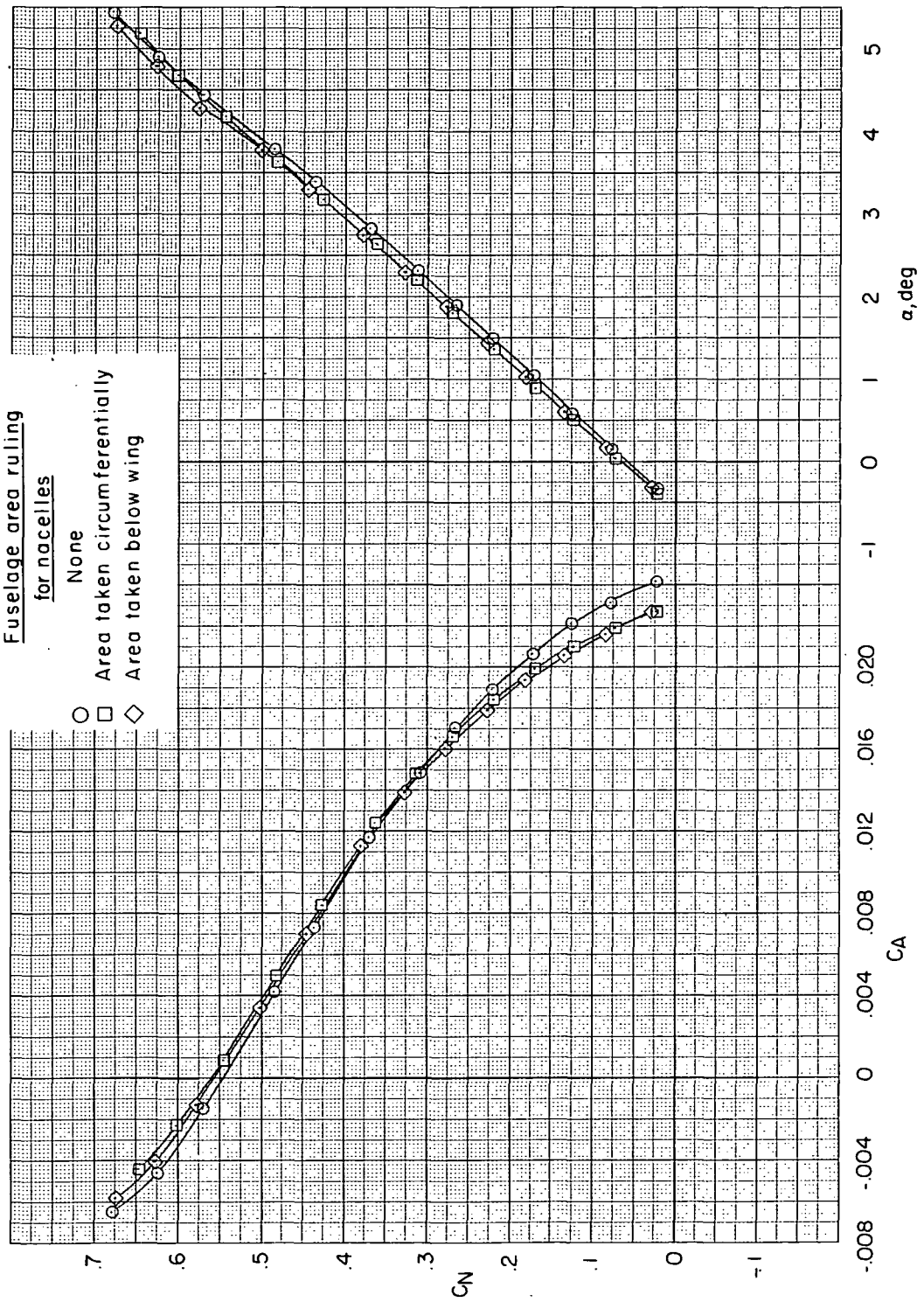

(b) Concluded.

Figure 36.- Continued.

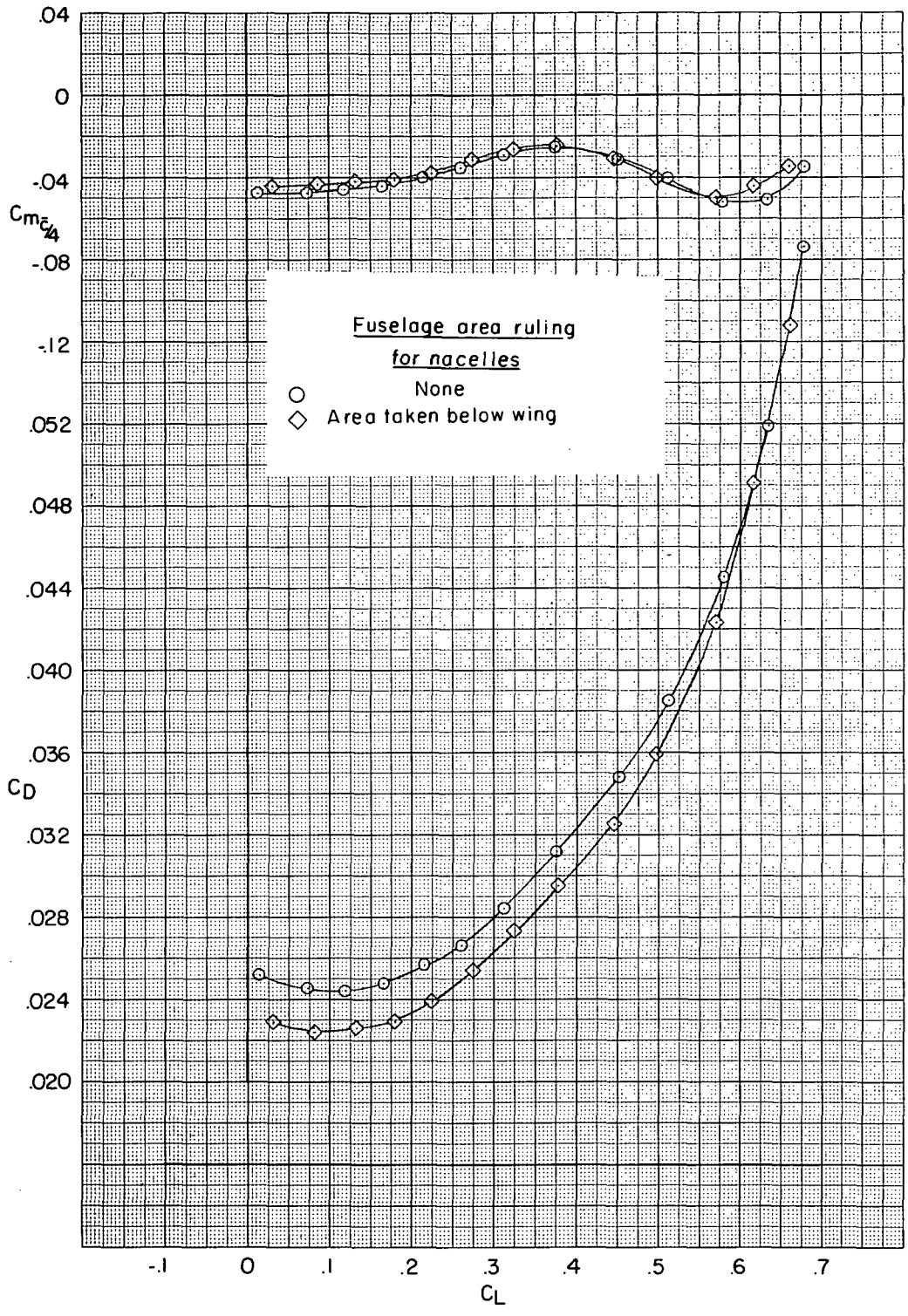

(c) M = 0.96.

Figure 36.- Continued.

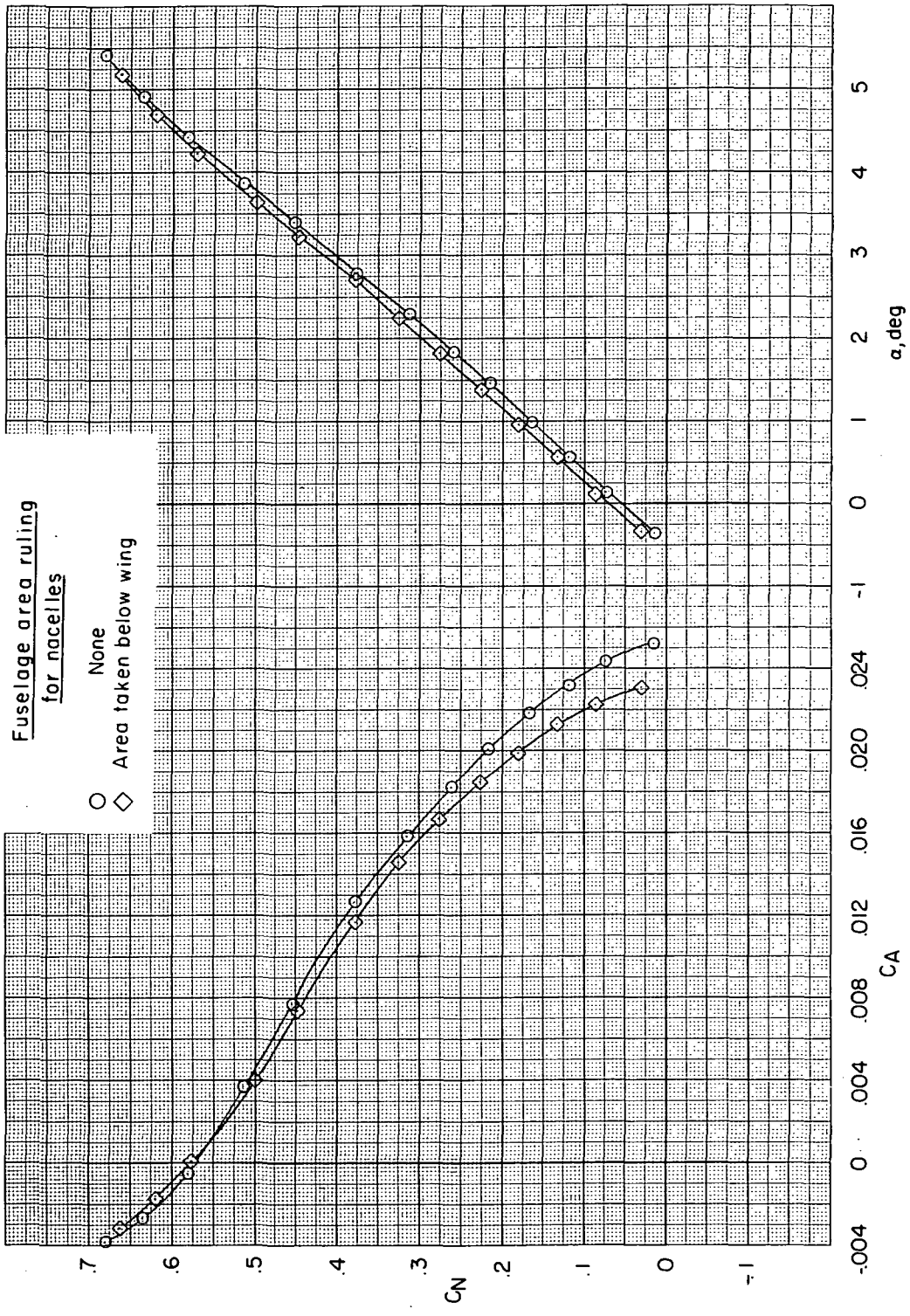

(c) Concluded.

Figure 36.--Continued.

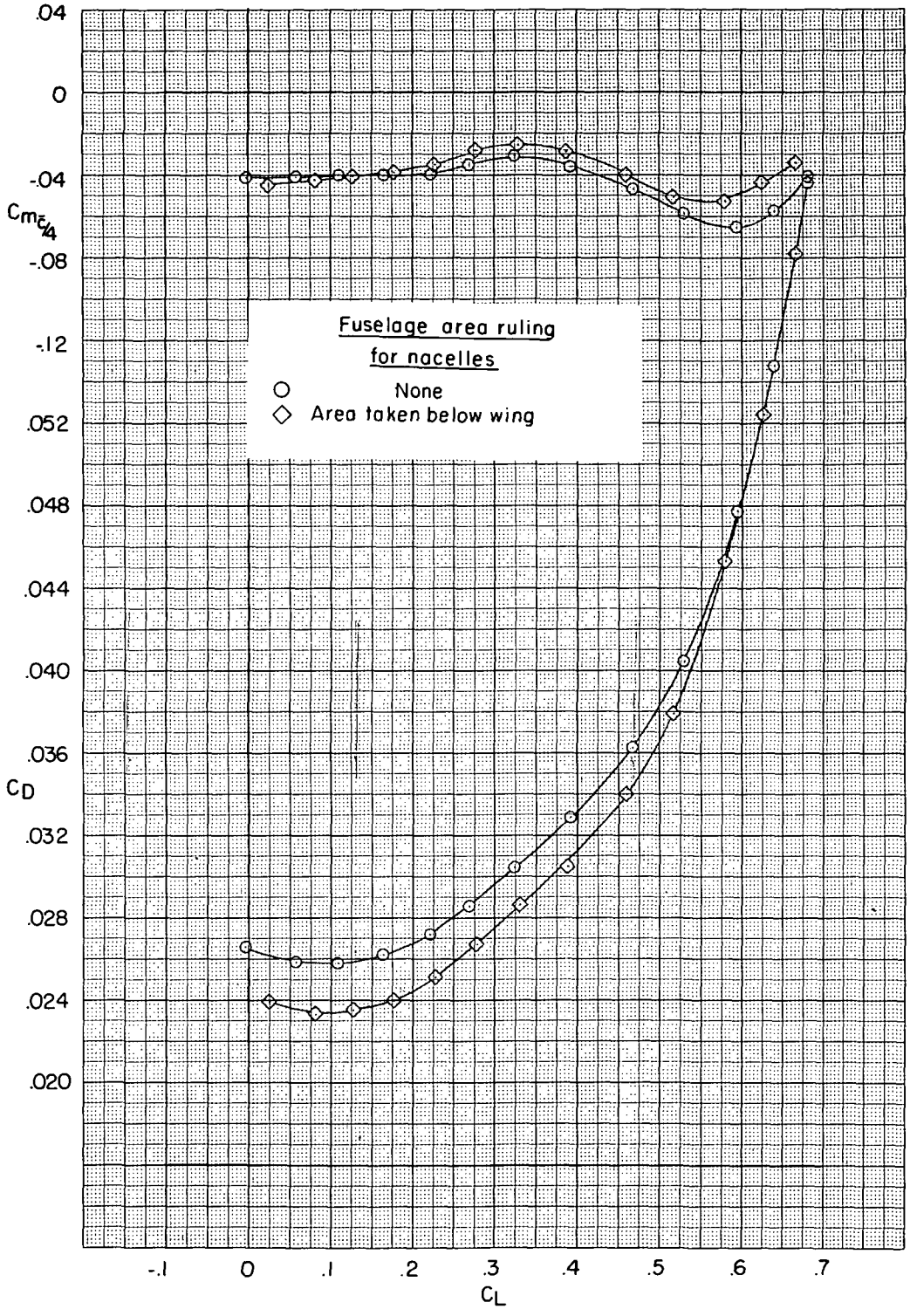

(d) M = 0.97.

Figure 36.- Continued.

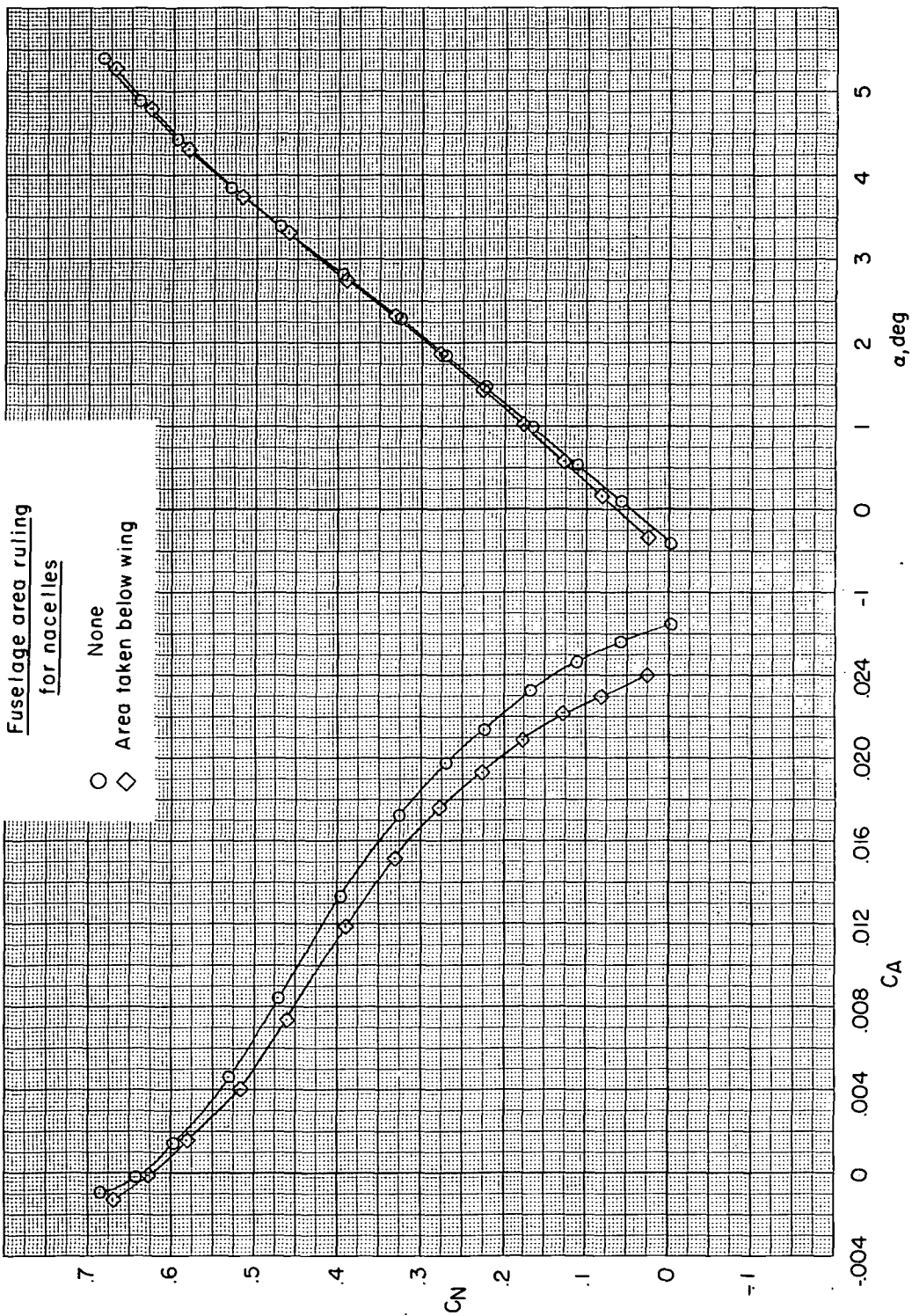

(d) Concluded.

Figure 36.- Continued.

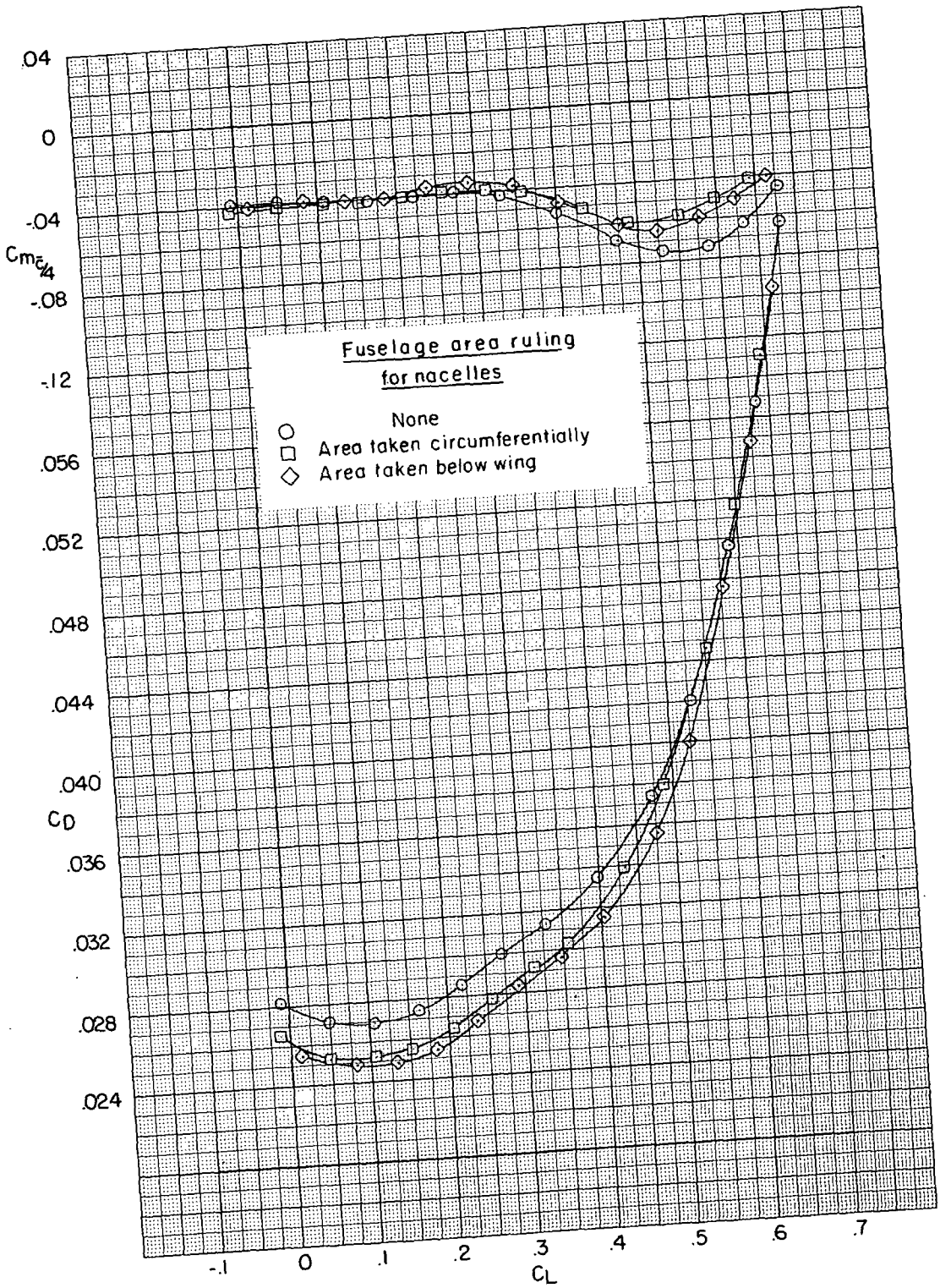

(e) M = 0.98.

Figure 36.- Continued.

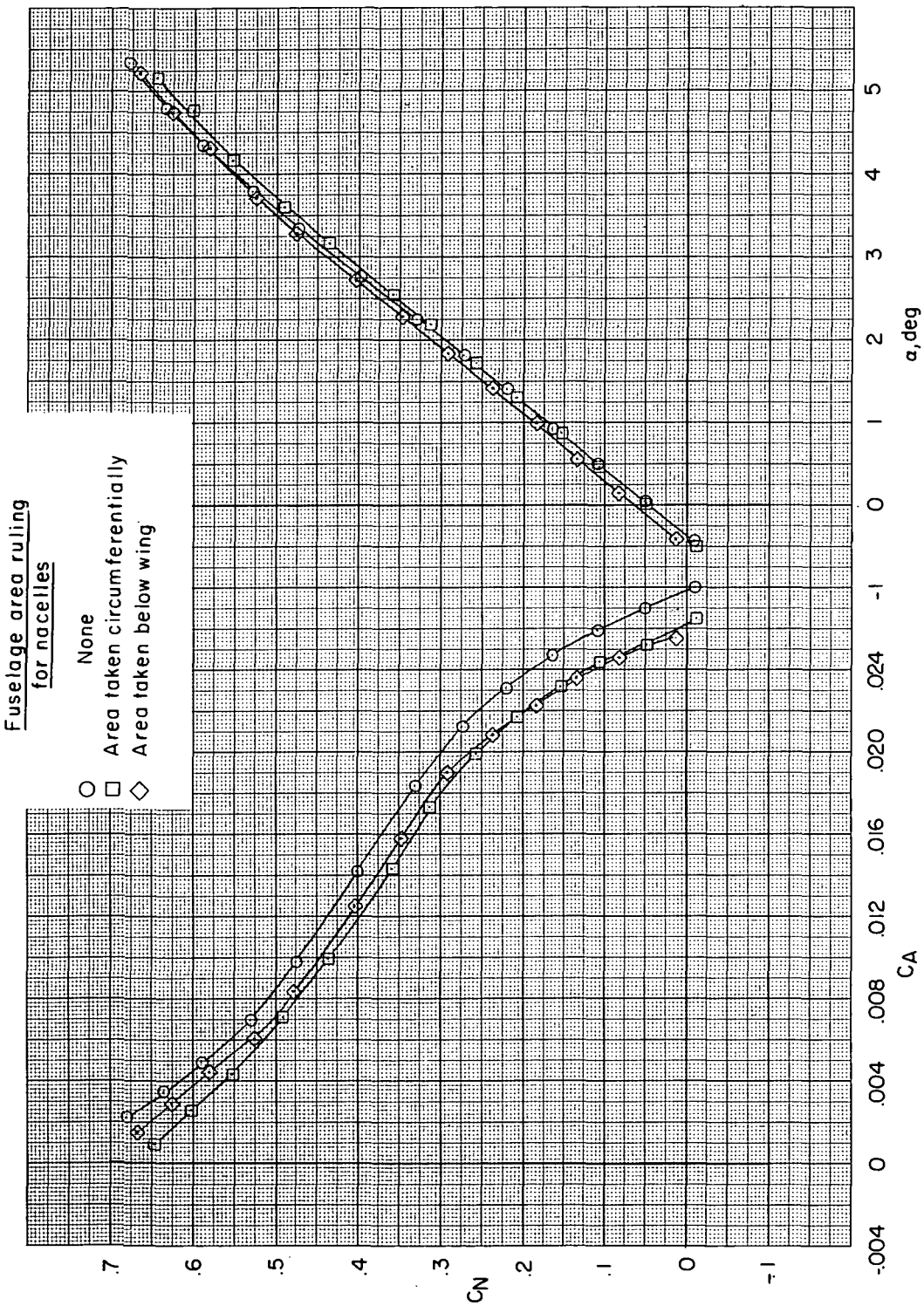

(e) Concluded.

Figure 36.- Continued.

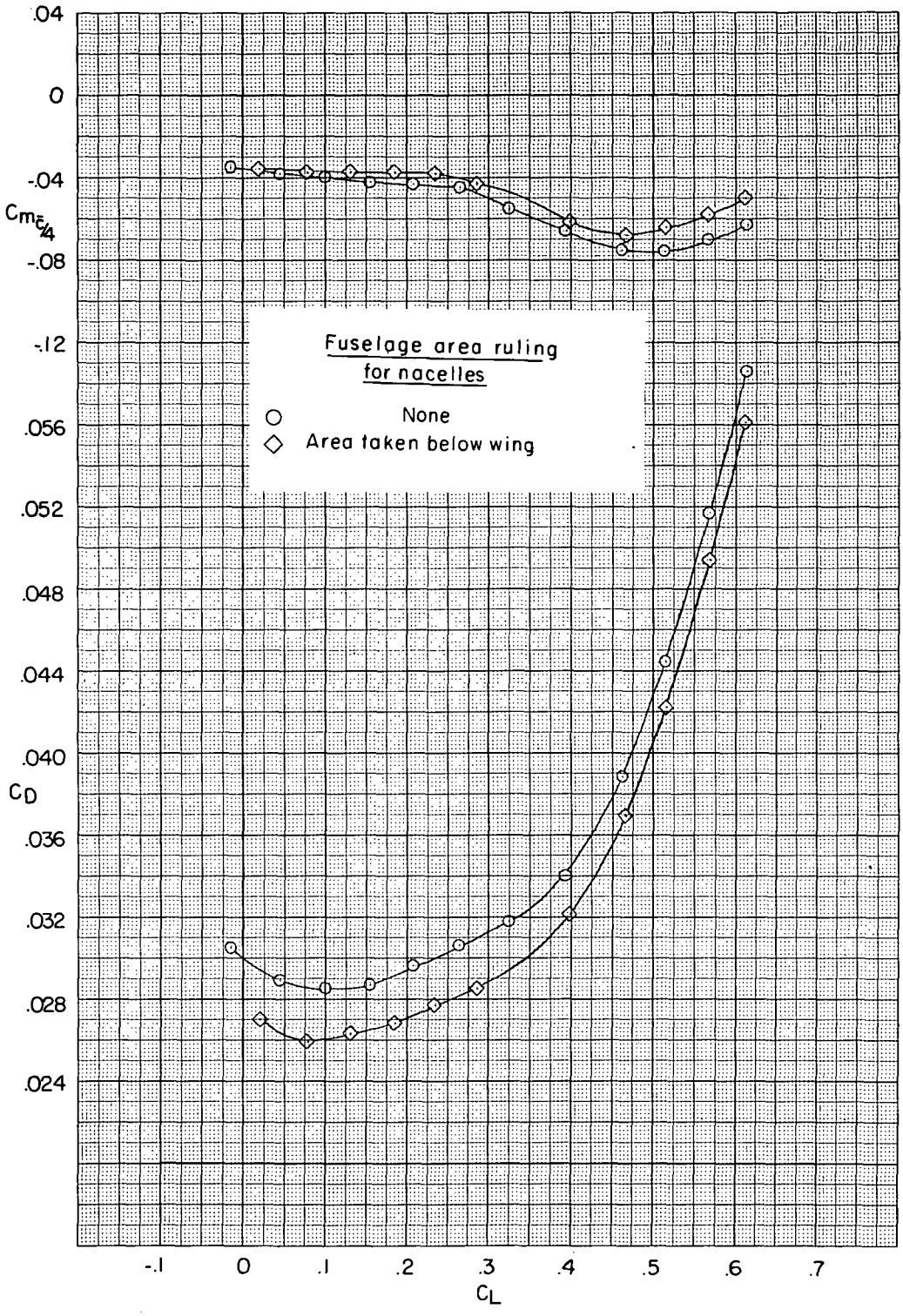

(f) M = 0.99.

Figure 36.- Continued.

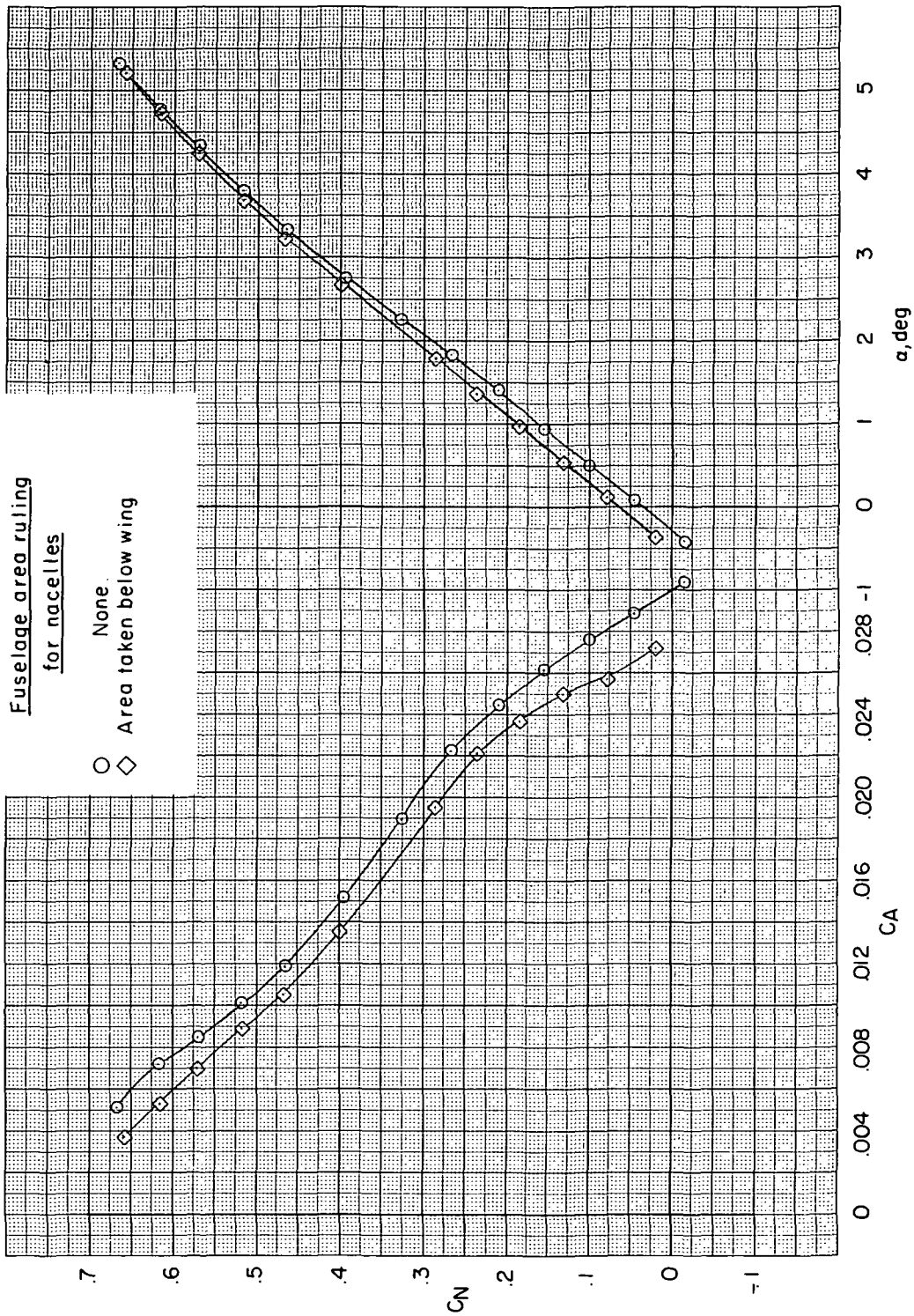

(f) Concluded.

Figure 36.- Concluded.

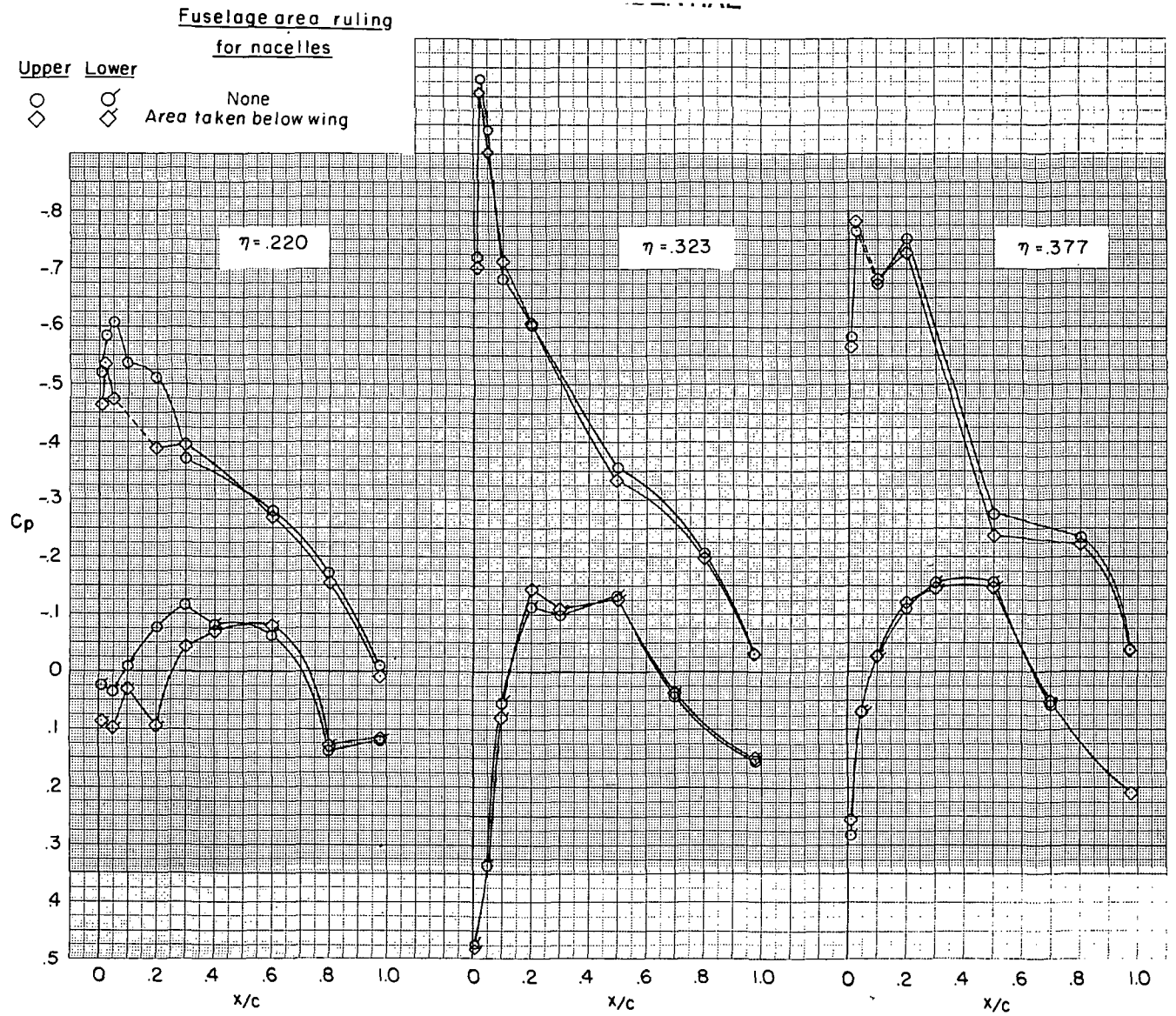

(a) M = 0.90.

Figure 37.- Effect of area ruling for nacelles located at 0.35b/2 on wing pressure distributions. $C_L \approx 0.40$.

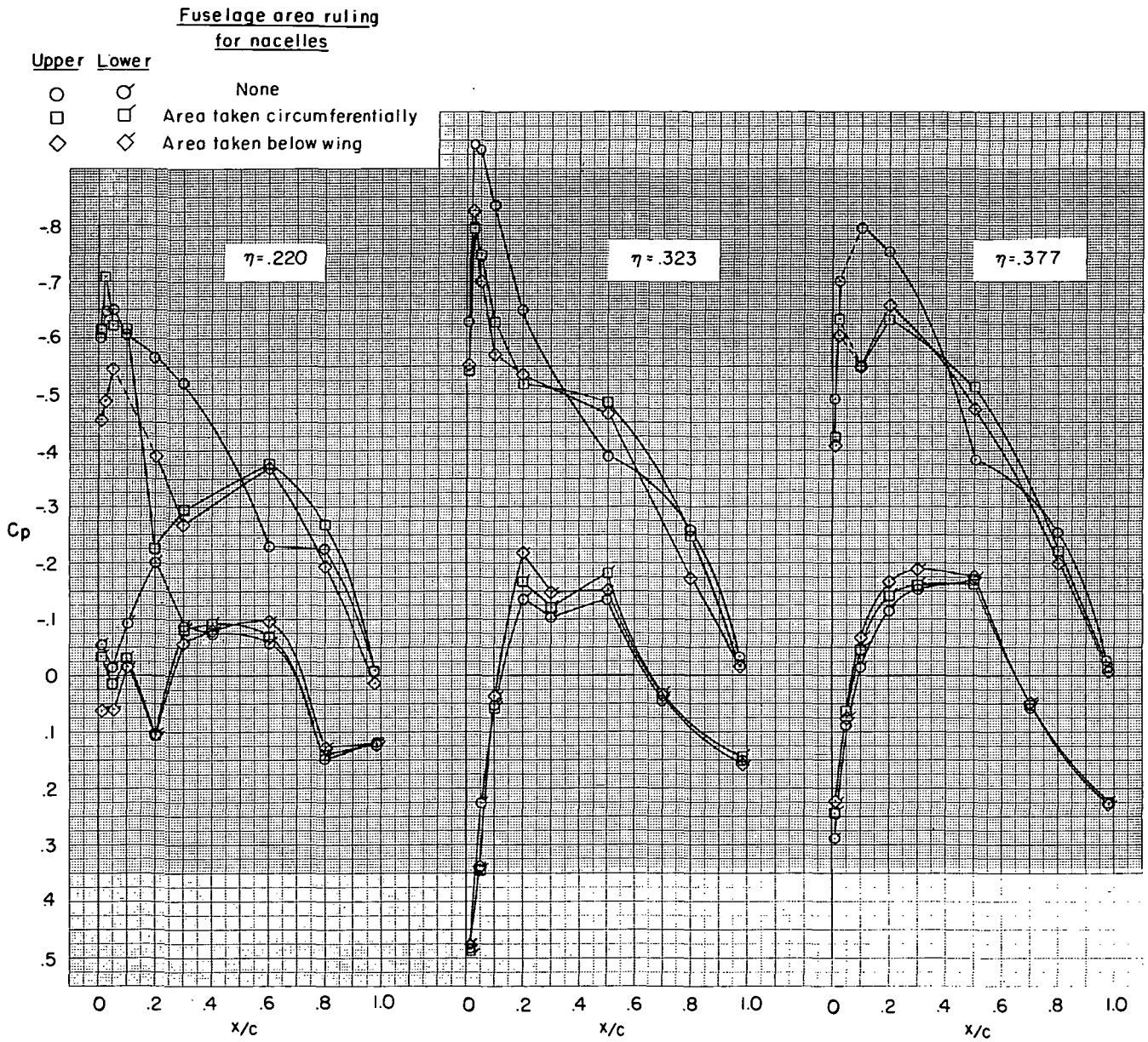

(b) M = 0.95.

Figure 37.- Continued.

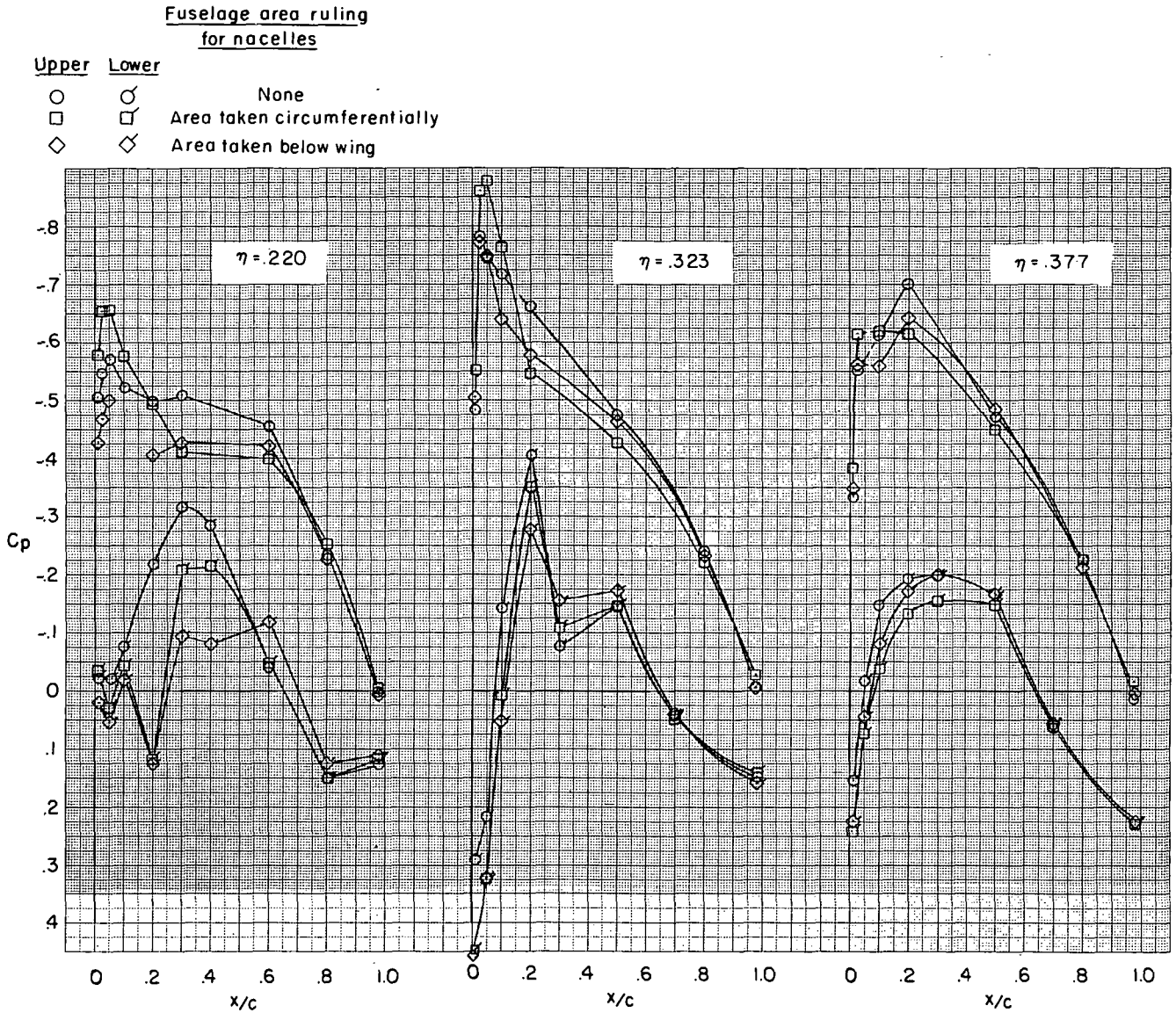

(c) M = 0.98.

Figure 37.- Concluded.

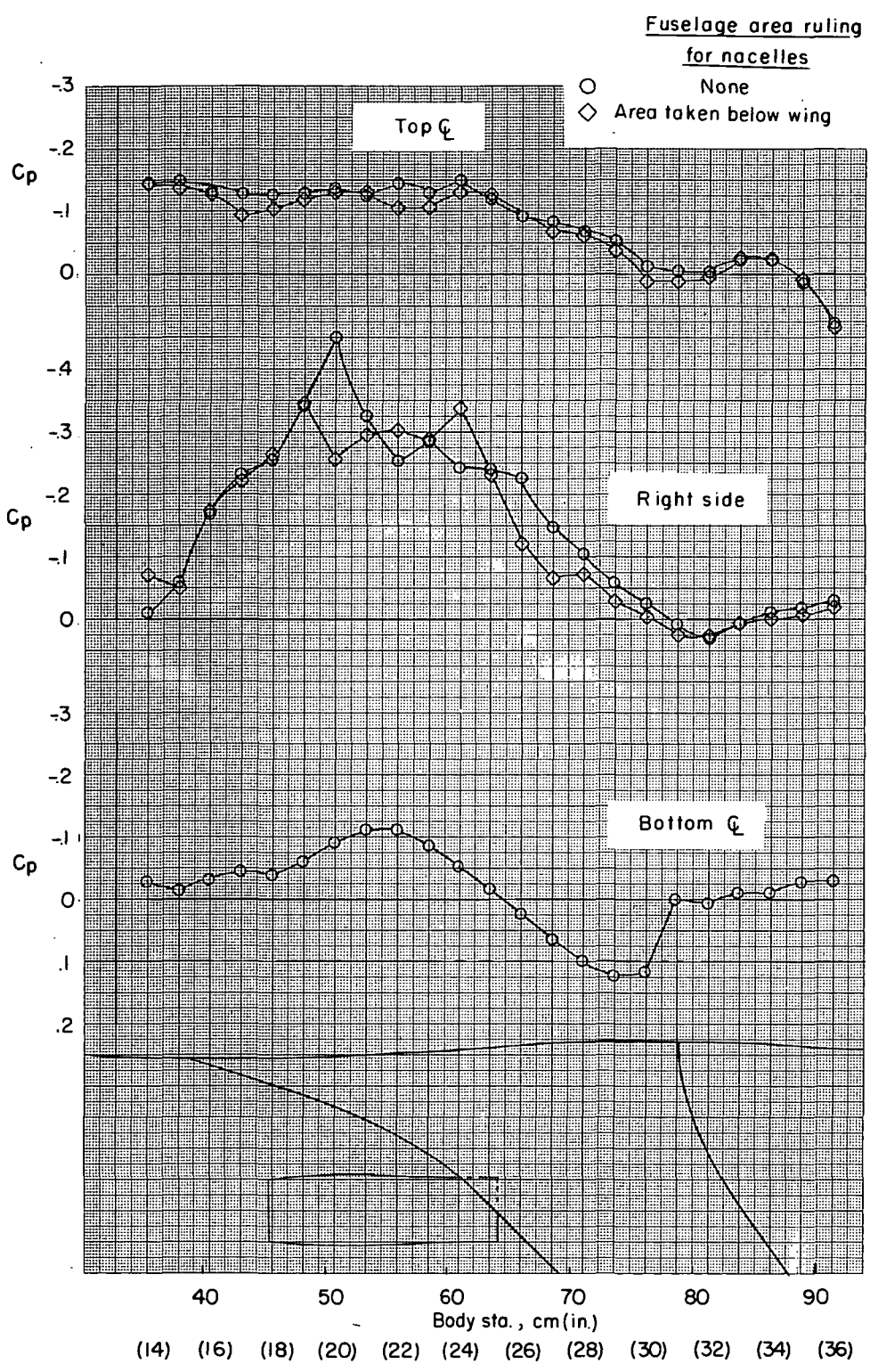

(a) M = 0.90.

Figure 38.- Effect of area ruling for nacelles located at 0.35b/2 on fuselage pressure distributions. $C_L \approx 0.40$.

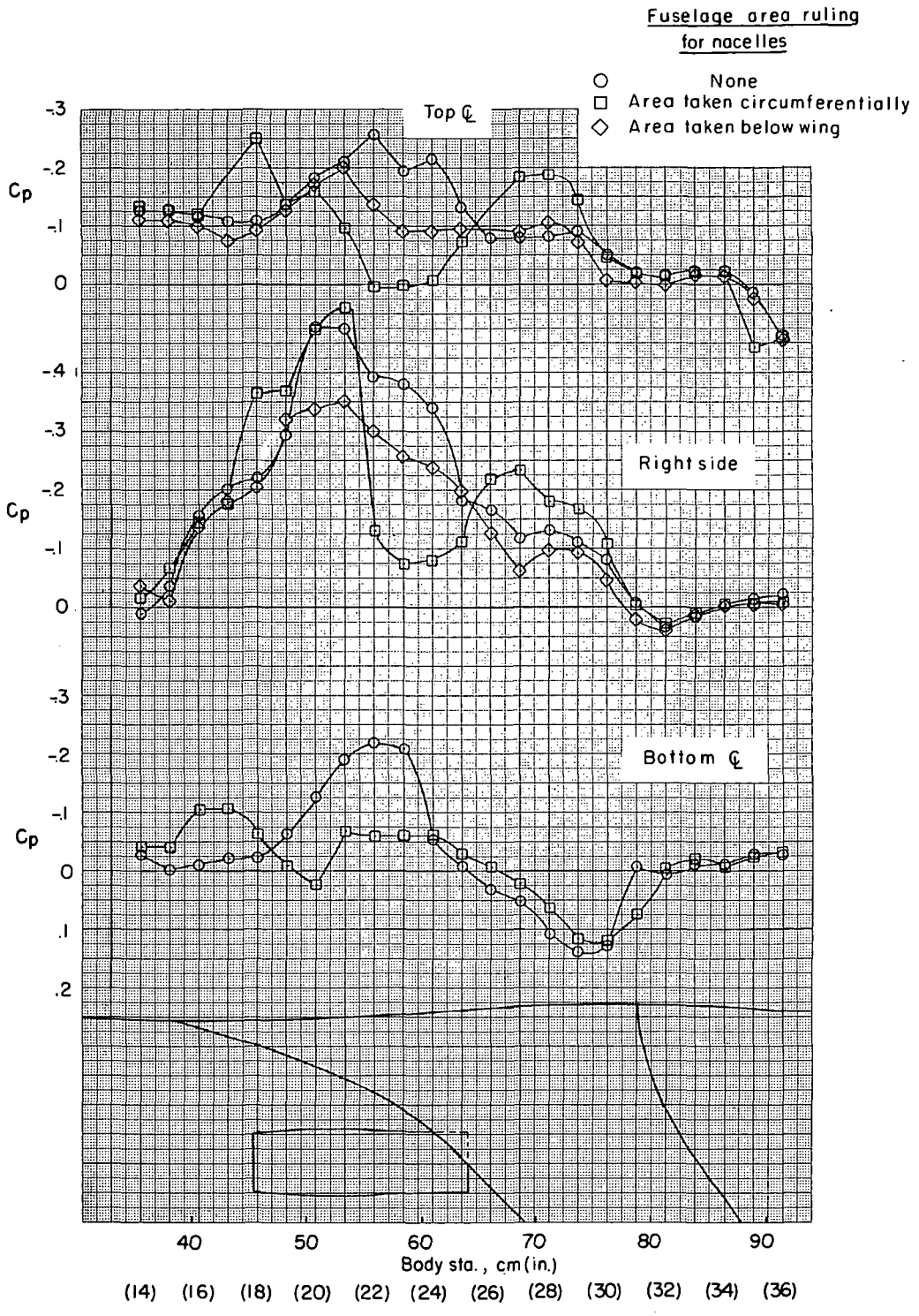

(b) M = 0.95.

Figure 38.- Continued.

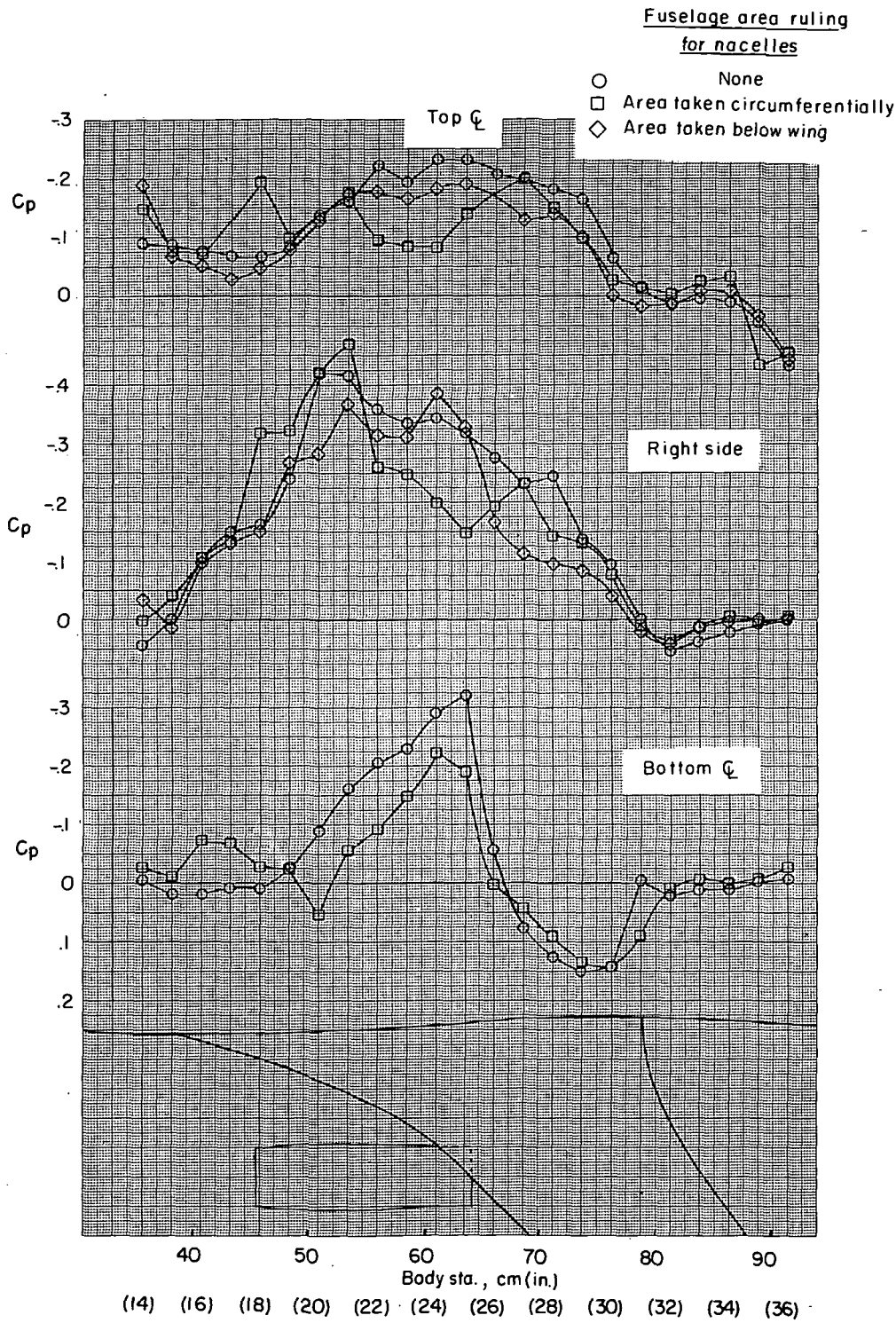

(c) M = 0.98.

Figure 38.- Concluded.

NASA-Langley, 1974 L-9267

"The aeronautical and space activities of the United States shall be conducted so as to contribute . . . to the expansion of human knowledge of phenomena in the atmosphere and space. The Administration shall provide for the widest practicable and appropriate dissemination of information concerning its activities and the results thereof."

—NATIONAL AERONAUTICS AND SPACE ACT OF 1958

NASA SCIENTIFIC AND TECHNICAL PUBLICATIONS

TECHNICAL REPORTS: Scientific and technical information considered important, complete, and a lasting contribution to existing knowledge.

TECHNICAL NOTES: Information less broad in scope but nevertheless of importance as a contribution to existing knowledge.

TECHNICAL MEMORANDUMS: Information receiving limited distribution because of preliminary data, security classification, or other reasons.

CONTRACTOR REPORTS: Scientific and technical information generated under a NASA contract or grant and considered an important contribution to existing knowledge.

TECHNICAL TRANSLATIONS: Information published in a foreign language considered to merit NASA distribution in English.

SPECIAL PUBLICATIONS: Information derived from or of value to NASA activities. Publications include conference proceedings, monographs, data compilations, handbooks, sourcebooks, and special bibliographies.

TECHNOLOGY UTILIZATION PUBLICATIONS: Information on technology used by NASA that may be of particular interest in commercial and other non-aerospace applications. Publications include Tech Briefs, Technology Utilization Reports, and Technology Surveys.

Details on the availability of these publications may be obtained from:

SCIENTIFIC AND TECHNICAL INFORMATION OFFICE

NATIONAL AERONAUTICS AND SPACE ADMINISTRATION

Washington, D.C. 20546